INVESTIGATIONS INTO THE REPRODUCIBILITY OF POWDER FLOW MEASUREMENTS AND THEIR RELEVANCE FOR PHARMACEUTICAL DOSAGE FORM MANUFACTURE

A THESIS SUBMITTED FOR THE DEGREE OF
DOCTOR OF PHILOSOPHY
IN THE FACULTY OF MEDICINE OF
UNIVERSITY OF LONDON

By

MOSUNMOLA TITILAYO OYEBOLA
BSc, MSc

THE SCHOOL OF PHARMACY
UNIVERSITY OF LONDON
BRUNSWICK SQUARE
LONDON WC1N 1AX

2004

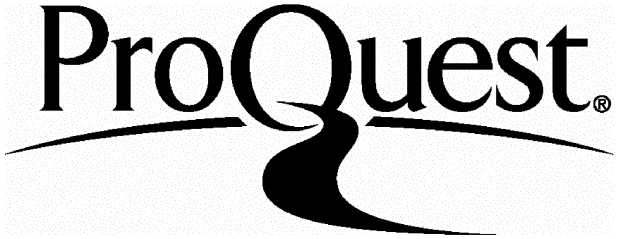

"Wisdom is the principal thing;
Therefore get wisdom;
And with all thy getting get understanding."
(Proverbs 4:7)

ABSTRACT

In the pharmaceutical industry, powder flow assessment methods are of great interest for the development and manufacture of solid dosage forms. Methods providing reproducibility, yet which are easy to perform, are sought. The aim of the thesis was to evaluate methods to determine powder flow for their ability to detect variability in flow, reproducibility of the results and ease of use. The operation and performance of the rotational split-level shear tester using a standard cell was evaluated by studying the flow and failure properties of pregelatinised starch, α-lactose monohydrate, precipitated calcium carbonate, microcrystalline cellulose type 105 and powder fractions of the first two of these powders. The results indicated that reproducible and reliable flow properties could be obtained using a set of derived parameters of operation. The instrument was able to detect differences in shear properties due to differences in particle size when using size-fractionated powder samples. An influence of relative humidity of the air (35 – 75 %) on the shear properties, however, was not evident. The results obtained for the powders in relation to static and dynamic packing demonstrated that the use of the Mohammadi and Harnby model (compaction constant, *T*) led to a better/distinct ranking of powders than the commonly employed Carr's compressibility index, and that the use of a classical tap volumeter as opposed to the fast tapping technique described in the European Pharmacopoeia enhances packing of powders. Pre-drying the powder prior to particle density measurements led to better values being obtained as indicated by the statistical evaluation of the pre and post - drying data. The critical orifice diameter measurement led to a different ranking of the powders compared to the other methods of powder flow evaluation. The studies have shown that the rotational split-level shear tester gave the most useful data which were reproducible and able to differentiate between the properties of the powders.

ACKNOWLEDGEMENTS

I would like to express my gratitude to the Almighty God for giving me the strength and courage to complete this wonderful, and yet emotional chapter in my life.

My sincere and deep appreciation also goes to my supervisor Prof. Fridrun Podczeck for giving me the opportunity to undertake this project, her excellent technical expertise, contribution, patience, encouragement and most of all her understanding. The financial support of the Engineering and Physical Sciences Research Council of Great Britain and of GlaxoSmithKline is gratefully acknowledged.

Special thanks to Prof. J. Micheal Newton for his technical expertise, 'words of wisdom' and for always being willing to share his knowledge with me even at 'short notice'. I would also like to say a big thank you to my industrial supervisor, Mr. Dave Barrett of GlaxoSmithKline, Harlow town, Essex, for his understanding, sharing his knowledge with me and also for the technical support. Many thanks to all his colleagues for making my research visit such an educating and memorable one, especially Dr. Chinedu Madichie for the training on the dynamic vapour sorption instrument.

A big thank you to all the Pharmaceutics postgrads, postdocs and my friends outside the school for their friendship, inspiration, motivation and also for having a good sense of humour. Thanks are due to Dr. Papa Boateng, Mr Dave McCarthy, the administrative and technical staff of the Pharmaceutics Department and the computer unit staff for their assistance.

Many thanks to my husband, Babajide for his love, understanding and support. My love and appreciation goes to my parents, Adetoun and all my beloved families for their encouragement and moral support. Not forgetting my 'little cherubs', Taiwo, Kehinde (the twins) and Idowu for believing in me, and also for always knowing when to allow mummy to do 'some work'. Hopefully, now that this is finished, we shall be able to spend more time together!

TABLE OF CONTENTS

List of Figures

CHAPTER 3

List of Tables

Abbreviations

PS – Pregelatinised starch

LM – Lactose monohydrate

PCC – Precipitated calcium carbonate

MCC 105 – Microcrystalline cellulose type 105

M – mass

V – volume

V_v – void volume

V_p – apparent particle volume

ρ_b - bulk density

D_o - minimum/aerated/initial bulk density

D_f - maximum/tapped/final bulk density

P/P_0 - relative pressure

cc - unit for volume of gas adsorbed (cubic centimeter)

g^{-1} - per gram

STP - standard temperature and pressure

TGA - Thermogravimetric analyser

C_S, C_F - Carr's index for slow and fast tapping respectively

T_S, T_F – Compaction constant for slow and fast tapping respectively

$AIFL_S$, $AIFL_F$ – Angle of internal flow for slow and fast tapping

COD - Critical orifice diameter

V_t - force applied for preconsolidation

S -shearing force

V - normal force

$\overline{V}$ - normal force prior to shearing.

τ - shear stress

σ - shear strain

δ - Effective angle of friction (EAF)

Φ - Angle of internal friction (AIF)

f_c - Unconfined yield stress

σ_1 and σ_2 - major and minor principal stress respectively

f_{ct} - Unconfined yield stress after an interval of time

FF - Flow Function

NCC – Normalised cohesion

EYL - Effective yield locus

PL – Preconsolidation load

CSL – Consolidation step load

CST – Consolidation step time

SST – Shear step time

ET – Expansion time of the powder during shear

PT – Preconsolidation time

SS – Sieve size

NSS - Number of shear steps

VS – Acceleration of vibration of the fill sieve

SD – Standard deviation from the automatically calculated values.

s.d. – standard deviation of replicate values

RH – Relative humidity of the storage air

r_s - rank correlation of Spearman

CHAPTER ONE

INTRODUCTION

OVERVIEW

1.1 PHARMACEUTICAL POWDERS

Many powder definitions exist depending on their application. The British standard considers a material as a powder if it is generally composed of dry, discrete particles with a size of less than 1000μm in any direction (BS 2955, 1993). This definition indicates that powders are composed of particles of different shapes and sizes, interspersed with void spaces and hence, non-homogenous in nature. Staniforth (2002) defined powders as solid particles of the same or different chemical compositions having equivalent diameters of less than 1000 μm. The British Pharmacopoeia (2003) defines powders as material consisting of solid, loose and dry particles of varying degrees of fineness. The degree of fineness, expressed in relation to a sieve size and sieve number, is classified as follows: coarse powders (> 350 μm), medium fine powders (100-350 μm), fine powders (50-100 μm), very fine (10-50 μm) and micronised powders (< 10 μm). Other terms considered by the British Pharmacopoeia include moderately coarse, microfine and superfine powders. Powders have various properties and functions due to the difference in contribution of the surface characteristics of the particles, and there are also different requirements for treatment and testing (Wanibe and Itoh, 1998). According to Podczeck (1998), the main characteristics of a powder bulk are packing, flow and mixing behaviour, which may or may not be governed by adhesion and friction at a particulate level.

Brittain et al (1991a) classified powder properties into three main levels, namely:

Molecular- in which the properties that are associated with the individual molecules, can be examined using electronic or vibrational spectroscopy and magnetic resonance techniques.

Particulate- in which the properties pertaining to individual solid particles studied include, for example, size distribution, particle morphology, X-ray and thermal analysis.

Bulk- in which properties associated with an assembly of particulate species are defined by micrometric and powder characteristics such as flowability.

The bulk level will be considered for now and future studies will look at the particulate level.

1.2 HISTORICAL BACKGROUND – POWDERS AS DOSAGE FORMS

Powders are the basis of many dosage forms, such as tablets or capsules and can also be a simple dosage form in their own right. A large number of drugs are in powder form before processing (Aiache and Beyssac, 1995).

The use of powder as a dosage form dates back as far as 500 BC where sacred bitters ("hiera Picra") was among the compound powders used as laxative (Buerki and Higby, 1993). Bitter powders containing aloe (the principal ingredient) bearing the name "hiera" were used in various pharmacopoeias and recognized up to 1926 in the 4th edition of the National Formulary. In addition, powdered dosage forms resulting from not only fine division of vegetable but also from animal, mineral and synthetic substances were used.

Powders were originally designed as a convenient mode of administering drugs obtained from hard natural materials such as roots, barks and wood. Insoluble chemicals such as mercury salts and chalk were conveniently dispensed in the form of powders (Aiache and Beyssac, 1995) and nauseous, excessively bitter drugs, or drugs with offensive taste were administered conveniently using powder mixtures. In relation to therapeutic activity, presentation in powder form permits reduction of drugs to a fine division that is claimed to enhance efficacy, e.g., homoeopathic triturations. Examples of compounds of the recent past include a variant of senna, Dover's powders introduced by Thomas Dover and Dr. James fever powder.

1.3 POWDER FLOW

In relation to powders, Neumann (1967) considered flow as being the state of continuous deformation with time, involving movement of the centre of gravity. In this definition the continuity of the powder bulk is preserved. This definition reflects what happens when powder deforms especially during shear testing and hence will be adopted in this work. The British standard (BS 2955, 1993) defined powder flowability as the ease with which a powder flows. Prescott and Barnum (2001a) went a step further by defining *powder flowability* as the ability of a powder to flow in a desired manner, in a specific piece of equipment. According to these workers, the flow behaviour of a powder is

multidimensional and depends on many powder characteristics. Powder flowability is the result of the combination of powder physical properties, which affect powder flow, and the equipment used for handling, storing or processing the powder. It is hence not an inherent powder property.

Powder flowability along with mixing and compression properties is of importance in the production of pharmaceutical dosage forms, for instance in the production of tablets and capsules (Staniforth, 2002). Flowability depends on a wide variety of factors in which particle size, particle shape, moisture content, porosity, and bulk density are just a few (Hanson 1998). Also, interparticulate forces play a role, but on the bulk level these are not specifically considered. The flow of a powder bulk is very complex as powders tend to exhibit different behaviour which is neither solid nor liquid like. Powders can deform and flow like a viscous liquid when sheared and can exhibit both elastic recovery and brittle fracture like solids. In addition, they can expand and contract when stressed and can even retain the shape acquired thereafter. This may be attributed to particle re-arrangement due to the presence of void spaces.

In relation to flow properties, there are two types of bulk materials, namely:

(a) *Free flowing materials*

(b) *Cohesive materials*

The terminology arises from how the resistance against shearing is developed (Bauer and Wu, 1995), a distinctive difference being that cohesive materials are able to sustain tensile stress up to a certain limit whilst free flowing materials cannot. Hence, a powder is termed free flowing if the force of gravity outweighs other forces that could be present such as interparticulate forces.

Powder cohesiveness is the property of powders that is of importance in powder handling (Pilpel, 1971). It describes the powder bulk behaviour. The term cohesion instead of 'cohesive' is often incorrectly used to describe this property of the powder. Cohesion should only be used if the surfaces in contact are of identical chemical nature. However, as pointed out by Rumpf (1962) identical chemical surfaces typically do not exist due to

impurities, gas adsorption etc. Hence, Zimon (1980) suggested using the term 'Autoadhesion' if particles of identical chemical nature are in close contact, for example two lactose particles. Adhesion describes the contact between surfaces of different chemical nature (Rumpf, 1962; Zimon, 1980).Cohesiveness expresses the ease or difficulty of a bulk powder to flow. The word *cohesiveness* has its origin in soil mechanics, where wet powder or powder masses are treated as a continuum as opposed to a *particulate* (properties of the powder bulk are obtained by summing individual interactions of the discrete particles), from which gross measures are taken. Jenike (1961, 1964) applied the theory to dry powder after it was developed from soil mechanics by Hvorslev (1937). In the continuum approach, the properties of the mass are assumed to be a continuous function, and the mass may be divided indefinitely without losing any of its defining properties (Thomson, 1997).

Flowability of powders must be consistent when fractionating the bulk material into a consistent volume e.g. when filling capsules or pressing tablets. A dependable and accurate measurement of flowability is therefore essential for defining the materials and in-process mixtures during pharmaceutical production (Hanson 1998, Kamath et al 1993). The specific bulk characteristics and properties of a powder that affect flow and that can, in principle, be measured are termed *flow properties* (Prescott and Barnum, 2001a).

1.4 FACTORS AFFECTING POWDER FLOWABILITY

Several factors affect the flowability of powder bulk; some of the factors will be considered here without claiming completeness.

1.4.1 PARTICLE SHAPE

Particle shape has a great influence on the flow properties of powders (Washington, 1992), and it is one of the most difficult problems encountered in powder technology (Podczeck, 1997). This influence is not only exerted on powders in the pharmaceutical industries but also in other industries where powder handling is involved. Luerkens et al., (1987) defined particle shape as the recognized pattern of relationships among all points which constitute the external surface. The effect of particle shape on the powder flow may be attributed to the alteration of interparticulate and/or frictional forces between particles. A good powder

flow may be attributed to particles with a shape that reduces interparticulate and frictional forces. Ridgway and Rupp (1969) concluded that the resistance to shear, or flow, of an assembly of irregular particles is greater than that of an assembly of spherical particles of the same size and density. Harwood and Pilpel (1969) concluded that angular particle shape may increase the friction coefficient and interparticulate forces compared to rounded particles. Podczeck and Sharma (1996) in their work on the influence of particle size and shape of components of binary powder mixtures on the maximum volume reduction due to packing, concluded that angular particles enhanced the packing properties of the binary mixtures, and that the addition of spherical and needle-shaped particles resulted in a lower value of the Kawakita constant a (this will be discussed later). This finding by the aforementioned workers is very important, for instance, in the production of solid dosage forms such as capsules, where packing properties of powders are very crucial for the effective filling of powders into smaller size capsules, even if the fill weight of the formulations is rather large (Podczeck and Sharma, 1996). Podczeck and Miah (1996) found that the particle shape influenced the friction and flow properties of powders and that the friction properties depended more on the asymmetry or elongation of the particles, while powder flow depended more on the geometric particle shape. It should be borne in mind that altering the particle shape is not a guarantee for good powder flow as the effect of particle shape on powder flow is more complicated (Zeng, et al. 2001).

According to Heywood (1963), the particle shape affects the surface area, bulk density, and other powder characteristics. The description of particle shape as being acicular, crystalline, dendritic fibrous, flaky, granular, angular, irregular, nodular or even spherical (BS 2955, 1993) is inadequate for the purposes of calculating particle properties which incorporate the effect of shape (See Figure 1.1 for different particle shapes and how cohesive powder behaviour is enhanced). The complexity of shape measurements makes the development of experimental methods for quantitative measurement of particle shape difficult. The interparticulate contact areas of powder particles also play a major role when considering particle shape. The reason for this is that powders with similar particle sizes but different shapes possess different interparticulate contact areas (Staniforth, 2002). For instance, a group of spheres has minimum interparticulate contact areas and thereby general optimal

flow properties, whereas a group of particle flakes or dendritic particles has a very high surface-to-volume ratio and thus a large contact area and poorer flow properties (Staniforth, 2002). Anisometric particles having high elongation or flatness ratio tend to build up open packings of high porosity, but can also be more readily deformed by compression than packings of isometric particles (Neumann, 1967). The author also pointed out that during flow anisometric particles tend to orientate their long axes in the direction of the flow, and if such orientation is achieved, they show less internal friction than more nearly isometric particles. Angular particles are more likely to form a good tablet possessing higher strength as they interlock mechanically after compression when compared with the rounded ones (Rupp, 1977). In the pharmaceutical industry, the spherical shaped particles are still the most desired ones, as it is believed that they produce the least interparticulate friction and, hence the best flow properties under normal conditions (Zeng et al., 2001).

Sophisticated methods such as laser diffraction can be used for particle characterisation but they all lack information on particle shape (Hundal, et al 1997). Common approaches used to assess particle shape include the determination of 'elongation ratio', 'aspect ratio', 'circularity', 'sphericity', irregularity factors and the use of Fourier analysis (Podczeck, 1997; Hundal et al., 1997). Fractal dimensions have also been employed but, according to Podczeck (1997), appear inappropriate. Podczeck (1997) developed a *shape factor NS* for particles on the basis of two-dimensional particle outlines obtained by image analysis. According to the author, this shape factor would ensure easy comparison between identical and non-identical particle shape. The worker pointed out that the proposed shape factor uses the deviations of the two-dimensional particle outline from standard images, for example, of a circle, triangle and square, and also considers the particle elongation and the number of characteristic corners of the apparent shape. Podczeck (1997) concluded after comparing the proposed new shape factor with standard shape factors such as aspect ratio and circularity that the new shape factor can differentiate between mathematically defined shapes. However, there are limitations to the use of the shape factor. Firstly, particles which cannot be classified into any mathematically defined model shape and with sufficiently large number of corners are classified as irregular. Secondly, the degree of roundness cannot be evaluated by the proposed shape factor *NS* (Podczeck, 1997). The algorithms to

measure this shape factor on an image analysis system are complex and the reader should refer to the original paper (Podczeck, 1997).

A very popular shape factor is the Aspect ratio (Schneiderhöhn, 1954) which is the ratio between the longest Feret diameter (see section 1.4.2) of the particle and its perpendicular value.

In this work, an image analyser was used to assess the particle shape and size of the various types of model powders. The use of an image analyser has a distinct advantage of measuring the particle size and deriving shape from particle size, area and circumference concurrently. The two-dimensional image or the contour line of a particle contains much of the relevant information on particle shape, and it is much easier to obtain than a three-dimensional image (Hundal et al., 1997).

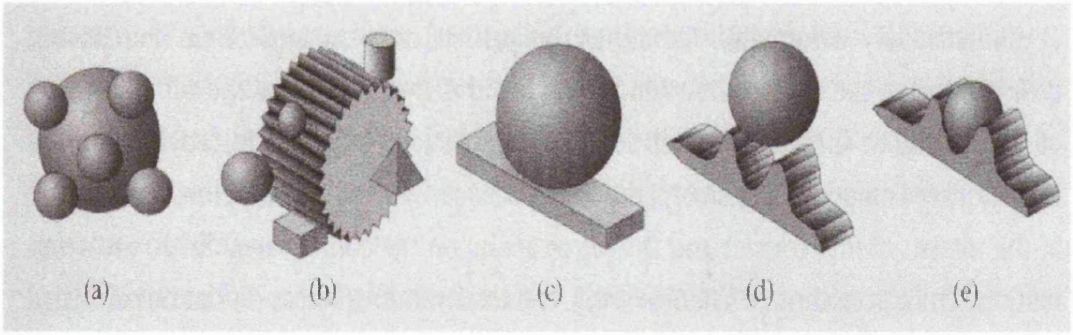

Figure 1.1 *Diagrammatic representation of some typical examples of interparticulate contact between particles, where (a) idealised situation; (b, c, d and e) common situation (Taken from Zeng et al, 2001)*

Image analysis involves more than one stage. The initial stage involves the acquisition/ storing of the image by the hardware. The acquired image is then converted into a digitised form, which is stored in the computer memory or a hard disc. The next stage involves the enhancement of the image to emphasise and define the required details. This is followed by the measurement operation to extract the required numbers or further information such as particle size distribution or shape. The instrumentation of an image analyser includes a

microscope, camera (e.g. charge-coupled device-CCD), frame grabber that enables the analogue signals to be converted to digital format, a computer and printer.

1.4.2 PARTICLE SIZE AND SIZE DISTRIBUTION

The particle size of powder particles is another important factor that is highly considered in pharmaceutical powder technology due to its impact on powder flow, since the forces that enhance powder cohesiveness are a surface phenomenon. Generally, fine particles with a very high surface to mass ratio are more cohesive than coarser particles, which are influenced more by gravitational forces. Particle sizes above 250 μm are usually free flowing, whereas, cohesiviness and flow problems are enhanced by sizes below 100 μm (Staniforth, 2002).

There are different methods to obtain the particle size. In the pharmaceutical industry, typically microscopy or laser light scattering techniques are employed. When using microscopy (typically in combination with image analysis) the Feret diameter (Hawkins, 1993) is the standard measure used. The Feret diameter of a particle is defined as the distance between two parallel tangents enclosing the particle outline.

In contrast to the above, Pilpel (1971) indicated that cohesiveness can still be exhibited by powders (e.g., carboxyl methyl cellulose) with a particle size up to 300 or 400μm, as mechanical interlocking caused by the irregular particle shape allows for this. Powders having a particle size less than 10 μm may be extremely cohesive and resist flow under gravity except possibly as large agglomerates (Staniforth, 2002). Jones and Pilpel (1966) concluded that the flow through an orifice increases with an increase in particle size until a maximum particle size is reached where any increase in particle size leads to a decrease in powder flow rate. The decrease in flow in relation to increase in particle size may be attributed to the limitations due to the size of the orifice relative to that of the particles. Conversely, the decrease in flow rate due to decrease in particle size may be due to the prevalence of surface tension and Lifshitz van der Waals attractive forces (Pilpel, 1964). According to Neumann (1967), an irregular shaped particle can be defined in more than one

way and in practice a single linear dimension, for example, the diameter of a sphere equivalent to the particle with respect to a selected property is usually assigned.

The particle size distribution is yet another important fundamental property. Defining the size of a single particle unequivocally could be difficult. Given a collection of many particles of varying sizes, the difficulty multiplies (Neumann, 1967). The preferred method involves separating the powder into many fractions containing particles of narrow range of sizes. This can then be expressed as either mass or number distribution or other collective values of the fractions in a statistical manner. Either cumulative values or frequency distributions are presented. The particle size distribution can affect bioavailability of certain drugs and exerts a major effect on powder flow. Pharmaceutical dosage forms must be produced in uniform units, and good content uniformity will be possible only when the particle size of the active component and excipients are also carefully controlled (Brittain *et al.*, 1991a). Many methods are available to measure the particle size distribution of powders. These include laser light scattering of particles suspended in inert solvents, optical microscopy usually combined with image analysis, sieve analysis and electrical zone sensing. In most of the techniques, only the size distribution present in the suspending medium is reflected and not necessarily what exists in the original powder sample. According to Brittain *et al.,* (1991a), microscopy and sieving are true indicators of the actual particle size of a powdered solid, and sieve analysis represents the simplest method for the determination of particle size distributions.

In the present work, laser light scattering was used to determine the particle size distribution. This principle relies on the fact that for light passing through a suspension, the diffraction angle is inversely proportional to the particle size. Early instruments related the diffraction angle to particle size utilising the Fraunhofer theory, which gives rise to large errors under some circumstances, for instance when the refractive indices of the powder particle and suspending medium approach each other. Though instruments using the Fraunhofer principle are still in use due to the low cost and fast computing, the results obtained are still questionable. The wavelength of light must be significantly smaller than the particle diameter for this principle to be valid. For smaller particles (< 10 μm), the Mie

theory is appropriate for the analysis of diffraction patterns. The factors cited by Etzler and Sanderson (1995), which may cause inaccuracies of particle size distribution determined by Frauhofer diffraction include the following: transparency of particles, appearance of *ghost particles* caused by high angle of diffraction due to the presence of edges on particles, and, finally, computer algorithms which are normally not known to the user vary with manufacturer. In view of these limitations, great care should be used particularly when Frauhofer devices are applied to pharmaceutical powders (Etzler and Sanderson, 1995).

The Mie theory utilised by the modern instruments allows particle size analysis in the range of 0.1 – 2000 μm. It requires knowledge of the refractive index of the powders and the dispersant for the calculation of particle size distribution (Rhodes, 1999). According to the Mie theory, particles approaching the dimension of the wavelength of the laser light scatter in the forward direction mainly and also produce some side scatter at different wavelengths and polarisations. Diffraction occurs when light emitted by a helium-neon laser is incident on the sample of particles. The scattered light is focused by a Fourier lens onto a photodetector, which measures the integral scattering of all particles simultaneously i.e. measures a particle cloud rather than individual particles. The light flux signals occurring at the photodetector are converted into electrical current, which is digitised and processed by a microprocessor into size distribution data (Staniforth, 2002).

1.4.3 APPARENT PARTICLE DENSITY

Powders normally flow under the influence of gravity, hence, dense particles are generally less cohesive and have better flow properties than less dense particles of the same size and shape. In addition to the apparent particle density other densities have been recognised e.g. the bulk, true, poured (minimum or aerated) and tapped (maximum or tapped) density. These will be discussed later. The apparent particle density can be measured with a pycnometer. The multipycnometer is designed to measure the true volume of various quantities of solid material based on the Archimedes principle of fluid displacement. Dry helium gas is the displaced fluid and it owes its suitability to its small atomic dimension and inertness, which assures penetration into crevices and pores thereby ensuring maximum accuracy. The apparent particle density of the powder is determined by measuring the

pressure difference when a known quantity of helium under pressure is allowed to flow from a precisely known reference volume into the sample cell containing the powdered or solid material.

1.4.4 SURFACE AREA AND SURFACE TEXTURE

The surface area determination is a very important concept in powder technology as it is related to powder flow. Carr (1970) and Staniforth (2002) attributed the variation in relative surface area of powder to the size of the powder particles and hence concluded that this property will play an important role in powder flow. The smaller the particle size, the greater is the relative surface area and ultimately the higher its surface area activity. However, the specific surface area depends on the surface texture and the amount of external pores. Hence, the specific surface area can vary considerably for powders of similar particle size (Roberts and Emödi, 1943). Several methods are available to measure the surface area of powders. The two most commonly available methods that allow direct calculation of surface areas are the *air permeability* and the *gas adsorption method* (Martin, 1993). According to the author, in the former, the rate at which a gas permeates a bed of powder is related to the surface area of the powder exposed to the gas (permeant). In the latter, the amount of gas that is adsorbed onto the sample of powder to form a monolayer is a direct function of the surface area of the powder sample. The adsorption of adsorbate or gas molecules onto the surface of a sample can either occur by *physisorption,* where weak forces bind the molecules to the sample surface, or by *chemisorption,* where chemical bonding, which is irreversible, prevails. At low temperature chemisorption occurs, which releases large amounts of energy and aids detection. Physisorption occurs during the formation of multiple layers, and little energy is released. For the purpose of this research, the gas adsorption technique will be discussed and used to determine the surface area of the powders.

The most widely used gas (adsorbate) is nitrogen as it is inert, less expensive and is available in high purity. By immersing the sample tube containing previously outgassed powder sample into the coolant - liquid nitrogen at 77 K (-195 °C), measurement is made. The outgassing process involves the removal of adsorbed gases and moisture from the

surface of the powder particles by evacuating them with the aid of a vacuum pump, followed by the heating of the sample tubes to a specified temperature and for a defined time. This process ensures that a clean sample surface is achieved and, hence, an increase in measurement accuracy.

After the immersion, helium is now admitted into the sample tube for the measurement of dead space, as helium does not adsorb onto the sample surfaces. The dead space is found to be linearly dependent on pressure (Allen, 1999). The next stage involves the removal of helium and the process being repeated with nitrogen. Some of the gas molecules admitted into the sample tube will adsorb onto the sample surfaces while the remaining gas will be free to exert a pressure. Increasing the amount of nitrogen gas admitted leads to an increase in the amount of gas adsorbed and an increase in the pressure in the sample tube. The volume of gas in cubic centimetre adsorbed per gram of powder sample (adsorbent) is plotted as a function of the relative pressure at a constant temperature.

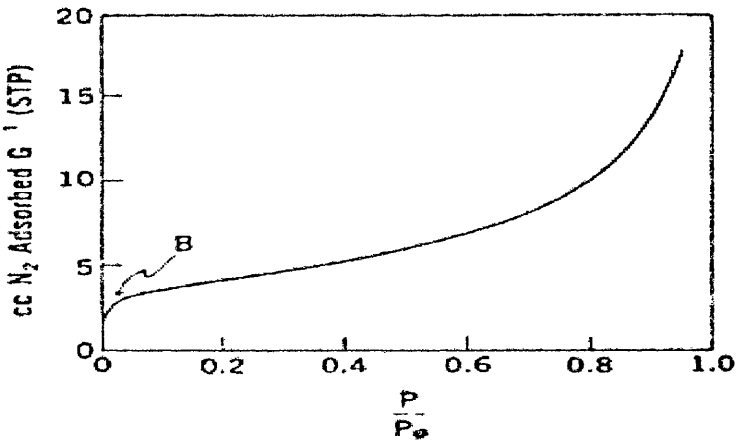

Figure 1.2 *Isotherm showing the volume of nitrogen adsorbed at increasing relative pressure (Taken from Martin, 1993).*

where:

B - completion of the monolayer

P/P_0 - relative pressure

cc - unit for volume of gas adsorbed (cubic centimeter)

G^{-1} - per gram

STP - standard temperature and pressure

The graph obtained is known as *Adsorption isotherm* (see Figure 1.2). Figure 1.2 is an example of a *Type II isotherm*, which is obtained by adsorption of gas on non-porous or macro porous powders and also represents unrestricted monolayer-multilayer adsorption on a heterogeneous substrate (Allen, 1999). The adsorbed layer is monomolecular at low pressures and multimolecular at higher pressures.

The most widely used equation to determine the volume of a monolayer of nitrogen V_m in cubic centimetres adsorbed by 1 gram of the powder sample is given by the BET expression (see Equation 1.1) named using the first letter of each surname of the original formulators - Brunauer, Emmett and Teller (Brunauer, Emmett and Teller, 1938). The workers developed this unified theory based on physical adsorption or *physisorption* and the theory itself is an extension of the Langmuir theory (Orr and Dallavalle, 1959).

Brunauer, Emmett and Teller (1938) arrived at Equation 1.1 by equating the rate of condensation of gas molecules onto an adsorbed layer to the rate of evaporation from that layer and summing for an infinite number of layers.

$$V = \frac{V_m C p}{(p_0 - p)\left[1 + (C-1)\frac{p}{p_0}\right]} \qquad \text{.....Equation 1.1}$$

By rearranging Equation 1.1, a linear form of the BET equation can be obtained (Equation 1.2)

$$\frac{p}{V(p_0 - p)} = \frac{1}{V_m C} + \frac{p(C-1)}{V_m C p_0} \qquad \text{.....Equation 1.2}$$

where:-

V = Volume Adsorbed

V_m = Monolayer Volume

C = Adsorption Energy Constant (ratio of the heat of adsorption to heat of liquefaction of nitrogen)

p = Sample Pressure

p_0 = Saturation Vapour Pressure of Adsorbate (liquid nitrogen)

A plot of $p/V(p_0 - p)$ as a function of p/p_0 yields a straight line having a slope of $(C - 1)/V_mC$ and intercept of $1/V_mC$. From the intercept and slope the values for the V_m and C can be obtained. The BET surface area (m^2/kg) can now be calculated using Equation 1.3:

$$S_w = \frac{A_m N}{M/\rho} \times V_m \qquad \text{.....Equation 1.3}$$

where

M/ρ = molecular volume of the gas (22,414 mL per mole)

N = Avogadro's number (6.02×10^{23} molecules $mole^{-1}$)

A_m = cross sectional area occupied by each nitrogen gas molecule (16.2 Å^2 or $16.2 \times 10^{-20} m^2$)

V_m = Monolayer Volume (ml/kg)

The BET equation owes its wide acceptability to its simplicity, non-destructive measurement, ease of use and high data reproducibility. Although the BET equation/theory is widely used, it is a mathematical model, and hence, it makes assumptions that include the following:

(a) The surface of the sample is homogenous, and hence, has uniform attraction for nitrogen molecules.

(b) Differences exist between the energy evolved by a nitrogen molecule adsorbing onto

a sample and a nitrogen molecule adsorbing onto a previously adsorbed nitrogen molecule in relation to multilayer formation.

(c) The molecules already adsorbed do not affect each other, hence, the nitrogen attractive forces are assumed to be normal.

Despite the widespread use of this theory/equation, limitations exist. For instance in the simple linear adsorption isotherm, deviations from linearity generally occur when relative pressures below 0.05 or above 0.35 are used (Orr and Dallavalle, 1959; Rudzinski and Everett, 1992).

Neumann (1967) described the two readily distinguishable groups of particle surface textures as those in which the particles appear to have smooth surfaces, and those with particles of rough surfaces. The former may show well developed crystal faces, or conchoidally fractured curved surfaces with sharp edges, or they may look like spherical, congealed or frozen droplets of liquid. The second type may seem to have a stepped or pitted, porous, but clearly coherent outer layer, or one showing regular or irregular aggregates of smaller particles. In this work a scanning electron microscope (Philips XL30 SEM) was used to study the surface topography of the powder particles qualitatively. This instrument is one of the most versatile and widely used tools in modern science. It is capable of visualising the particle topography (surface features) and also the morphology, which includes the shape and size of particles smaller than 0.5 μm using electrons rather than a conventional tungsten filament (light). Useful magnifications in excess of 200,000 times are obtainable, which translate to a resolution of 3.5 nm at an accelerating voltage of 30 kV.

The electron gun in the SEM produces a stream of monochromatic electrons, which is condensed by the first condenser lens. This lens is used both to form the beam and limit the amount of current in the beam. In conjunction with the condenser aperture, it eliminates the high-angle electrons from the beam. The electrons are now constricted to form a thin, coherent beam by the second condenser. Further elimination of the high-angle electrons from the beam is achieved by the objective aperture. This is followed by the scanning of the

surface in a grid fashion, dwelling on points for a period of time (this is determined by the scan speed). The objective, which is the final lens, focuses the scanning beam onto the sample. This results in interactions inside the sample, which are detected, and the number of interactions is displayed as pixels. The intensity of the pixels depends on the number of interactions (the more the interaction the brighter the pixel). This process is repeated until the grid is finished, which is a high resolution image of the morphology or topography of a material with great depth of field, at a low or very high magnification. It should be noted that for materials or powders that are not electrically conductive, pre-treatment of the sample surface with a thin conductive metallic film material (Skoog et al., 1998) like gold is required before analysis. It is advisable to dry materials before analysis as volatile substances or materials having a substantial amount of water do tend to deform and may impact on the level of vacuum in the sample chamber.

1.4.5 MOISTURE

According to Pilpel (1971), much of the work that has been done on the effects of moisture on the cohesive strengths of powders originated in the field of soil mechanics, and hence, it is appropriate to draw on these results when considering the effects of the moisture on pharmaceutical powders. When powders are exposed to high relative humidity, problems arise, which may lead to poor powder flow and consequently impact on operations such as storage in hoppers and silos, transportation, formulation and mixing, compression and even packaging. Powders tend to adsorb water, which may form liquid bridges between powder particles. This results in greater powder cohesiveness and, hence, reduced powder flow (Teunou and Fitzpatrick, 1999b). Conversely, as the relative humidity decreases, powders tend to desorb water, and liquid bridges will disappear for moist insoluble material. For soluble powders, solid bridges may form causing the powder to cake. It is important to note that the adsorption of water by a mass of powder from the atmosphere is time dependent as water must diffuse from the air into the powder and thus the effect of relative humidity on powder flow will depend on the time required for moisture to diffuse and on the dimensions of the bed of powder (Teunou and Fitzpatrick, 1999b).

Lowes and Perry (1965) showed that the cohesiveness of sand with an average particle size of 83 μm and a bulk density of 1.08 g/cm^3 was 3.92 Pa when exposed to 42 % relative humidity, but when the relative humidity was raised to 92 % relative humidity, the cohesiveness increased tremendously to 11.77 Pa at the same bulk density. Craik and Miller (1958) showed that adding a small amount of light magnesia to starch made starch less cohesive after exposure to relative humidities between 4 and 81% for 24 hours. A similar result was obtained with fine sucrose having a particle size of 10 μm, but with coarse sucrose of 100 μm size the addition of magnesia only made it less cohesive after being exposed to relative humidities above 60 %. According to Pilpel (1971), it has been shown that cohesiveness of relatively packed starch, lactose and griseofulvin increased as their moisture content increased and that this had an effect on the powder flow i.e. poor powder flow. The adsorption of water not only increases the area of contact between particles but can also produce a softening of the surfaces of many powder bulks, e.g., starches and water-soluble drugs. Hence, there may be increments in cohesive strength of the powder bulk. The impact of moisture on pharmaceutical powders has been well documented (Pilpel and Esezobo, 1974; Teunou and Fitzpatrick, 1999b). Moisture can be present in powders in different physical forms, namely as: adsorbed monolayers, multilayers on the surfaces of particles, normally condensed water on the surface, physically absorbed water within the particles or as strongly bound chemisorbed water. The rule of thumb is "as the moisture content of a powder increases, so does its cohesive strength (Marinelli, 2003).

In this work, the moisture content was determined using the Halogen Moisture Analyser based on the thermogravimetric principle while the moisture uptake was assessed using the Dynamic Vapour Sorption which is based on a gravimetric principle.

The Halogen Moisture Analyser emits/radiates infrared rays from the halogen radiator situated in the instrument. Some of the emitted rays are absorbed by the sample and the rest ultimately converted to heat. This heat is then transferred via contact with adjacent molecules in the sample to lower lying layers. The greater the thermal conductivity of the sample the faster and more homogenously the sample heats up. The thermal conductivity of

the sample changes with decreasing water content as drying progresses. The weight loss due to drying is determined by a balance incorporated and interpreted as moisture content.

The gravimetric study using the Dynamic Vapour Sorption technique (DVS) is undertaken in a humidity controlled ultra-sensitive recording microbalance system. This instrument is capable of measuring changes in sample mass to ± 0.1 μg. It also enables the accurate recording of the mass of a sample following exposure to a humidified or dry Nitrogen atmosphere. The ultra-sensitive recording microbalance system is housed in a precisely controlled constant temperature incubator.

1.4.6 TEMPERATURE

Powder cohesiveness is also affected by the rises in powder temperature or that of the surroundings. This is another important factor that impacts on powder flow. Some powders are sensitive to the temperature at which they are handled or stored and, hence, become more difficult to handle. Powders may agglomerate or soften at high temperature or may undergo phase changes, e.g. changes in crystalline form that result in caking (Teunou and Vasseur, 1996) when cooled. The yield strength of the powder has been found to increase significantly when temperature changes occur for example when powders are dried, then loaded hot into storage silos and allowed to consolidate (Thomson, 1997).

1.4.7 PACKING GEOMETRY

Neumann (1967) described powder packing simply as a system of particles where each individual is supported by direct contact with other particles or with the wall of the container. Particles filled into a volume of space will produce a powder bed that is in static equilibrium due to the interaction of gravitational and adhesion forces. A different spatial volume can be occupied by a powder bed, which was once in static equilibrium, by slight vibration of the particles. A higher driving force is required by more tightly packed powders to produce a flow than more loosely packed particles of the same powder. The reason for this is that the rearrangement of the packing geometry produces a different bulk volume, which generally results in a transition from loosely packed particles to more tightly packed particles (Staniforth, 2002).

1.4.7.1 Characterization of Packing Geometry

Porosity and bulk density:

The characterization of packing geometry using porosity is linked to the bulk density of the powder. The bulk density of a powder can be defined as the mass of the powder divided by the volume occupied by the powder. The volume specified here includes the volume of the particles as well as the voids (spaces between particles). Different geometric configurations can be illustrated using a set of monosize spherical particles ranging from one extreme, where the spheres form a cubical arrangement having a porosity of 0.48 (Fig. 1.3a), to the other extreme having a porosity of 0.26 (Fig. 1.3b) with a rhombohedral arrangement (Staniforth, 2002). Porosity values ranging from 0.9 to 0.1 have been obtained for powders of various types including anisotropic particles (Neumann, 1967).

The density of a powder bulk can be defined as the weight per unit volume of the entire powder particle assembly and the relationship is as follows:

$$\rho_b = \frac{M}{V} \ (\text{kg m}^{-3}) \qquad \text{....Equation 1.5}$$

where ρ_b is the bulk density of the powder, M the mass and V the volume occupied by the powder.

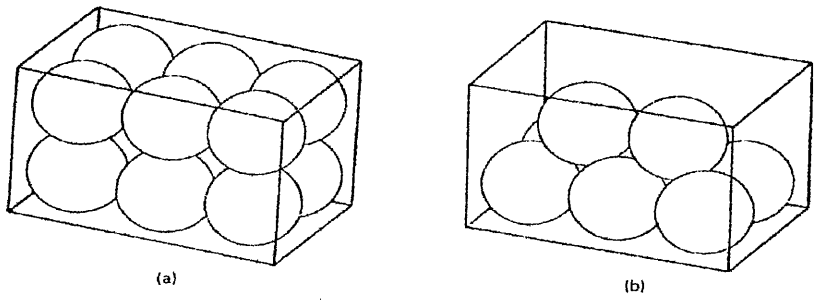

Figure 1.3 *Different geometric packings of spherical particles: (a) cubical (b) rhombohedral packing (Taken from Staniforth, 2002.)*

Hence, the bulk density is a characteristic of the powder rather than individual particles and is dependent on the particle packing. The density of a powder is always less than the

density of its component particles, and this is due to the presence of interparticle voids. This shows that a powder can possess many different bulk densities depending on the particle packing and porosity, but a single value for the particle density. Having a high bulk density value does not necessarily mean a close packing and low porosity bed since bulk density is directly proportional to particle density (Staniforth, 2002).

Bulk density $\propto$ particle density

i.e., Bulk density = k * apparent particle density

$$\Rightarrow \quad k = \frac{bulk\ density}{apparent\ particle\ density} \qquad \text{.....Equation 1.6}$$

Also, k is defined as $k = 1 - e$, where k is the constant of proportionality, which is known as the *packing fraction or fractional solids content* and e is the porosity. Fractional voidage (or bed porosity) e can also be expressed using the ratio of apparent particle volume Vp to bulk volume Vb:

$$e = 1 - (Vp/Vb) \qquad \text{.....Equation 1.7}$$

The ratio of void volume Vv to apparent particle volume represents the voids ratio:

$$\frac{Vv}{Vp} = \frac{e}{(1-e)} \qquad \text{.....Equation 1.8}$$

This voids ratio provides information about the stability of the powder mass.

According to Staniforth (2002), an increase in bulk density of powders with similar apparent densities leads to a decrease in porosity, and hence, an increase in the number of

interparticulate contacts and contact areas causing an increase in cohesiveness. However, a decrease in bulk density may be associated with a reduction in particle size and produce a loosely packed powder bed, which although porous is unlikely to flow because of the inherent cohesiveness of the fine particles.

Using porosity to characterize packing geometries can sometimes be misleading as a powder having a high porosity may be relatively closely packed when compared with a powder with a lower porosity. A typical example is that of loosely packed monosize cubic crystals with a porosity of 20% compared to a closely packed system of spheronised crystals with a porosity of 30% (Staniforth, 2002).

In the case of powder mixtures, different models have been proposed and used to predict the maximum packing density. In the Furnas model (1931), the packing of particles is such that, very small particles are introduced into a bed of powder containing large particles and allowed to fill up the voids, hence, reducing the porosity of the powder. Furnas (1931) gave the theoretical maximum packing density (PE_{max}) for binary mixture i.e. coarse and fine particles as:

$$PE_{max} = PE_c + (1 - PE_c)\, PE_f \qquad \text{.....Equation 1.9}$$

PE_c – packing density of the the coarse particles
PE_f - packing density of the fine particle fractions
$(1 - PE_c)$ - interstitial pore fraction of packed particles of a single size (fine or coarse)

The maximum packing density is the highest density attained by a powder bed after tapping or application of external vibration. Zheng et al, (1995) used the Furnas model to predict the maximum particle packing density in a binary powder system. They found that the packing density decreased when the ratio of coarse particles to fine particles decreased, which is governed by the volume fraction of coarse to fine particles. The Westman and

Hugill model (1930) has also been used to predict the ideal packing density of more than two particle component mixtures, but the application is limited to spherical shaped particles and powder mixures with uniform particle size and shape (Westman and Hugill, 1930). According to these authors, the prior introduction of fine fractions to large powder particles is crucial; so as to reduce the occurrence of powder segregation during powder packing i.e. the fine fractions will fill the voids as opposed to settling at the bottom. Newton and Bader (1981) utilized the Staple model to predict the composite packing density of binary mixtures consisting of different but narrow particle size fractions. Staple (1975) pointed out that the Westman and Hugill (1930) model loses power with each additional powder component. Podczeck and Sharma (1996) used the Kawakita model (this will be discussed later) to predict the maximum packing of binary powder mixtures. They stated that the particle shape of each single component of the binary powder mixtures influences the maximum volume reduction due to packing, represented by the Kawakita constant *a*.

1.5 DETERMINATION OF POWDER FLOW

Many widely accepted methods exist to measure flow properties of powders. The measurement of powder bulk flowability is not limited to traditional methods or ideas such as Carr's compressibility index (Carr, 1965), angle of repose (Train, 1958), Hausner's ratio (Hausner, 1967) and critical orifice diameter (Walker, 1966). Other technologies without claiming completeness include: shear cell measurements (Jenike, 1961 and 1964; Carr and Walker, 1967/1968; Peschl, 1984), studying avalanching behaviour (Kaye et al, 1992), electronic powder flow meters (Gold *et al.,* 1966a), powder rheometer (Podczeck, 1999a, 1999b) and torsional device (Orband and Geldart, 1997).

For the purpose of this research a few of the former and latter methods will be discussed with more emphasis on the shear cells.

1.5.1 STATIC AND DYNAMIC POWDER PACKING

According to Neumann (1967), the bulk density and bed porosity are common parameters used to describe the state of packing of a powder bed. The worker also stated that the most logical way of describing the state of packing of a powder is by its porosity which is

defined as the ratio of interparticulate void space to the total volume of packing. Conversely, the bulk density is less satisfactory for comparing different packings as it includes the particle density. The static powder behaviour relates to the property of the powder when at rest (as in maximum bulk density), while the dynamic powder packing reflects the property of the powder during volume reduction as in powder bed densification (Podczeck and Newton, 2000). The bulk density of a powder is the ratio of mass per unit volume and is dependent on the particle packing, and changes as the powder consolidates. The bulk density is not useful in measuring the flow of powders unless its effect on compressibility is considered (Carr, 1965). The consolidation of powder can be used as an indirect method of measuring powder flow. Generally in bulk density measurements, two types of bulk densities are considered i.e., *aerated and tapped bulk density.*

Aerated bulk density: This is also known as fluff, poured, loose, minimum or untapped bulk density and is denoted by D_0. The aerated bulk density can be obtained by pouring powder carefully into a calibrated or graduated container (e.g. a cylinder). The powder bed is leveled off and the net weight noted. The net weight is multiplied by the reciprocal of the powder volume to obtain the aerated bulk density. The values of the aerated bulk density are operator and procedure dependent.

Tapped bulk density: Also called the packed, equilibrium, consolidated, maximum or final bulk density and is denoted by D_f. The tapped bulk density can be determined by subjecting the powder in the aerated bulk density state described above to tapping using for example a mechanical tapping device or jolting volumeter. The volumeter follows the change in packing volume that occurs when void space diminishes and consolidation occurs. The volumeter taps the powder in the cylinder by means of a constant velocity cam. This activity leads to increase and ultimately final bulk density from an initial bulk density after attaining its most stable arrangement (Staniforth, 2002). Podczeck and Sharma (1996) found that the accuracy with which the tapped density can be obtained using modern tapped density volumeters is very limited. This finding was also supported by Abdullah and Geldart (1999). These authors reported that the modern tap density volumeter (Copley tap density volumeter) gave inaccurate measurements when compared with the Hosokawa

powder tester, which is similar in operation to the slow tap density volumeter used in the sixties and seventies. Hausner (1967) pointed out that in order to achieve conditions for the particles to become free from their adhesion and friction force interactions during tapping, the tap volumeter should not exceed a tapping velocity of 30/minute, and the free fall (i.e. cam) height should be at least 25mm. Hence, particle packing (decrease in volume) using modern BP/EP equipment remains incomplete, even at numbers of taps as high as 50,000 (Podczeck and Sharma, 1996). The European Pharmacopoeia (2002) stipulates that tapping experiments should be performed at a tapping speed of 250 ± 15 taps/minute from a height of 3 ± 0.2 mm. Incomplete particle packing is the result, as this procedure will lead to redispersion of the powder particles as opposed to close packing.

The process of volume reduction varies from powder to powder due to differences in particle properties (e.g., shape and size) and due to a different degree of interparticulate friction (Podczeck and Sharma, 1996). The larger the forces are, the less reliable become the tapping results under BP/EP conditions (Podczeck, 1998). The two methods will be used in this research and the results obtained will be compared to ascertain the differences between the two methods.

1.5.1.1 Static Packing

In the static powder packing, the behaviour of the powder bed packing at rest is considered and, hence, utilized to assess powder flow. The aerated (initial) and the tapped (final) density are considered and used in the calculations.

1.5.1.1.1 Carr's Compressibility Index

Carr (1965) developed this indirect method of measuring powder flow from bulk densities. He deduced that compressibility is a very important flow characteristic. The percentage compressibility (% compressibility) of a powder is a direct measure of the potential powder arch or bridge strength and is given by the following equation:

$$C\,[\%] = 100(D_f - D_o) / D_f \qquad \text{.....Equation 1.10}$$

where D_f and D_o are the maximum and minimum bulk density, respectively. The more compressible a powder is the less flowable it will be and vice versa. In addition, any increase in frictional forces and interparticulate adhesion leads to an increase in Carr's compressibility index. The transition between a free-flowing powder to a non-free flowing powder is about 20% to 21% for the value of C (Carr, 1965). Values below 15% are indicative of good flow characteristics whereas values above 25% correspond to poor powder flow. The use of Carr's index to characterize powder flow comes with some advantages. For instance, the method is simple; less powder is employed in the analysis compared with the angle of repose, and the method can be used to evaluate free-flowing or non-free flowing powders. The draw back of this method is that it does not represent the actual compaction behaviour a powder may undergo during bulk transfer operations (Prescott and Barnum, 2001b).

1.5.1.1.2 Hausner Ratio

Hausner (1967) observed that the density of an uncompacted mass of powder is a characteristic figure of the powder and that it reflects the friction conditions between the powder particles. The reason for this is that those particles, between which high frictional and adhesion forces exist while at rest, will have a low bulk density because gravity alone will not be able to overcome the forces. Conversely, during tapping powder particles are forced to jump thereby losing contact with each other and for a moment no friction exists between the particles. This process encourages powder particle rearrangement resulting in stable packing conditions and hence a reduction in volume due to strong adhesion and /or friction forces.

Grey and Beddow (1968/69) termed the ratio of the tapped bulk density to the aerated bulk density "Hausner ratio *HR*" following work by Hausner on metallurgical powders.

$$HR = D_f/D_o \qquad \text{.....Equation 1.11}$$

Hausner (1967) concluded that the ratio could be used to predict powder flow properties. Powders with low interparticulate friction such as spheres have Hausner ratios of approximately 1.2 and in contrast, less free-flowing or cohesive powders such as flakes have Hausner ratios above 1.6. Hamby et al (1987) also used the HR values obtained to detect critical relative humidity values for powders thereby indicating points at which an incremental change in the flow of the powder would occur. The threshold limit of HR equivalent to Carr's compressibility index is 1.25 (Podczeck, 1998).

1.5.1.2 Dynamic Packing

The dynamic packing of a powder bed relates to the rate of packing down from loose/aerated to tight packing under controlled experimental conditions. This involves observing the initial volume of powder that has been loosely filled into a graduated cylinder, followed by mechanical tapping with volume readings taken at intervals until a final volume is reached where no further change is observed. Powders having the most heterogeneous size and shape distribution take a longer time to reach their closest packing and show much greater total change of volume (Neumann, 1967). This is due to the fact that during tapping the particles not only have to find their optimum orientation to eliminate arching, but they also have to re-arrange until the small particles find their way into the voids between the larger particles. The smaller the difference between loose/aerated and tight packings (high rate of packing down), the better the powder flow.

1.5.1.2.1 Kinematic constants of packing

Hauer et al (1993) observed that the compression velocity (i.e., velocity with which a powder bed reduces its volume during tapping) was directly related to the flow properties of the powder. This observation was derived from their work on capsule filling.

This is expressed by the equation below:

$$f(x) = a + b * e^{-k_1 x} + c * e^{-k_2 x} \qquad \text{.....Equation 1.12}$$

where $f(x)$ = packing volume after x tappings

k_1 = compression velocity during initial tapping

k_2 = compression velocity during the final tapping

x = number of taps

The workers found a large difference between the kinetic constants (k_1, k_2) derived for the powders studied (anhydrous lactose, Avicel PH 101 and various size fractions of lactose). Podczeck and Newton (1999) found a very small difference between the powders they studied. The workers also stated that a complex relationship exists between the powder filling properties and the powder properties such as dynamic densification profile, Carr's compressibility index, angle of internal flow, particle size and shape. Podczeck and Newton (1999) presumed that direct comparisons between powders are only possible, if the powders are composed of for instance, identical particle shape but different particle size.

1.5.1.2.2 Angle of Internal Flow

Varthalis and Pilpel (1976) were able to establish that a relationship exists between the porosity e and number of taps n from data obtained from tapping experiments that will be described later. By plotting K (K= n/(1-e)) against the number of taps n, a linear relationship was found. Plotting K-Ko (Ko is the intercept on the ordinate of the series of straight lines obtained from the above) against n, the slopes of the lines defined as $\tan \theta$ was obtained.

According to Kočova and Pilpel (1973), since cohesiveness of a powder is a measure of the difficulty with which the particles can flow past each other when tapped, θ appears to be related to the powder bulk angle of internal friction and can be termed the angle of internal flow.

1.5.1.2.3 Mohammadi and Harnby Model

Mohammadi and Harnby (1997) used bulk density modelling as a predictive tool to characterize cohesive powders. The approach used was to place more emphasis on the tapped bulk density D_f and to add an extra descriptor- the constant of compaction, T. The constant of compaction characterizes the ease of compaction. The workers paid less

emphasis on the value of aerated bulk density D_o which is subject to significant experimental error. A modification of the model of Cooper and Eaton (1962) was used, where the density (d_n) reached after a certain number of taps *(n)* is given by:

$$d_n = d_f - (d_f - d_o) \exp^{-n/T} \qquad \text{.....Equation 1.13}$$

where d_f and d_o are the fitted final values of the theoretical tapped and bulk density of the powder, and T is the compaction constant. Densification of powder is fast if the values of T exceeds 35 and conversely slow if the value of T is below 35 for pharmaceutical processes such as capsule filling. Podczeck and Newton (1999) deduced that for pharmaceutical processes such as capsule filling, the optimum value of the compaction constant T appears to lie between 20 and 25. Values below the optimum led to variability in capsule fill weight presumably caused by powder flooding. The workers encountered major filling problems for values above 30. Caligaris et al (1985), derived the above equation from first principles (thermodynamics principle), assuming that the densification of a powder sample after the application of a load is either an adiabatic or an isothermal process.

1.5.1.2.4 Kawakita Model

Kawakita and Lüdde (1970/71) have reviewed the Kawakita model otherwise called the Kawakita's compression equation extensively. The use of this model makes it possible to predict a maximum in volume reduction of powder achieved by application of vibration, small pressure or tapping.

The equation with regards to volume reduction of a powder due to tapping is as follows:

$$N/C = 1/(a\,b) + N/a \qquad \text{.....Equation 1.14}$$

where

$a = (V_o - V\infty)/V_o$ and $C_T = (V_o - V_N)/V_o$

a = maximum possible volume reduction that can be achieved by tapping

b = constant related to the tensile strength of the powder bed

N = tapping number

C = degree of volume reduction after N taps

V_o = initial apparent volume

V_N = bulk volume of the powder after N taps

$V\infty$ = minimum bulk volume

Based on single powder observations, the value of *a,* was found to be smallest for spherical and largest for irregular particles (Lüdde and Kawakita, 1966). The workers also concluded that *a,* which quantifies the maximum volume reduction, is theoretically equal to Carr's compressibility index for tapping experiments. The above conclusion was confirmed experimentally by Podczeck and Lee-Amies (1996). The authors pointed out that the Kawakita equation has no advantage over the use of Carr's compressibility index as an indicator of possible volume reduction. They indicated that an estimate of the volume reduction due to low-force compression as applied in capsule filling machines can be found by adding 5% to Carr's compressibility index. Lüdde and Kawakita (1966) and Tan and Newton (1990a) found no correlation between Kawakita constant *a,* and the angle of internal friction. They concluded that hence no correlation exists between the friction properties of the powders and Carr's compressibility index or even Hausner's ratio. Podczeck (1998) stated that it remains unknown whether this is due to the shear cell not reflecting the friction forces between individual particles adequately, or the measurements being flawed.

1.5.1.3 Relationship between Powder Packing and Flow

Packing characteristics of powder beds when tapped are often used to evaluate the powder flow properties and are even used to group or rank powders with regards to powder flowability. Podczeck (1998) reprocessed some data on the relationship between powder bulk properties and capsule filling performance of microcrystalline cellulose powders using bulk density modelling as described by Mohammadi and Harnby (1997) and obtained

values for T (compaction constant) leading to a different ranking of the microcrystalline cellulose powders compared to the ranking reported by Patel and Podczeck (1996). The T values strongly correlated with the capsule filling performance, hence helping to understand the influence of powder flow on the filling process.

The structural strength and packing characteristics of an aerated powder play a major role during powder consolidation. The reason for this is that on application of an external force such as tapping or vibration on a powder bed in a container, the powder bed undergoes structural (strength) collapse and hence, there is an increase in bulk density (mass per unit volume). The bulk density and bed porosity are the common parameters used to describe the state of powder bed packing. According to Mohammadi and Harnby (1997), the amount of consolidation or densification depends on the structural strength and packing characteristics of the aerated sample. In addition, the values of the bulk density are of little absolute value but are used as a sensitive secondary measure to identify any slight changes in the morphology of the primary particles and their flow characteristics within the process. Powder packing depends on the density, shape, rugosity, size and size distribution of the particles and on the amplitude and frequency of the vibration that may have been applied to them (Varthalis and Pilpel, 1976).

1.5.2 OTHER METHODS

Other methods such as the angular methods are applicable to relatively free-flowing/mildly cohesive powders containing particles larger than about 100 μ m (Pilpel, 1971). In addition, the angular properties of powders depend to a marked extent on the details of the experimental techniques employed in measuring them and hence, it is inadvisable to assess the cohesiveness of powders on the basis of such measurements except in a qualitative manner (Pilpel, 1971). The reason being that such powders cannot be investigated satisfactorily in shear cells and tensile test apparatus as the particles become crushed during consolidation. In addition, such powders do have low tensile strength and cohesiveness (Pilpel, 1971). Harwood and Pilpel (1968) assessed the flow properties of glass beads, silica sand, magnesia and two batches of griseofulvin with wide range of particle sizes,

using three different methods. The investigators concluded that the discharge hopper method is ideal for the study of large, free-flowing granular mass, the shear cell for cohesive powders, and the rotational viscometer for materials with a particle size that falls in-between the particle size range not considered by the two other methods. Though the results obatined using angular tests are still debatable, they are still being used along with other methods for quality control purposes (Pilpel, 1971). Examples of angular methods are given below.

1.5.2.1 Angle of repose (α)

This is the maximum angle that can be obtained between the freestanding surface of a powder heap and the horizontal (Carr, 1965; Pilpel, 1965).

The angle α is defined by the equation:

$$\tan \alpha = 2H/D \qquad \text{.....Equation 1.15}$$

where H is the height of the heap and D is the diameter of the cone.
In addition, if the diameter of the orifice is considered, a correction factor is introduced to account for this. That is:

$$\tan \alpha = 2H/(D - d/2) \qquad \text{.....Equation 1.16}$$

where d is the diameter of the orifice.

A particle begins to slide when the angle of inclination is large enough to overcome frictional forces and conversely, will stop sliding if frictional forces cannot be overcome. The behaviour of a powder heap is based on this principle. The angle of repose is a characteristic of the internal friction/cohesiveness of the powder (Marshall, 1986). Cohesive powders will have a high value of angle of repose whilst the non-cohesive will have a lower value. In addition, the powder heap of a very cohesive powder may be characterized by more than one angle of repose (Staniforth, 2002). Values of α are rarely

less than 20°, and values of up to 40° indicate reasonable flow potential. On the other hand, powders with values above 45° flow with great difficulty (Carr, 1970). The angle of repose may be determined by dynamic or static methods. Methods to determine the dynamic angle of repose are preferably used, because these methods closely mimic the manufacturing situation in which the powder is in motion.

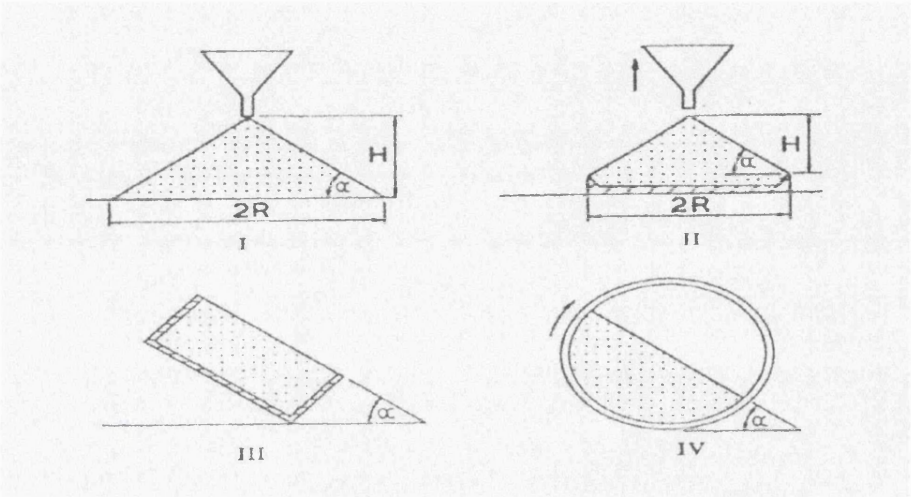

Figure 1.4 *Four main methods of measuring the angle of repose. (I) Fixed funnel and freestanding cone. (II) Fixed base cone. (III) Tilting box. (IV) Rotating cylinder;* Diameter of cone, *D = 2R (see equation 1.15 and 1.16). (Taken from Train, 1958)*

A typical dynamic test involves the use of a hollow cylinder half-filled with the test powder, which is carefully tilted until the powder begins to slide. The powder surface is made to cascade by rotating the cylinder about its horizontal axis (see Fig. 1.4). Static measuring methods, which include the fixed funnel-free standing cone and the fixed base cone technique (Train, 1958) tend to give lower values than the dynamic methods (Cole, 1987). Train (1958) and many workers assessed the various methods of measuring the angle of repose critically. Some of the advantages cited include simplicity in measurement, sensitivity to changes in particle size and moisture (Pilpel, 1965), rapid measurement and an indirect measure of properties affecting flow. The limitations include poor reproducibility and variability in results of the same powder when different methods are

used. Neumann (1967) reported that the angle of repose is not srongly dependent on average particle size, but on specific surface area of a powder, which is also one of the factors affecting powder flow. Craik and Miller (1958) determined the angle of repose of some powders at various moisture contents and after the addition of different amounts of light magnesium oxide. However, Ridgway and Rupp (1969) found that the angle of repose of sand of different size ranges increased with increasing departure of the particle shape from being spherical.

Gold et al. (1966b) used the powder flow meter to evaluate various glidants and compared the results obtained with those determined based on angle of repose. The workers concluded that the flow meter is a valuable instrument for selecting the best glidant and to determine the optimum concentration of a particular glidant, and that the angle of repose is not a reliable method for evaluating the flow of the powders. Powder flow meters are often equipped with vibrators in order to study poorly flowing powders (Gold et al., 1966a; Podczeck, 1998).

1.5.2.2 Angle of Spatula (Φ_S)

This gives the relative angle of internal friction or rupture for each dry powder. A spatula blade is taken, stuck into the bottom of a mass of dry bulk material to obtain enough mass that will give a true picture of the angle. This is then lifted straight up and out of the powder. One angle of rupture or internal friction will be obtained for a free-flowing powder whereas a number of irregular angles of rupture will be obtained on the blade for non-free flowing powder (Carr, 1965). In the latter case, the angle of spatula is obtained by averaging the average angles to the horizontal and the average of the lower angle/angles of the spatula obtained (Carr, 1965).

The angle of spatula indirectly measures powder properties such as surface area, particle size, particle shape and porosity. Carr (1965) also stated that the angle of spatula evaluates the relative flow of particles en mass and gives more indication of the action of a powder in a hopper. The higher the angle of spatula of a powder the poorer the powder flow. Generally, powders with angle of spatula lower than 40° are considered free flowing. Some

of the limitations of using this method include poor reproducibility, and powders with non-uniform particle size distribution and shape require a different spatula blade width (Carr, 1965).

1.5.2.3 Flow Through Orifices

Measuring the rate at which powder discharges through an orifice of a container or hopper under the influence of gravity is one of the most direct methods of assessing powder flow. The effects of powder properties such as particle size and shape, density, diameter and size of the container hole/outlet are well documented (Neumann, 1967; Harwood and Pilpel, 1969; Flemming and Mielck, 1995; Lavoie *et al.,* 2002). Several methods exist to measure flow rates. These include: measuring the mass of powder which flows through the outlet or hopper at a given time or even using discs with a central hole of varying diameter/sizes. In the latter, the flow category to which a powder belongs is identified by establishing the exact diameter of a hole the powder could flow through without any hindrance. The diameter of the hole is termed the *critical orifice diameter.* Critical orifice diameter is a direct measure of powder cohesiveness and arch strength and is proportional to the attractive forces between particles in the powder bulk (Podczeck, 1998; Staniforth, 2002).

The flow of powder through an orifice plays an important role whenever powder has to be fed into a system through a hopper as in capsule, tablet or sachet filling machines. Richards (1966) described a hopper to be a tall cylinder with an orifice at the base.

When the orifice at the base of a hopper full of free-flowing powder is opened, a flow pattern emerges as the powder is discharged. The pattern is such that particles just above the orifice fall freely through first due to the influence of the gravitational force. This leads to the formation of a depression at the upper surface, which spreads outwards to the sides of the hopper. This activity leads to the formation of a trumpet-shaped flow region once the particle movement has reached the top free surface of the powder bulk (Neumann, 1967). Finally, the flowing region now spreads outwards to the sides of the hopper. In Figure 1.5, particles move quickly from zone A to feeding zone C, leading to downward and inwards flows.

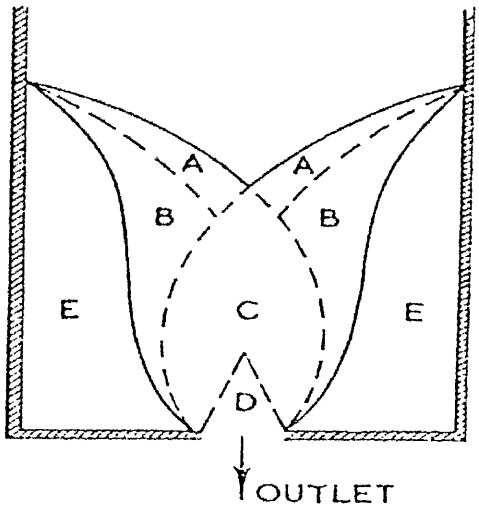

Figure 1.5 *A developed flow pattern of a free-flowing powder (Taken from Pilpel, 1965)*

Particles slide slowly along each other in zone B, consequently, particles in zones B and C converge to a 'tongue' D just above the orifice. At this point the particle movement is most intense and the packing density of the particles decreases and is loosest just before falling through the orifice (Podczeck, 1998). Outside the tongue shaped region above the orifice, denoted E, the powder is at rest.

The effect of the flow pattern could be consequential in practice if the particles in the zone towards the base and sides of the container are not discharged. This may lead to degradation or the static zone may enhance the segregation of previously homogenous powders (Staniforth, 2002).

A proportionality of the flow rate to the (approximately) third power of the orifice diameter has been reported and can be derived by dimensional analysis (Neumann, 1967). It confirms that the orifice diameter is the most important single factor controlling the flow of powders through the openings. To avoid the formation of arches i.e. a stable obstruction at

or near, for example, a bin outlet, mass flow could be encouraged by designing hoppers that will ensure continuous and uniform powder flow (Pilpel, 1965). Mass flow hoppers are particularly tall, and the conical outlet has steep sides. The determination of the critical orifice is, however, not only important for hopper design, but equally applies to dosage form manufacture, for example, using dosator nozzles in capsule filling (Tan and Newton, 1990b).

1.5.2.4 Avalanching

Held et al. (1990) studied the behaviour of a sand heap and described the catastrophic failure of the stability of the sand heap (termed avalanche) after progressively adding a grain of sand to a sand heap. They described the gently and slowly generated heap as *pseudo-static.* They also found that the size distribution of sand avalanches created in pseudo-static heaps could be described by a *hyperbolic function.* The study of the flow of powders in such heap is described as *holistic rheology* (Kaye, 1997), while the phenomenon whereby a powder avalanches on arriving at the top of a powder heap is termed *critically self-organised system* (Bak et al, 1988).

Kaye et al., (1995) used an advanced system that utilizes a rotating disc in which a fixed amount of powder is kept in motion to study the avalanching behaviour of powders with respect to their flow properties. The principle of operation is based on fractal dimensions (in data space), in which the fractal data are treated as a pattern of events that can be used to describe a chaotic system (Kaye et al. 1993; Howard, 2002), and deterministic chaos theory. In the deterministic chaos theory, the interaction of events is considered and described by deterministic physics (Howard, 2002). In the previous design, powders were fed continuously onto a ramp with a defined tilting angle. By doing so the powder gains weight until the accumulated powder bulk suddenly collapses.

In the current design, the rotating disc is placed into a light box, fitted with electronic light sensors. The position of the powder bulk can continuously be monitored, and avalanching can be measured as a real time process, depending on the speed of rotation, time and height of the powder bed at the moment of avalanching. A *Chaotic fingerprint* is left, which is

indicative of the flow property of each individual powder. Powders with considerable adhesion characteristics appear to climb upwards the disk wall in direction of the rotation until it suddenly drops down avalanche-like. Podczeck (1998) indicated that avalanching behaviour could be observed in tamp filling capsule machines and, hence, could be used to predict problems during capsule filling on tamp filling capsule machines. During the capsule filling operation, the powder has to flow round the transfer station. Powders with poor flow tend to form a growing heap in front of the transfer station. At certain intervals, the heap collapses avalanche-like, and a larger amount of powder passes the transfer station. According to Lee et al., (2000), a dual approach in which visual observation of the type of motion of the powder bed in the rotating drum and the numerical descriptors such as mean time to avalanche (MTA) and scatter are considered, is more accurate in assessing powder flow. These workers pointed out that without visual observation, powders with low MTA but with a different powder movement in a rotating drum, slippage in this case, could be mistaken to have good powder flow properties.

The advantage of using this device cited by Podczeck (1998) includes the unlimited time span, over which a powder could be tested. The limitation cited by the same author includes tribo-electric charging, which could cause increased adhesion between powder particles, and hence, change in powder flow properties during motion.

1.5.3 SHEAR AND FAILURE PROPERTIES OF POWDERS

Podczeck (1998) stated that shear cell measurements directly reflect the level of attractive forces between particles in a powder bulk, although the assessment of the powder properties is here based on the continuum approach. They involve measuring the strength of powder beds when subjected to a shearing force as opposed to a tensile force.

Jenike (1961) pioneered the idea of using shear cells to investigate the cohesiveness of dry powders by subjecting them to shear and measuring the relationship between stress and strain under a series of different normal loads. The idea originated from measurement of failure of remolded cohesive soils saturated with water and subjected to strain under a given

normal load (Pilpel, 1971). Further strain on the sample after reaching the end point produced no further change in shear force or voidage.

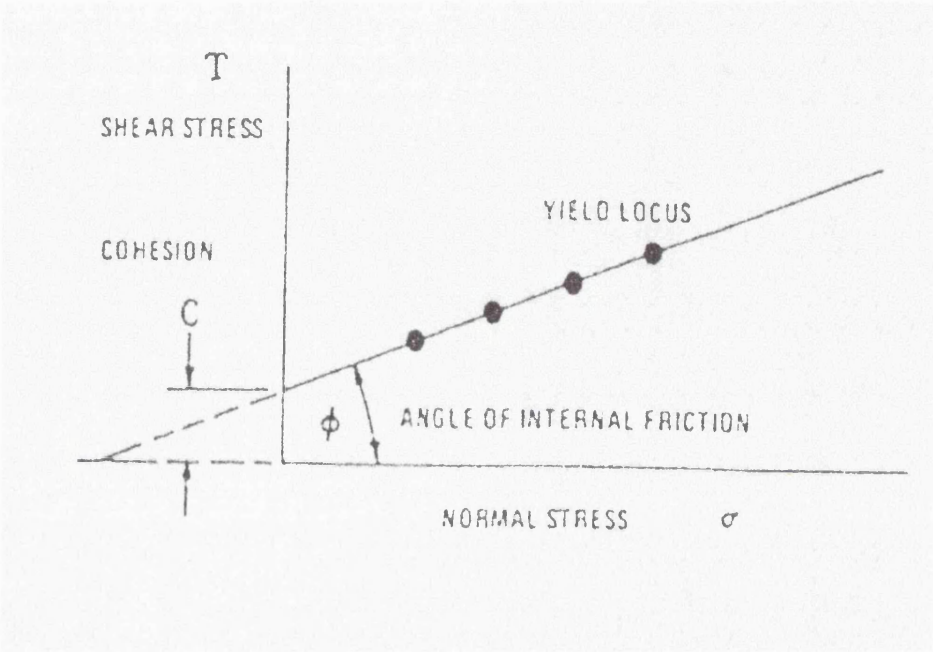

Figure 1.6 *Yield locus of a Coulomb solid (Taken from Thomson, 1997).*

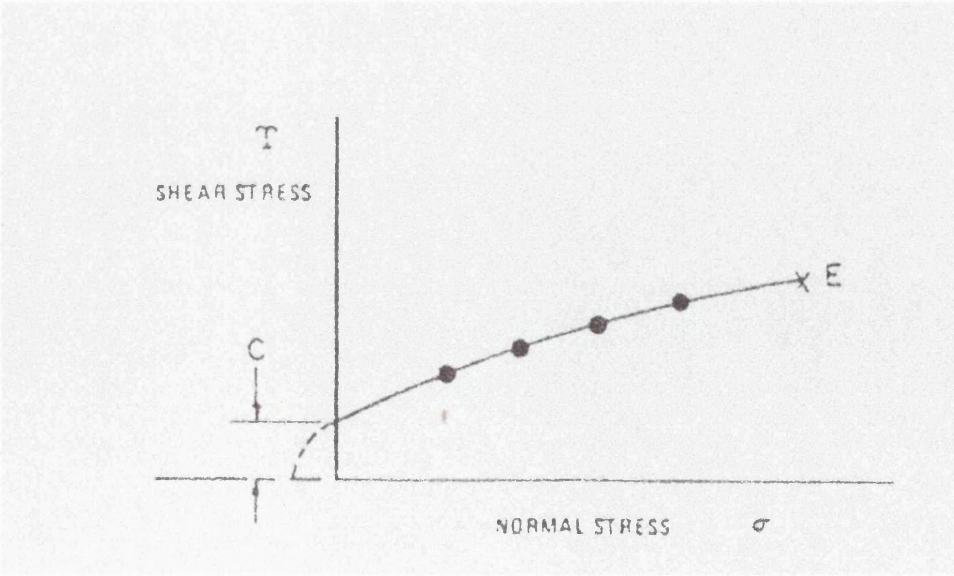

Figure 1.7 *Yield locus of a cohesive solid (Taken from Thomson, 1997).*

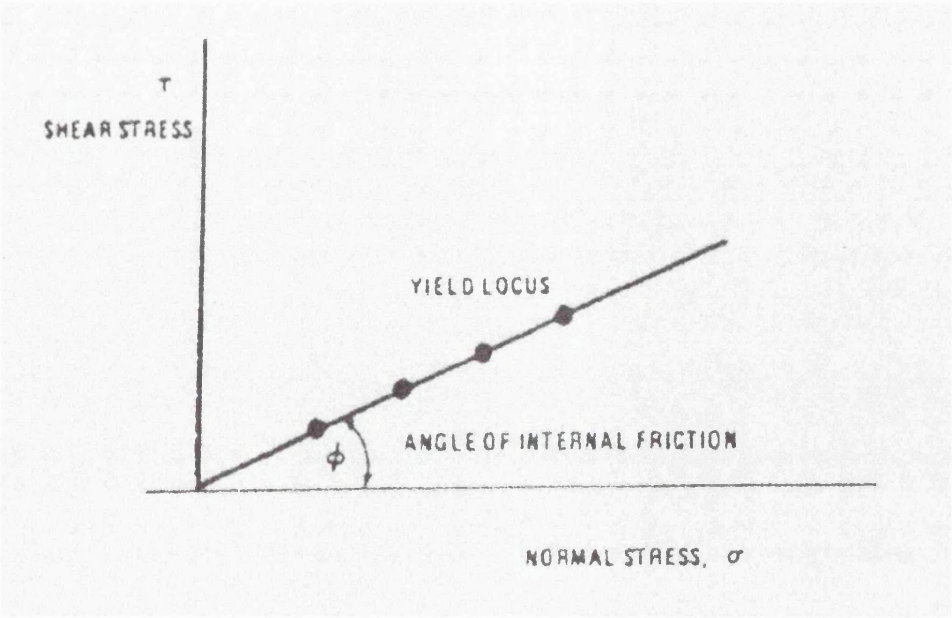

Figure 1.8 *Yield locus of free-flowing sand (Taken from Thomson, 1997).*

According to Thomson (1997), Jenike assumed that a bulk solid could be closely approximated by a rigid-plastic Coulomb solid. From soil mechanics, such a solid is characterized by a *yield locus* that defines the limiting shear strength under any normal stress (Fig. 1.6). A Coulomb solid has a linear yield locus. Plotting shear stress τ against normal stress σ, the yield locus for a Coulomb powder intersects the τ axis at a value of τ defined as "*cohesion coefficient*" *C* at an angle ϕ, defined as the *angle of internal friction.*

Jenike deduced after many experimental measurements that with real bulk solids, at low pressures, the locus deviates from a straight line (Fig. 1.7). The yield locus does not increase indefinitely with increasing values of σ but terminated at some point *E*: and the position of the locus is a function of the degree of consolidation of the material. During flow the stresses in the plastic regions of the solid are continuously defined by point *E*. The yield locus for a cohesive solid is shown in Fig. 1.7 and a free flowing powder material has a locus as shown in Figure 1.8.

Furthermore, Jenike assumed that in the plastic region, the solid properties at any point are the same in all directions (isotropic), and that they are frictional, cohesive, and

compressible. During incipient failure, the bulk solid expands and during steady flow it can either expand or contract. Stress at any point does not change with time, and stresses are not significantly affected by velocity changes.

1.5.3.1 Stress - Strength Relationships

During powder flow through a bin outlet, the major consolidating stress σ on the powder changes and continuous shear deformation occurs, causing slip planes as the powder particles slide on one another. In addition, the strength (resistance to shear failure) and density are a function of the last set of stresses, and when flow stops it is assumed that these stresses remain. As the powder remains stationary under these stresses, it may gain strength and resist flow for instance when the bin outlet is opened.

1.5.3.2 Classification of shear cells

Many shear testers exist to measure flow properties of powders, however no single universal tester or standard exists to measure the required properties accurately (Kamath et al 1993).

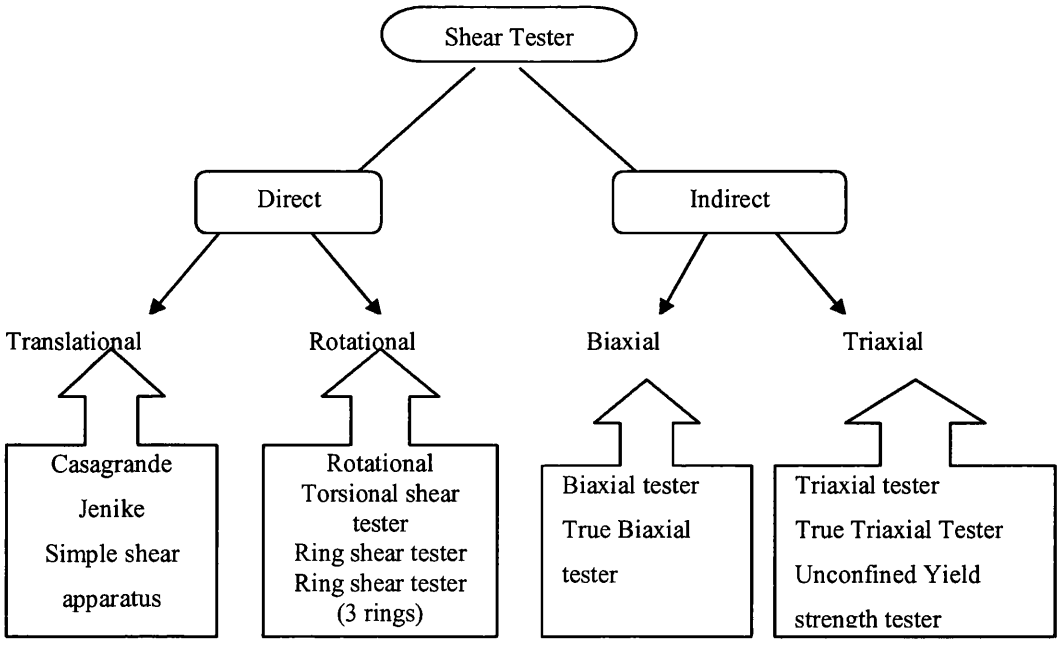

Figure 1.9 *Shear testers (Adapted from Schwedes and Schulze, 1990).*

Schwedes (1984), Schwedes and Schulze (1990), reviewed the classification of shear testers used in powder technology. A possible shear principle survey and names of shear testers is shown in Figure 1.9.

1.5.3.2.1 Direct Shear Testers

In the direct shear testers, the shear zone is defined by the design of the apparatus. The directions of the principal stresses are fixed and remain constant during the test. They are distinguished by either rotational or translational displacement.

(A) *Direct Shear Testers with Translational Displacement*

The direct shear testers with translational displacement have only limited shear displacement e.g., the Jenike tester with a maximum of 4 to 5 mm (this will be described shortly). For direct shear of a sample two ideal cases can be distinguished (Fig. 1.10). (a) is the case of pure Coulomb-friction without volume change. (b) is a shear process, where the shearing takes place homogeneously throughout the sample with possible volume changes. The available shear testers behave neither as in case (a) nor as in case (b). The shear process in the tester of Jenike is shown for comparison in Figure 1.10 (c). Inside the lens-shaped shearing zone case (b) is nearly realised; outside this zone the powder is moving as in case (a) (Schwedes, 1984).

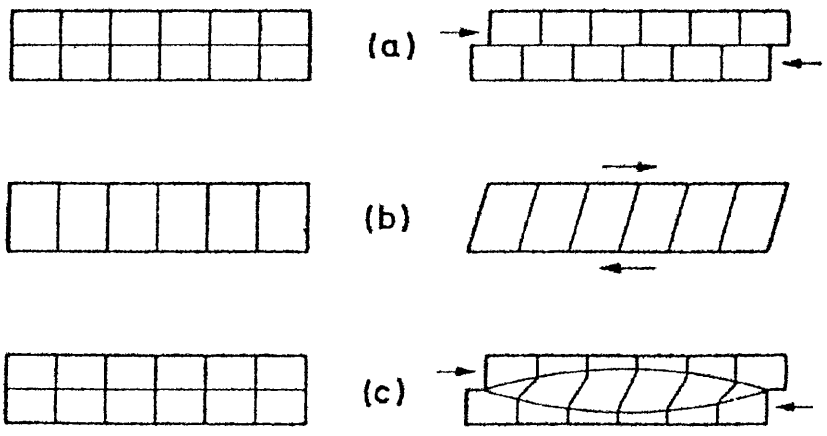

Figure 1.10 *Shearing of a bulk solid sample during translational displacement (Taken from Schwedes, 1984).*

(i) *Jenike shear cell*

The Jenike shear cell consists of a base located on the frame of the machine, a ring resting on top of the base, and a lid (Figure 1.11). The ring mostly used has an inside diameter of 95mm (3.75 in.). A 65mm (2.5 in.) ring is sometimes used when high consolidating forces are required.

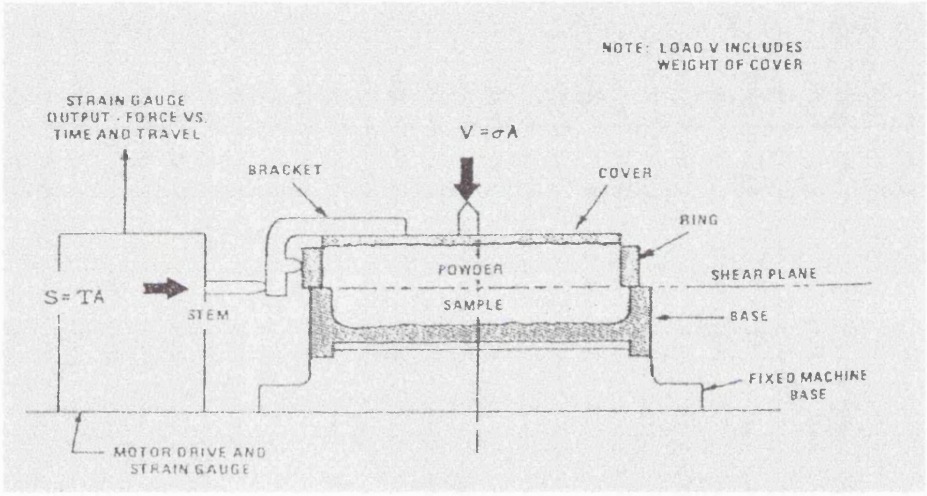

Figure 1.11 *Jenike shear cell (V = normal force, σ = normal stress, T = shear stress, A = cross sectional area* and S = shearing force). *(Taken from Thomson, 1997).*

The base and ring are filled with the powder bulk and a vertical force is applied to the lid. On a bracket attached to the lid a motor-driven stem applies a horizontal shearing force. Some of the shearing force is transferred to the ring by a loading pin attached to the cover bracket. This helps to ensure more uniform distribution of the shearing force across the cell during shear. With 60 Hz electrical supply, shearing is applied at a constant rate of 0.91 mm/min (0.036 in./min) in older machines, and 2.7 mm/min (0.108 in./min) in newer machines. With 50 Hz electrical supply, the rates are 0.76 mm/min (0.03 in./min) and 2.3 mm/min (0.09 in./min). The shearing force is transmitted through the pin to a load cell and displayed as shear force versus time and displacement (Thomson, 1997). Using identically preconsolidated samples under different normal loads the maximum shearing force S for every normal force V can be obtained (Schwedes and Schulze, 1990).

Each normal force and the corresponding shearing force represents a point on the line of yield of the powder bulk i.e. yield locus. Dividing V and S by the cross-sectional area of the shear cell gives the normal stress σ and the shear stress τ. Figure 1.12 shows the Jenike shear cell sequence.

Many workers including Kamath et al, (1993), Carr and Walker (1967/68) and Johnson (1992) have used this tester to measure, compare and assess the flow properties of powders. Among the advantages cited are:

(1) The Jenike shear cell is widely used in the technical industry
(2) The flow function (see below), which is valuable in predicting the flowability of powder, can be obtained from the test result.

The limitations include:
(1) The test results vary significantly from one technician to the other. Significant time investment is needed to attain a sufficient level of expertise.
(2) The non-uniform stresses in the shear cell cause the major principal stress to be undefined.
(3) Requires a sample volume about 450 times the particle size cubed.
(4) The cell can only handle samples with particle size of up to 2000 μm (Bagster, 1984).
(5) The limited shear displacement available results in a rather arbitrary and laborious sample preparation prior to the shear consolidation.
(6) Sample consolidation pressure is applied non-uniformly, hence, sample consolidation pressure is not known until three or more tests (hopefully at the same pressure) are complete (Johanson, 1992).

The Jenike shear cell can be used when time is not a critical factor, when the flow function is required and to measure flowability of powder with particle size less than 2 mm. Larger diameter Jenike-type cells offer somewhat longer stroke lengths and are better able to tolerate larger or high-aspect ratio particles (The et al, 1995). In addition, the Jenike shear cell can be used to measure flow properties of powders with similar characteristics i.e.,

medium bulk density, coarse particles (less cohesive), texture, etc (Kamath et al, 1993). At this stage before discussing the other types of shear cells, it is necessary to give an overview of the properties measured that are used to analyse flowability in shear testers. The Jenike shear tester as discussed by Thomson (1997) and other workers will be used in this respect.

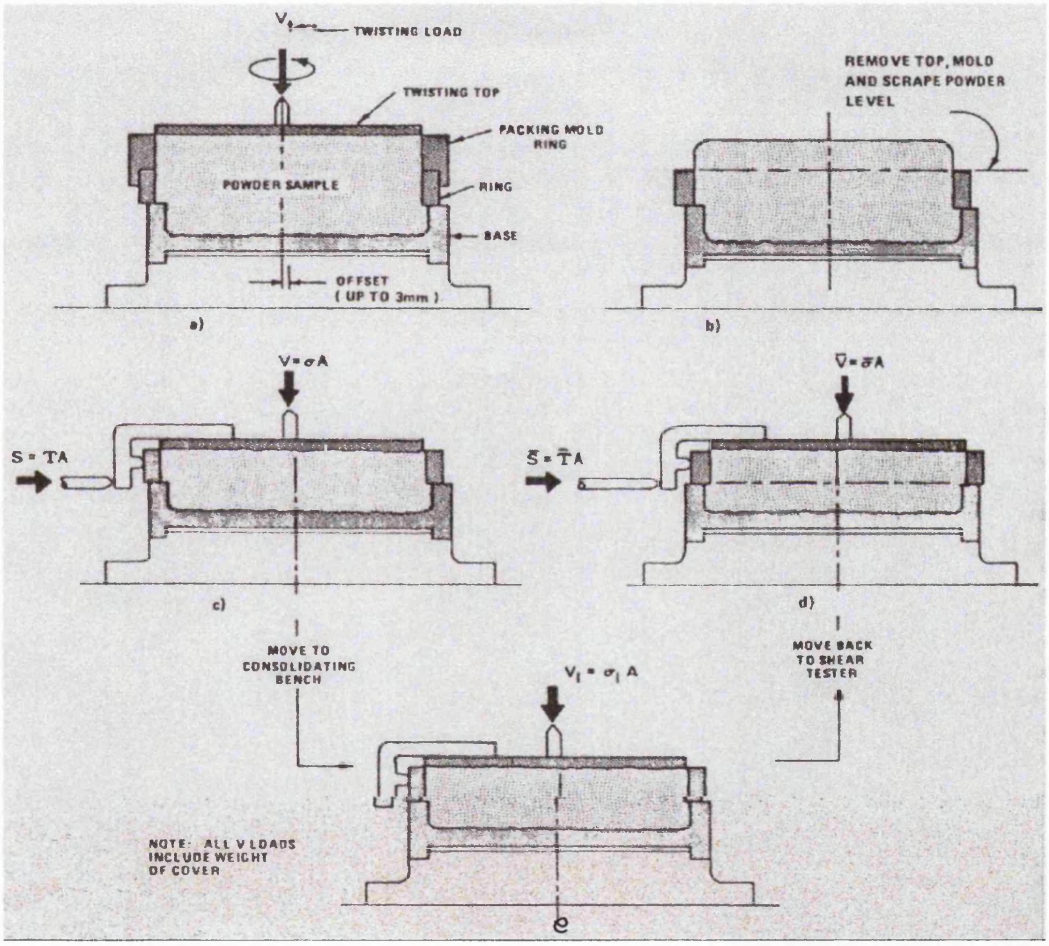

Figure 1.12 *Jenike shear test sequence: (a) preconsolidation, (b) Removal of twisting top and packing mold ring, (c) consolidation, (d) shear, (e) time consolidation,* V_t *= force applied for preconsolidation;* S *= shearing force;* V *= normal force;* $\overline{V}$ *= normal force for shearing;* A *= cross-sectional area;* T *= shear stress;* σ *= normal stress;* $\overline{\sigma}$ *= normal stress for shear;* σ_1 *= normal stress for consolidation;* V_1 *= consolidation stress;* $\overline{T}$ *= shear stress during shear . (Taken from Thomson, 1997).*

1.5.3.2.1.1. Properties measured in shear cells

(a) *Yield locus*

This is a curve joining several points on a shear stress versus normal stress graph, which represents stress states that lead to flow in powder samples of the same initial bulk density (Ladipo and Puri, 1997).

(a)Mohr Stress Semicircle.

Mohr stress semicircles are used to identify the frictional and strength properties of the sample from the yield as shown in Figure 1.13. The state of stress on any plane within the bulk solid can be represented by a Mohr circle. For any stress condition represented by a Mohr semicircle tangent to the yield locus, the bulk solids will be at yield, and the major principal stress σ_1 and minor principal stress σ_2 at this condition will be defined by the intersection of the semicircle with the σ axis. The yield locus terminates at the point of tangency of the Mohr semicircle through Point *E*. This circle intersects the σ axis at the principal stresses σ_1 and σ_2.

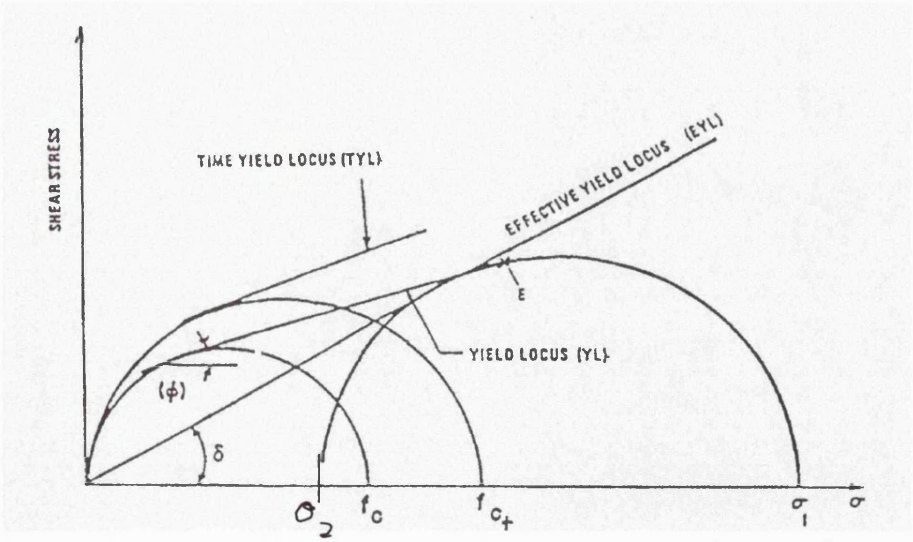

Figure 1.13 *Graph of shear stress (τ) as a function of normal stress (σ) showing the Yield locus, Mohr Stress semicircle, Effective angle of friction (δ), Angle of internal friction (ϕ), Unconfined yield stress (f_c), major and minor principal stress respectively (σ_1 and σ_2), Unconfined yield stress after an interval of time (f_{c1}), Time yield locus (Taken from Thomson, 1997).*

(b) Effective Angle of Friction (δ)

The effective angle of friction, angle δ (Figure 1.13) is a measure of resistance of the solids to flow while they are in a steady-flow condition. The higher the value of δ, the lower is the flowability of a bulk solid. The value usually increases slightly with decreasing stress for a given solid. The values for δ range from 15 to 70° for most materials that have been tested. The ratio of major principal consolidation stress σ_1 and minor principal consolidation stress σ_2 during steady flow can be expressed by the effective yield function:

$$\sigma_1 / \sigma_2 = (1 + \sin \delta) / (1 - \sin \delta) \qquad \text{.....Equation 1.17}$$

Mobility (m) may be defined as:

$$m = \frac{(1 - \sin \delta)}{(1 + \sin \delta)} \qquad \text{.....Equation 1.18}$$

Mobility is an intrinsic property of particles, since shear stress is independent of shear strain and consequently of the specific volume. The values for m range from 0.03 – 0.6 and for powders with interlocking particles or with rough surfaces, m may be four times greater than for powders, which flow easily. Mobility (m) may be small, but never reaches zero (Deleuil et al., 1994).

(c) Effective Yield Locus (EYL)

It has been found that the Mohr circles representing steady-flow stress are approximately tangential to a straight line through the point of zero stress. The envelope is tangent to the Mohr semicircle that defines the major and minor principal stresses σ_1 and σ_2. The effective yield locus (EYL) can be defined by:

$$\sin \delta = (\sigma_1 - \sigma_2)/(\sigma_1 + \sigma_2) \qquad \text{.....Equation 1.19}$$

(d) Angle of Internal Friction (ϕ)

The slope of the yield locus at the point tangential to the Mohr circle, which passes through the origin, and the Mohr circle, which defines the end of the yield locus, defines ϕ i.e. the angle of internal friction of the solid. This is also called the *kinematic angle of internal friction* since it is determined by the instantaneous yield locus. Fine and dry solids have lower values of ϕ and δ. Coarse, wet solids and cohesive solids have higher values. Another angle of internal friction that can be considered is the *static angle of internal friction (ϕ_t)*. Here, the slope of the time yield locus at the point tangential to the Mohr circle, which passes through the origin, defines ϕ_t, the static angle of internal friction of solids.

(e) Unconfined Yield Strength (f_c)

The minor consolidating stress σ_2 acting normal to the surface formed on the bottom surface of an arch is equal to zero, and the major stress σ_1 is tangential to the surface. Therefore a Mohr circle through the origin, tangential to the yield locus, defines the largest stress σ_c that the solid can withstand at a free, unsupported surface. The value of σ_c defines the unconfined yield strength f_c. For each value of consolidating stress, there is a corresponding value of f_c and as the consolidating stress increases, f_c increases.

(f) Flow Function (FF)

The flow function also called the failure function, characterizes the "flowability" of a bulk solid. The unconfined yield strength, defined by the yield locus, is a function of the major consolidation stress σ_1 and for a value of σ_1 the corresponding value of f_c can be found from the yield locus. Therefore if a family of yield loci is constructed as shown in Figure 1.14 (i), the corresponding values for f_c for each family member can be plotted against σ_1 to produce

a flow function as depicted in Fig. 1.14 (ii). In addition, the upper curve in Figure 1.14(ii) depicts the greater ability to support an arch or the strength of the powder.
The flow function for a bulk solid can be defined as the relationship:

$$f_c = f(\sigma_1) \qquad \text{.....Equation1.20}$$

where f_c is a function of the moisture content of the powder, temperature, and the major consolidation pressure (Jenike, 1961).

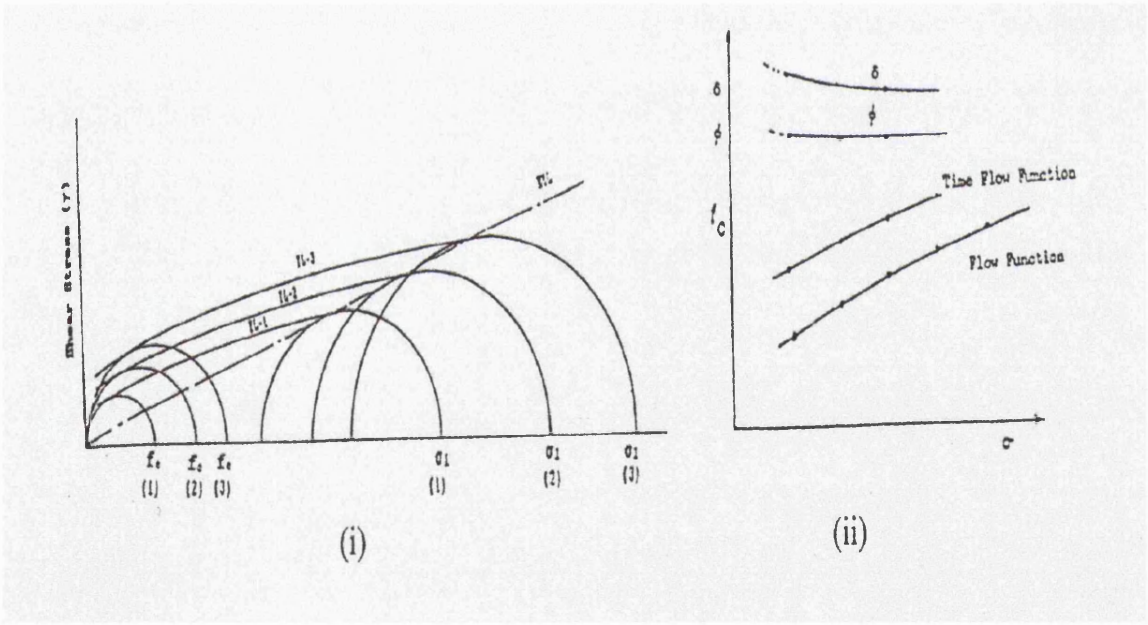

Figure 1.14 *Flow Function (Taken from Thomson, 1997).*
(i) - Graph of shear stress (τ) as a function of normal stress (σ) showing theYield locus, Mohr Stress semicircle, Effective yield locus – EYL; (ii)- Effective angle of friction (δ), Angle of internal friction (ϕ), Unconfined yield stress (f_c), major principal consolidating stress (σ_1); (Taken from Thomson, 1997).

Instantaneous flow functions are determined under conditions of zero consolidation time. Time flow functions are determined under conditions occurring during time consolidation. Many materials gain strength with time consolidation. However, the flow function of a powder (*FF*), which is a function of only the powder properties (Rhodes, 1998), should not be confused with the hopper flow factor (*ff*). According to Rhodes (1998), the hopper flow factor, relates the stress developed in a powder bulk with the compacting stress acting in a particular hopper.

(ii) *The simple shear apparatus*

The simple shear cell apparatus can be used to determine completely the state of stress of powders. The sample is stressed with a normal force V, whereas a shearing force S is acting on the bottom of the apparatus. With this apparatus complete Mohr stress circles can be determined. A yield locus in a σ, τ- graph is obtained as the envelope to the greatest Mohr stress circle. Comparative tests carried out using this shear cell and Jenike's shear cell showed that the assumption of coincidence of the horizontal plane with a slip plane is not correct but of little influence, when, for example, a hopper has to be designed for storing bulk solids (Schwedes, 1984). The disadvantage of the simple shear tester is the high amount of time, electronic and mechanical equipment that is needed for running shear tests (Schwedes, 1984).

(B) *Direct Shear Testers with Rotational Displacement*

In the direct shear cells with translational displacement, powder samples have to be preconsolidated first to be sure that maximum values of shear stresses are obtained within the short time for strain allowed. This is not the case with the direct shear cells with rotational displacement. Preconsolidation is not necessary due to their unlimited shear strain. Four versions of these testers are given in Figure 1.15. The cross-section of the sample is either circular or annular. The shear process is induced by rotation around the vertical axis. The covers of all testers shown in Figure 1.15 are roughened to be sure that the shear process takes place within the bulk solid and not between solid and the cover. In most testers the base is rotating and the shear moment acting on the cover is measured.

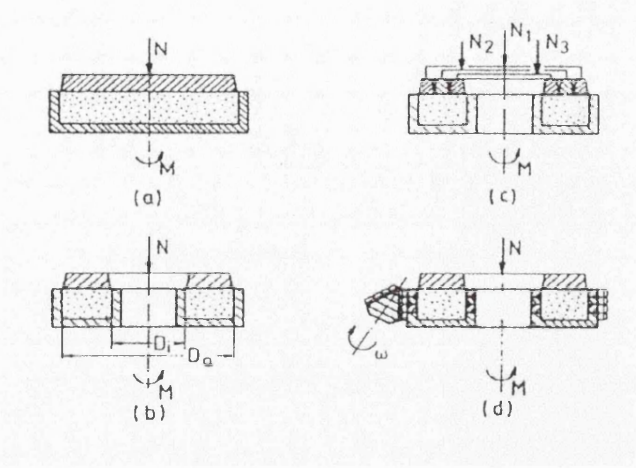

Figure 1.15 *Rotational shear testers. N = normal force,* M = *shear moment, Di and Da = inside and outer diameter respectively. (Taken from Schwedes, 1984)*

An influence of the ratio *Di/Da* (Fig. 1.15b) on the results is to be expected as can be seen in Fig. 1.16. Upon an angle α of rotation the strain in the middle of the ring is s, $s + \Delta s$ at the outer wall and $s - \Delta s$ at the inner wall. According to Cleaver (2004), if an over-consolidated sample is sheared, the maximum value of shear stress is just reached in the middle and remains at maximum level between the middle and the outer wall. However, other opinions exist here, and Schwedes (1994) clearly states that "if an over-consolidated sample is sheared and the maximum value of shear stress is just reached in the middle, it is beyond the maximum on the outer wall and has not yet reached the maximum at the inner wall." The total shear moment is measured thus resulting in a mean value of shear stress, which is less than the maximum value, which is needed for the determination of yield loci. Only the determination of steady state flow is without problems, since it is obtained and maintained on all radii after some time.

To investigate the influence of the ratio *Di/Da,* ring shear testers with different values of *Di/Da* are used (Fig. 1.15 b) or the cover consists of three concentric rings, which do not touch each other (Fig. 1.15 c).

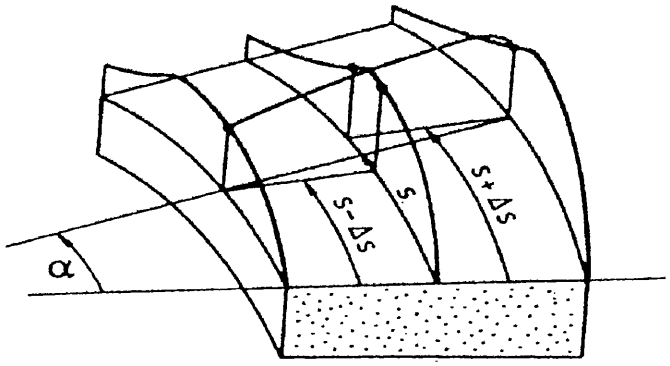

Figure 1.16 *The influence of the ratio Di/Da on shear stress. s = strain in the middle of the ring, Δs = strain change, α = angle of rotation, (Taken from Schwedes, 1984)*

Another complicated method of running a ring shear test is given in Fig. 1.15d. The shear cell consists of several rings, which rotate at different speeds thus producing a deformation similar to that in the simple shear apparatus. The advantage of the direct shear testers with rotational displacement is the unlimited shear strain. The disadvantage is the still unknown radial distribution of shear stresses (Schwedes, 1984).

Carr and Walker (1967/68) developed the first ring shear tester used in powder technology. More have now been introduced based on the original idea by several workers (Scarlett and Todd, 1968; Peschl, 1984). This shear tester and the Peschl shear tester are discussed below.

(i) The Annular Shear Cell

This type of shear cell is also known as a *rotational single level shear tester.* The annular shear cell which is also a ring shear apparatus, was invented with a view to remove stringent limitations associated with some shear testers (Carr and Walker, 1967/68; Bagster, 1984), for example, to combat the problem of non-uniformity of strain and stress within the sample, to permit the study of flow properties of bulk solids after failure, and to ease sample preparation. Many workers including Carr and Walker (1967/68), and Klausner et al. (2000) have fabricated and used the annular shear cell to measure and assess the

behaviour of cohesive powders. Kočova and Pilpel (1971/1972), employed an annular shear cell to investigate the failure properties of α - lactose monohydrate and calcium carbonate. The investigators concluded that the angle of internal friction provides a satisfactory single parameter for describing their properties. York (1975) used an annular shear cell to assess the flowability of powder/glidant systems. The investigator concluded that the optimum concentrations of magnesium stearate, talc and fine silica required to improve the flowability of lactose are 1.75, 2.25 and 0.85 wt. %, respectively. Teunou et al. (1999a) used the annular shear cell to measure the flowability of four food powders (flour, skim-milk, tea and whey-permeate) with reference to their physical properties and relative humidity of the surrounding atmosphere. They deduced from the flow index (which is the slope of the flow function) that skim-milk is a free flowing powder, whey permeate is easy flowing, tea powder is moderately flowing and flour powder is very cohesive. Tan and Newton (1990a) characterised the shear and failure properties of size fractions of microcrystalline cellulose (Avicel PH101), heavy, precipitated calcium carbonate, milled, fine lactose, maize starch and pregelatinised starch. They deduced that for a particular excipient, the flow function (*FF*) is dependent on particle size. The coarse particles exhibited better flow than the fine powder fractions.

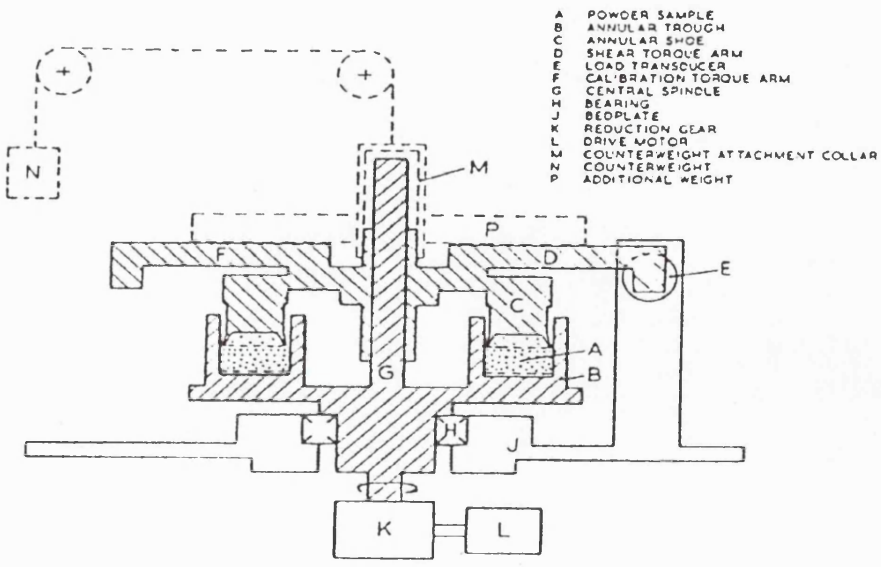

(a)

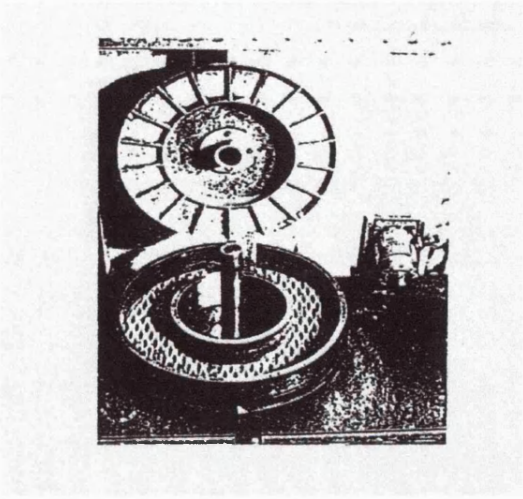

(b)

Figure 1.17 *Schematic diagram of the Portishead shear cell (a), and view of trough and shoe of Portishead shear cell (b). (Taken from Carr and Walker, 1967/68).*

Podczeck and Newton (2000) used the annular shear cell to investigate the powder and capsule filling properties of lubricated granulated cellulose powder. According to the workers, the results obtained using the shear cell indicated that "the addition of 0.2 % magnesium stearate and more impairs granule flow and does not reduce interparticulate friction".

The Portishead ring shear cell (Carr and Walker, 1967/68), which is an annular shear cell, is described below. Figure 1.17a & b show the schematic diagram and the view of trough and shoe of the Portishead ring shear tester, respectively. The Portishead was designed for performing shear tests under normal pressures up to 6.9 kPa on bulk materials up to a mesh size of approximately 6.3mm. The gun-metal trough has an inner wall diameter of 150 mm and an outer diameter of 250 mm. These dimensions help to minimize the ratio of extreme strain rates. The gun-metal shoe is mounted on a plate attached to a brass collar, which forms a sliding fit on a central spindle integral with the trough: the shoe is thus held accurately concentric with the trough. According to the workers, the clearance between the shoe and the trough must be uniform throughout, but its actual magnitude is probably not critical. The powder is loosely packed into the trough and the trough is then rotated slowly

(at a specific rpm), by a motor driving through reduction gears. Integral with the shoe is a radial torque arm, which is prevented from rotating with the cell by a load transducer. The powder is thus sheared under the chosen normal load until a steady shear stress indicates that the required state of compaction has been achieved. The behaviour of the prepared sample can be investigated at another chosen stress condition, by reversing the cell to remove the shear stress, reducing the normal load to the desired value and then re-shearing. The sample can readily be returned to the original prepared state by re-adjusting the normal load (it is necessary to retract the cell for this operation). A series of measurements can be made on a single sample without having to refill the cell, provided of course that it is first established that the physical nature of the material does not change significantly due to such factors as moisture loss, segregation, etc. This is achieved by placing disc-shaped weights symmetrically and progressively on the lid giving increasing yields strengths, or in the case of low pressures, by partially counter-balancing the weight of the lid with weights added to a hanger attached to a nylon cord passing over two pulleys. The final load is equal to the consolidation load. The compaction or dilation can be monitored with a linear displacement transducer clamped onto the frame with its finger resting vertically on the shoe.

The shear stress S developed can easily be calculated from the total shear torque given by the transducer reading. If R_i and R_0 are the inner and outer radii of the shear lid, then

$$\text{Total Shear Torque} = \int_{R_0}^{R_I} S \times R \times 2\pi R \, dR \qquad \text{.....Equation 1.21}$$

(ii) The Peschl Shear Tester

The Peschl shear tester also called the *rotational split level shear tester* was developed by Peschl at the University of Eindhoven, Netherlands, to overcome the shear strain limitation of the translational shear testers and to reduce the needed operator skill and the time required to complete a shear test (Eiserhart-Rothe and Peschl, 1977; Peschl, 1984; Thomson, 1997). The rotational movement ensures that there is no limitation of shear strain and the presence of the split-level results in a shear plane development in the middle of the

sample where the condition of the sample is not disturbed throughout the top or bottom of the lid. Figure 1.18 shows the Peschl rotational split level shear tester. The cell containing the material sample is clamped to a turntable that rotates at about 0.050 rpm. A consolidating load is applied to the cover, which is kept stationary through a vertical shaft attached to the cover. The stationary shaft allows the application of loads to be automated if desired. The shaft is mounted on an air bearing to minimize friction and to hold the cover parallel with the cell base. The torque applied to the cell cover during cell rotation is transmitted through a torque arm (Figure 1.19 (ii)), which is attached to the cover, to a strain gauge load cell. The vertical movement of the cover that occurs during expansion of the sample during shear is transmitted through a vertical rod to a vertical displacement transducer. Shear force and cover displacement are measured and recorded for each test.

The test procedure includes initial preconsolidation, as with the Jenike cell. Multiple shear tests can be made on the same sample to obtain the complete yield locus because greater shear strain is possible. Generally, a maximum of three to five yield loci (depending on the reproducibility of the steady-state shear values) can be made with a single sample (Thomson, 1997).

There are two types of model available: a *manual machine* where the consolidation loads are placed manually onto the shaft by the operator, and an *automatic machine* where the values for the consolidating loads are selected by the operator but the placement of the weights onto the cell is done by programmed electromagnets. In addition, the sequencing of the consolidating and shearing procedures and acquisition and evaluation of the data are controlled by a programmed microprocessor. The resulting data for the yield locus, flowability index, bulk density, and angle of internal friction can be printed out, displayed, or stored on floppy disc.

According to Peschl (1984) the advantages of using this shear cell include:
(1) Independent measurement results.
(2) High accuracy and reproducibility.
(3) Measurement of one or more yield loci with the same sample.

(4) Can be used to obtain a yield locus quickly for a cohesive powder (Kamath et al, 1993).

(5) Very quick measurement compared to Jenike and other shear testers.

(6) Automatic measurement and the flowability of the sample can be evaluated using the flow function or the absolute flowability index (Kamath et al, 1993).

(7) The sizes available:

Volume of specimen 2.5 and 5 cm^3- pharmaceutical equipment

" " 50 cm^3- standard equipment

" " 450 cm^3- raw material equipment

Limitations include:

(1) Not widely used or acceptable in the pharmaceutical industry.

(2) The precise location of the shear profile within the rotational shear cell is still discussed (Thomson, 1997).

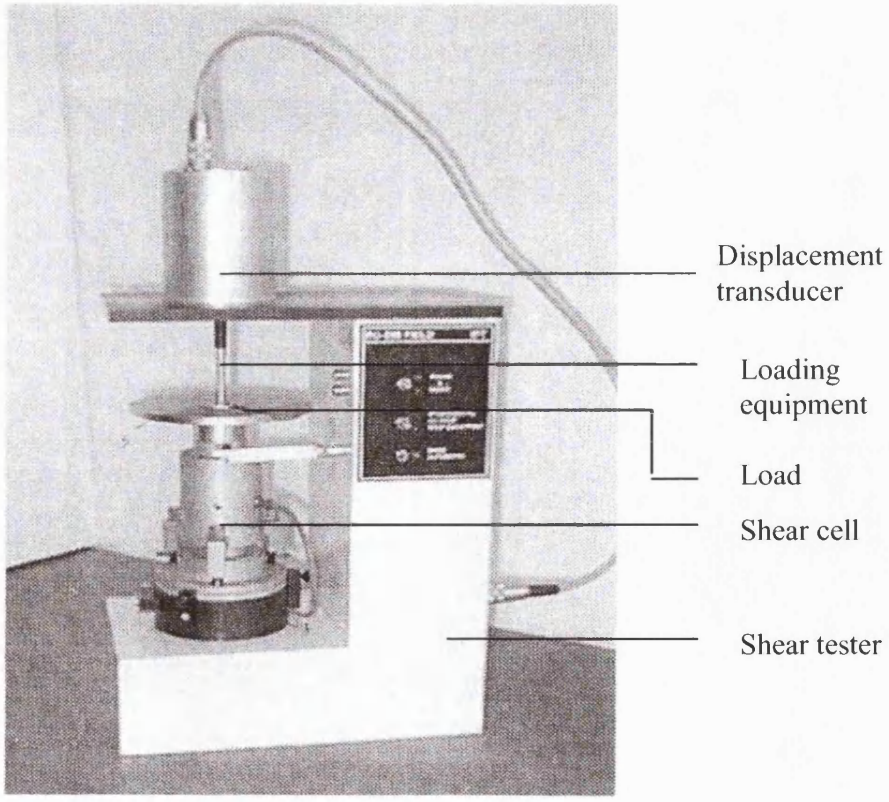

Figure 1.18 *Semi - automatic Shear tester R0-200 (Peschl Shear tester operating manual)*

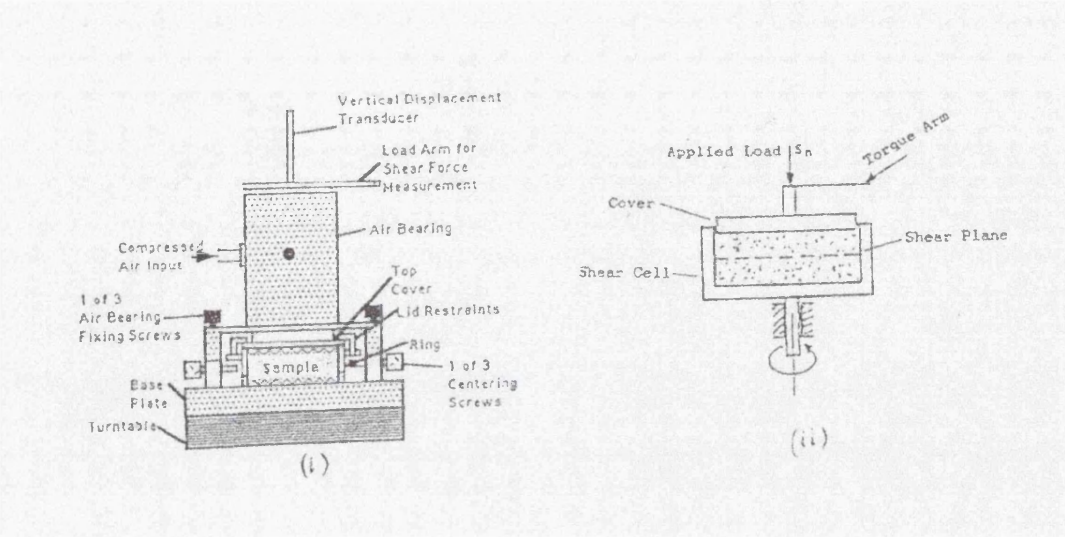

Figure 1.19 *Schematic diagram of the Peschl rotational shear tester*

(i) – shear tester set-up with the sample, (ii) – shear cell with powder sample undergoing test. (Taken from (i) Kamath et al, 1993; (ii) Thompson, 1997).

The Peschl rotational shear tester can be used when results are needed quickly (except in time consolidation analysis), when flowability is to be evaluated, and the equipment can also be used to measure flow properties of powders with low bulk density and fine particles (Kamath et al, 1993).

Podczeck and Wood (2003) utilised this equipment to study the formation of different liquid states during wet massing for granulation. Using lactose monohydrate as a model bulking agent, the investigators found the upper limit of funicular state to be approximately 15% (w/w) of liquid binder, and the threshold between pendular and funicular state to be 6% (w/w) of liquid binder (5% colloidal solution of HPMC in water). The workers also deduced that the threshold values obtained from the shear cell measurements correlated with values obtained from the final dry granule characteristics such as granule density and compressive Young modulus determined by Dynamic Mechanical Analysis.

Margreiter and Schlocker (2002) used this instrument to characterize the flow properties of a mixture of coarse particle fractions and micronised lactose for dry powder inhalers. They concluded that the extent of the flow improvement of the coarse particle fraction and the

mixtures of the coarse particle fraction with micronised lactose depends on the increase in particle size and isometry. The split- level shear tester has also been used to obtain the yield locus of wet masses for a model formulation system consisting of microcrystalline cellulose, lactose and hydroxypropylmethylcellulose (Shah *et al.,* 1995).

Figure 1.20 gives a schematic view of the development of shear stresses during the shearing of a sample using the split-level rotational shear cell (Peschl cell) R0-200. The principle as given by Peschl (1984) is as follows:

(a) *Elastic deformation* $0 < \phi < \phi_1$

Shear stress τ_1 changes linearly with radius R until the shear stress has reached the maximum value.

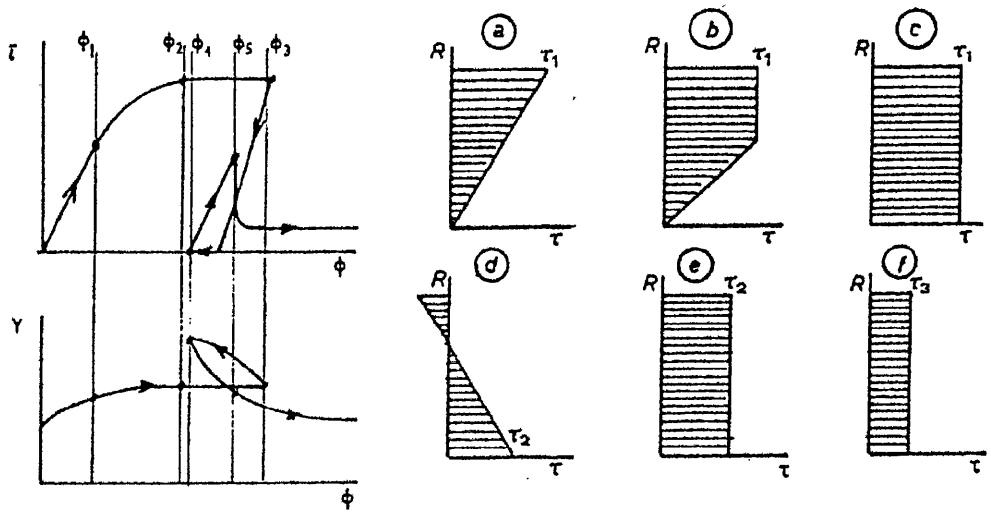

Figure 1.20 *Schematic view of development of shear stresses during the shearing of a sample using the split level rotational shear cell R0-200.*
R - radius of the shear plane, ϕ - angle of rotation, γ - density, τ - shear stress and a-f: significant points (see explanation below). (Taken from Peschl, 1984).

(b) *Transition elastic-plastic* $\phi_1 < \phi < \phi_2$

On the area outside the shear plane, the maximum shear stress (plastic deformation) is reached. By continuing the shearing the area of maximum shear stress increases and the elastic area decreases.

(c) *Plastic deformation* $\phi_2 < \phi < \phi_3$

The development of shear stresses across the shear cell area depends on the shear strain. The distribution of shear stresses changes from linear distribution along the radius in the case of elastic deformation up to the uniform distribution along the radius in the case of plastic deformation. Over the whole area of the shear plane the shear stress reaches the maximum, except in a small area around the center, which can be neglected. The sample is now *ready* for further shear procedure. The rotational shearing of the sample will be reversed (d), so that the measuring arm gets free. The sample undergoes elastic deformation so that the sum of the moments over the shear area becomes zero. The sample rotates in the opposite direction to previous shear steps a - c until equilibrium is reached. The biggest shear stress can be found in the center of the sample.

(e) *Second shear-points at static yield locus* $\phi_4 < \phi < \phi_5$

By repeated shearing of the sample, under a lower vertical load, the sample deforms elastically until the stresses reach the maximum value τ_2 corresponding to the vertical load. Due to the elastic deformation, the maximum shear stress τ_2 will be reached at the same moment along the radius of the sample. At this moment the peak is measured, which represents the point at the yield locus valid for the maximum consolidation pressure p.

(f) *Second shear - point at dynamic yield locus* $\phi > \phi_5$

Once the maximum shear stress over the whole area of the sample has been attained, the stress starts to decrease until the stationary value is reached. This stationary value represents a point on the dynamic yield locus, which can be approximated as a straight line through the origin. The particles change their position continuously in the shear plane. In

this respect, the dynamic yield locus corresponding to the stationary value of the shear stress looks like a yield locus of a free-flowing material (Peschl, 1984).

1.5.3.2.2 Indirect Shear Testers

The shear zone develops unhindered according to the applied state of stress. Here, the principal stresses are given and the shear plane is adjusted accordingly. Indirect shear testers consist of uniaxial (Maltby et al, 1993; Thompson, 1997), biaxial and triaxial testers (Schwedes and Schulze, 1990). Generally, no direct shear tester is capable of measuring the complete Mohr stress circle. The only exception is the simple shear apparatus. In the indirect shear testers the principal stresses in two or three directions are measured. Hence, the Mohr stress circles can easily be drawn (Schwedes, 1984).

(A) Biaxial Shear Tester

The biaxial tester is an improvement over the conventional shear testers. In the biaxial shear testers/cells two independent and perpendicular stresses are applied to the powder sample (Kamath and Puri, 1997) and no deformation is possible in the z-direction thus resulting in a plane deformation (Schwedes, 1984). The usefulness of this tester is limited by the two-dimensional attributes. Example of biaxial tester includes the true *biaxial tester.*

(i) True Biaxial Shear Tester (TBT)

In the true biaxial shear tester (Fig. 1.21) the boundaries of the sample remain plane and parallel. The sample is constrained in the lateral x- and y- directions by four steel plates. Rigid top and bottom plates restrict vertical deformations of the sample.

The sample can be loaded by the four lateral plates, which are linked by guides so that the horizontal cross-section of the sample may take different rectangular shapes. In deforming the sample, the stresses in the x- and y -directions, σ_x and σ_y, can be applied independently of each other. The plates can be covered with a thin rubber membrane to avoid friction between the plates and the sample. Silicone grease is applied between the steel plates and the rubber membrane.

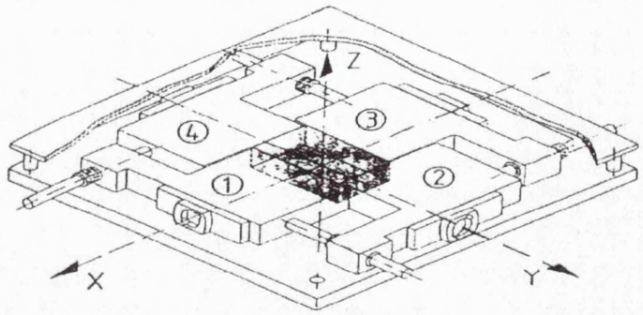

Figure 1.21 *True Biaxial Tester (Taken from Schwedes and Schulze, 1990)*

Since there are no shear stresses on the boundary surfaces of the sample, σ_x and σ_y are principal stresses. With the True Biaxial Shear tester, the measurement of both stresses and strains is possible (Schwedes and Schulze, 1990). The true biaxial tester can also be used for the low stress region of interest in powder technology. This is not possible with the normal biaxial tester, where the sample has to be placed into a rubber membrane outside the apparatus before testing. To stabilize the form of the sample, the rubber membrane has to be prestressed. Therefore high stresses have to be used during the shear process to be sure that the prestresses of the rubber membrane can be neglected (Schwedes, 1984).

(B) *Triaxial Shear Tester*

The triaxial tester was mostly used in the field of soil mechanics, where samples have to be tested at high stresses (above 100 kPa). It offers the possibility of measuring yield loci. Here principal stresses are directly measured in a steady state situation or incipient failure, leading to Mohr circles, the envelope of which is the yield locus. The triaxial tester also gives the opportunity of direct measurement of flow characteristics, thereby avoiding the need for cumbersome measurement of the complete yield locus (Haaker and Rademacher, 1984). The conventional triaxial tester (Figure 1.22), despite its name, is also effectively a two-dimensional tester. The reason for this is that two of the three principal stresses, σ_2

(intermediate) and σ_3 (minor), are equal. In addition, there is virtually no strain at the interfaces at the two ends of the test sample due to frictional constraints at the base and cap of the test sample. This restricts the failure to specific parts of the sample, leading to the familiar shear plane seen during triaxial tests. Ideally, the powder at the interfaces should be free to deform as well. Another draw back is that the stress distributions at the cap and base are non-uniform (Kamath and Puri, 1997). The normal construction of the apparatus is hardly suitable for measuring the flow characteristics of bulk materials (see Fig. 1.23). For this reason, a modified triaxial tester also called *cubical or true triaxial tester* (Fig. 1.22b and 1.24) was developed (Haaker and Rademacher, 1984). One difference between the normal triaxial and true triaxial tester is the shape of the sample, which is cylindrical (see Figure 1.22a) in the normal triaxial tester (Schwedes, 1984).

The principle of testing using the triaxial tester is simple. The sample to be tested is enclosed in a thin cylindrical rubber membrane whilst the top and bottom membrane is closed using metal covers sealed by o-rings (Figure 1.23). The membrane is placed in a pressure chamber and a hydrostatic pressure is applied thus supporting the sample. By increasing the force on the top cover an additional vertical pressure can be introduced until the sample fails. This is not the case with a bulk material such as powder, as filling of the membrane has to take place within a rigid mold to sustain the sample.

This mold can only be removed after supporting the sample by the hydrostatic pressure, which means manipulation of the mould in the pressure chamber, which is rather unattractive. Another possibility is applying underpressure within the sample, letting the atmosphere serve as a hydrostatic pressure. In this case the pressure chamber can be omitted, but the method is only suitable for sufficient permeable materials and there is a risk of changing the moisture content of the sample when evacuating (Haaker and Rademacher, 1984). This now leads to the *modified triaxial cell/tester* that is better suited for bulk materials (Figure 1.24). A cylindrical cavity that has been drilled in the vertical split axial brass block serves as the pressure chamber.

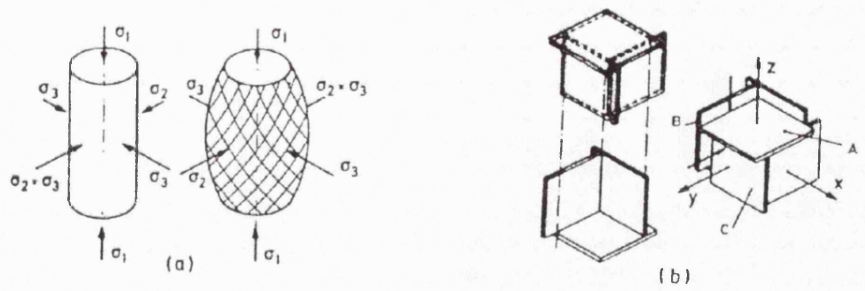

Figure 1.22 *Shape of sample in (a) normal triaxial tester and (b) true triaxial tester. σ_1, σ_2 and σ_3 are the principal stresses; A,B,C – sample boundaries/walls; x,y,z – direction of deformation (Taken from Schwedes, 1984).*

The mold consists of two half cylinders made from perforated steel plates, mounted in the pressure chamber. Both parts of the mold are moveable from outside the pressure chamber by means of a spindle and are guided by two guiding pins.

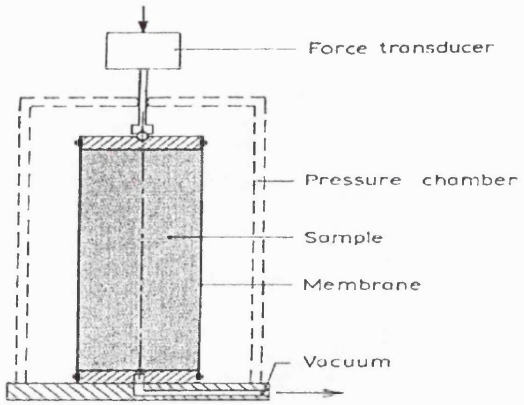

Figure 1.23 *Schematic diagram of the normal triaxial tester (Taken from Haaker and Rademacher, 1984)*

The pressure chamber is connected to a pressure or vacuum source by a transit in the mold spindle. Both half blocks of the apparatus are separately fixed to one vertical column of the

existing triaxial pressing machine such that they can rotate in a horizontal plane, like a waffle iron. With a detachable clamp both parts can be firmly fixed together. A very thin cylindrical rubber membrane, with the top and bottom fixed to a rigid ring, encloses a sample to be tested. The rigid rings on the outside have o-rings, which seal off the pressure chamber. The sample can now be fitted with covers at the top and bottom. The upper cover is fixed to a force transducer in the central vertical axis of the pressing machine, the loose undercover rests on the moveable base of the machine (Haaker and Rademacher, 1984).

The consolidation of the sample follows after preconsolidation. Reducing the horizontal pressure to the desired value and simultaneously doing the same to the vertical stress so that the values are the same, achieves this. Now the sample is forced to shear by vertical displacement of the sample against the upper cover. Displacement of the sample is continued until the steady state is attained, which is characterized by a steady value of the vertical stress, measured by the force transducer on the upper cover.

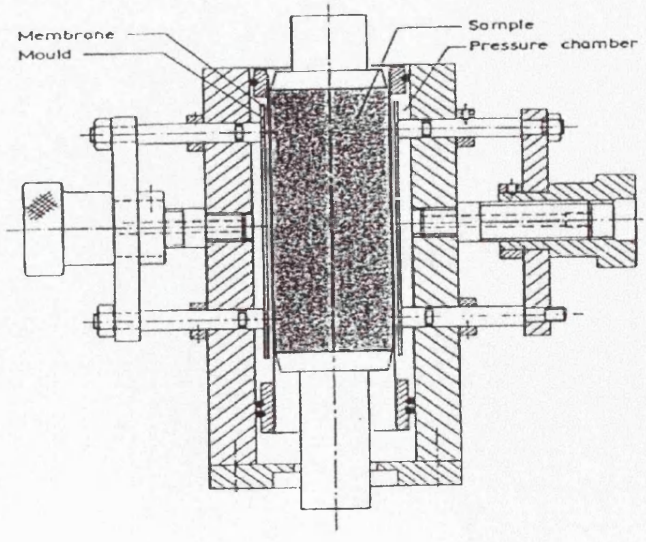

Figure 1.24 *Schematic diagram of the Modified Triaxial Tester (Taken from Haaker and Rademacher, 1984)*

Shearing of the sample is achieved by reducing the horizontal and vertical stresses simultaneously to the desired value and continuing the displacement until the vertical stress goes through a maximum and incipient failure occurs. Up to this point the principal stress of the circle touching the yield locus is known. For further circles the whole procedure is repeated with the same values of vertical preconsolidation stress and horizontal pressure at consolidation but with different horizontal pressure values (Haaker and Rademacher, 1984). The advantage of the true triaxial tester is the fact that the three principal stresses can be varied independently (Schwedes, 1984).

An example of the uniaxial shear tester is the POSTEC-Research shear tester developed by POSTEC-Research. (Maltby et al, 1993). Using the uniaxial shear tester the comprehensive failure strength similar to the unconfined yield strength f_c or the flow function can be determined directly as a function of the consolidation stress. The measurement is undertaken within a fraction of the time needed by most testers. In addition, repeatability using the tester has been proven to be good (Maltby et al, 1993).

1.5.4. USE OF MODELS

Several models have been postulated and their use demonstrated in predicting certain bulk powder behaviour prior to flow (Tripodi et al, 1992; Klausner et al, 2000).

1.5.4.1 Critical State Models

An extensive body of literature exists in which powders are modeled as a plastic continuum using soil mechanics. Critical state models based on critical state theory have recently been applied to cohesive powders (Klausner et al., 2000). The critical state theory is a widely accepted plasticity theory used to describe failure of powders (Kamath and Puri, 1997) and it states that a bulk powder reaches a volume after which additional loading produces flow with no further volumetric change (Tripodi et al., 1992; Tripodi et al., 1995). In other words, when powder is loaded, particles rearrange, causing the volume to decrease. The material then reaches some point at which additional load may change the shape of a given mass, but not its volume. The failure surface defined at the critical state becomes the final state of the powder, after which it flows without volume change (Tripodi et al., 1994).

Constitutive models such as the modified Cam-clay and elasto-viscoplastic models are based on this theory. The most common critical-state models are those patterned after the Cam-clay model - a basic soil model upon which many other constitutive models are based. The Cam-clay model used three critical-state parameters: M (slope of critical-state line); λ (slope of loading path); and κ (slope of unloading path). Based on numerous observations from implementation of the original model, a 'modified' Cam-clay model was formed in which the definition of dissipated work during plastic strain was added. The modified Cam-clay model redefined the flow function.

The modified Cam-clay model is given by the following equation:

$$\delta\epsilon_s^p / \delta\epsilon_v^p = (M^2 - \eta^2) \qquad \text{.... ...Equation 1.22}$$

where $\delta\epsilon$ is the differential strain, superscript p the plastic state, subscripts s and v refer to shear and volumetric components, respectively, and η is the ratio between mean effective stress p' and deviatoric stress q. The strain components during flow are separated into elastic volumetric; plastic volumetric and plastic shear strains (elastic shear strains are assumed to be negligible). The constitutive equations, which represent the relationship of stress to strain in a given powder, help to predict successive stress states in a powder if the constitutive parameters, the initial conditions of the material, and the loading conditions imposed on the powder are given.

1.5.5. POWDER RHEOMETER

The FT3 powder rheometer (see Figure 1.25) is a fairly new instrument and the first independent research into its use was carried out by Podczeck (1999a, 1999b). The worker used the instrument to study the rheological properties of different grades of dry microcrystalline cellulose masses. Podczeck (1999a, 1999b) concluded that the instrument could detect small differences and similarities in the flow, shear and packing properties of powders. Luukkonen et al., (2001) employed this instrument to study the properties of two different grades of microcrystalline cellulose and silicified microcrystalline cellulose wet masses and compared the results to the mixer torque rheometer. The workers pointed out

that the FT3 powder rheometer was able to distinguish any wet granules from wet powder masses after liquid saturation, whereas the mixer torque rheometer could not. Cassidy and Thomas (2001) studied the rheological properties of normal lactose, different sieve fractions of lactose and spray dried lactose. They concluded that the equipment could detect differences with respect to particle size and morphology. The aforementioned workers used the 200 ml vessel in their studies. However, a 25 ml vessel also exists and no data have as yet been reported in the literature. The benefit of using a smaller vessel to characterise powder flow in the pharmaceutical industry cannot be over-emphasised especially during preformulation stages and quality control, since this allows for easy handling during the procedures and is also more cost efficient.

Figure 1.25 *The FT3 Powder Rheometer (Taken from FT3 Powder Rheometer operating manual)*

According to the manual of this equipment, some of the benefits of the FT3 powder rheometer include the following:

- Operator independent / automated testing
- Ability to investigate flowability and robustness in relation to any key variable
- Powder conditioning, which allows tests to be repeated and compared
- Ability to measure the rheology of powders and complex semi-solids
- Ability to measure the shear strength of powders
- Small volume of powder
- High repeatability between instruments

1.5.5.1. The FT3 operating principle

The instrument measures continuously the forces causing the deformation and flow of the powder as a twisted blade is forced along a helical path through the powder at a required flow pattern and flow rate. The forces acting on the blade, rotational force (torque) and the axial force, determine the direction of the helical path and are also used as the basis of flowability assessment. The force transducers measure these forces by producing a voltage output that is proportional to the force applied.

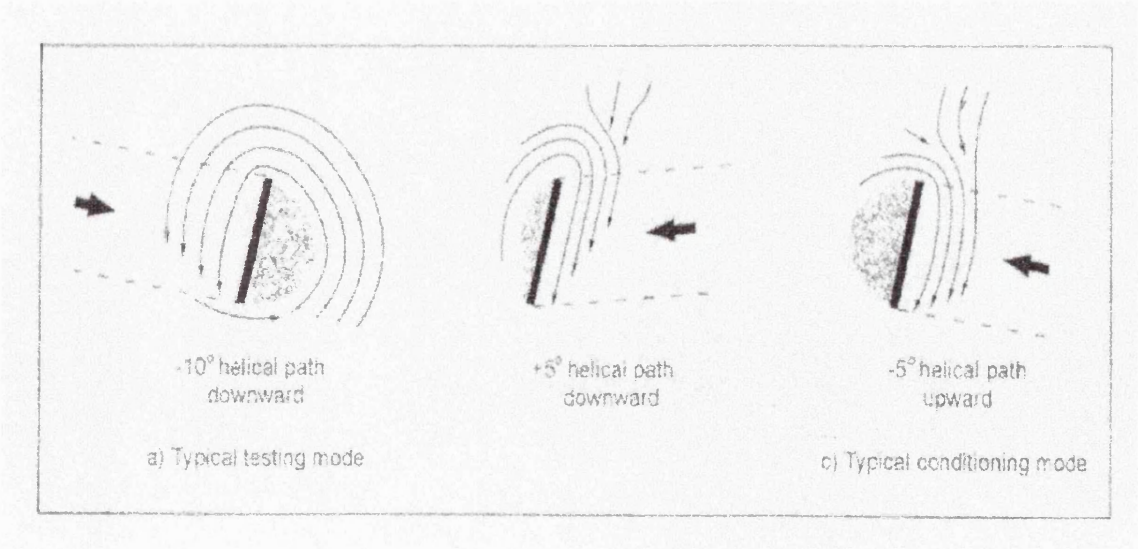

Figure 1.26 *Examples of different helical paths (Taken from FT3 operating manual)*

The helical path may be small or steep and depending on the direction in which the blade rotates, it may be right or left-handed. The work done or energy consumed during the process is measured as a function of distance (height) moved. The energy calculation is done whilst the blade moves from the top to the bottom of the powder column under test, which is termed *downward traverse.* In addition, energy calculations are made every 0.25 mm of vertical displacement of the blade. Each individual calculation is called the *energy gradient* as each is the energy per small vertical displacement and is expressed in *mJ/mm.* The *Total energy utilised* during the downward traverse is the area underneath the energy gradient versus height curve. The following basis of flowability measurements and indices is assessed by the FT3 powder rheometer:

i. Total Energy – energy consumed in displacing the powder.
ii. Basic flowability energy (BFE) – energy required to displace a constant volume of conditioned powder at a given flow rate and pattern.
iii. Stability index (SI) – factor by which the measured energy changes during repeated testing.
iv. Flow rate index (FRI) – measures the extent to which the BFE is changed when the flow rate of the standard test is reduced by a factor of 10.
v. Zero Torque Limit (ZTL) – the largest torque exerted by the powder column on the rotor blade for a defined test condition.
vi. Zero Force Limit (ZFL) – the largest force exerted on the rotor blade for a defined test condition.

1.5.6. STATISTICAL METHODS

1.5.6.1. ANOVA

Analysis of variance, frequently abbreviated to ANOVA, is an extremely powerful statistical technique which is used to compare the variation of group means to the variation of individual values within the groups. Hence, it separates and estimates the different causes of variation. It can test whether changing the controlled factor leads to a significant difference between the mean values obtained (Miller and Miller, 1993). ANOVA is one of the techniques known as General Linear Model (GLM). A GLM is usually indicated for a

model with multiple factors/variables or relationships between those variables, specifically linear relationships. Hence, the assumptions for ANOVA stem from GLM. The assumptions include the following: All variables must exhibit independent variance, equality of variance and data are random samples from a normal distribution (SPSS training manual). The ANOVA table includes the *source, degrees of freedom, sum of squares (SS), mean squares (MS)*, and the probability based on the statistical test (F-ratio). The degrees of freedom are the total number of observations minus one i.e. $(N_t - 1)$. The mean squares are equal to the sum of squares divided by the degrees of freedom (Bolton 1997). However, the derivation of these values is much more complex, if more than one factor has been tested simultaneously.

1.5.6.1.1 F-Ratio

If the null hypothesis of equal treatment means is not accepted, the distribution of the "between-groups mean square" to "within-groups mean square" ratio is described by the *F distribution*, and is expressed as follows;

$$F = \frac{Between - groups\ mean\ square}{Within - groups\ mean\ square} \qquad \text{.....Equation 1.22}$$

The *F distribution* is probably the most important probability distribution used in statistics. This distribution results from the sampling distribution of the ratio of two independent variance estimates obtained from the same normal distribution. It is defined by two parameters, degrees of freedom in the numerator and the denominator. Comparison of the observed *F*- ratio to a table of the *F* distribution with appropriate degrees of freedom at the specified level of significance enables significance testing. A ratio of about one indicates no population or group difference. If the *F* value is large (greater than one), then there is a higher proportion of between groups variability, and therefore it is much more likely that the groups differ in the population (Bolton, 1997; SPSS training manual 2000). According

to Miller and Miller (1993), differences from 1 occur as a result of random variation. However, it should be noted that this test does not indicate which of the groups differ, and hence further tests e.g. multiple mean comparison ("post-hoc tests") would need to be carried out to determine this.

1.5.6.1.2 t-Test

The t-test can be viewed as a special case or the simplest form of ANOVA in which two means are compared (SPSS training manual; Bolton, 1997). There are two types of t-tests; first, the *un-paired* and secondly the *paired – samples* t-test. In the unpaired –samples t-test, the means of two different groups are compared e.g. comparing the means of the angle of internal friction of different starch fractions. Conversely, the paired – samples t-test is used to compare the means of the same group under two different conditions e.g. the means of the time flow function (FF), where the sample remains in the shear cell and the yield loci are obtained twice to study the effect of time consolidation.

The t-test is not ideal for comparing the means of more than two groups. This is due to the fact that when multiple comparisons are made among a set of group means, the probability of at least one test showing significance even when the *null hypothes cannot be rejected* is higher than the significance level at which each test is performed.

1.5.6.1.3 Post – hoc Testing

The aim of "post hoc" testing is to determine exactly, which groups differ from which others in terms of mean differences. They are performed after the main ANOVA test revealed that population group means are unlikely to be equal. Post-hoc tests can be performed on all possible pairs of comparisons. However, performing multiple tests (i.e. multiple t-tests) increases the chances of making a Type I error, and each of the variety of post hoc tests available attempts to combat this potential problem in a different way. The ideal post-hoc test would demonstrate tight control of Type I error, have good statistical power (probability of detecting true population differences), and be robust over assumption violations (failure of homogeneity of variance, non-normal error distributions). Unfortunately, there are implicit tradeoffs involving some of these desired features (Type I

error and power) and no one current post hoc test is best in all areas (SPSS training manual).

In this work the *Scheffé test* was employed to determine if any statistical significant difference exists between for instance the cohesion coefficients of all the powders and also if any difference exists between the powder size fractions, as it controls the overall error rate. The Scheffé test not only adjusts for the pairwise comparisons but also any possible comparison the investigator might require. Most importantly, it is the most conservative of the available methods (false positive rate is least). Despite the proven attributes of this test, it has less statistical power as a larger difference between means is required for significance (Bryman and Cramer, 2001; SPSS training manual).

1.6 IMPORTANCE OF POWDER FLOW FOR DOSAGE FORM MANUFACTURE

The importance of powder flow for dosage form manufacture in the pharmaceutical industry cannot be over-emphasised. In the pharmaceutical industry, several processes are affected by powder flow, mainly in the development and production of solid dosage forms. As such, the identification of the best technique to evaluate powder flow in a cost effective manner has received much attention. Processes involving powder handling may involve separation of a small quantity (unit dose) of powder from a large blend, for instance when producing tablets. Although measured by volume, the uniformity of content of dose and weight uniformity are affected. During tabletting, a powder blend with poor flow properties may impact on the high speed process that previously worked well. For most high speed automated systems, consistent flow at this point is essential to provide consistent weight of individual doses. Hence, powders with poor flow cannot be used to produce tablets on these systems. Powder flow is a function of the powder being handled and the equipment and hence, in order to increase die feeding efficiency powders may either be forced into the die cavity, or one needs to improve the flow properties of the powder above the die cavity physically (Shangraw, 1989). In addition, powder flowability could also be enhanced through machine modification, which may serve to aerate the powder to allow it to flow naturally and improve die filling (Prescott and Barnum, 2001a). Furthermore, in capsule

filling the operation requires the powder to form a plug and the plug be ejected into the capsule shell, and the remaining powder to be sufficiently free flowing to collapse to fill the void created (Prescott and Barnum, 2001a). Other applications in which a unit dose is created and powder flow is a concern include inhalers (Prescott and Barnum, 2001a).

According to Prescott and Barnum (2001a), the following processes without claiming completeness are also affected by powder flow in the pharmaceutical industry:
Powder transfer of, for instance, raw or in-process materials through a comparatively large equipment as in transfer from a bin or drum hopper for transportation, storage or processing. *Mixing,* in which the quality of the resulting mixture depends on the type of mixer used and the flow behaviour of the powder during the mixing cycle. *Compaction* processes used for instance in dry granulation processes to improve powder flow properties. *Powder storage,* which could result in, for instance, caking within a drum or bin after storage or shipping. *Quality control,* in which flow property measurements are intended to distinguish between powders or batches. *Fluidization,* for fluidized bed processing such as granulation.

1.7 AIMS AND OBJECTIVES OF THE WORK

The aims of this thesis were to evaluate the operating parameters of the Peschl rotational shear tester in order to use the derived parameters (standard operating procedure) to assess the flow and shear properties of four model powders. The relative humidity of the storage air was varied to establish whether the shear cell is able to detect the influence of the formation of capillary forces on powder flow and interparticulate friction. The influence of particle size on shear cell behaviour was investigated using size fractionated samples. In addition, it was attempted to assess other techniques to observe powder flow and to compare the results obtained in terms of variability and reproducibility.

The work reported in this thesis is divided into two general sections. It is seen from the review work that little work has been done using the Peschl rotational split-level shear tester to assess powder flow. This may be attributed to the lack of wide-acceptance of the

instrument by the industry. The first part of the research is concerned with the characterisation of the powder with regards to particle size and size distribution, particle shape and distribution, surface area, particle topography and apparent density.

The second part of the work relates to the assessment of the operating parameters of the Peschl rotational shear tester. The standard operating procedure was used to evaluate the effect of relative humidity of air on the shear properties of the model powders and also to evaluate the flow properties of powder size fractions (pregelatinised starch and α-lactose monohydrate). Other methods such as determination of static and dynamic bulk density, critical orifice diameter were employed also to study powder flow and the results obtained were then compared with that of the Peschl split-level shear tester.

CHAPTER TWO

MATERIALS AND METHODS

2.1 MATERIALS

2.1.1 MICROCRYSTALLINE CELLULOSE

Microcrystalline cellulose is a purified, partially depolymerised cellulose and is prepared by treating α-cellulose, obtained as a pulp from fibrous plant material, with mineral acids (Bolhuis and Chowhan, 1996). The material occurs as a white or almost white, odourless, tasteless, crystalline powder composed of porous particles (BP, 2002; Bolhuis and Chowhan, 1996; Wheatley, 2000). It is used as filler-binder in direct compression. In addition, it works to a limited extent as a disintegrant and lubricant (Bolhuis and Chowhan, 1996). The cellulose fibres in the starting material are composed of millions of microfibers. Two different regions can be distinguished in the microfibers; a para-crystalline region, which is an amorphous and flexible mass of cellulose chains, and a crystalline region, which is composed of tight bundles of cellulose chains in a rigid linear arrangement. The amorphous fraction is largely removed due to the effect of controlled hydrolysis, yielding aggregates of the more crystalline portion of cellulose fibers. Subsequently, dry porous microcrystals can be obtained after purification by filtration and spray drying. By controlling the atomisation and drying conditions, particle size and moisture content can be varied (Doelker, 1993; Bolhuis and Chowhan, 1996). In 1964, microcrystalline cellulose under the brand name Avicel was first marketed by FMC Corporation in four different particle sizes. In 1992 the range of products was extended to seven types (Bolhuis and Chowhan, 1996). Other grades with different particle sizes and moisture content, which have different properties and applications, are commercially available. Examples include: Emcocel 50M by Edward Mendell Co. Inc. and Vivacel 101 by J. Rettenmaier and Söhne GmbH (Wheatley, 2000). Microcrystalline cellulose exhibits low bulk densities (0.32- 0.45 g/cm^3) and poor flow, and is hygroscopic (Bolhuis and Chowhan, 1996). The varying morphological properties influence the flow characteristics (Szabó-Révész et al., 1995). The powder is slightly soluble in 5% w/v NaOH (when 5 g of NaOH are dissolved in 100 ml of water, volume contraction will occur and hence, the British Pharmacopoeia (2003) prescribes the use of % w/v as mandatory unit), practically insoluble in water, dilute acids and most organic solvents (BP, 2003).

Microcrystalline cellulose under the name Vivapur® type 105 (J. Rettenmaier and Söhne GmbH & Co, Ellwangen-Holzmühle, Germany), batch number 5610590848 was used. According to the manufacturer, MCC 105 has a bulk density of 0.25 g/cm^3.

2.1.2 α - LACTOSE MONOHYDRATE

α - lactose monohydrate also referred to, as lactose, hydrous or regular lactose is the most common used form of lactose monohydrate, and is used in the pharmaceutical industry as diluent for solid oral dosage forms or as carrier in inhalation products and even in lyophilised products, where it helps to increase plug size and aids caking. It is a natural disaccharide obtained from cow's milk. Lactose monohydrate occurs as odourless, white or almost white crystalline powder (BP, 2003; Kibbe, 2000) with a slightly sweet taste. Chemically, lactose consists of one galactose unit and one glucose unit. Lactose exists in two isomeric forms, α -lactose and β -lactose, and can be either crystalline or amorphous. Crystalline α -lactose occurs in the monohydrate and anhydrous forms, whereas, crystalline β -lactose exists in anhydrous form only (Bolhuis and Chowhan, 1996). Lactose monohydrate is stable in air and is insignificantly affected by humidity at room temperature. Regular lactose has a surface area value ranging from 0.24-0.25 m^2/g (Kibbe, 2000). It is soluble in water and practically insoluble in alcohol (BP, 2003). In this research, α-lactose monohydrate supplied by Borculo Whey Products, Saltney, UK, batch number 749035 was used.

2.1.3 PREGELATINISED STARCH

Pregelatinised starch (Starch 1500®) formerly marketed as STA-Rx 1500 by A.E. Staley cp., Decatur, Illinois, is prepared by subjecting corn starch to physical compression or shear stress in high-moisture conditions causing an increase in temperature and a partial gelatinisation of some of the starch. Pregelatinised starch occurs as a moderately coarse to fine, white to off white coloured powder. It has a slight characteristic taste and is odourless (Bolhuis and Chowhan, 1996; Lordi and Rowley, 2000). Pregelatinised starch is used as a disintegrant, binder and diluent in oral tablet and capsule formulations. Pregelatinised starch is self-lubricating but when used with other excipients it may be necessary to add a lubricant to the formulation (Lordi and Rowley, 2000). The product consists of both

individual starch grains and aggregates of starch grains bonded to hydrolysed starch (Bolhuis and Chowhan, 1996). Pregelatinised starch typically contains 5% of free amylose, 15% of free amylopectin and 80% unmodified starch (Lordi and Rowley, 2000). The content of free amylopectin is used as a quality criterion and identified as "cold water solubility". Pregelatinised starch has poor flow properties when compared with other filler-binders because of the large specific surface area of the powder, resulting in strong forces between particles despite claims that pregelatinised starch is a free-flowing material with better flow properties. Pregelatinised starch swells in the presence of moisture (Bolhuis and Chowhan, 1996). This starch is practically insoluble in organic solvents, slightly soluble to soluble in cold water, depending upon the degree of pregelatinisation. Pregelatinised starch is hygroscopic. Pregelatinised starch (Starch 1500®) with cold water solubility of 18.9% supplied by Colocon, Indianapolis, Indiana, U.S.A, batch number IN 501833 was used.

2.1.4 CALCIUM CARBONATE

Calcium carbonate can be obtained from the naturally occurring minerals aragonite, calcite, and vaterite. Calcium carbonate can also be prepared by double decomposition of calcium chloride and sodium bicarbonate in aqueous solution. Calcium carbonate occurs as a white, tasteless, odourless powder or crystals (Pharmaceutical codex, 1979; Armstrong, 2000; BP, 2003). The density and fineness are governed by the concentration of the solution (Armstrong, 2000). Calcium carbonate is stable (Armstrong, 2000) and absorbs insignificant amounts of moisture at 25° at a relative humidity up to about 90% (Pharmaceutical Codex, 1979). It is used as diluent in solid-dosage formulations and also as a base for medicated dental preparations. Calcium carbonate is used as an opacifier in tablet film-coating and as a bulking agent in tablet sugar-coating processes (Armstrong, 2000). In addition, calcium carbonate is used as an antacid and calcium supplement and as a food additive (Armstrong, 2000). Calcium carbonate is practically insoluble in 95% ethanol and water (Armstrong, 2000). The solubility in water is increased by the presence of carbon dioxide (Pharmaceutical codex, 1979; Armstrong, 2000) and ammonium salts (Armstrong, 2000). Solubility is further reduced in the presence of alkali hydroxides. Precipitated calcium carbonate supplied by Merck, Poole, UK; batch 618535 was used.

2.1.5 SUMMARY OF SALTS USED FOR MAINTAINING SPECIFIED RELATIVE HUMIDITIES

Table 2.1 outlines the salts used to prepare the saturated solutions and the relative humidity they provide at various temperatures.

Table 2.1 *Saturated salt solutions and their relative humidity over a range of temperatures (Reproduced from Nyqvist (1983) and Wade (1980).*

SALT	TEMPERATURE (°C)					BATCH NO.	SUPPLIER
	20	25	30	35	40		
Calcium Chloride, $CaCl_2,6H_2O$	35.0	31.0				330-A743500	Merck, Poole, UK
Potassium Carbonate, K_2CO_3	44.0	43.0	43.0	43.0	43.0	A158736-924	Merck, Poole, UK
Magnesium Nitrate, $Mg(NO)_2,6H_2O$	55.0	53.0	52.0	50.0	48.4	D8670B	Avocado Research Chemicals Ltd., Heysham, UK
Sodium Chloride, NaCl	76.0	75.3	75.1	74.8	74.7	K26081033-903	Merck, Poole, UK

The temperature of the saturated salts solutions was maintained at 20 °C.

2.1.6 WATER

The water used was obtained from a purifying system (Option 4 water purifier, USF Elgar, USA). The purification of water involved an initial pre-filtering through an active-carbon membrane filter to remove chlorine and particulate contaminations. The remaining impurities (organic and inorganic ionic) were removed by further purification using reverse osmosis and demineralisation.

2.1.7 ABSOLUTE ALCOHOL AND ACETONE

Ethanol of analytical grade (99.7 - 100 % v/v) was used to disperse the powders before particle size analysis using the Malvern Matersizer. Absolute alcohol was supplied by BDH Lab Supplies, Poole, UK; Lot number L008907, L206007 and L286807. Acetone was used to clean the glass ware before analysis, for example, the glass ware for the surface area measurement. Acetone was also supplied by BDH Lab Supplies, Poole, UK; Lot number K29459005.

2.2 METHODS

2.2.1 PARTICLE SIZE AND SIZE DISTRIBUTION

The particle size and size distributions of the powders and the powder fractions were analysed using the Malvern Mastersizer (model SS, 1997, Malvern Instruments Ltd., Malvern, England). This instrument uses the principle of Low Angle Laser Scattering using vertically polarised light in the form of a low power helium-neon laser beam. The instrument was fitted with a lens having 300 mm focal length and active beam of 14.3 mm. This setting allowed particles with the particle sizes in the range of 0.5 μm to 900 μm to be measured. Using the polydisperse analysis model, the following refractive indices were used: 1.530, 1.596, 1.589 and 1.480 for pregelatinised starch, lactose monohydrate, precipitated calcium carbonate and microcrystalline cellulose type 105, respectively. Before analysis, the 15 ml magnetic stirrer was thoroughly cleaned internally using the dispersing solvent i.e. analytical grade ethanol and 95 % alcohol before analysing the other powders and precipitated calcium carbonate, respectively. Lint-free tissues were used to clean the lens and the external glass surfaces of the magnetic stirrer. The magnetic stirrer was filled with the dispersing solvent, and bubbles, which may be mistaken for particles by the instrument and, hence, introduce errors, were removed by repeated acceleration and deceleration of the stirrer speed. The laser beam was aligned followed by background noise measurement and zeroing. A few milligrams of the powder was dispersed (by manual shaking) in 14 ml scintillating vials (supplied by Scientific Laboratory Supplies, Nottingham, England) and added dropwise to the ethanol-filled measuring cell using a 2 ml disposable Pastuer pipette until an obscuration between 15 – 20 % was attained. Several runs were performed until three measurements with a residual value (deviation between the

fitted and corrected data) of < 1% were obtained. The particle size distributions were expressed as the volume proportions in each class of particle size, and the total volume of each distribution was set to one. The calculation was carried out automatically (Mie model) using the in-built algorithm of the software (Mastersizer Malvern version 1.2b, Malvern, England).

2.2.2 PARTICLE SHAPE

The particle shape factor and size of the pharmaceutical model excipients were assessed concurrently using an image analyser (Seescan Solitaire 512, Cambridge, UK) attached to a microscope (Olympus BH – 2, Hamburg, Germany) via a black/white CCD– 4 miniature video camera (Rengo Co., Toyohashi, Japan).

A small amount of the powder sample was suspended in 1- iodonaphthalene sulphur, a high refractive index liquid, on a glass slide. A cover slip was gently lowered on to the homogenous suspension so that the suspension was allowed to settle evenly between the two glass surfaces.

By clicking on "Live" from the created user menu, the image from the microscope (with the appropriate magnification) was viewed using the monitor. Afterwards, the slide was removed and replaced with a graticule, which was viewed under the microscope. Calibration was selected from the created user menu and the image of the graticule was used to calibrate the pixel size. In addition to this, the number of corners as determined by visual inspection of the two-dimensional particle outline on viewing the particles on the slide under the microscope was entered. Using the right button on the mouse, the calibration menu was changed to the created user menu and the graticule was replaced with the slide. The focus was adjusted and a suitable field of vision was selected. From the user menu, 'Interactive threshold' was selected. The correct grey shade was achieved by moving the mouse forward and backward to obtain a good contrast. By going back to the users menu, "Kill small" followed by "Fill Holes was selected. The captured image was edited by selecting "Draw in blue" from the users menu. By zooming followed by clicking on 'edit' on the bottom of the screen using the mouse, particles slightly touching at corners were

separated by drawing in a blue line." Draw in red" was used to fill in incomplete images. Unwanted images were removed by selecting "Remove objects" from the created user menu. The remaining particles in the field were measured by selecting "Measure all" from the created user menu. Each field was measured once. The measurement was analysed statistically by selecting "Show Statistics" afterwards. Using different fields from the same slide at least 500 particles were analysed. Three slides were prepared per powder and the procedure repeated for each powder (i.e. re-calibration and using the appropriate magnification). Thus, a minimum number of 1500 particles were studied. The pixel aspect ratio of the camera attached is 1.417 for which automatic correction is undertaken and a pixel size of $\pm$ 2.308 μm was used for all powders, i.e. all measurements are accurate to $\pm$ 2 μm. The parameters measured include Feret diameter, Aspect ratio and the Shape factor *NS* (see section 1.4).

2.2.3 SURFACE AREA/SURFACE RUGOSITY

The surface area of the powders was measured by the gas adsorption method based on the Brunauer-Emmett-Teller or otherwise called the BET equation (Brunauer *et al.*, 1938) and analysed on the automated bench top surface area analyser (SA 3100 Surface Area Analyser, Beckman Coulter U.K Ltd., High Wycombe, England). The instrument is fitted with three outgassing stations, a vacuum pump and one analysis sample port. The powders were dried to constant mass by infrared radiation in a moisture balance (Sartorius, model YTC 01LT Thermo Control Unit, Sartorius GmbH, Gottingen, Germany). The dried powders were stored immediately over silica gel in desiccators for 48 hours to protect the particle surfaces against moisture adsorption.

About 5 g of powder (between 1-3 g for MCC 105 and precipitated calcium carbonate) was weighed into the flat bottom sample tube, a glass rod was inserted to reduce the free space in the sample tube, and the sample tube was subsequently sealed with glass wool and rubber cap. This weight was noted and subtracted when the powder was added to obtain the powder weight. The sample tube containing the powder sample without the cap was inserted into the outgassing station of the surface area meter. Three samples per powder

were outgassed simultaneously overnight at 90°C under vacuum after flushing with pure nitrogen.

After outgassing, the sample tubes including the tube insert and sample were removed and covered immediately with caps and left to equilibrate to room temperature prior to re-weighing. The caps were replaced promptly after weighing and the new weight used in the analysis. As only one tube could be analysed at a time, each tube was cleaned with a lint-free tissue to remove fingerprints before analysis. The sample tube without the cap was loaded into the sample port and the Dewar flask, filled with liquid nitrogen, was loaded as prompted by the message on the screen. The sample analysis commenced after an initial evacuation process using pure nitrogen gas within 90 minutes. After analysis the sample tube was removed, covered immediately with a cap and left to equilibrate to room temperature. The sample tube was re-weighed again to determine the final weight of the sample that was analysed. This weight was used in the final BET calculations.

The outgassing and BET profiles are given below:

Parameter	**Setting**
Sample Tube size	9 ml (3 ml for calcium carbonate)
Sample weight:	5.60 ± 0.70 g (Pregelatinised starch and α – lactose monohydrate)
	2.55 ± 1.34 g (MCC 105 and calcium carbonate)
Outgas Temperature	90°C ± 0.5°C (Pregelatinised starch, MCC 105 and α – lactose monohydrate)
	250°C ± 0.5°C for calcium carbonate
Outgas Time	90 minutes
Analysis Method	Vacuum
Calculation	10 points BET
Adsorbate	Nitrogen at liquid nitrogen temperature
Partial Pressure Range	0.05 – 0.20 relative pressure (P/P_o)
Sensitivity	High

The coefficient of rugosity was calculated according to Robertson and Emödi (1943), which is given below;

$$Rugosity = \frac{BET\ surface\ area}{Theoretical\ surface\ area} \qquad \text{.....Equation 2.1}$$

According to the workers, the closer the value is to unity, the less rough is the particle surface.

2.2.4 APPARENT PARTICLE DENSITY

The apparent particle densities of the powders were evaluated using a helium pycnometer, otherwise called the Quantachrome multipycnometer by Quantochrome Corporation, Syosset, NY, USA, model number MVP-1. Prior to measurement, the instrument was allowed to stabilise for about an hour and calibrated using the two microspheres of 2.156 cm^3. The powders were dried in an oven for 16 hours at 105 °C with the exception of α-lactose monohydrate that was dried 90 °C for 24 hours. The powders were stored over silica gel in a desiccator for a few hours. Preliminary experiments have shown that it is essential to dry the samples to mass constancy prior to the measurements to obtain a value for the apparent particle density as close as possible to the material density. The powders were weighed into the tared sample cell and weights recorded. Using a standard operating procedure, five determinations were carried out for each powder. The particle density was then calculated from the volume data and the weight of each sample used.

2.2.5 STATIC AND DYNAMIC POWDER PACKING

The static and dynamic powder packing was assessed using two different types of tap volumeter as described in detail below.

2.2.5.1 Slow Tapping

The tap density volumeter by Jencons Scientific equipment, Hemel Hempstead, Bedfordshire, England was utilised. The container for the tapping was a glass cylinder of

250 cm^3 capacity, and the equipment worked with a lift height of 2.54 cm and a tapping frequency of 29 taps /min. This equipment complies with Hausner's work and the standards provided in his paper (Hausner, 1967).

2.2.5.2 Fast Tapping

Fast tapping device: tap volumeter by Copley instruments, Nottingham, UK, having a lift/drop height of 3 mm, tapping frequency of 253 taps /min. Similarly, a glass cylinder with a nominal capacity of 250 cm^3 was used. This equipment complies with EP/BP regulations.

Procedure

A funnel fitted with a 3 mm screen was mounted on top of the cylinder. The powder was carefully screened into the cylinder to form a bed of 200 – 250 cm^3. The powder was carefully levelled off with a spatula without causing disturbance of the packed powder column. The maximum bulk volume, which corresponds to the minimum bulk density of the powder bed, was noted and not the weight, as any movement could encourage disturbance of the powder bed, hence, introducing some errors. The cylinder was allowed to fall freely (mechanically tapped) and the volume readings were taken at specific tap intervals. The whole container was covered after a few tappings and not before tapping as it was discovered that the volume of the powders reduced immediately when covering the packed cylinder before starting the tapping. The measuring cylinder was weighed to determine the weight of the powder after a constant minimum bulk volume was reached. The powder density was evaluated as a function of the number of taps (dynamic packing) using the models described by Mohammadi and Harnby (1997) and Varthalis and Pilpel (1976).

2.2.6. SCANNING ELECTRON MICROSCOPY

Scanning Electron Microscopy (SEM) is a technique, which is used to examine the surfaces of structures. Due to its very large depth of field it encourages the production of images having almost a three-dimensional quality. Samples were mounted onto adhesive double sided carbon discs attached to the SEM aluminium stubs and coated with gold by sputtering

(EmitechK550 sputter coater, Emitech, Kent, UK) for 3 minutes at 20 mA, after which a thin gold film had formed. Scanning electron micrographs were obtained using a Philips XL30 SEM (Philips, Eindhoven, Netherlands).

2.2.7. MOISTURE CONTENT

A Halogen Moisture Analyser was employed to evaluate the moisture contents of the powders (Mettler Toledo GmbH, Grėifense, Switzerland). A tared aluminium dish was placed in the pan holder followed by the addition of about 5 g of powder, which was evenly spread. The drying temperature was set to 90 °C and program 5 was chosen for the switch-off-criterion. The switch-off-criterion corresponds to the time when the drying is complete and there is no or very minimal or insignificant moisture lost. The weight loss was determined by the balance incorporated in the instrument and interpreted as moisture content.

2.2.8. MOISTURE UPTAKE

The gravimetric studies using the Dynamic Vapour Sorption (DVS) were undertaken in a humidity controlled ultra-sensitive recording microbalance system (DVS-1, Surface Measurements Systems, London, UK). The experimental method was set up (i.e. the required %RH, temperature and exposure time, which ranged between twenty four hours to sixty two hours depending on the powder) and saved. The pan was placed gently on the hang down wire and the door closed. The weight was allowed to stabilise before taring the balance. A sample weight between 18 – 60 mg was then weighed directly into the glass sample pan in the microbalance (a small card was placed underneath the pan to prevent the pan or sample from dropping into the DVS glassware just below the pan) housed in an incubator to ensure accurate temperature control. A smaller quantity was used for hygroscopic powders and more for the hydrophobic ones. After sample weighing, the glass arm was tightened and the oven closed. The sample pan was allowed to stabilise before proceeding to the next step. The *Auto M(0)* button on the main panel of the DVS program was clicked to record the initial mass. The experiment was initiated by clicking the *ON* button on the right hand bottom corner of the screen, after which a green light came up indicating the experiment has commenced. At completion of the experiment (indicated by

the red light), data from the experiment was converted to a form recognised by excel and used to obtain the sorption-desorption isotherm.

2.2.9. SHEAR AND FAILURE PROPERTIES

The acceleration of vibration of the fill sieve was determined using the 2237B Controller Hand-Arm vibration meter (Bruel and Kjaer, Naeium, Denmark), and the flow properties of the model pharmaceutical excipients were measured using the Peschl shear tester RO- 200 semi automatic (IPT Industrial Powder Technology, Vaduz, Liechtenstein). The stages involved in the assessment are given below;

2.2.9.1 Calibration of the fill sieve

The acceleration of vibration of the fill sieve was determined using the 2237B Controller Hand-Arm vibration meter by Bruel and Kjaer, Naeium, Denmark.

The accelerometer was attached to the top front of the instrument. This was achieved by screwing the accelerometer into one of the holes on the mounting bracket attached to the instrument. The straps holding the mounting bracket in place were attached firmly to eliminate free vibration of the mounting bracket.

Using the measurement acceleration range of 0.1 to 316 m/s^2, frequency weighting of 5Hz to 1500 Hz and 10 seconds measurement time, the A_{mp} (maximum peak acceleration) and the A_{eq} (equivalent constant root mean square acceleration for the entire measurement period) was measured. The measurements were taken after a 15 seconds warm up time for the hand-arm vibration meter. The acceleration of vibration of the remaining (two) sides were also taken.

2.2.9.2. Evaluation of the operating parameters of the Peschl shear tester

Preparation of Peschl shear cell

The shear ring was placed on top of the cleaned cell base, using the three centering pins, whereby the shear cell was centered ensuring that the notches of the ring faced upwards.

The weight of the empty shear cell was noted and the protection ring placed on top of the shear cell.

The fill ring (1 cm high for pregelatinised starch and the 2 cm for the other powders) was placed on top of the shear cell ring. Using the "Fill sieve RO- 220", the shear cell was then filled as uniformly as possible with powder that had been stored in a desiccator for twenty-four hours. The different sieve sizes i.e. fine, intermediate and coarse were explored along with the different acceleration of vibration (low, medium and high). After using the various sieve sizes and acceleration of vibration, the medium acceleration of vibration and intermediate sieve were selected for further analysis as it was found that this combination ensured that there is minimal segregation of particles (intermediate sieve) and minimal electrostatic effect (medium acceleration of vibration). The powder above the upper edge of the fill ring was scraped off and a "porous consolidation lid" was placed centrally on top of the powder. The shear cell was placed on the consolidation bench and the shear cell including the porous consolidation lid was loaded with load corresponding with the consolidation load during the shear. Different preconsolidation times were explored i.e. 4, 8, 10 and 12 minutes. For further analysis, the 8 minutes preconsolidation time was used. The shear cell was removed from the consolidation bench after completion followed by the porous lid. The fill ring was removed gently and the additional powder above the top of the shear cell ring was scraped off. Spilled powder was removed from the shear cell base using a fine brush and the shear cell filled with powder was weighed. The weight of the powder was obtained by subtracting the weight of the empty shear cell with shear cell ring from this final weight.

Procedure for shear cell assembly

The three- legged top lid of the shear cell was placed gently on the cell base ensuring that the loading lid (top cover) of the shear cell did not make any contact with the powder in the shear cell. The loading lid was gently lowered until the top cover touches the powder. The three clamp screws were immediately tightened.

Mounting of the shear cell on the shear tester

The three screws on the turntable of the shear tester were loosened and the shear cell assembly was placed on it. The shear cell was turned so that the position of the loading arm on the shear cell was connected to the loading linkage on the shear tester. Using the three screws, the shear cell was fixed to the turntable and the loading bar was connected to the shear cell. The three centering screws were loosened gently so as not to disturb the powder packing and to ensure that the top cover could move freely. The air supply was connected afterwards.

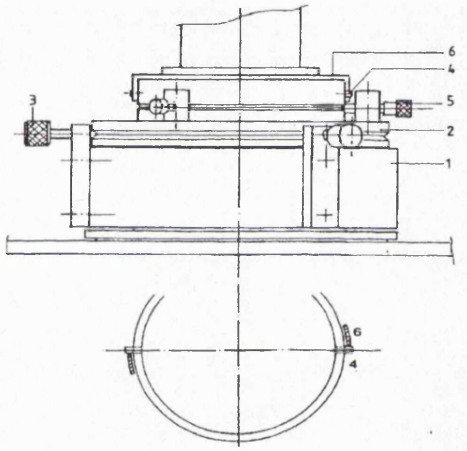

Figure 2.1 *Shear cell assembly on shear tester. 1. Turntable, 2. Cell base, 3. Clamp screws for fixing the cell, 4. Pin on cell ring, 5. Centering screw for cell ring, 6. Lips on loading lid (Taken from Peschl shear tester operating manual)*

Measurement

From the main menu, the number corresponding to "set up parameters for measurement" was selected. A set up/measurement parameters was chosen. The initial measurement parameters that served as the starting point for the analysis are as follows:

Consolidation step load of 50 g/cm^2	- (4.905 kPa)
Shear step value per step	- 10 g/cm^2 (0.981 kPa)
Time factor consolidation step	- 2 min
Time factor shear step	- 2 min
Expansion time	- 1 min

Measurement type - Standard

Data input - 1 yield locus

Standard deviation - 0.029 kPa (from linear approximation)

After the initial analysis, the effects of varying the above chosen parameters were studied in addition to varying the evaluation parameters and the already discussed parameters i.e. (sieve size, acceleration of vibration, preconsolidation load and expansion time). The idea was to vary the parameter one at a time leaving the other parameters intact.

Table 2.2 *Summary of experimental set up to determine the parameters of operation*

PL (g)	CSL (g)	CST (min)	SST (min)	ET (min)	PCT (min)	SS (mm)	NSS	VS (m/s^2)	SD (kPa)
1500	1500	2	2	1	8	2.1	6	18.5	0.029
600 2400	600 2400	2	2	1	8	2.1	6	18.5	0.029
1500	1500	1 3 5	2	1	8	2.1	6	18.5	0.029
1500	1500	2	1 3 5	1	8	2.1	6	18.5	0.029
1500	1500	2	2	0.5 2	8	2.1	6	18.5	0.029
1500	1500	2	2	1	4 10 12	2.1	6	18.5	0.029
1500	1500	2	2	1	8	1.1 3.1	6	18.5	0.029
1500	1500	2	2	1	8	2.1	5 10	18.5	0.029
1500	1500	2	2	1	8	2.1	6	12.0 25.0	0.029
1500	1500	2	2	1	8	2.1	6	18.5	0.020 0.049

Table 2.2 depicts this experimental set-up and the following abbreviations are used :
PL – Preconsolidation load, CSL – Consolidation step load, CST – Consolidation step time, SST – Shear step time, ET – Expansion time of the powder during shear, PCT – Preconsolidation time, SS – Sieve size, NSS - Number of shear steps, VS – Acceleration of vibration of the fill sieve, SD – Standard deviation from the calculated plot.

2.2.9.3. Influence of relative humidity of the storage air on shear properties of pharmaceutical powders

In this experiment a relative humidity (RH) of 35, 45, 53 and 76 % was employed. The powder samples were stored in triplicate in each RH for 24 hours. The storage and measurement temperature was maintained at 20 ± 3 °C. During analysis a relative humidity of 42 ± 0.3 % was maintained. The parameters of operation derived from the evaluation of the shear tester were used in this work. In addition, the experiment was randomised to exclude systematic errors.

2.2.10. CRITICAL ORIFICE DIAMETER

The critical orifice diameter was evaluated using the Flotest® tester (Copley Scientific Limited, Nottingham, UK). The instrument consisted of a stainless steel cylinder of 7.6 cm in height and an inner diameter of 5.7 cm (outer diameter of 6 cm) with an approximate capacity of 200 ml. Starting with the 16 mm disc, 150 ml of powder was introduced into the cylinder through the funnel with the shutter in place. The powder was levelled carefully using a spatula to ensure uniform powder bed surface. The shutter was opened after 30 seconds (to allow for any possible formulation of flocs). The test was deemed positive if the powder flowed through the hole leaving an upside – down truncated cone in the cylinder (rathole - like). The process was repeated (using fresh powder) by increasing the size of the disc hole until a positive result was obtained. For the powders that were positive first time when the 16 mm disc was used, smaller discs were used until the smallest disc to give a positive result was obtained. The test was repeated three times using the disc above that which gave no flow.

2.2.11. FRACTIONATION OF THE POWDERS

The Alpine Air Jet Sieve (Alpine, Augsburg, Germany) was used to prepare two different size fractions for α-lactose monohydrate and pregelatinised starch. Size fractions of <56 μm and >56 μm were prepared for the two powders. Calcium carbonate was not fractioned due to its small particle size (mean particle diameter of 12 μm), and the needle shape of the microcrystalline cellulose powder particles would require a slotted sieve to achieve defined size fractions. Using the 56 μm sieve, 40 grams of the powder was sieved for 40 minutes. The fractions in the sieve and on the filter (in the lower part of the instrument) were collected separately. This procedure was repeated to obtain about 1.5 kg of each powder fraction.

2.2.12. PREPARATION OF SATURATED SOLUTIONS FOR MAINTAINING SPECIFIED RELATIVE HUMIDITIES

At a given temperature air has the ability to take up water vapour until it is saturated. On raising the temperature the air can up more moisture if water is available. Relative humidity (%) may be defined as:

$$RH = \frac{Partial\ pressure\ of\ water\ vapour\ in\ the\ air}{Vapour\ pressure\ of\ water\ vapour\ in\ air\ saturated\ at\ the\ same\ temperature} \times 100$$

Saturated salt solutions were use to maintain the specific relative humidities in closed chambers.

Saturated salt solutions were prepared by adding distilled water to the salt of interest in a desiccator, ensuring that a large amount of excess of salt remained at the bottom of the desiccator. The solution was stirred for about 15 minutes. The quantity of salt and water used depended on the solubility of the salt and the final solution volume required. The desiccator was covered with the lid having some grease at the underside of the rim to

ensure an air-tight sealing. The saturated solution was left to equilibrate for twenty four hours prior to use at 20 °C.

2.2.13. STATISTICAL DATA PROCESSING

SPSS 11.0 for Windows (SPSS Inc., Woking, Surrey, England) software package was employed for all the statistical data analysis and Microsoft Excel for Microsoft Windows XP Professional (Microsoft Corp., WA, USA) was used for the statistical analysis of data obtained during the shear testing to derive the optimum operational parameters of the Peschl shear tester. In addition, the effect of moisture and the sensitivity of the instrument to changes in the powder particle size were also assessed statistically. Other uses without claiming completeness include the comparison of the packing properties of the powders.

CHAPTER THREE

RESULTS AND DISCUSSION

3.1 CHARACTERISATION OF POWDERS

Powder characterisation is a core element or rather an integral part in powder technology as all materials must have been in one form of solid or another. For instance in the pharmaceutical industry, much attention is directed towards characterisation of powders be it during formulation or better still, prior to processing as solid-handling properties of a bulk mass are influenced by any factor that can have an effect on the interpaticulate interactions of powder particles (Howard, 2002). The importance of solid-handling properties, especially flow properties cannot be overemphasised, as this property impacts on the tabletting and encapsulation processes. These dosage form manufacturing processes require the flow of powder materials from a stage container to filling stations, such as tablet dies or capsule fillers (Howard, 2002). In the manufacture of solid dosage forms such as capsules, the filling of capsules using tamp filling machines relies on the measurement of volume by the dosing disc. Powder flowability needs to be accurately evaluated to ensure a smooth and efficient manufacturing operation so as to achieve tablets and capsules with uniform fill weights.

In this study, the characteristics that were deemed to be important with respect to powder flow were investigated. These are particle size, particle shape, particle outer surface morphology, apparent particle density, surface area, surface rugosity, water loss, equilibrium moisture content and bulk density. Though other characteristics exist, these are outside the scope of this work and will not be investigated.

3.1.1. SCANNING ELECTRON MICROSCOPE IMAGES

Images of the powder particle morphology were produced using the scanning electron microscopy (SEM) with a view to gaining a visual impression of the external surfaces of the particles. This is quite useful as the angle of internal friction is dependent on surface properties. SEM does not have any statistical power as the observed sample fraction was selected under considerable subjective bias and should not be relied upon as a representative of the sample population.

Figures 3.1 – 3.8 *SEM images of the powders in 294 and 978 – fold magnification (Pregelatinised starch, α-lactose monohydrate and MCC 105) and 2935 and 4892 – fold magnification (Precipitated calcium carbonate)*

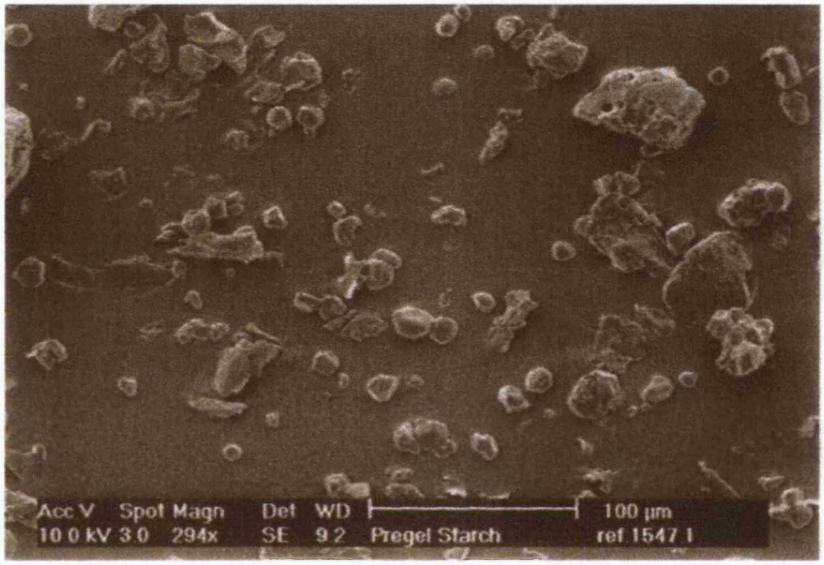

(a)

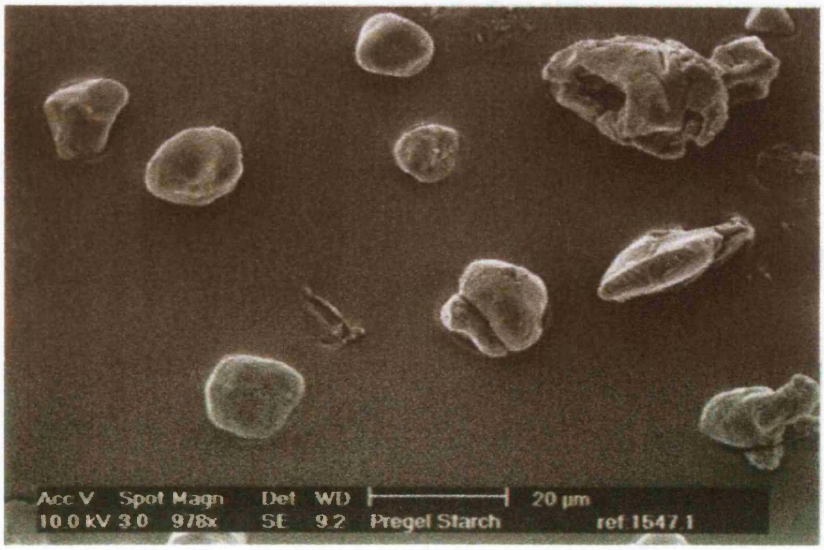

(b)

Figure 3.1 *Pregelatinised starch (a) 294 – fold magnification (b) 978 – fold magnification*

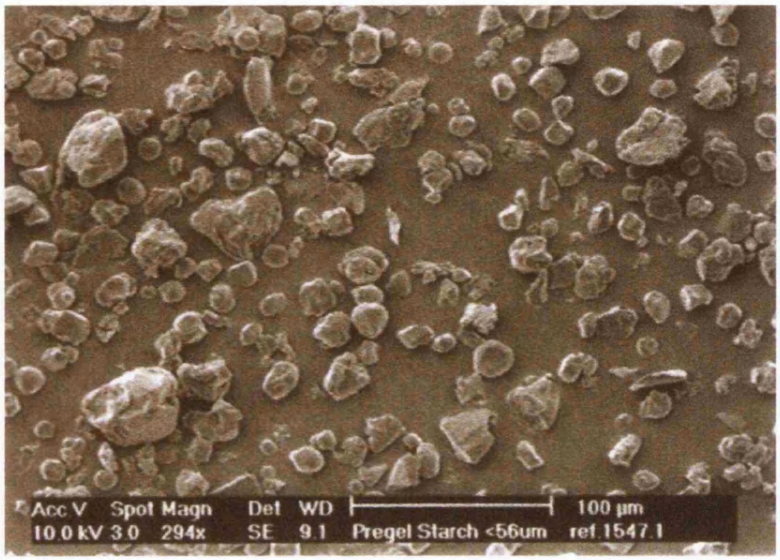

(a)

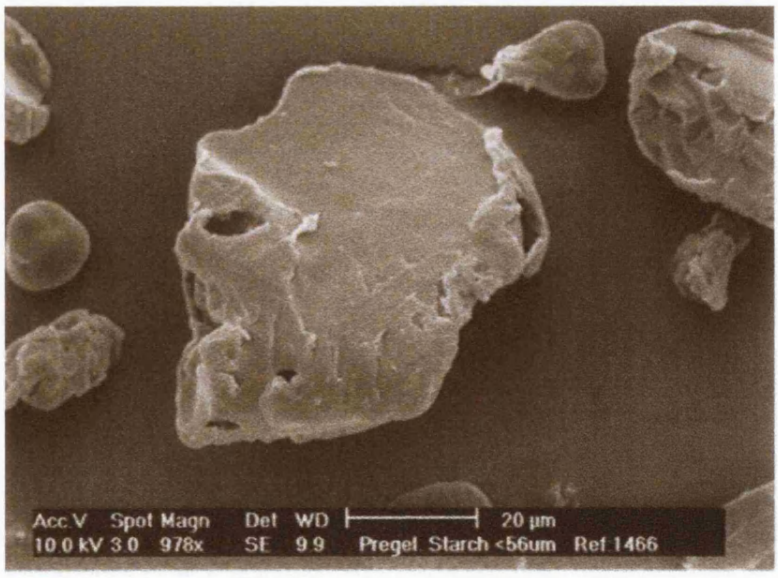

(b)

Figure 3.2 *Pregelatinised starch < 56 µm (a) 294–fold (b) 978-fold magnification*

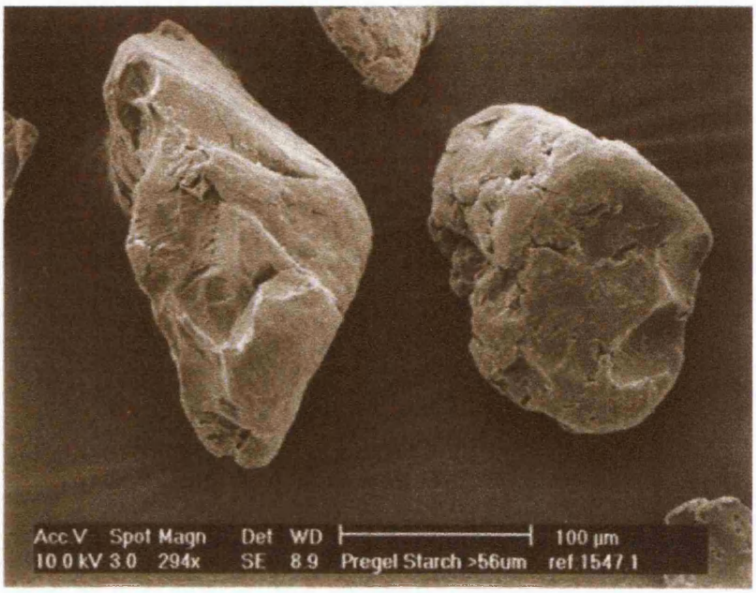

(a)

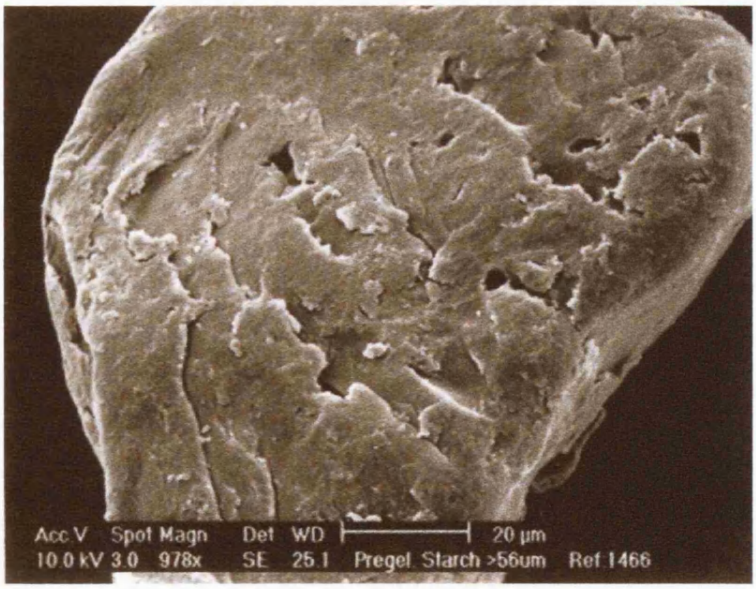

(b)

Figure 3.3 *Pregelatinised starch > 56 µm (a) 294–fold (b) 978-fold magnification*

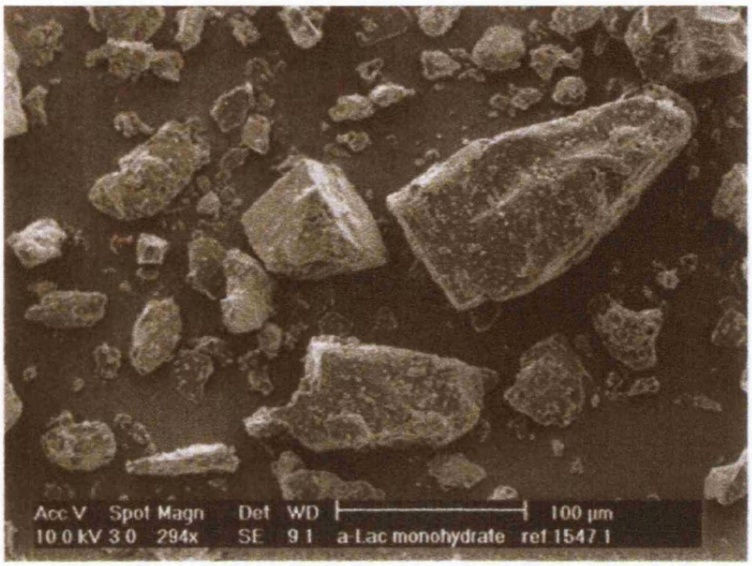

(a)

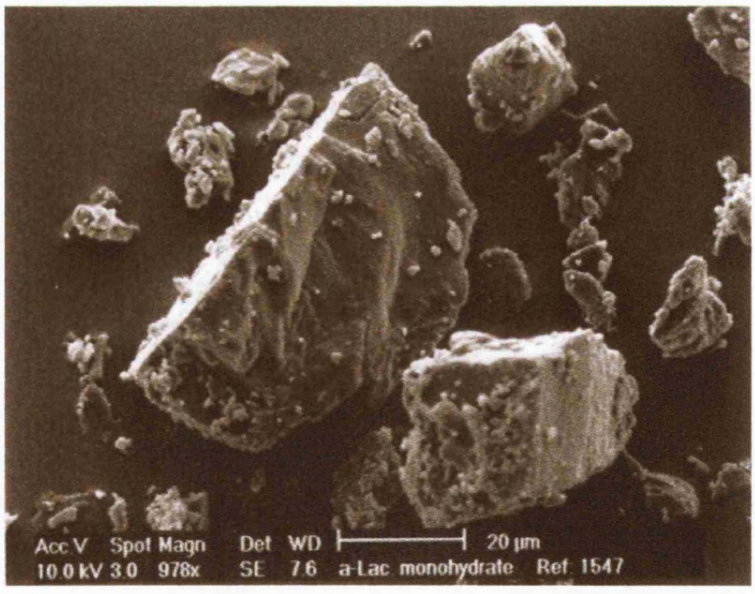

(b)

Figure 3.4 *α – lactose monohydrate (a) 294 – fold magnification (b) 978 – fold magnification*

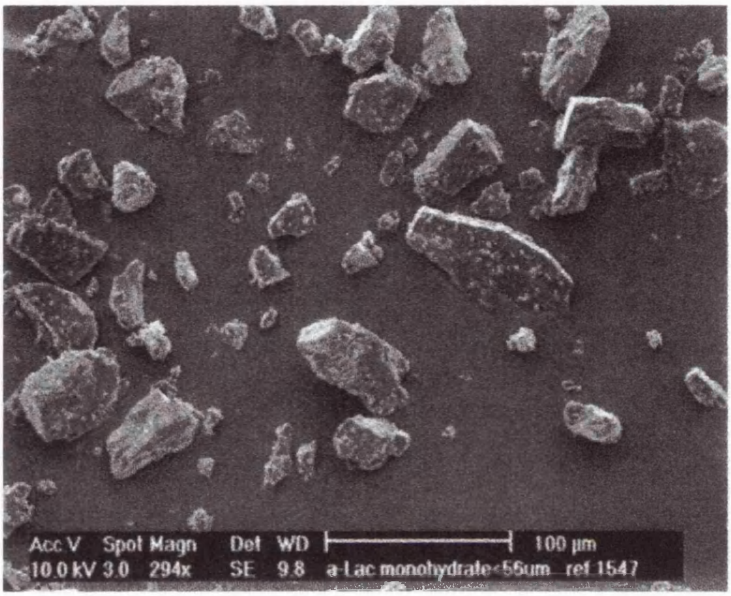

(a)

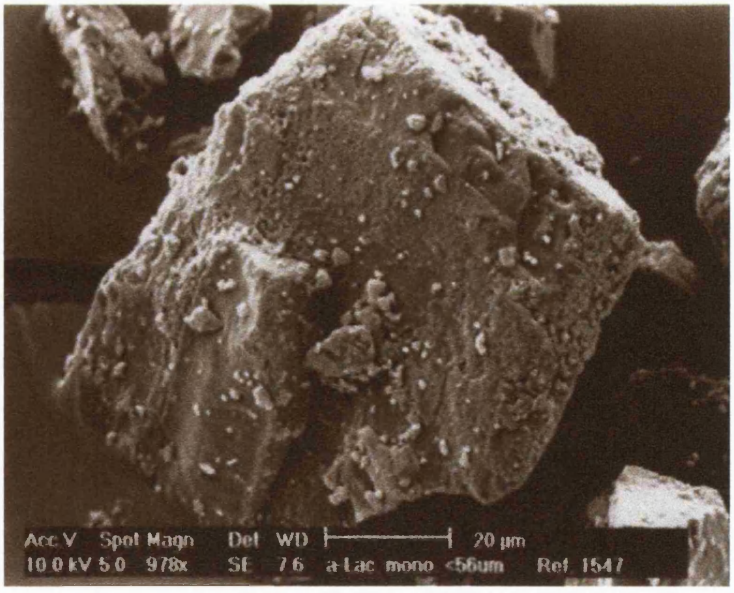

(b)

Figure 3.5 *α – lactose monohydrate < 56 µm (a) 294-fold (b) 978–fold magnification*

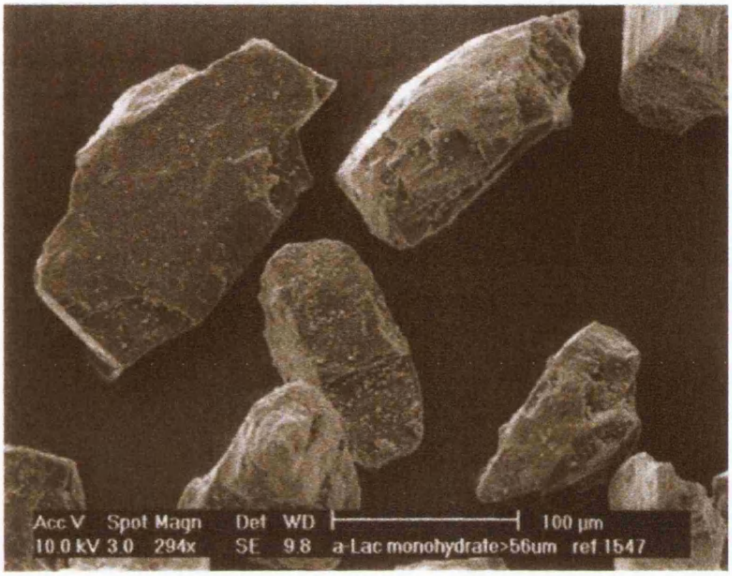

(a)

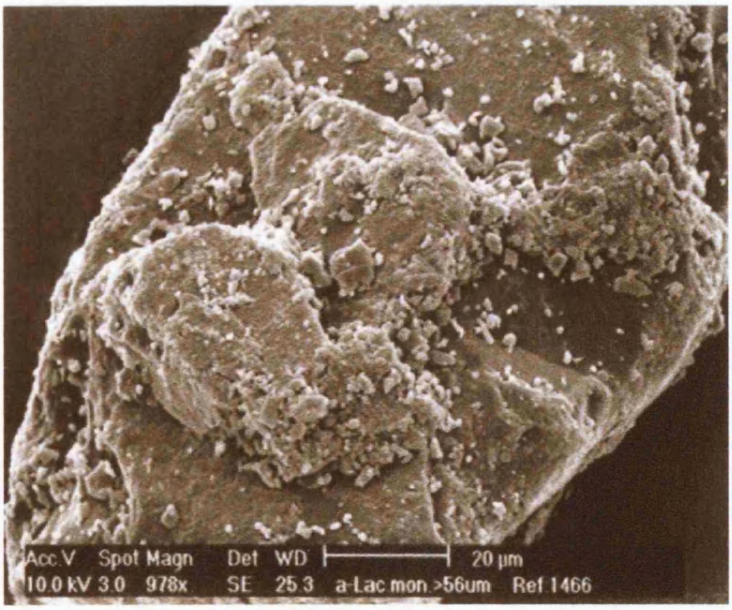

(b)

Figure 3.6 *α – lactose monohydrate > 56 µm (a) 294-fold (b) 978 – fold magnification*

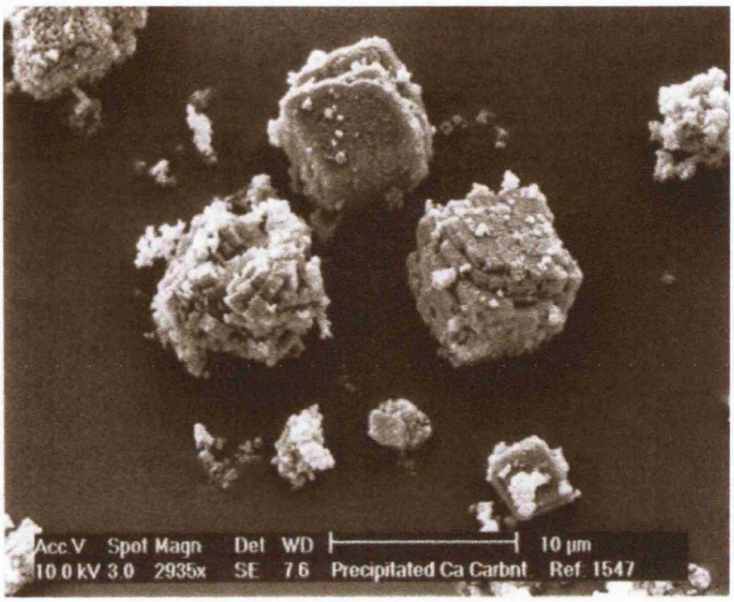

(a)

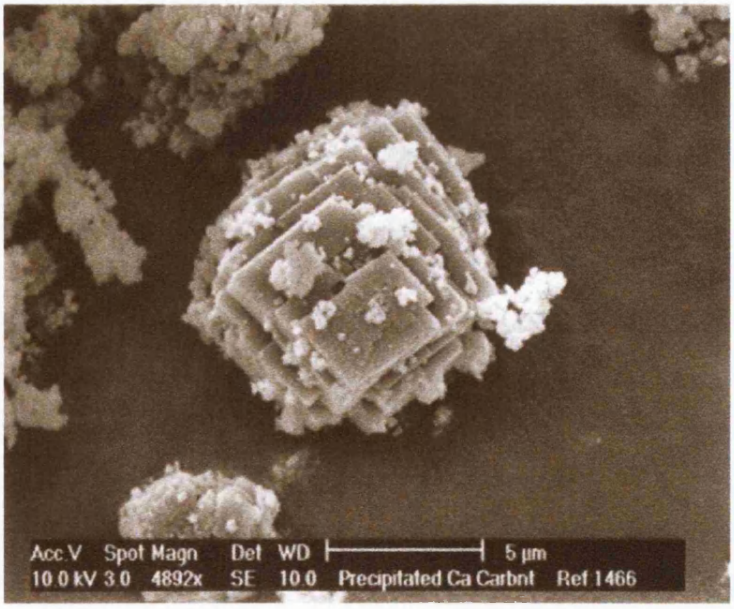

(b)

Figure 3.7 *Precipitated calcium carbonate (a) 2935-fold (b) 4892 –fold magnification*

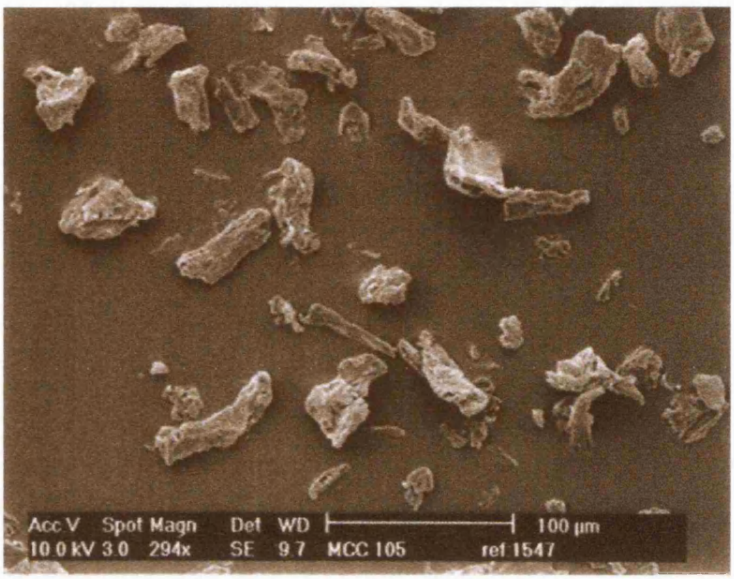

(a)

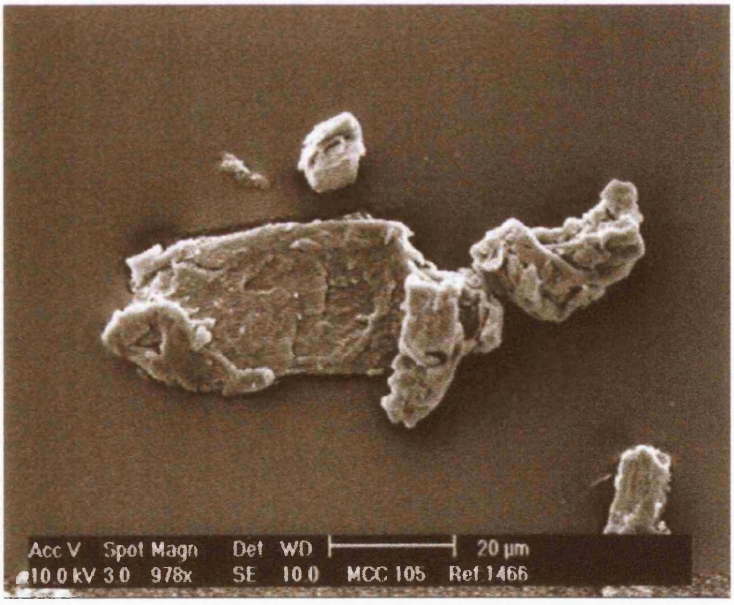

(b)

Figure 3.8 *Microcrystalline cellulose type 105 (a) 294-fold (b) 978 –fold magnification*

With the exception of precipitated calcium carbonate, an image of 294 and 978 –fold magnification is shown for each powder, which provides a picture of several individual particles, and higher magnification of the surface of the particles respectively.

Scanning electron micrographs show that both the particle shape and size of pregelatinised starch vary (Figure 3.1), with some particles having angular or rounded shape. In addition, the particle surfaces vary, with some having smooth surfaces and, some possessing slightly rough surfaces. The presence of deformed/ruptured particles as shown in Figure 3.1b may be attributed to the elevated temperature encountered during the pregelatinisation process (Bolhuis and Chowhan, 1996). The low magnification scanning electron microscopy micrographs of pregelatinised starch < 56 μm (Figure 3.2a) show again the varied particle size and shape. While most of the particles are found as individuals, fused particles can also be observed. The surfaces of the particles appear smooth under low magnification, but higher magnification shows that some have smooth to rough/ruptured-like surfaces (Figure 3.2b).

Figure 3.3 shows the SEM micrographs of pregelatinised starch > 56 μm. The magnification chosen was not adequate to ensure better observation of particle size and shape distribution. Hence, the micrograph presented above (Fig. 3.3a) is not a true representation of the powder population. The magnification chosen is to aid in the comparison of the powders considered with the exception of calcium carbonate which required a higher magnification due to the very small particle size. Figure 3.3b shows a higher magnification of the pregelatinised starch particles, and it can be seen that the surface of the particles are not smooth and some pores are evident. These pores may actually account for the lower apparent particle density (1.467 g/cm^3) obtained in contrast to that of pregelatinised starch < 56μm particles (1.480 g/cm^3, see Table 3.5).

The images of α–lactose monohydrate (Figure 3.4a and b), show that lactose possesses a heterogenous size distribution. A closer view (Figure 3.4b), indicates that the lactose particles were angular in shape with rough surfaces. These rough surfaces may impact on powder flow, as it is generally known that rough particle surfaces enhance particle-particle

interaction, and hence, impair powder flow. It can also be observed, that very fine particles are strongly adhered to the surfaces of the larger particles, which adds further to the surface roughness of this powder.

Scanning electron micrographs of α – lactose monohydrate < 56 μm are shown in Figure 3.5a and b. Figure 3.5a illustrate that α – lactose monohydrate < 56 μm particles are angular in shape and the particle size is heterogeneous. A higher magnification (Figure 3.5b) revealed that not only are the particles angular, but the bigger particles still have adhered particles on the already less smooth surfaces, as observed earlier.

Figure 3.6a – b illustrates SEM of α – lactose monohydrate > 56 μm. The shape and surface of the particles are similar to that of α – lactose monohydrate < 56 μm (Figure 3.5a – b). In addition, the particles exist in more or less individual states with smaller sized particles still firmly attached to the surfaces. Hence, although the two size fractions are obtained by air-jet sieving, the fine particles have not been removed. This is a clear documentation of the adhesion strength between the fine and coarse particles.

Scanning electron micrographs show that the calcium carbonate particles consist of plate like arrangements that confer a cuboid-like structure to the particles. The sizes of the particles are varied and a higher magnification (Fig. 3.7b), reveals that smaller particles are attached to the bigger particles. In addition, the entire surface of each particle is uneven due to the protuberances/edges of the plate-like arrangement that makes up each particle.

The scanning electron micrographs of microcrystalline cellulose type 105 (Figure 3.8) show that the shape of the particles is somewhat varied with some possessing elongated or rod-like shape and others angular shape. The majority of particles shown (Figure 3.8a) though tend to have an elongated shape. The particle surfaces as illustrated in Figure 3.8b appear rough. This surface attribute and shape may impact on powder flow.

3.1.2. PARTICLE SIZE AND SIZE DISTRIBUTION

The particle size analysis was carried out by laser diffraction using a Malvern Mastersizer. This method makes use of particle dispersions as opposed to agglomerates and hence, might provide a better characterisation. The mean and standard deviation of the median volume [D (v, 0.5)] particle size distribution are listed in Table 3.1.

***Table 3.1**: Mean particle size and standard deviation of 5 observations*

Powder	Particle size (μm)	Std. dev. (n = 5)
Pregelatinised starch	29.4	0.5
Pregelatinised starch < 56 μm	33.5	0.7
Pregelatinised starch > 56 μm	109.1	1.3
α - lactose monohydrate	34.4	0.2
α - lactose monohydrate < 56 μm	43.7	1.0
α - lactose monohydrate > 56 μm	119.4	0.9
Precipitated calcium carbonate	9.9	0.2
Microcrystalline cellulose 105	26.9	0.6

From Table 3.1 it can be seen that α – lactose monohydrate > 56 μm has the largest mean particle size (119.4 μm) closely followed by pregelatinised starch > 56 μm with a mean particle size of 109.1 μm. Pregelatinised starch, pregelatinised starch (< 56 μm) and α – lactose monohydrate possess similar mean sizes of 29.4, 33.5 and 34.4 μm, respectively. However, their particle densities vary considerably (see Table 3.5). According to Howard (2002), larger particles flow faster than smaller particles, and with relatively small particles, the flow through an orifice may be restricted because the interparticulate forces between the particles may enhance the formation of bridges. It should be noted that having a larger particle size does not necessarily confer good flow behaviour, as other factors such as particle shape or even the particle size of the powder particles may impact on powder flow by blocking the orifice.

3.1.3. PARTICLE SHAPE

The particle shapes of the powders were assessed using an image analyser attached to a microscope via a black/white CCD-4 camera. The particle shape affects flow and packing properties of powders (Martin, 1993).

Table 3.2 *Shape of particles*

Powder	Shape	Mean Aspect Ratio	Mean Shape Factor
Pregelatinised starch	parallelogram	1.33 ± 0.28	7.52 ± 0.46
α – lactose monohydrate	parallelogram	1.41 ± 0.34	7.49 ± 0.51
Precipitated calcium carbonate	irregular	1.29 ± 0.25	11.59 ± 0.44
Microcrystalline cellulose 105	parallelogram	1.77 ± 0.59	7.31 ± 0.47

Table 3.2 summarises the particle shape of the powders. The aspect ratios of the powders, defined as the ratio between the largest Feret diameter and its perpendicular (Podczeck, 1997) are also shown. MCC 105 has the highest aspect ratio, indicating that this powder consists of mainly elongated particles, which is supported by the visual observation (see Figure 3.8a and b for the scanning electron micrograghs). On the other hand, precipitated calcium carbonate has the smallest aspect ratio. The geometric shape assessed as shape factor indicates that pregelatinised starch, α – lactose monohydrate and microcrystalline cellulose 105 have parallelogram-like shape, as the values of the shape factor range from 7.0 – 8.0. The shape factor of calcium carbonate indicates that the powder particles have irregular shape, as the shape factor is greater than 10.

3.1.4. SURFACE AREA

The surface areas of the powders were evaluated by employing gas adsorption technique, which is based on the Brunauer-Emmett-Teller theory (Brunauer *et al.,* 1938). The knowledge of the surface area is very crucial in powder technology and is required in every powder handling process, as powders with high surface area have been linked generally with poor powder flow. The surface area of each powder was measured in triplicate.

Table 3.3 shows the surface areas of the powders. As can be seen from Table 3.3, the surface area of precipitated calcium carbonate is the largest (2.855 m^2/g), with pregelatinised starch > 56 μm having the smallest surface area. The surface area value of 0.327 m^2/g obtained for pregelatinised starch varies from that cited (0.26 m^2/g) in the literature (Newman *et al.*, 1996; Rowley, 2003).

Table 3.3 *Surface area (m^2 /g) of each powder determined by gas adsorption*

Powder	Mean	Std. dev. (n = 3)
Pregelatinised starch	0.327	0.005
Pregelatinised starch < 56 μm	0.433	0.012
Pregelatinised starch > 56 μm	0.174	0.003
α – lactose monohydrate	0.332	0.005
α – lactose monohydrate < 56 μm	0.437	0.006
α – lactose monohydrate >56 μm	0.221	0.006
Microcrystalline cellulose Type 105	1.807	0.010
Precipitated calcium carbonate	2.855	0.020

This could be attributed to either sampling error or according to Bolhuis and Chowhan (1996), changes in particle size distribution during handling. The surface area of microcrystalline cellulose type 105 is larger than that of pregelatinised starch despite the little difference in particle size as determined by Malvern mastersizer. This distinct difference may be due to the rough surface texture of the microcrystalline cellulose type 105 particles as indicated by SEM.

3.1.5. APPARENT PARTICLE DENSITY

The apparent particle density was determined using the helium-pycnometer, which is a non-destructive method. The accuracy of this technique is limited to the degree to which the fluid (helium) can penetrate the pores. The apparent densities shown are the mean values of five observations and their standard deviations (see Table 3.4).

From Table 3.4 it can be concluded that precipitated calcium carbonate having the smallest median particle size (9.9 μm) has the largest apparent density (2.794 g/cm^3), and pregelatinised starch > 56 μm has the smallest apparent density (1.467 g/cm^3) and an average median particle size of 109.1 μm. Another observation is the marked difference between particle densities of the smaller and the larger size fractions.

Table 3.4 *Mean apparent density and standard deviations of 5 observations per powder*

Powders	Density (g/cm^3)	Std. dev. (n = 5)
Pregelatinised starch	1.510	0.005
Pregelatinised starch < 56 μm	1.480	0.001
Pregelatinised starch > 56 μm	1.467	0.003
α – lactose monohydrate	1.549	0.005
α – lactose monohydrate < 56 μm	1.513	0.000
α – lactose monohydrate > 56 μm	1.507	0.001
Microcrystalline cellulose Type 105	1.623	0.007
Precipitated calcium carbonate	2.794	0.016

This difference may be attributed to the presence of inaccessible pores or voids in the bigger size fractions in contrast to the smaller size fractions having dense structures. The value (1.549 g/cm^3) obtained for α – lactose monohydrate agrees with 1.535 g/cm^3 obtained by Berlin *et al.*, (1971) using the same method i.e. helium displacement method.

3.1.6. RUGOSITY

The rugosity or surface roughness values of the pharmaceutical powders and powder particle fractions are shown in Table 3.5.

Table 3.5 lists the rugosity of all the powders and the size fractions. The theoretical surface area was calculated according to the shape of the powder particles. In this work the shape of the particles was assumed to be spherical, as the Malvern data (particle size analysis) is based on the model of a sphere. For the estimation of the theoretical or hypothetical surface

area, the median diameter of each powder was used to calculate the radius (converted to meters) and used in the formula for the area of a sphere. This was also adopted to obtain the volume of each particle (volume of a sphere). The density of each powder particle was converted into kg/m^3 to aid in the determination of the particle weight, and hence the number of particles in one gram of the powder was detemined.

Table 3.5 *Rugosity*

Powder	**Hypothetical surface area (m^2/g)**	**Rugosity**
Pregelatinised starch	0.135	2.417
Pregelatinised starch > 56 μm	0.037	4.637
Pregelatinised starch < 56 μm	0.121	3.575
α – lactose monohydrate	0.112	2.946
α - lactose monohydrate > 56 μm	0.033	6.588
α – lactose monohydrate < 56 μm	0.090	4.811
Microcrystalline cellulose Type 105	0.137	13.137
Precipitated calcium carbonate	0.216	13.150

This was multiplied with the surface area of a particle to obtain the hypothetical surface area. The ratio of the measured surface area to the hypothetical gave the rugosity values.

In Table 3.5, pregelatinised starch powder has the lowest rugosity value indicating that the particles have smoother surfaces or in otherwords are more rounded than the particles of the other powders. This is supported by the SEM (see Figure 3.1). Surprisingly it would have been expected that the pregelatinised starch fractions would give similar rugosity value to the original powder. The difference may be attributed to the handling process i.e. the sieving process, which may have caused particle surface attrition, ultimately leading to less smooth particle surfaces. A similar trend could be observed for α – lactose monohydrate and its size fractions. Brittain et al., (1991b) found that handling materials (i.e. sieving, tumbling and forcing through a mesh screen) before its analysis strongly influenced an experimentally determined particle size distribution. Precipitated calcium carbonate has the highest rugosity value; suggesting irregularly shaped powder particles or rather unsmooth

particle surfaces. This value is a true reflection of the powder particles as the SEM supports this (see Figure 3.7). Robertson and Emödi (1943) found that the closer the rugosity value is to unity, the more rounded are the powder particles. This has an implication on powder flow. In general, the greater the interparticulate interaction due to increased surface roughness, the greater is the hinderance on powder flow i.e. the more cohesive the powder will be. According to Carr (1970), powder particles exhibiting irregular shapes have many points of contact as edges, corners, and ragged asperities, and as such tend to have many effective surface forces.

3.2. MOISTURE CONTENT

The moisture content of the model powders after storage in desiccators for 24 hours at 45% relative humidity was determined using the 'TGA 2950' *Thermogravimetric Analyser* (TGA). The moisture content of the powders and powder fractions after storing under various humidity conditions was measured prior to shear cell analysis using a halogen Moisture Analyser. The hygroscopicity of the model powers was investigated using the Dynamic Vapour Sorption.

3.2.1. MOISTURE CONTENT DETERMINED BY TGA

The TG – curves are shown in Figures 3.9a – d and the moisture content obtained using the TGA and halogen moisture analyser are presented in Tables 3.6a – b.

Figures 3.9a – d illustrate the weight – loss curves (TG–curve) and their derivatives (DTG-curve) as a function of temperature for the four model powders. For pregelatinised starch (see Figure 3.9a), there was a steady loss in water on increasing the temperature up to 200 °C. The moisture content value of 9.52 % obtained for pregelatinised starch is similar to the 9.48 % obtained by Gohil (2002) and also agrees with the 8 to 9 % obtained by Newman *et al.,* (2001) using the same method. According to Bolhuis and Chowhan (1996), the total moisture content of α – lactose monohydrate is about 5. 2 % and about 0.2 % of this value constitutes the free moisture. In Figure 3.9b, it can be seen that the initial water loss at a temperature less than 100 °C is not substantial and may account for the free moisture most likely due to loss of crystal water.

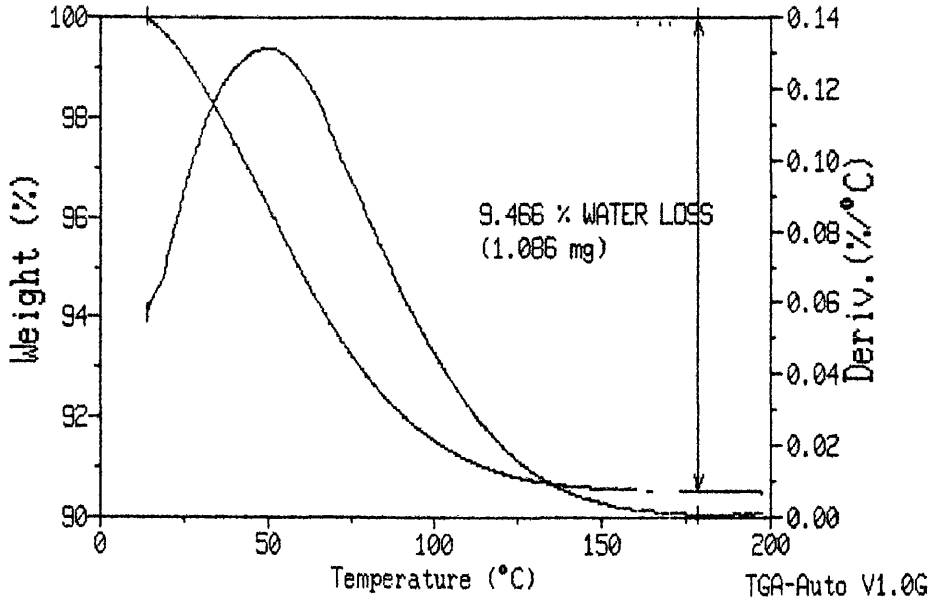

Figure 3.9a *TG – curve of pregelatinised starch*

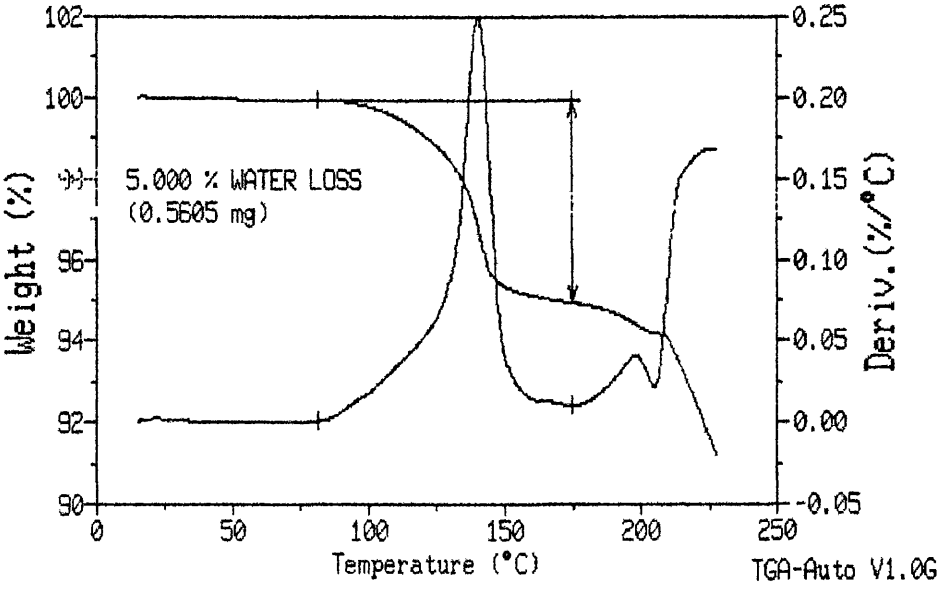

Figure 3.9b *TG – curve of α – lactose monohydrate*

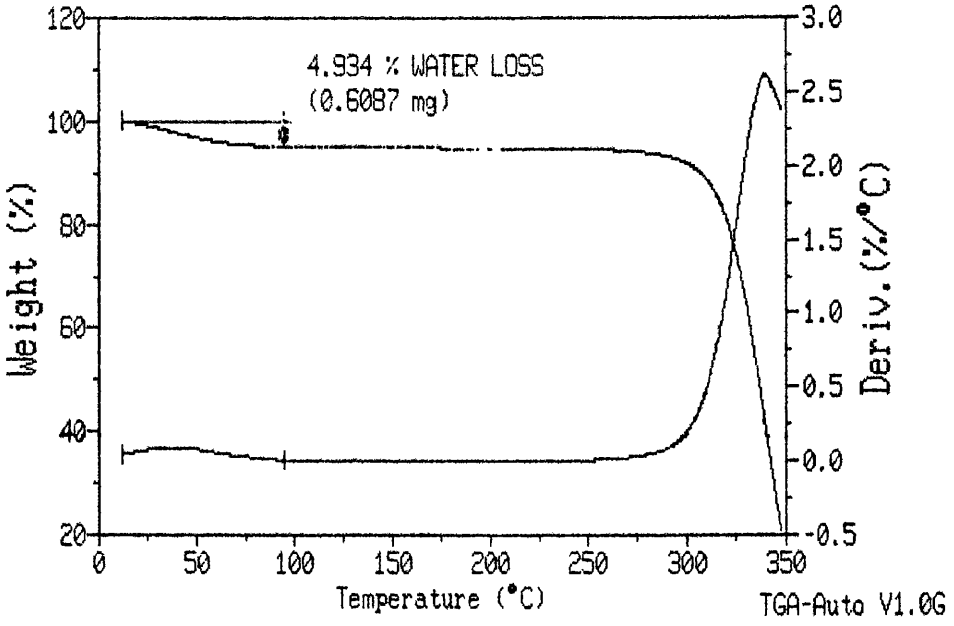

Figure 3.9c *TG – curve of MCC 105*

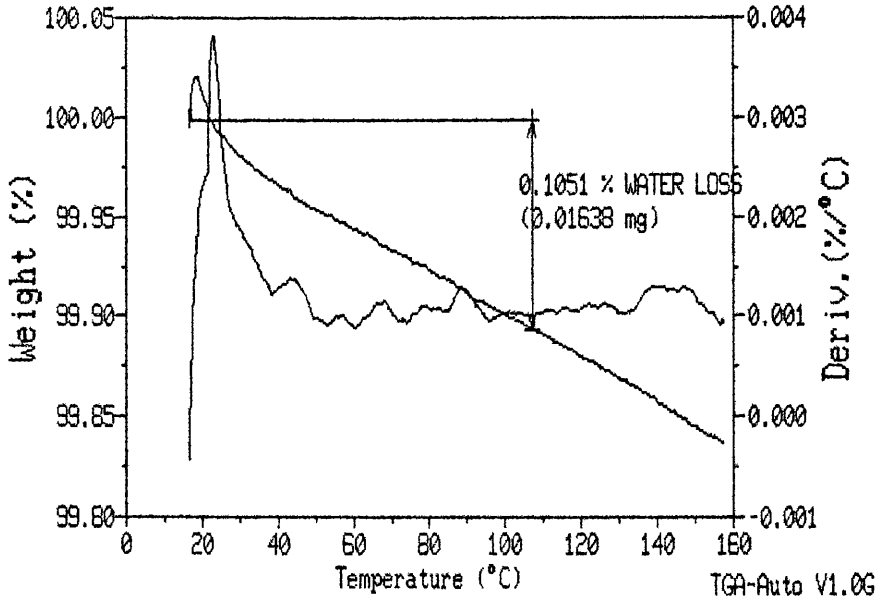

Figure 3.9d *TG – curve of precipitated calcium carbonate*

Increasing the temperature beyond 100 °C led to a substantial moisture loss. The TGA curve indicates that the crystal structure of α – lactose monohydrate used in this research was indeed a monohydrate. The moisture content for α – lactose monohydrate using this technique was 5.01 %, this agrees with that of the aforementioned authors.

The moisture content of calcium carbonate was 0.1 %, which agrees with the value 0.2 % obtained by Tan and Newton (1990a). It must be pointed out that these investigators dried the powder to constant weight in a vacuum oven. It is right to say that calcium carbonate contained very little free water and no bound water, unlike α – lactose monohydrate with little free, but substantial amounts of bound water. The moisture content of microcrystalline cellulose was 4.92 %. This value agrees with that stipulated (less than 5% w/w) by Weller (2003). Most of the water will be within the porous structure of microcrystalline cellulose and a large proportion of this bound moisture is expected to be hydrogen-bonded to molecules of cellulose within the particle (Bolhius and Chowan, 1996).

Table 3.6a *Moisture contents as determined by Thermogravimetric analysis (TGA)*

POWDERS	MOISTURE CONTENT (%)
Pregelatinised starch	9.52 ± 0.05
α – lactose monohydrate	5.01 ± 0.02
Microcrystalline cellulose 105	4.92 ± 0.06
Precipitated calcium carbonate	0.10 ± 0.00

3.2.2. MOISTURE CONTENT AS DETERMINED BY HALOGEN MOISTURE BALANCE

Table 3.6b lists the moisture content of the powders after exposing them to different relative humidity of air for 24 hours.

The value obtained for pregelatinised starch, precipitated calcium carbonate and microcrystalline cellulose type 105 compares to those obtained using the thermogravimetric analyser – TGA (see Table 3.6a). The halogen moisture analyser detects no water of crystallisation as opposed to the TGA, hence, the low value observed for α – lactose monohydrate (Table 3.6b).

Table 3.6b *Moisture contents as determined by Halogen moisture analyser*

Powder	Moisture content at different RH (%)			
	35	45	53	76
Pregelatinised starch	8.03 ± 0.04	8.20 ±0.04	8.18 ± 0.02	8.33 ± 0.11
α – lactose monohydrate	0.10 ± 0.02	0.11 ± 0.01	0.11 ± 0.01	0.11 ± 0.02
Precipitated calcium carbonate	0.10 ± 0.02	0.11 ± 0.01	0.11 ± 0.01	0.12 ± 0.00
Microcrystalline cellulose 105	4.78 ± 0.04	4.91 ± 0.02	4.99 ± 0.02	5.14 ± 0.01
Pregelatinised starch (> 56 μm)	8.29 ± 0.02	8.64 ± 0.09	8.92 ± 0.02	9.35 ± 0.02
Pregelatinised starch (< 56 μm)	9.45 ± 0.01	9.51 ± 0.06	9.75 ± 0.08	9.95 ± 0.13
α – lactose monohydrate (> 56 μm)	0.09 ± 0.01	0.09 ± 0.01	0.09 ± 0.01	0.10 ± 0.00
α – lactose monohydrate (< 56 μm)	0.10 ± 0.00	0.11 ± 0.01	0.09 ± 0.01	0.12 ± 0.02

Despite this limitation, the simplicity of the technique i.e. moisture determination using a halogen moisture analyser, made it a favourable option, especially for in-process control prior to shear experiments.

3.2.3 EQUILIBRIUM MOISTURE CONTENT

The hygroscopicity of the powders was evaluated using Dynamic Vapour Sorption. The relative humidity (RH) ranged from 25 – 85 % and the temperature of the incubator was set to 25 °C. The sorption – desorption isotherms are illustrated graphically in Figures 3.10a – d. The amount of water sorbed by the powders is here expressed in terms of mass change at equilibrium and the amount of water sorbed termed equilibrium moisture content. The sorption-desorption curves (Figures 3.10a - d) for the powder samples are quite similar as there was a progressive increase in water sorbed on increasing the relative humidity.

The type of isotherm exhibited by the powder samples is similar to that of a Type III isotherm. From 3.10a it can be seen that pregelatinised starch sorbed more moisture than the rest of the powders and the magnitude of the hysteresis is larger in the range of 30 – 80 % RH. This observation agrees with that of Newman *et al.,* (1996) and Wurster *et al,* (1982). Microcrystalline cellulose type 105 as shown in Figure 3.10d sorbed more moisture than α – lactose monohydrate and precipitated calcium carbonate.

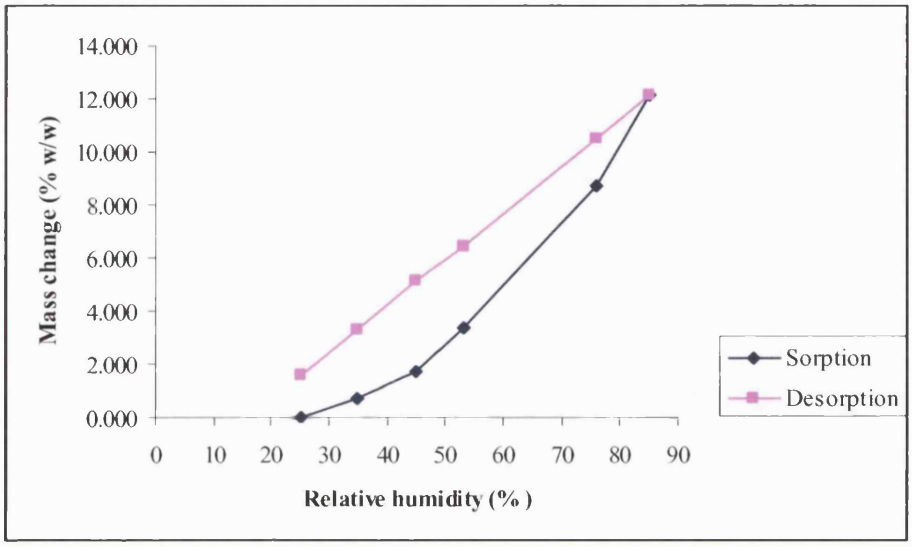

Figure 3.10a *Moisture sorption-desorption isotherm for pregelatinised starch*

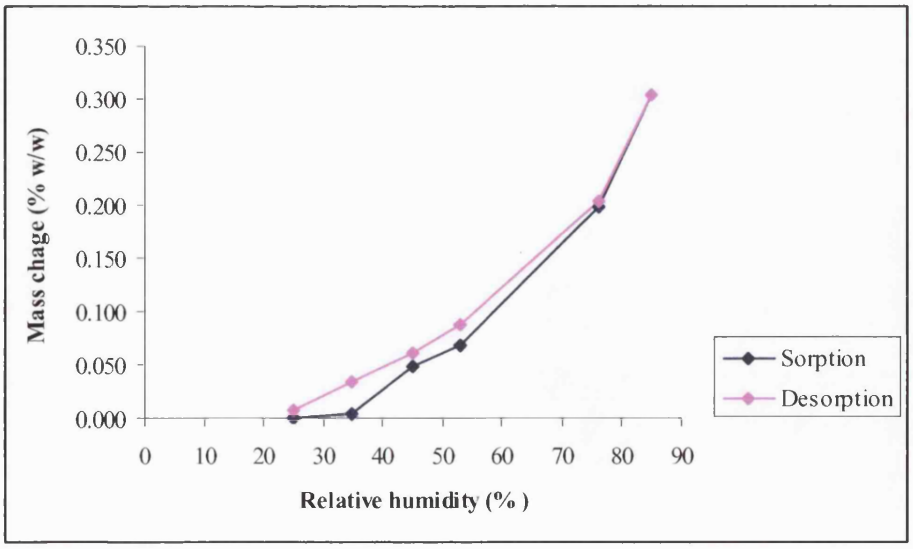

Figure 3.10b *Moisture sorption-desorption isotherm for α –lactose monohydrate*

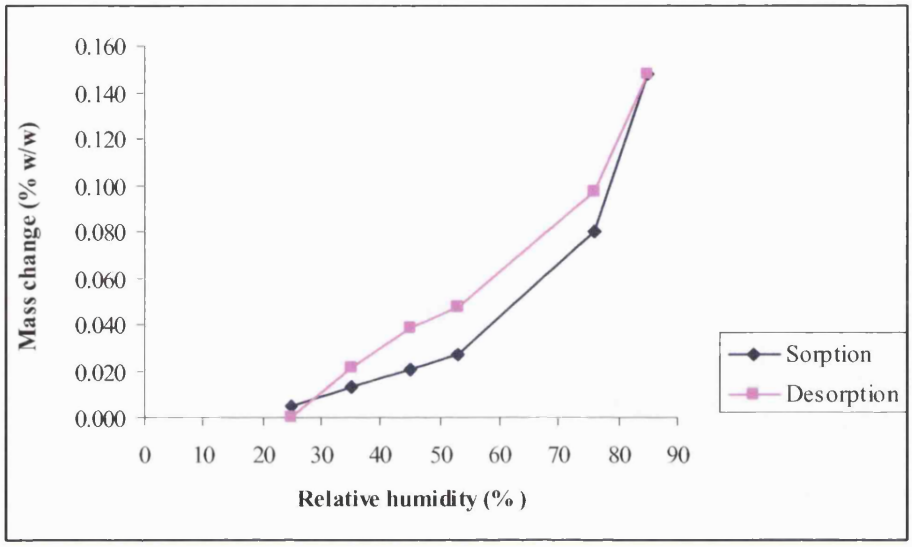

Figure 3.10c *Moisture sorption-desorption isotherm for precipitated calcium carbonate*

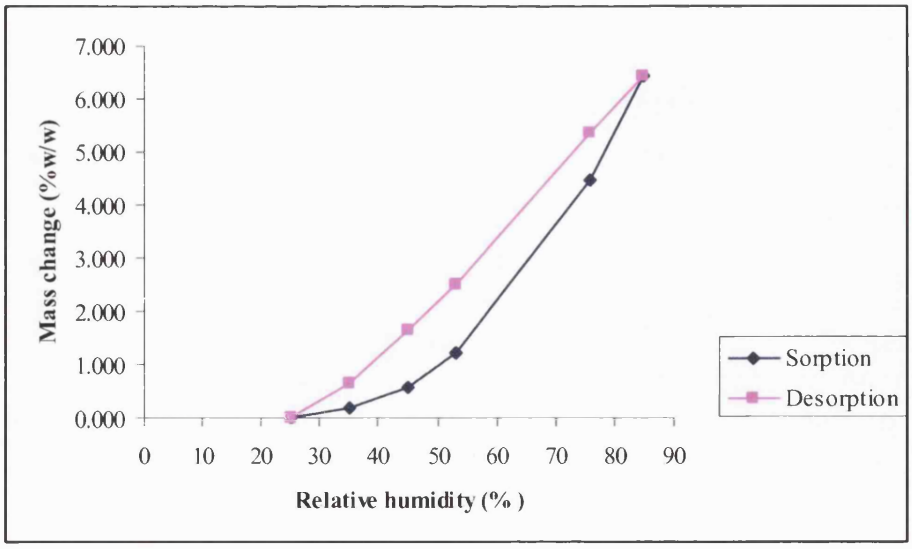

Figure 3.10d *Moisture sorption-desorption isotherm for microcrystalline cellulose Type 105*

Here calcium carbonate sorbed the least amount of moisture. This is hardly surprising as calcium carbonate is hydrophobic in nature and the total amount sorbed (about 0.2 %) agrees with that obtained by Tan and Newton (1990a). It should be noted that the samples were not dried prior to analysis as drying may have an impact on the structural/chemical form of the powders (Madichie, 2003).

However, adsorption of moisture depends on the initial moisture content of the samples, and hence reproducibility of these results is impaired. Nevertheless, this approach appeared more useful as it coincided with the use of the powder in the experiments and in general during handling.

3.3 STATIC AND DYNAMIC POWDER PACKING

The packing characteristics during tap consolidation are widely used to evaluate the flow properties of powders, as both packing and flow are dependent on the friction between the particles during sliding and rearrangement (Podczeck, 1998). This test enables the comparison of different powders in terms of their flowability. In this work, the dynamic packing profile was used to evaluate the powder density (as a function of number of taps) using the Mohammadi and Harnby model (1997) and the angle of internal flow (Varthalis and Pilpel, 1976). The Carr's compressibility index (Carr, 1965) was calculated from the minimum and maximum densities for each powder.

3.3.1 MINIMUM AND MAXIMUM BULK DENSITY

Figures 3.11a – f show the relationship between the powder bulk densities as a function of number of taps.

The graphical illustrations presented (Figures 3.11a – f) represent the trend of the powder densities during tapping. The differences in the method of tapping i.e. slow and fast tapping technique are well pronounced in the early tapping phase. In Figure 3.11a it can be seen that there was rapid densification in the early stages i.e. before 100 taps, followed by a gradual increase in the densities and finally the attainment of constant tapped density values.

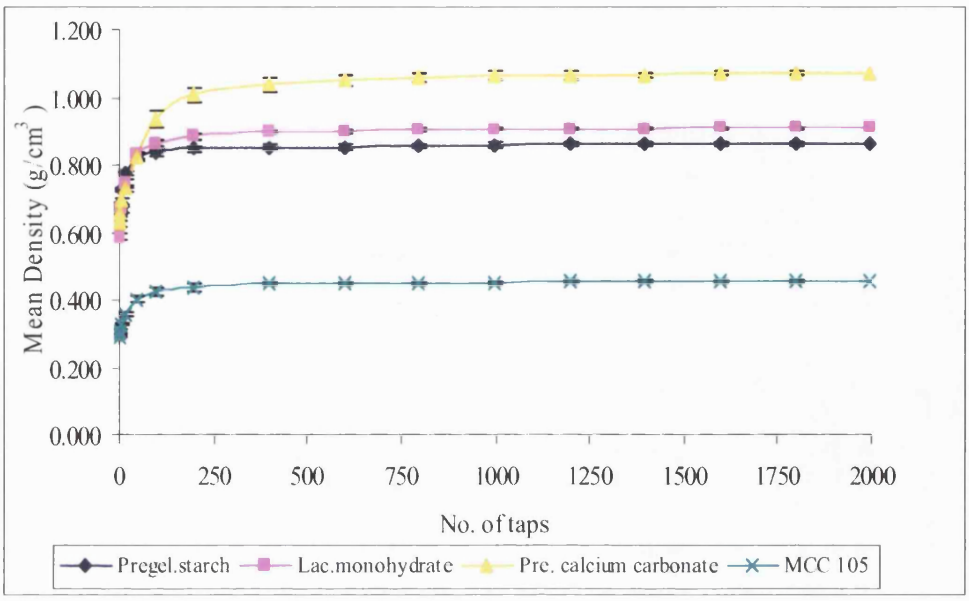

Figure 3.11a *Measured density as a function of number of taps for powders using slow tapping technique*

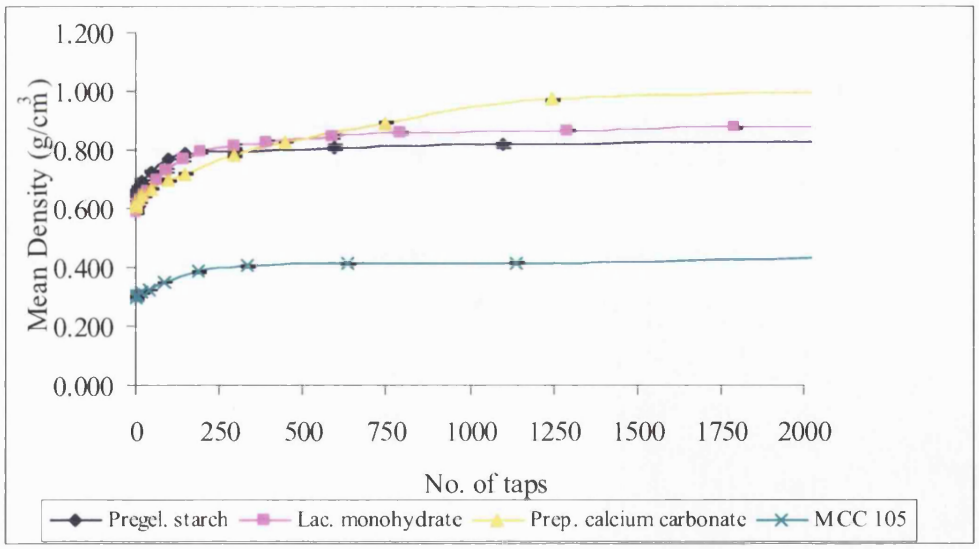

Figure 3.11b *Measured density as a function of number of taps for powders using fast tapping technique*

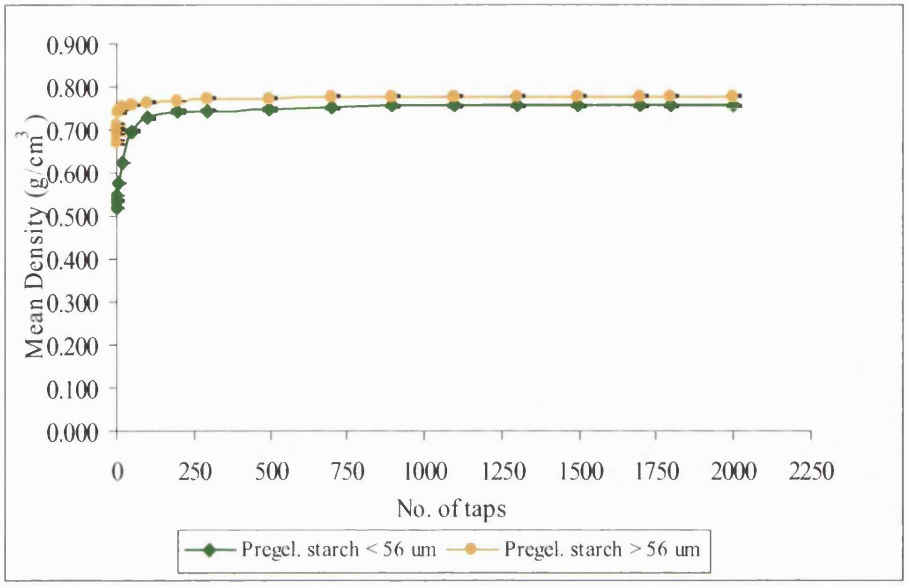

Figure 3.11c *Measured density as a function of number of taps for Pregelatinised starch size fractions using slow tapping technique*

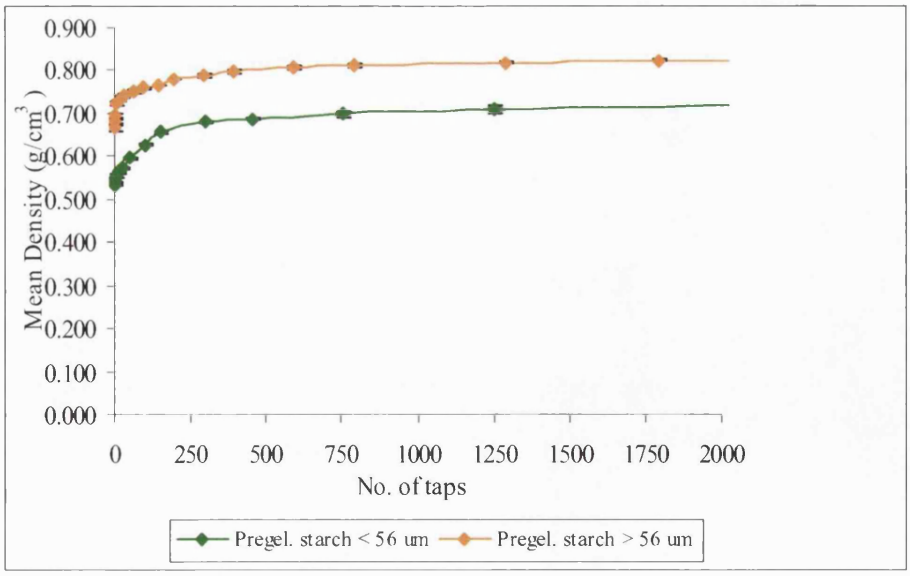

Figure 3.11d *Measured density as a function of number of taps for Pregelatinised starch size fractions using fast tapping technique*

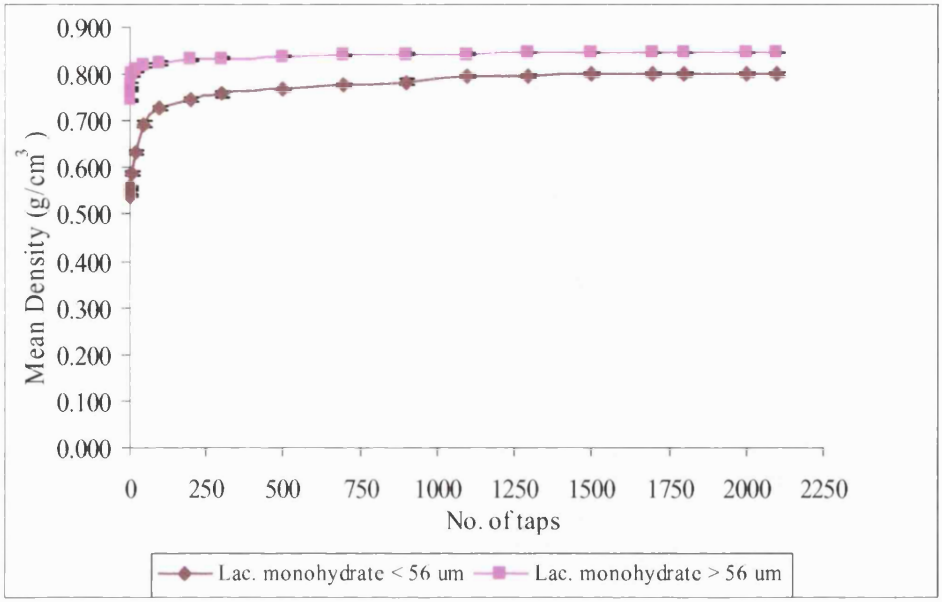

Figure 3.11e *Measured density as a function of number of taps for α – lactose monohydrate size fractions using slow tapping technique*

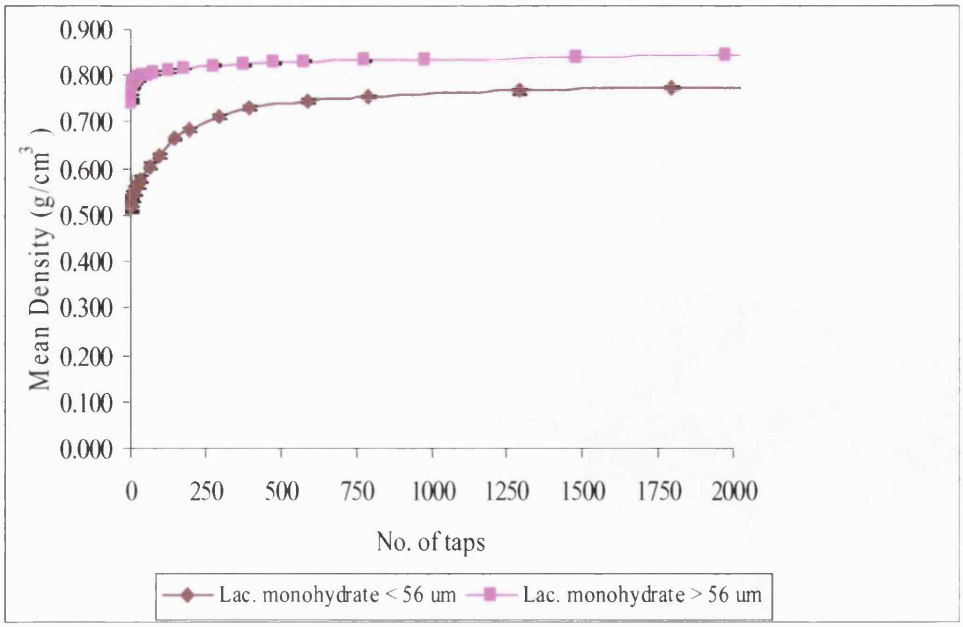

Figure 3.11f *Measured density as a function of numberof taps for α – lactose monohydrate size fractions using fast tapping technique*

In contrast, when the four pharmaceutical powders were subjected to fast tapping (see Figure 3.11b), the densification was slower at the early stages and even slower subsequently without attaining constant tapped density values. In Figure 3.11a, the densities of the four pharmaceutical powders after just about 100 taps were found to be more than that obtained at tappings higher than 500 taps on using the BP/EP method in Figure 3.11b (fast tapping technique).

Continous tapping in excess of 2000 did not yield constant tapped density values (see Fig. 3.11b). During slow tapping, the particles were able to re-arrange themselves so that the smaller particles fill the void spaces between the large ones, thereby creating a dense packing (Abdullah and Geldart, 1999). This has an implication for in-process control where much emphasis is placed on working effectively (obtaining reliable and reproducible results at cost effective time). Podczeck and Sharma (1996) concluded that due to high speed of the tapped density volumeter, redispersion of the powder particles occurs instead of closer packing. The workers attributed this to the vibration-like tapping action compared to clear fall of the cylinder when using the slow tapping device. In this respect, Abdullah and Geldart (1999) reported that the Hosokawa powder tester with a fall height of 25 mm, which is similar in operation to the Jencons tap volumeter (used for the slow tapping) gave more accurate bulk density measurements than when the Copley tap volumeter with a fall height of 3 mm was used. This according to the authors could be attributed to the weak in-built tapping mechanism hence, rendering the Copley volumeter unsuitable for assessing the flowability of powders as the tapping provided cannot sufficiently overcome the interparticulate forces in cohesive powders.

The curves of the four pharmaceutical powders are distinct from each other on using the slow tapping technique (see Figure 3.11a), with calcium carbonate having the highest mean density and MCC type 105 having the lowest. Having the lowest bulk density does not indicate best powder flow as the bulk density of a powder is not useful in evaluating the flow of powders (Carr, 1965). The only effect bulk density has is on powder compressibility and according to Carr (1965), the more compressible a powder is the less free flowing is the powder and vice versa. The bulk density of a powder is not a single

definite number; rather it is any of several values (Carr, 1965) and is dependent on both the physical characteristics of the constituent particles of the powder and the method of packing the particles within a prescribed volume (Harnby et al., 1987). The curves of the powders with the exception of MCC 105 overlapped at the initial stage of densification when the fast tapping technique was used.

Figures 3.11c and d illustrate the curves of the pregelatinised starch size fractions using the slow and fast tapping technique, respectively. It can be seen in both plots that pregelatinised starch > 56 μm has the higher density value regardless of the number of taps. Similarly, the curves obtained when the slow tapping technique was used are similar to that obtained for the four pharmaceutical powders using the same technique. The reason remains the same. The bigger size fraction also attained the dense packing structure earlier than the smaller size fraction. The reason may be the smaller amount of fines which could not ensure the alteration of the primary structure, hence no rearrangement of the particles as such (Abdullah and Geldart, 1997).

In Figures 3.11e and f, the same observation as seen for pregelatinised starch size fractions could be observed for α – lactose monohydrate size fractions. There is not much difference between the aerated and the tapped density of the bigger size fraction of lactose monohydrate. This is not a surprise as repeated tappings were not able to dislodge the adhered fines on the surfaces of the bigger particles to aid the alteration of the structure/packing. When using the slow tapping device, the difference between the minimum and maximum bulk density is highest for precipitated calcium carbonate. This can be attributed to the finer/smaller particle size. The smaller the particle size the longer it takes the powder to attain its maximum bulk density. Prior to tapping, smaller size particles are able to form stable powder bridges depending on the level of interparticulate forces present. If the forces are strong as in the case of calcium carbonate, then a greater effort is required to overcome these forces. Hence, there is a higher number of taps necessary, which leads to a higher maximum bulk density.

Table 3.7 Packing properties using slow tapping technique

	CALCULATED			MODEL				
POWDER	D_o	D_f	C (%)	D_o	D_f	C (%)	T	A.I.F
PS	0.650 ± 0.005	0.859 ± 0.007	24.4 ± 0.4	0.660 ± 0.005	0.852 ± 0.008	22.6 ± 0.4	19.1 ± 0.3	18.0 ± 0.5
α-LM	0.587 ± 0.010	0.907 ± 0.003	35.3 ± 1.0	0.597 ± 0.009	0.898 ± 0.005	33.4 ± 0.8	28.6 ± 1.9	16.6 ± 0.2
PCC	0.626 ± 0.009	1.068 ± 0.007	41.4 ± 0.6	0.644 ± 0.007	1.060 ± 0.011	39.2 ± 0.5	83.0 ± 7.1	44.7 ± 0.4
MCC 105	0.291 ± 0.004	0.454 ± 0.006	35.9 ± 1.7	0.298 ± 0.005	0.450 ± 0.006	33.7 ± 1.9	41.6 ± 7.3	61.6 ± 0.5
PS > 56 µm	0.669 ± 0.003	0.778 ± 0.002	13.7 ± 0.9	0.678 ± 0.007	0.770 ± 0.002	11.9 ± 0.8	6.3 ± 0.9	22.5 ± 0.2
PS < 56 µm	0.519 ± 0.002	0.755 ± 0.001	31.2 ± 0.3	0.529 ± 0.005	0.749 ± 0.002	29.4 ± 0.4	32.3 ± 0.5	25.1 ± 0.1
α-LM > 56 µm	0.744 ± 0.003	0.847 ± 0.001	12.1 ± 0.3	0.754 ± 0.009	0.837 ± 0.002	9.5 ± 0.3	13.1 ± 2.8	19.1 ± 0.1
α-LM < 56 µm	0.539 ± 0.003	0.802 ± 0.006	32.8 ± 0.2	0.552 ± 0.005	0.784 ± 0.005	29.6 ± 0.1	55.1 ± 1.8	22.3 ± 0.4

PS – Pregelatinised starch

LM – Lactose monohydrate

PCC – Precipitated calcium carbonate

MCC 105 – Microcrystalline cellulose type 105

Calculated – experimental bulk densities values obtained

Model – fitted values deduced from the Mohammadi and Harnby (1997) model, D_o - minimum/aerated/initial bulk density, D_f - maximum/tapped/final bulk density, C (%) – Carr's compressibility index, T – Compaction constant, *A.I.F* – Angle of internal flow.

Table 3.8 Packing properties using fast tapping technique

	CALCULATED			MODEL				
POWDER	D_a	D_f	C (%)	D_a	D_f	C (%)	T	A.I.F
PS	0.643 ± 0.004	0.864 ± 0.007	25.5 ± 1.0	0.657 ± 0.004	0.839± 0.008	21.7 ± 0.7	121.6 ± 2.9	17.9 ± 0.4
α-LM	0.584 ± 0.006	0.913 ± 0.006	36.0 ± 0.2	0.603 ± 0.006	0.887± 0.005	32.1 ± 0.4	183.6± 12.2	16.5 ± 0.4
PCC	0.608 ± 0.001	1.026 ± 0.005	40.8 ± 0.3	0.626 ± 0.002	1.041± 0.005	38.3 ± 0.4	604.4 ± 2.7	47.4 ± 0.3
MCC 105	0.296 ± 0.003	0.479 ± 0.004	38.2 ± 0.9	0.306 ± 0.003	0.456± 0.004	33.0 ± 0.9	369.1± 18.2	59.6 ± 0.3
PS > 56 µm	0.666 ± 0.007	0.834 ± 0.002	20.1 ± 1.0	0.705 ± 0.006	0.819± 0.003	13.9 ± 0.8	211.9 ± 19.5	19.5 ± 1.0
PS < 56 µm	0.533 ± 0.001	0.765 ± 0.001	30.4 ± 0.2	0.549 ± 0.003	0.738± 0.006	25.6 ± 0.2	247.3 ± 11.0	25.8 ± 0.9
α-LM> 56 µm	0.742 ± 0.004	0.863 ± 0.001	14.1 ± 0.4	0.775 ± 0.004	0.850± 0.003	8.8 ± 0.8	265.9 ± 24.6	19.4 ± 1.1
α-LM< 56 µm	0.518 ± 0.014	0.822 ± 0.002	37.0 ± 1.7	0.535 ± 0.014	0.793± 0.002	23.5 ± 0.00	251.3 ± 32.1	32.5 ± 1.7

See Table 3.7 for abbreviations.

The differences in the values of the minimum and maximum bulk densities are a result of the changes in the packing arrangements of the powder particles, which are due to the differences in the shapes, density, rugosity, size, and size distribution of the particles (Varthalis and Pilpel, 1976). Other workers such as Hamby et al., (1987) also stipulated that the variation could be due to variation in surface roughness, porosity and specific gravity.

3.3.2 CARR'S COMPRESIBILITY INDEX

According to Carr (1965), the percentage compressibility indirectly provides a picture of uniformity in size and shape, deformity, surface area, moisture content and cohesiveness of powders. Hence, the index provides a very important flow characteristic. The more compressible a powder is, the less flowable it will be, or in other words, the less compressible a powder, the more flowable it is.

The compressibility values of the powders using the slow and fast tapping technique are shown in Tables 3.7 and 3.8. α – lactose monohydrate has the lowest value and according to the index has a good flowability. Precipitated calcium carbonate has the highest value, hence, an extremely poor flow. The flow behaviour of the remaining powders ranges from fair to poor flow.

With regards to the technique used, the order of decrease in compressibility using the slow tapping technique (calculated values) is precipitated calcium carbonate > MCC 105 > α - lactose monohydrate > α - lactose monohydrate (< 56 μm) > pregelatinised starch (< 56 μm) > pregelatinised starch > pregelatinised starch (> 56 μm) > α-lactose monohydrate (> 56 μm). In contrast, the order of decrease using the fast tapping technique is calcium carbonate > MCC 105 > α - lactose monohydrate (< 56 μm) > α - lactose monohydrate > pregelatinised starch (< 56 μm) > pregelatinised starch > pregelatinised starch (> 56 μm) > α-lactose monohydrate (> 56 μm). The reason for the difference has already been discussed. However, it must be pointed out that such a change in ranking order would severely influence the choice of excipients in a formulation problem. The difference could mean failure or success in the extremes. The value (about 24.4 %) obtained for pregelatinised

starch (Table 3.7) is similar to that (26.7 %) obtained by Podczeck and Newton (1999). The reason for the slight difference may be attributed to the difficulty in determining the minimum bulk density with reasonable accuracy (Podczeck and Newton, 1999) or sample preparation prior to analysis, or simply batch to batch variability.

Statistical evaluation did reveal a difference between the Carr's compressibility values of α - lactose monohydrate fine fraction and the unsieved powder ($p < 0.05$) when the slow tapping technique was used. There was also a significant difference between the larger size fraction of α-lactose monohydrate and the unsieved powder ($p < 0.05$) and also between the fine fraction and the large size fraction of α-lactose monohydrate powder ($p < 0.05$). This difference may be due to the presence of less fines in the large size fraction.The presence of more fines in the unsieved powder may have aided in the high densification and ultimately the high compressibility value observed. There was a statistical difference between the compressibility values obtained for the unsieved pregelatinised starch powder and the large size fraction of pregelatinised starch, between pregelatinised starch fine and the large size fraction ($p < 0.05$), and finally between unsieved pregelatinised starch powder and pregelatinised starch fine fraction ($p < 0.05$).

Statistical evaluation of the compressibility values obtained after the use of the fast tapping technique, revealed that a statistical difference exists between the unsieved pregelatinised starch powder and its size fractions ($p < 0.05$), and also between the size fractions themselves. However, a statistical difference was found between α – lactose monohydrate and the large size fraction, fine fraction and the large fraction of α – lactose monohydrate, but none was found between α – lactose monohydrate and the fine size fraction ($p > 0.05$).

3.3.3 ANGLE OF INTERNAL FLOW (θ)

The angle of internal flow was determined by the packing profile using the empirical equation by Varthalis and Pilpel (1976).

The lower the value of the angle of internal flow the better is the powder flow. Surprisingly, from Tables 3.7 and 3.8 α - lactose monohydrate should have a better flow than

pregelatinised starch using both slow and fast tapping technique. In addition, MCC 105 now has a very poor flow in contrast to the ranking obtained based on the Carr's index (with calcium carbonate having an extremely poor flow). Precipitated calcium carbonate having the highest surface area and the smallest particle size would have been expected to have the highest angle of internal flow, but mechanical interlocking caused by the needle-like fibrous shaped particles of MCC 105 may have encouraged the poor flow and hence, the largest angle of internal flow. The order of decrease in angle of internal flow is MCC 105 > calcium carbonate > pregelatinised starch (< 56 μm) > pregelatinised starch (> 56 μm) > α- lactose monohydrate (< 56 μm) > α-lactose monohydrate (> 56 μm) > pregelatinised starch > α- lactose monohydrate. There is a difference in the order of decrease of the angle of internal flow obtained when the fast tapping technique was used. In addition, there are differences in the values for θ obtained from slow and fast tapping. The ranking of α - lactose monohydrate (lowest value), calcium carbonate and MCC 105 (highest value) is similar for both techniques, while the ranking of the other powders differs. Though MCC 105 has a lower rugosity and surface area value than precipitated calcium carbonate, the particle shape may have contributed to the higher angle of internal flow observed. The change in ranking of the other powders may be due to the alteration of the powder particle surfaces due to the fast tapping motion, as particles were more likely to rub against each other, and hence cause particle surface attrition. The value of the angle of internal flow obtained (18.0°) for pregelatinised starch in this work (Table 3.7) differs greatly from that obtained by Podczeck and Newton (1999), who obtained about 37.7° for the angle of internal flow. This difference may be due to either batch to batch variability or the fact that in this work the powders were exposed to 45 % RH of air prior to analysis. This may have enhanced the lubricating properties of water and hence, may have ensured easy particle movement and ultimately a reduction in inter-particulate forces. Podczeck and Newton (1999) analysed the powder as received. Statistical evaluation of the angles of internal flow obtained after the use of the slow tapping technique revealed that a significant difference exists between pregelatinised starch powder and the fine fraction ($p < 0.001$), between pregelatinised starch and the large size fraction ($p < 0.001$), and even between the large and fine size fraction ($p < 0.001$). Similarly, a significant difference exists between α – lactose monohydrate and its size fractions ($p < 0.001$), and also between the size fractions ($p <$

0.001). This is hardly a surprise, as the powders do have different particle morphology as revealed by the SEM. In addition, the rugosity and surface area values indicate that the powders are all different, and hence will most likely have different flow behaviour as reflected by the angles of internal flow obtained. Using the fast tapping technique, similar results were obtained for α – lactose monohydrate when the angles of internal flow were analysed statistically (i.e $p < 0.05$). The reason remains the same. Statistical evaluation revealed that no difference exists between the angle of internal flow of unsieved pregelatinised starch powder and the large size fraction ($p = 0.092$). However, slight differences could be observed when the angles of internal flow of all the powders using the slow tapping technique were compared with those obtained using the fast tapping technique.

3.3.4 MOHAMMADI AND HARNBY MODEL

In Figures 3.11a – f all the powders exhibit the same trend with regard to bulk density. There is an initial stage of rapid consolidation followed by a slower rate stage. Tables 3.7 and 3.8 list the compaction constant, *T*. The ranking (not shown) of the powders as displayed by the compaction constant is different to the ranking obtained for the Carr's index. The only similarity is the ranking of calcium carbonate, having the largest value. The distinct ranking provided by the compaction constant, *T*, compared to that based on Carr's index may be advantageous. The values of *T* obtained using the fast tapping technique are much larger than those obtained from the slow tapping technique. This may be due to the smaller dropping distance/ fall height of the Copley volumeter (Abdullah and Geldart, 1999). In Table 3.7 the *T* value obtained using the slow tapping technique for pregelatinised starch powder is higher than that obtained for the fine fraction, but lower than that of the pregelatinised starch larger fraction i.e. > 56 μm size. The reason may be attributed to the particle size and size distribution. The larger size fraction densified faster because there was minimal or no fines and the bigger particles were able to reach their densest packing quickly as there was minimal particle re-arrangement. The more fine components, the slower was the rate of densification and, hence the tendency to go beyond the threshold value stipulated by Mohammadi and Harnby (1997). The same trend was observed for α - lactose monohydrate and the size fractions, and the reason remains the same. Statistical

analysis also revealed differences between the powders and their size fractions and also between size fractions ($p < 0.001$).

The use of fast tapping technique produced a different T value pattern for pregelatinised starch powder and its size fractions, and also between α – lactose monohydrate and its size fractions (see Table 3.8). Here pregelatinised starch powder densified faster than the fine and large size fractions. The same was noticed for α – lactose monohydrate and its size fractions. A statistical difference exists between the T value of pregelatinised starch powder and the fine fraction ($p < 0.001$), pregelatinised starch powder and the large size fraction ($p = 0.001$), but not between pregelatinised starch large and fine size fraction ($p = 0.068$). In the case of α – lactose monohydrate, statistical difference exists between α – lactose monohydrate and the large size farction ($p = 0.005$), between α – lactose monohydrate and the fine size fraction ($p = 0.430$), but not between the large and fine size fraction ($p = 0.567$). This result is not unexpected, as the rate of powder densification is affected by the tapping rate, which did not encourage proper particle rearrangement. Overall, the T value obtained for the two powders and size fractions using the fast tapping technique were much larger than than obtained using the slow tapping technique. These results suggest that the two powders and their size fractions did undergo slow rate of densification using the fast tapping technique. Calcium carbonate has the smallest particle size and is amongst other things the most cohesive of the powders considered for the tapping experiments. From Table 3.7 (slow tapping technique) it can be seen that it has a slow rate of densification and a mean T value above 35. Only, the remaining powders show a similar trend.

Mohammadi and Harnby (1997) suggested that the product of T and the minimum bulk density could be used to dissociate the effect of minimum density and to relate the T value better to the powder structure under compaction. The use of this relationship (the product), though not shown, did not lead to a major re-classification of the powders based on the T values. The value of T obtained for pregelatinised starch (Table 3.7) was about 19.1, which agrees with the 20.4 obtained by Podczeck and Newton (1999) on similar material.

3.4 CRITICAL ORIFICE DIAMETER

The results of the critical orifice diameter (COD), which is a direct method of assessing arch strength and powder cohesiveness of the model powders and the size fractions, are shown in Table 3.9. Although α – lactose monohydrate size fraction (>56 μm) has the largest median particle diameter (see Table 3.1), its critical orifice diameter is larger than that of pregelatinised starch size fraction (> 56 μm). As discussed before, there is a critical particle size to orifice ratio; if particles become too large they can block the orifice mechanically and the method looses its power in determining arch strength and flow. In addition, pregelatinised starch size fraction (> 56 μm) was observed to flow better than the rest of the powders, as the powder could flow through all the orifices (including the 4 mm) available without arching.

Table 3.9 *Critical orifice diameter (COD) of powders*

Powder	Weight of powder (g)	COD (mm)	Observation*
Pregelatinised starch	98.5 ± 0.0	26	CR
α – lactose monohydrate	85.5 ± 0.0	30	CR
Precipitated calcium carbonate	95.4 ± 0.0	28	CR
MCC 105	50.0 ± 0.0	30	RH
Pregelatinised starch (> 56 μm)	105.3 ± 0.0	≤ 4	F
Pregelatinised starch (< 56 μm)	73.1 ± 0.0	22	CR
α – lactose monohydrate (> 56 μm)	113.8 ± 0.0	5	CR
α – lactose monohydrate (< 56 μm)	77.6 ± 0.0	30	CR

* CR - collapsed rat hole
RH - rat hole
F - free flow

The particle shape of pregelatinised starch coupled with other factors may have enhanced the powder flow. Also from the result obtained, the precipitated calcium carbonate with the largest shape factor (Table 3.2), lowest particle size and largest apparent particle density (Table 3.4) flows better with a COD of 28 mm than MCC 105, α – lactose monohydrate and α – lactose monohydrate size fraction (< 56 μm). The critical orifice diameter obtained

for pregelatinised starch (26 mm) is comparable to the value (24 mm) obtained by Lee et al., (2000). The slight difference may be attributed to differences in standing time, the filling procedure, other operator-related variations of procedure (Lee et al., 2000), other powder characteristics and/or prevailing atmospheric conditions.

3.5 SHEAR AND FAILURE PROPERTIES

3.5.1 CALIBRATION OF FILL SIEVE

The results of the in-house calibration of the fill sieve are given in Table 3.10.

Table 3.10 *Acceleration of vibration (m/s^2)*

	Front - B		Side - A		Side - C	
Number	A_{mp}	H A_{eq}	A_{mp}	H A_{eq}	A_{mp}	H A_{eq}
0	1.34	0.81	0.62	0.36	1.67	0.81
1	4.57	3.09	3.54	2.42	3.54	2.34
2	5.68	3.93	7.41	4.73	4.21	2.95
3	8.91	6.23	9.66	6.83	8.71	6.02
4	11.80	8.31	12.30	8.71	11.80	8.41
5	13.60	9.22	14.10	9.88	13.80	9.66
6	16.90	11.60	17.10	12.10	17.10	12.10
7	18.40	12.80	18.60	12.70	18.60	13.30
8	19.70	13.80	19.70	13.60	19.90	13.90
9	21.60	15.10	21.10	14.60	21.60	15.10
10	22.60	15.80	22.60	15.40	22.90	15.80
11	24.50	16.90	24.20	16.60	24.50	16.70
12	25.10	17.50	24.80	16.70	24.80	16.90
13	26.30	17.90	25.70	17.30	26.00	17.50
14	27.20	18.40	26.00	17.50	26.30	17.90
15	27.80	18.60	26.60	17.70	27.20	18.40

A_{mp} – maximum peak acceleration

H A_{eq} – equivalent constant RMS acceleration for the entire measurement period

According to the instruction manual, the hand-arm vibration meter used is for indication purposes. The settings that correspond to low, intermediate and high acceleration of vibration are 4, 7 and 15. From Table 3.10, 4 corresponds therefore to a acceleration of

vibration of approximately 12.0 m/s^2, 7 to medium acceleration of vibration of 18.5 m/ s^2 and 15 to high acceleration of vibration of 27.4 m/s^2 (mean A_{mp} value). The three acceleration of vibration were used in studying the effect of acceleration of vibration on the flow properties of the pharmaceutical excipients.

3.5.2 ASSESSMENT OF PARAMETERS OF OPERATION OF THE PESCHL SHEAR TESTER

The operating parameters of the rotational split-level shear tester were evaluated by assessing the shear and failure properties of the four model powders (see Table 2.2.) for the experimental set up. The following definitions were adapted from the standard test method for measuring the shear stresses of powders using the Peschl rotational split-level shear tester (D 6682 – 01).

Preconsolidation load (PL) – This is the load applied to the test powder to de-aerate/densify the powder.

Consolidation step load (CSL) – This is the maximum load applied to the powder sample prior to execution of a yield locus.

Consolidation step time (CST) – This is the time employed for shearing under the consolidation normal stress until the shear stress reaches a maximum.

Shear step time (SST) – This is the time used for the shearing of the powder sample (after the consolidation step).

Expansion time of the powder during shear (ET) – This is the time allowed for powder expansion during shearing.

Preconsolidation time (PCT) – Time employed for the application of the normal stress (load) prior to testing.

Number of shear steps (NSS) – number of shear steps that is used to obtain the yield locus.

Standard deviation (SD) – standard deviation of the measured points from the calculated plot.

Sieve size (SS) – the size of the sieve (i.e. 1.1, 2.1 or 3.1 mm).

Acceleration of vibration (VS) – acceleration of vibration of the fill sieve (i.e. 12.0, 18.5 and 27.4 m/s^2)

In addition the following abbreviations will be used for the pharmaceutical powders:

PS – Pregelatinised starch

LM – lactose monohydrate

PCC – Precipitated calcium carbonate

MCC 105 – Microcrystalline cellulose type 105

Table 3.11 *Experimental set up for the rotational split-level shear tester (see text below for abbreviations)*

PL (g)	CSL (g)	CST (min)	SST (min)	ET (min)	PCT (min)	SS (mm)	NSS	VS (m/s^2)	SD (kPa)
1500	1500	2	2	1	8	2.1	6	18.5	0.029
600 2400	600 2400	2	2	1	8	2.1	6	18.5	0.029
1500	1500	1 3 5	2	1	8	2.1	6	18.5	0.029
1500	1500	2	1 3 5	1	8	2.1	6	18.5	0.029
1500	1500	2	2	0.5 2	8	2.1	6	18.5	0.029
1500	1500	2	2	1	4 10 12	2.1	6	18.5	0.029
1500	1500	2	2	1	8	1.1 3.1	6	18.5	0.029
1500	1500	2	2	1	8	2.1	5 10	18.5	0.029
1500	1500	2	2	1	8	2.1	6	12.0 25.0	0.029
1500	1500	2	2	1	8	2.1	6	18.5	0.020 0.049

3.5.2.1. Effect of acceleration of vibration and sieve size on failure and flow properties

Under this section, the effect of varying the acceleration of vibration of the fill sieve and sieve size will be considered. The fill sieve was used to eliminate lumps and agglomerates in powder samples and for ensuring uniform filling of the shear cell. The acceleration of vibration refered to in this section is the acceleration of vibration of the fill sieve. Three speed settings were considered i.e. 12.0 (low acceleration of vibration), 18.5 (intermediate acceleration of vibration) and 27.4 (high acceleration of vibration) m/s^2. The sieve sizes assessed were 1.1 (Fine - F), 2.1 (Intermediate - I) and 3.1 mm (Coarse - C).

The flow properties that were determined in this research using the rotational split-level shear tester were; angle of internal friction, effective angle of friction, flow function and normalised cohesion coefficient. The normalised cohesion coefficient is the value obtained after correcting the cohesion coefficient for the change in bed density (density of the consolidated powder in the shear cell) during a shear experiment (Podczeck and Wood, 2003). The former flow properties have already been defined (see Chapter One, section 1.5.3.2.1).

Angle of internal friction: The angle between the line (yield locus) joining the points obtained after consolidation of powder samples with the same pressure, but sheared under different load, gives the angle of internal friction. The angle of internal friction is also a measure of inter-particulate friction during shear.

The mean of the angle of internal friction (ϕ) obtained from three different yield loci using the same consolidation load, low acceleration of vibration (12.0 m/s^2) but different sieve size for the filling of the cell are illustrated graphically in Fig. 3.12a. The effect of using 18.5 and 27.4 m/s^2 acceleration of vibration with varying sieve sizes on the angle of internal friction is shown in Figures 3.12b and 3.12c, respectively.

The effect of acceleration of vibration and sieve size on powder failure properties was investigated for any statistical significance using "Univariate ananlysis of variance" (ANOVA). The statistical analysis revealed that a significant difference exists between the

angle of internal friction of the powders, as ANOVA calculated an F – value of 285.00 which corresponds to a $p < 0.001$ (Table 3.12). In addition, a statistical difference could be observed for the angle of internal friction considering the sieve size as influence factor. However, as seen from the table, there is an interaction between sieve size and acceleration of vibration i.e. the effect that sieve size has on the angle of internal friction depends on the acceleration of vibration employed and vice versa. The sieve size is hence not a true effect. Any interpretation has to be done under consideration of the other factors. A "post hoc test" (Scheffé) was applied to evaluate differences among the means. The Scheffé-test generated two subsets of sieve sizes (Table 3.13a) and shows that no significant difference exists between the angles of internal friction if a fine (1.1 mm)or coarse sieve (3.1mm) has been used.

From Figure 3.12b, it could be observed that the use of 18.5 m/s^2 acceleration of vibration promoted better distinction of the powders as opposed to when the 12.0 or 27.4 m/s^2 acceleration of vibration was used (Figures 3.12a and 3.12c, respectively). This diference may be attributed to the different packing exhibited by the powder. This was reflected in the bed densities of each powder in the cell (not shown) when subjected to low acceleration of vibration and different sieve sizes, where a variation in bed density values was observed. Microcrystalline cellulose type 105 gave in general the highest angle of internal friction (ϕ). Pregelatinised starch exhibited the lowest angle of internal friction (ϕ). Based on available data of powder surface area (Table 3.3), the order of increase of the angle of internal friction (ϕ) could be pregelatinised starch < α–lactose monohydrate < microcrystalline cellulose type 105 < precipitated calcium carbonate. It would have been expected that the surface area is related to the level of powder cohesiveness. This ranking, which also reflects the order of increase in the shape factors (see Table 3.2) is similar to the findings by Ridway and Rupp (1969). They reported that an increase in shape coefficient (criterion the workers used for the degree of departure of particle shape from spherical, which is the ratios of the surface area of the particles to their volumes), led to a decrease in powder flow rate through an orifice.

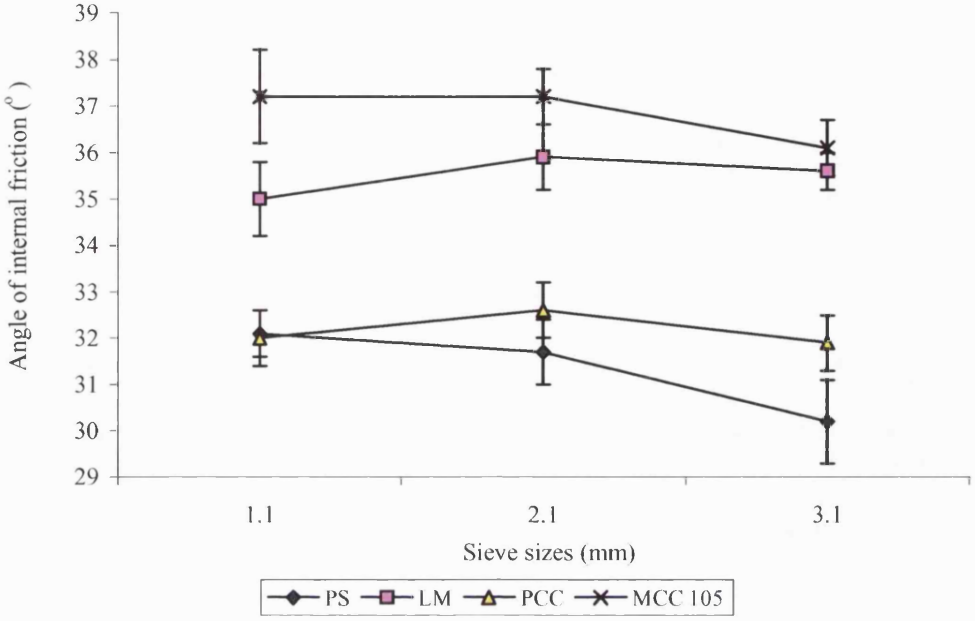

Figure 3.12a *Effect of different sieve sizes (acceleration of vibration 12.0 m/s^2) on the angle of internal friction (mean and s.d. for 3 replicates).*

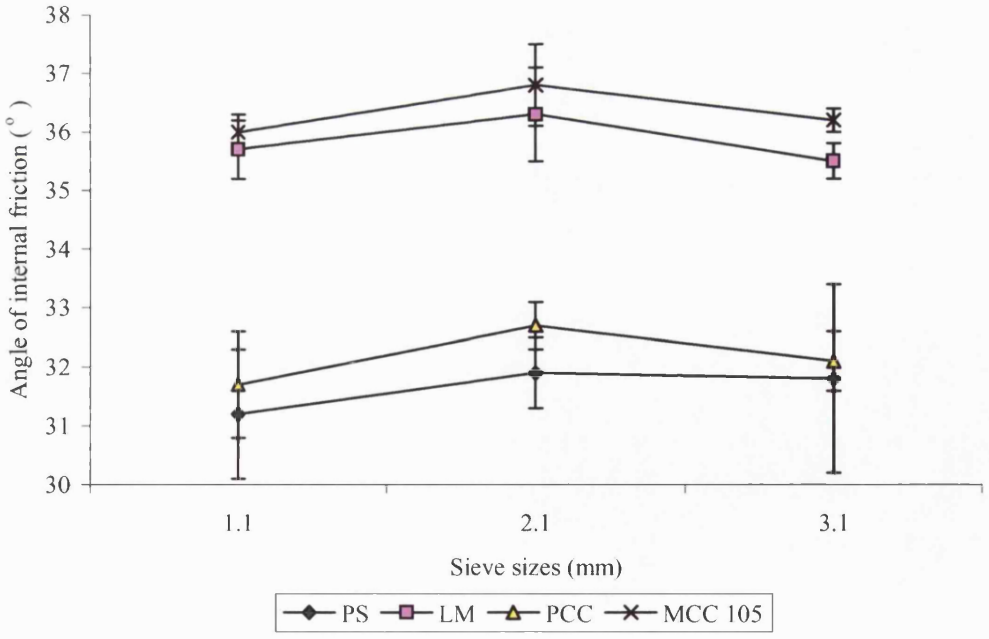

Figure 3.12b *Effect of different sieve size (acceleration of vibration 18.5 m/s^2) on angle of Internal friction (mean and s.d. for 3 replicates)*

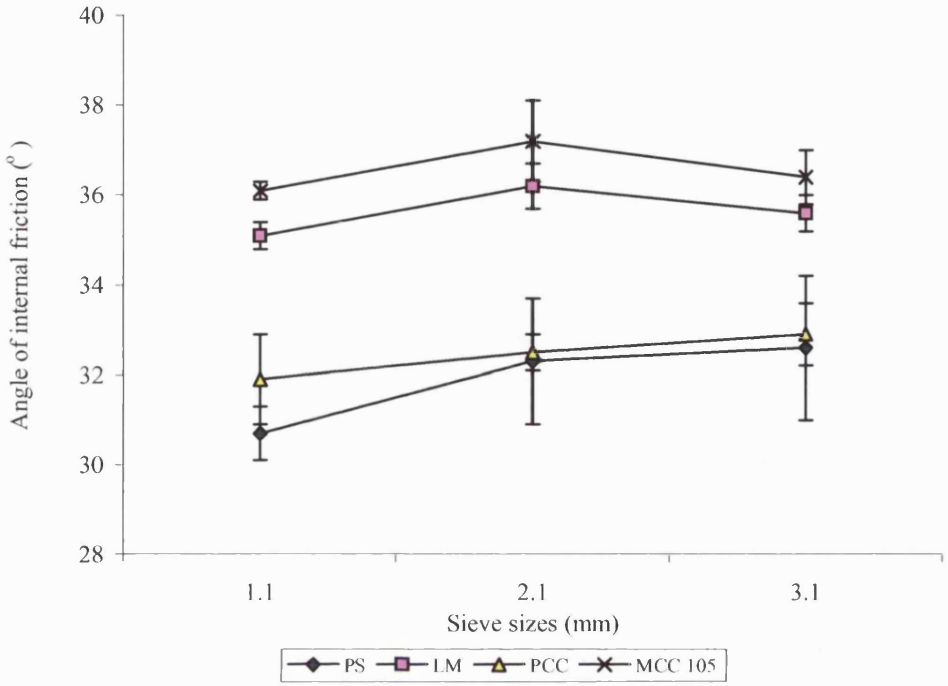

Figure 3.12c *Effect of different sieve sizes (acceleration of vibration 27.4 m/s^2) on angle of internal friction (mean and s.d. for 3 replicates)*

However, the finding by these workers is not supported by Figures 3.12a-c. Microcrystalline cellulose has an aspect ratio of 1.77 (see Table 3.2), an indication of largely elongated particles. The particle shape of microcrystalline cellulose type 105 allows for particle interlocking.

On the contrary, the fine particle size in addition to the irregular shape as shown by the Feret diameter and shape factor, respectively (Table 3.2) may have changed the ranking of precipitated calcium carbonate in this case, as opposed to that obtained when the surface areas of the powders were considered. This finding is similar to that reported by Podczeck and Miah (1996). They found that powder particles having a large aspect ratio such as needle shaped particles, have a high angle of internal friction.

Table 3.12 *Tests of significance for effects of acceleration of vibration and sieve size*

FLOW PARAMETERS		SOURCE		
		Powder	Sieve	Accevib*sieve
Angle of Internal Friction	*df*	3	2	4
	F	285.00	7.22	3.40
	p	< 0.001	0.001	0.013
Effective Angle of Friction	*df*	3	2	4
	F	1343.88	2.47	1.77
	p	< 0.001	0.091	0.144
Flow function	*df*	3	2	4
	F	229.83	1.96	1.35
	p	< 0.001	0.147	0.259
Normalised cohesion coefficient	*df*	3	2	4
	F	4170.70	7.94	2.64
	p	< 0.001	0.001	0.040

Accevib – Acceleration of vibration

Table 3.13a *Post hoc test for sieve size*

Homogeneous Subsets- Angle of internal friction
Scheffé

SIEVE	N	Subsets	
		1	2
1.1 mm sieve	36	33.7	
3.1 mm sieve	36	33.9	
2.1 mm sieve	36		34.4
Sig.		0.615	1.000

Table 3.13b *Post hoc test for Powder*

Homogeneous Subsets- (Angle of internal friction)
Scheffé

POWDER	N	Subsets			
		1	2	3	4
PS	27	31.6			
PCC	27		32.3		
LM	27			35.7	
MCC 105	27				36.5
Sig.		1.000	1.000	1.000	1.000

Table 3.13c *Post hoc test for acceleration of vibration*

Homogeneous Subsets- (Angle of internal friction)
Scheffé

VIBSPEED	N	Subset
		1
18.5 m/s^2	36	33.9
12.0 m/ s^2	36	34.0
28.0 m/ s^2	36	34.1
Sig.		0.634

Table 3.13c shows that no significant difference exists in the angle of internal friction of the powders when a different acceleration of vibration was used to pack the powders. Though the statistical evaluation did not detect a difference in the acceleration of vibrations, 18.5 m/s^2 will be used for further analysis based on better distinction of the powders (Fig. 3.12b) and also on visual observation of the powder filling efficiency (minimal powder agglomerates in cell and better uniform powder filling).

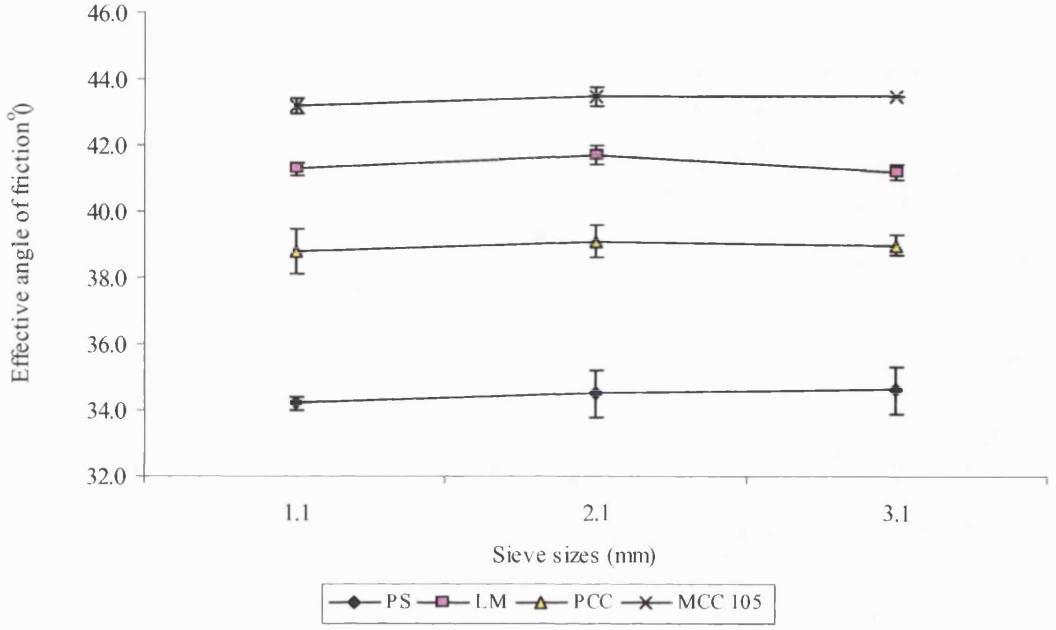

Figure 3.12d *Effect of different sieve sizes (18.5 m/s^2 acceleration of vibration) on effective angle of friction (mean and s.d. for 3 replicates)*

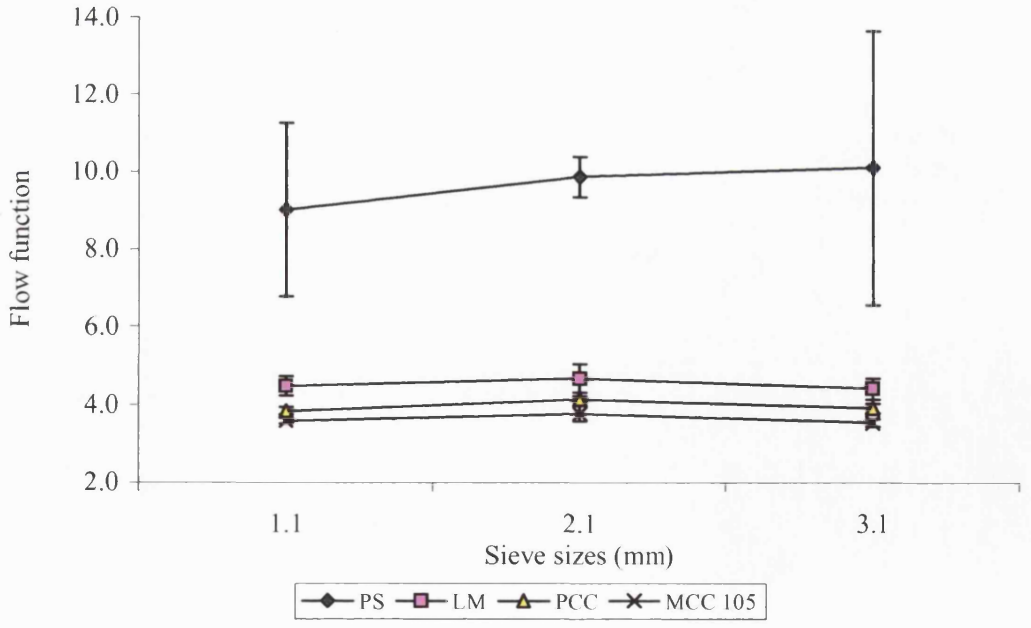

Figure 3.12e *Effect of different sieve sizes (with 18.5 m/s^2 acceleration of vibration) on flow function (mean and s.d. for 3 replicates)*

Effective angle of friction (δ): The effective angle of friction is the angle of the line joining the end points of each yield locus and the normal stress axis (abscissa). The effective angle of friction is a measure of resistance of powders to flow while being sheared. In this work, the mean values of the effective angle of friction of three different effective yield loci were plotted against different combinations of acceleration of vibration and sieve sizes. The graphical illustration of the effect of 18.5 m/s^2 acceleration of vibration with different sieve sizes on effective angle of friction is shown in Figure 3.12d.

From Figure 3.12e, it could be seen that the effective angle of friction separates all powders into *distinctive individuals* unlike the angle of internal friction that grouped powders into two distinctive main groups (Figure 3.12b) i.e. α-lactose monohydrate plus microcrystalline cellulose against pregelatinised starch plus calcium carbonate. This interesting finding could be very important for the quality control of pharmaceutical materials, where a property that can distinguish between materials of such different nature and properties as used here is certainly more useful.

Table 3.13d *Post hoc test on Powders*

Homogenous Subsets- Effective angle of friction

Scheffe

POWDER	N	Subset			
		1	2	3	4
PS	27	34.5			
PCC	27		39.1		
LM	27			41.3	
MCC type 105	27				43.6

From Table 3.12, it can be seen that using any of the sieve size or acceleration of vibration did not have any significant effect on the effective angle of friction, as the probabilities were higher than the threshold of 0.05. This was not the case for the model powders with error probability of $p < 0.001$. Using Scheffé test, the statistical significance between the powders was determined. The post hoc test generated four subsets as shown in Table 3.13d.

A similar finding to what was discovered in terms of calcium carbonate having a larger angle of internal friction than α-lactose monohydrate is repeated here.

Flow function: The flow function, *FF* is used to characterise flowability of powders. In Figure 3.12e, it can be seen that the order of flowability as obtained from this measure has changed, compared to the order based on angle of internal friction (Fig. 3.12b), to pregelatinised starch > α-lactose monohydrate > calcium carbonate > microcrystalline cellulose type 105. Jollife and Newton (1982) also found a difference between the angle of internal friction and the flow function. The workers suggested that the angle of internal friction and flow function provide different powder bulk characteristics. Hence, a powder may have a good powder flow but still can exhibit some cohesiveness, as seen for pregelatinised starch. Hence, the angle of internal friction and the flow factor represent truly different powder bulk properties as suggested by Jenike (1961).

Statistical testing for significance (Table 3.12) revealed different behaviour of the powders ($p < 0.005$). The Scheffé test confirmed that pregelatinised starch behaved completely different from the other powders (see Figure 3.12e). The overlap of subsets 1 and 2 (Table 3.13e) illustrates, however, that although statistically significantly different, the behaviour of the remaining three powders is fairly similar in terms of the flow function.

Table 3.13e *Post hoc test on Powders*

Homogenous Subsets- FF (Flow function)

Scheffé

POWDER	N	Subset		
		1	2	3
MCC 105	*27*	3.63		
PCC	*27*	3.94	3.94	
LM	*27*		4.50	
PS	27			9.30
Sig.		0.681	0.178	1.000

Normalised cohesion coefficient: The cohesion coefficient values obtained were normalised to remove the effect of variation in cohesion coefficient values due to the error arising from differences in filling and packing and operation of the apparatus. It is very difficult to ensure that samples of the same powder have been packed in an identical manner in two separate determinations (Pilpel, 1971), plus different powders packed under identical conditions will not have identical packing densities. As the position of the yield locus depends on the packing density, a comparison of the intercepts is only possible under reference to the packing density. The normalisation removes this problem (Podczeck and Wood, 2003).

Cohesion coefficient and packing density are related via $k = \tau_0/S_p$, where k is the normalised cohesion coefficient, τ_0, is the cohesion coefficient and S_p the powder packing density. The units of k are *J/kg*, implying that this parameter reflects the energy required to overcome the interparticulate forces to make a powder flow. The higher the energy required, the more cohesive behaves the powder.

Figure 3.12f shows the mean of the normalised cohesion coefficient using 18.5 m/s acceleration of vibration but different sieve sizes. Statistical analysis (Table 3.12) showed that there is a significant difference in the normalised cohesion coefficient caused by the factors 'powder' and 'sieve'. Further evaluation to identify where the difference lies is shown in Table 3.13f - g.

Table 3.13f shows that the difference is due to the use of 2.1 mm sieve and Table 3.13g shows that all the powders are different in behaviour. Hence, the variation in their normalized cohesion coefficient values is a property of the powders. As observed for the effective angle of friction, the normalized cohesion coefficient is able to distinguish between the powders and hence might be a more suitable in-process parameter than, for example, the flow function. The highest energy is required to cause MCC 105 to flow. This finding is consistent with for example, the impossibility of filling into capsules as reported by Patel and Podczeck (1996). In contrast, low energy is required to cause pregelatinised starch to flow.

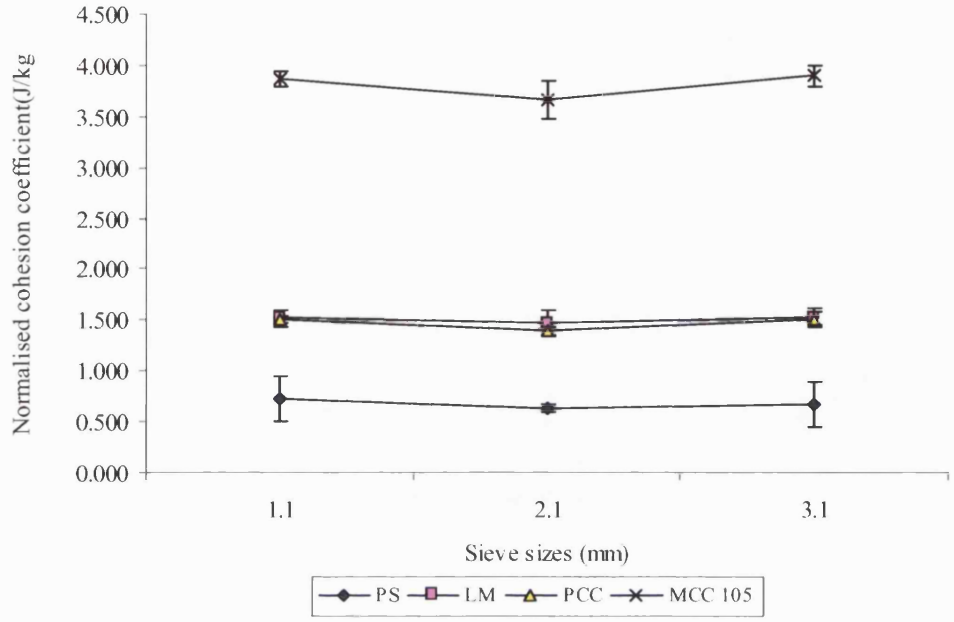

Figure 3.12f *Effect of different sieve sizes (18.5 m/s^2 acceleration of vibration) on normalised cohesion coefficient(mean and s.d. for 3 replicates)*

Table 3.13f *Post hoc test on sieve size*

Homogenous Subsets- Normalised cohesion coefficient

Scheffe

SIEVE	N	Subset	
		1	2
2.1 mm	36	1.82	
3.1 mm	36		1.90
1.1 mm	36		1.91
Sig.		1.000	0.916

Table 3.13g *Post hoc test on powder*
Homogenous Subsets- Normalised cohesion coefficient

Scheffe

POWDER	N	Subset		
		1	2	3
PS	27	0.697		
PCC	27		1.48	
LM	27		1.54	
MCC 105	27			3.82
Sig.		1.000	0.679	1.000

This is consistent with very good filling properties observed (Podczeck and Newton, 1999). The combination of 2.1 mm sieve and 18.5 m/s^2 acceleration of vibration better powder packing. This behaviour could be attributed to reduction in electrostatic charges as high electrostatic charges discourage close packing of powder particles, segregation and reproducible powder packing. The cohesion coefficient pattern of the powders (not shown) is supported by the flow function (Figure 3.12f), i.e. the powders being grouped into two distinct groups. An overlap of the curves of lactose monohydrate and calcium carbonate was observed after the normalisation of the cohesion coefficient values (Figure 3.12f).

In conclusion, the statistical analysis regarding the acceleration of vibration and sieve size revealed that the 2.1 mm sieve size probably ensures that reliable and reproducible flow properties (i.e. angle of internal friction, effective angle of friction flow function, normalized cohesion coefficient) for the powders are obtained. However, the results did not suggest any acceleration of vibration that will encourage reliable flow properties. The use of 18.5 m/s^2 acceleration of vibration might be considered to be nearest to providing reliable conditions. The reason for this could be that this acceleration of vibration appears to reduce electrostatic charges, which in return allows particles to bounce/jump more easily thereby encouraging close powder packing.

3.5.2.2. Effect of manual packing using the spatula (no acceleration of vibration)

The effect of manual packing using the spatula on the flow properties of the powders is shown in Table 3.14, and compared with combinations of medium acceleration of vibration and different sieve size.

Table 3.14 *Comparison of the medium acceleration of vibration and different sieve sizes with manual packing*

PARAMETER	FLOW PROPERTY	PS	LM	PCC	MCC
Med/fine sieve	AIF (°)	31.2 ± 1.1	35.7 ± 0.5	31.7 ± 0.9	36.0 ± 0.3
	EAF(°)	34.2 ± 0.2	41.3 ± 0.2	38.8 ± 0.7	43.2 ± 0.2
	FF	9.02 ± 2.25	4.48 ± 0.25	3.84 ± 0.10	3.59 ± 0.07
	NCC (J/kg)	0.73± 0.22	1.52±0.09	1.51±0.04	3.87±0.08
Med/ intermediate sieve	AIF (°)	31.9 ± 0.6	36.3 ± 0.8	32.7 ± 0.4	36.8 ± 0.7
	EAF (°)	34.5 ± 0.7	41.7 ± 0.3	39.1 ± 0.5	43.5 ± 0.3
	FF	9.87 ± 0.52	4.68 ± 0.37	4.15 ± 0.07	3.77 ± 0.20
	NCC(J/kg)	0.63 ± 0.04	1.47 ± 0.12	1.40 ± 0.04	3.66 ± 0.18
Med/coarse sieve	AIF (°)	31.8 ± 1.6	35.5 ± 0.3	32.1 ± 0.5	36.2 ± 0.2
	EAF (°)	34.6 ± 0.7	41.2 ± 0.2	39.0 ± 0.3	43.5 ± 0.0
	FF	10.11 ± 3.54	4.42 ± 0.27	3.92 ± 0.12	3.54 ± 0.10
	NCC (J/kg)	0.67±0.22	1.53 ± 0.09	1.51 ± 0.07	3.90 ± 0.11
Spatula	AIF (°)	31.8 ± 1.3	35.6 ± 0.6	32.1 ± 1.0	36.3 ± 0.2
	EAF (°)	34.9 ± 0.6	41.2 ± 0.5	39.0 ± 0.7	43.0 ± 0.1
	FF	8.53 ± 1.72	4.52 ± 0.28	3.95 ± 0.11	3.83 ± 0.12
	NCC (J/kg)	0.77 ± 0.15	1.50 ± 0.09	1.46 ± 0.03	3.54 ± 0.10

Med – medium acceleration of vibration

PS – Pregelatinised starch

LM – Lactose monohydrate

PCC – Precipitated calcium carbonate

MCC – Microcrystalline cellulose type 105

A.I.F – Angle of internal friction

E.A.F – Effective angle of friction

FF – Flow function

NCC – Normalised cohesion coefficient

Statistical evaluation revealed that differences exist between the powders but not between the various sieves and the spatula (Table 3.15). Further analysis shows that on this occasion the angle of internal friction of pregelatinised starch is comparable to that of precipitated calcium carbonate, while that of α-lactose monohydrate is similar to microcrystalline cellulose 105 (not shown). No statistical difference exists in the angle of internal friction when different sieve sizes or the spatula were used to pack the powders.

The effective angles of friction of the powders using the spatula/no vibration, different sieve size and medium acceleration of vibration are shown in Table 3.14. Statistical analysis (Table 3.15) indicates that *F* is significant for the effective angle of friction of the powders and not for the use of different sieve sizes (which includes the use of spatula for packing).

Table 3.15: *Tests of significance for effects of manual packing (spatula).*

Source	df	Angle of Internal friction		Effective Angle of friction		Flow function		Normalised cohesion coefficient	
		F	*p*	F	*p*	F	*p*	F	*p*
Powder	3	113.82	< 0.001	886.93	< 0.001	65.62	< 0.001	1566.77	< 0.001
Sieve	3	1.41	0.136	0.98	0.411	0.30	0.820	1.70	0.312
Pow*sv	9	0.25	0.981	0.72	0.684	0.33	0.955	1.98	0.074

Pow*sv – Powder*sieve

Sieve – includes the three different sieves (1.1, 2.1, 3.1 mm) and the spatula

Further analysis using the post hoc test revealed that all the powders are different as the effective angles of friction of the powders were grouped individually.

The mean of the flow function using medium vibration speed and different packing technique are shown in Table 3.14. In Table 3.15, the value of F is significant for the flow functions of the powders. Further analysis indicates that pregelatinised starch having the highest flow function is different from the remaining powders, which occupy the second subset.

Table 3.14 also shows the mean of the normalised cohesion coefficient using medium vibration speed and different packing technique. In Table 3.15, the powders have been identified to be statistically different from each other using the post hoc test. After normalisation, with the exception of pregelatinised starch and microcrystalline cellulose type 105, the powders were found to have similar normalised cohesion coefficient values.

Using the spatula or a different sieve size did not have any effect on the cohesion coefficient or the normalized cohesion coefficient of the powders.

3.5.2.3. Effect of preconsolidation time

In a shear experiment, the preconsolidation stage is carried out to remove trapped air and to provide samples of similar condition. In this experiment, the preconsolidation time was varied to determine the effect this will have on the failure properties of the model powders. The preconsolidation times used were 4, 8, 10 and 12 minutes. Figures 3.13a – d compares the individual shear properties as a function of preconsolidation time. All the results are the mean and standard deviation of three experiments.

Figure 3.13a –b illustrates the effect of preconsolidation time on the angle of internal friction and effective angle of friction. Statistical evaluation reveals that a significant difference exists between the angles of internal friction of the powders ($p < 0.05$). The post

hoc test (Scheffé) for the angle of internal fricition (Table 3.17b) shows that pregelatinised starch and calcium carbonate have different powder behaviour, while the angle of internal friction of α-lactose monohydrate and microcrystalline cellulose type 105 are similar and hence, these two materials may possess similar powder behaviour. The table also shows a significant effect when the preconsolidation time is varied. The post hoc test for the preconsolidation time (see Table 3.17a) shows that similarities exist between the angles of internal friction of the powders at 12, 4 and 10 minutes. There is also a similarity between the angles of internal friction of the powders at 4, 8 and 12 minutes. A closer look at the table indicates that the biggest difference is between 8 and 10 minutes preconsolidation time. However, with the exception of the curve obtained for pregelatinised starch that showed a maximum at 8 minutes preconsolidation time (see Figure 3.1.3a), other curves obtained for the remaining of the powders did not reveal any distinctively pattern. In terms of variability, a more consistent pattern could be seen when 8 minutes preconsolidation time was utilised.

Figure 3.13b shows the effect of varying the preconsolidation time on the effective angle of friction. As can be seen from Table 3.16, a significant difference exists between the effective angles of friction considering the powders, but not between these values when considering the preconsolidation time as influence factor. This is indicated by the calculated F-value which corresponds to a *p-value of <0.001*. Further analysis using the post hoc test revealed that the powders do behave differently, as each occupies a different subset (see Table 3.17c). This is well illustrated graphically in Figure 3.13b, where the powders are grouped distinctively.

Figure 3.13c shows the effect of using different preconsolidation time on the flow function of the powders. Table 3.16 shows that a significant difference exists between the flow function of the powders caused by the preconsolidation time. Table 3.17e shows that microcrystalline cellulose type 105 and precipitated calcium carbonate are similar in their flow functions, while α-lactose monohydrate and calcium carbonate are also similar. However, pregelatinised starch does not share any similarity to the other powders. The graphical illustration (Figure 3.13c) confirms this.

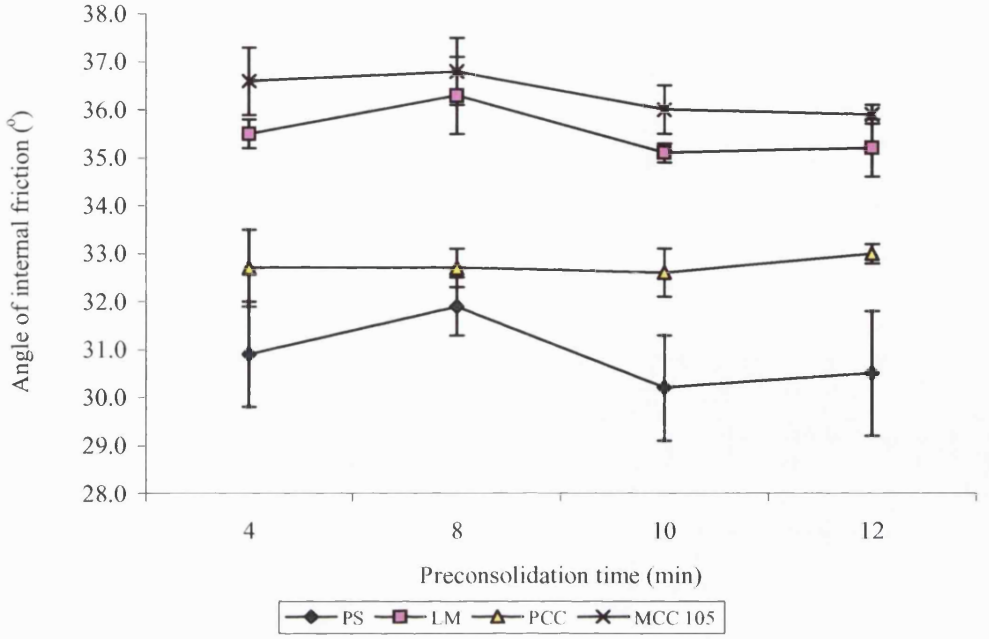

Figure 3.13a *Effect of preconsolidation time on angle of internal friction (mean and s.d. for 3 replicates)*

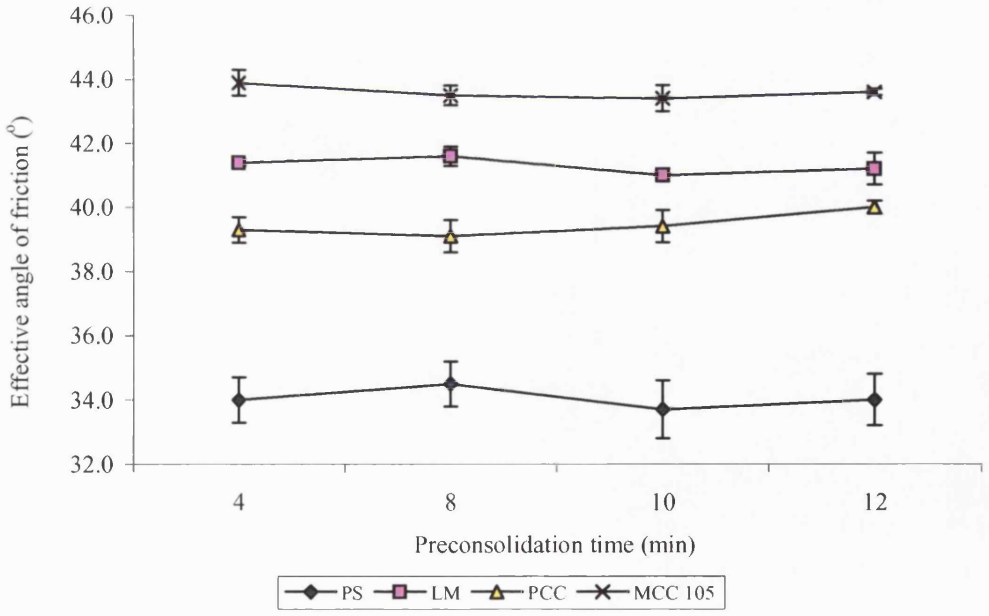

Figure 3.13b *Effect of preconsolidation time on effective angle of friction (mean and s.d for 3 replicates)*

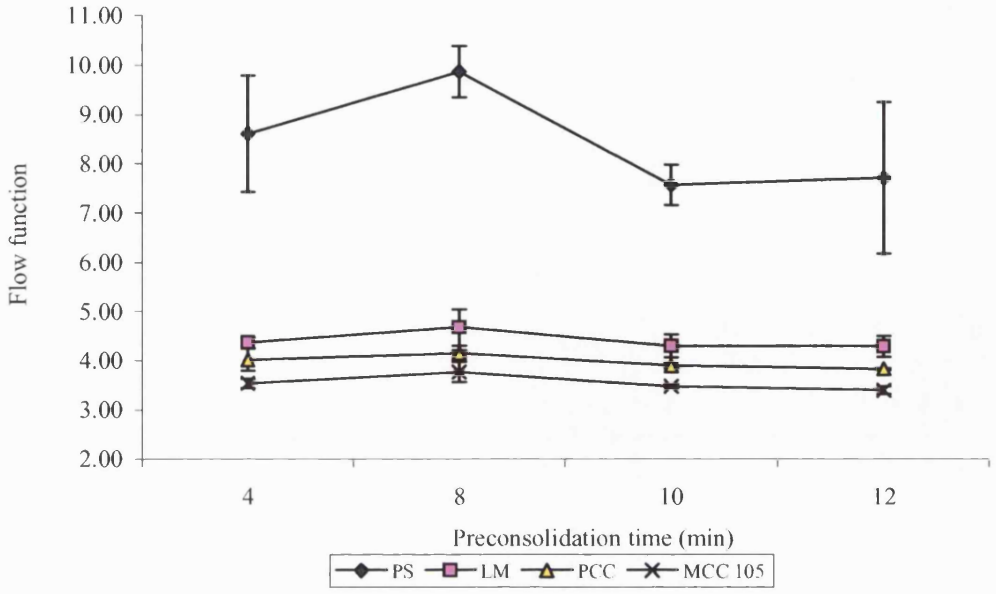

Figure 3.13c *Effect of preconsolidation time on flow function (mean and s.d. for 3 replicates)*

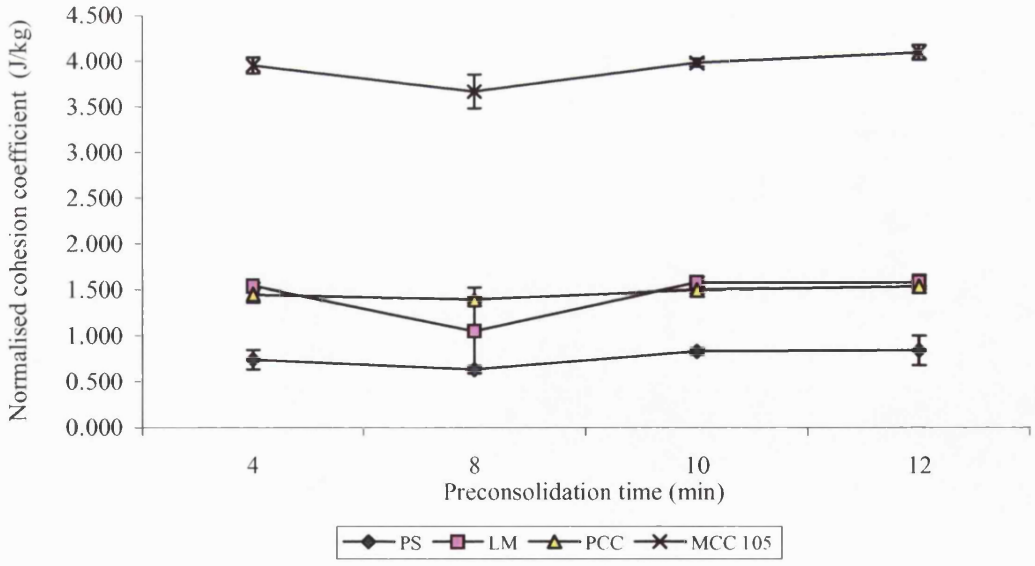

Figure 3.13d *Effect of preconsolidation time on normalised cohesion coefficient (mean and s.d for 3 replicates)*

In this plot, the flow function values obtained for pregelatinised starch is distinct from that of the other powders regardless of the preconsolidation time used. The use of 8 minutes preconsolidation time produced the largest flow function value as seen in Table 3.17d. A slight similarity exists also between 4 and 8 minutes preconsolidation time while 12, 10 and 4 minutes are forming another group of similar experiments as they occupy the same subset.

The largest flow function values were obtained when 8 minutes preconsolidation time was used as shown in Figure 3.13c.

Table 3.16 *Tests of significance for effects of preconsolidation time*

SOURCE	df	Angle of Internal Friction		Effective Angle of friction		Flow Function		Normalised cohesion coefficient	
		F	*p*	F	*p*	F	*p*	F	*p*
Powder	3	154.51	< 0.001	822.58	< 0.001	216.17	< 0.001	3408.39	<0.001
Other	3	4.06	0.015	1.009	0.401	6.171	0.002	10.09	<0.001
Powder*other	9	0.79	0.624	1.173	0.345	2.187	0.050	0.598	0.789

Other – 4, 8, 10 and 12 minutes preconsolidation time

The effect of different preconsolidation time on the normalised cohesion coefficient is shown in Figure 3.13d. Statistical evaluation indicates that a significant difference exists between the normalised cohesion values obtained for the powders with preconsolidation time as the influence factor. All powders with the exception of α-lactose monohydrate experienced a decrease in the normalized cohesion coefficient values when preconsolidated for 8 minutes (Figure 3.13d). This trend probably indicates that the optimum time for preconsolidation is 8 minutes. Further analysis (see Table 3.17g) revealed that using 4 or 8 minutes preconsolidation time could result in equal powder behaviour. Table 3.17f shows

that the normalised cohesion coefficients of pregelatinised starch and microcrystalline cellulose are different while calcium carbonate and α-lactose monohydrate are similar in behaviour.

Table 3.17a *Post hoc test for preconsolidation time*

Homogenous Subsets- Angle of internal friction

Scheffé

OTHER(Preconsolidation time)	N	Subset	
		1	2
10 minutes	12	33.5	
12 minutes	12	33.7	33.7
4 minutes	12	33.9	33.9
8 minutes	12		34.4
Sig.		0.460	0.109

Table 3.17b *Post hoc test for powder*

Homogenous Subsets- Angle of internal friction

Scheffé

POWDER	N	Subset		
		1	2	3
PS	12	30.9		
PCC	12		32.8	
LM	12			35.5
MCC 105	12			36.3
Sig.		1.000	1.000	0.069

Table 3.17c *Post hoc test for powder*

Homogenous Subsets- Effective angle of friction

Scheffé

POWDER	N	Subset			
		1	2	3	4
PS	12	34.0			
PCC	12		39.5		
LM	12			41.3	
MCC 105	12				43.6
Sig.		1.000	1.000	1.000	1.000

Table 3.17d *Post hoc test for preconsolidation time*

Homogenous Subsets- Flow function

Scheffé

OTHER (Preconsolidation time)	N	Subset	
		1	2
12 minutes	12	4.81	
10 minutes	12	4.81	
4 minutes	12	5.13	5.13
8 minutes	12		5.62
Sig.		0.530	0.197

Table 3.17e *Post hoc test for powder*

Homogenous Subsets- Flow function

Scheffé

POWDER	N	Subset		
		1	2	3
MCC 105	12	3.55		
PCC	12	3.98	3.98	
LM	12		4.41	
PS	12			8.44
Sig		0.291	0.288	1.000

Table 3.17f *Post hoc test for powder*

Homogenous Subsets- Normalised cohesion coefficient

Scheffé

POWDER	N	Subset		
		1	2	3
PS	12	0.759		
PCC	12		1.47	
LM	12		1.54	
MCC 105	12			3.98
Sig.			0.234	1.000

Though statistical evaluation did not identify precisely an optimum preconsolidation time (see Table 3.17g), the probably most reliable one is 8 minutes preconsolidation time.

Table 3.17g *Post hoc test for preconsolidation time*

Homogenous Subsets- Normalised cohesion coefficient

Scheffé

OTHER	*N*	Subset	
		1	*2*
Preconsolidation time 8	12	1.84	
Preconsolidation time 4	12	1.92	1.92
Preconsolidation time 10	12		1.96
Preconsolidation time 12	12		2.02
Sig.		0.139	0.058

Increase in preconsolidation time can facilitate particle-particle contact, and hence, an increase in the cohesion coefficient. In addition, the use of 8 minutes preconsolidation time produced a consistent pattern in standard deviation of results i.e. small deviation values.

3.5.2.4. Effect of preconsolidation load

The effect of different consolidation load on the flow properties of the pharmaceutical excipients was studied using three different loads i.e. 1.962, 4.905 and 7.848 kPa. Using the right load is crucial to the consolidation of the powder sample. The right load will ensure the curve (shear stress/strain curve) reaches a limiting value (Pilpel, 1971) as opposed to the powder being under or over consolidated (no limiting value observed). The effects are illustrated graphically in Figures 3.14a – d.

The preconsolidation load is the load used to consolidate the powder before the commencement of shear test. This load is equal to the vertical load during shear test. For each preconsolidation load, a fresh sample was used before the shear test.

Figure 3.14a and b show the angle of internal friction and effective angle of friction, respectively.

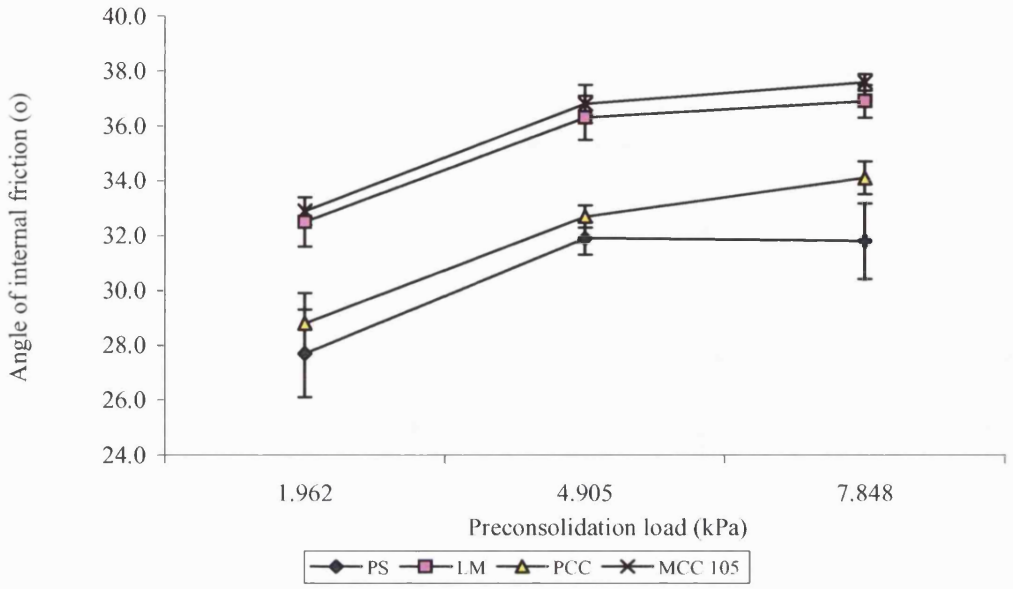

Figure 3.14a *Effect of preconsolidation load on angle of internal friction (mean and s.d. for 3 replicates)*

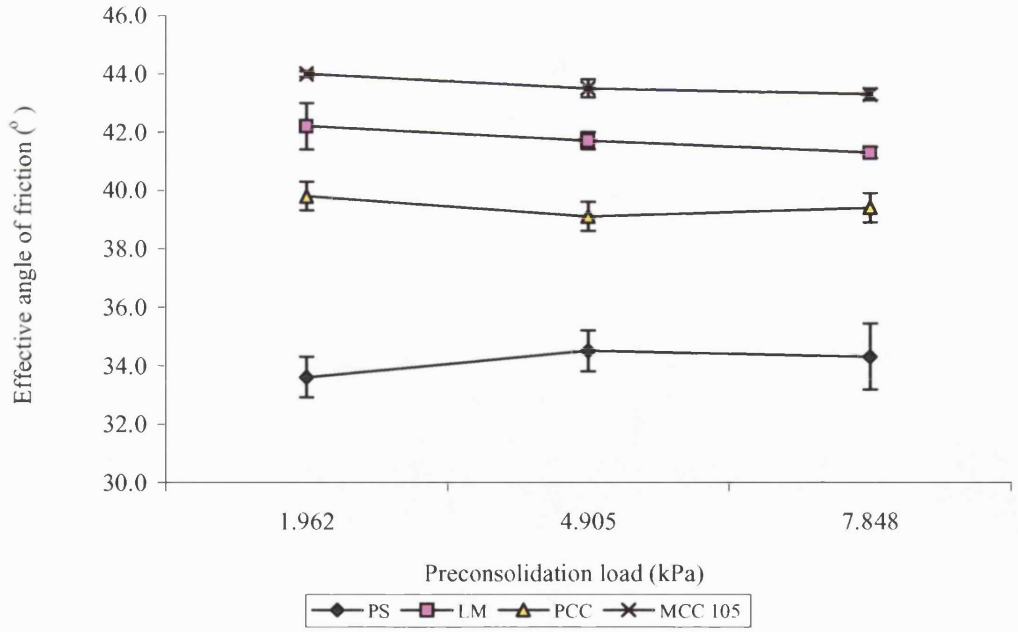

Figure 3.14b *Effect of preconsolidation load on effective angle of friction (mean and s.d. for 3 replicates)*

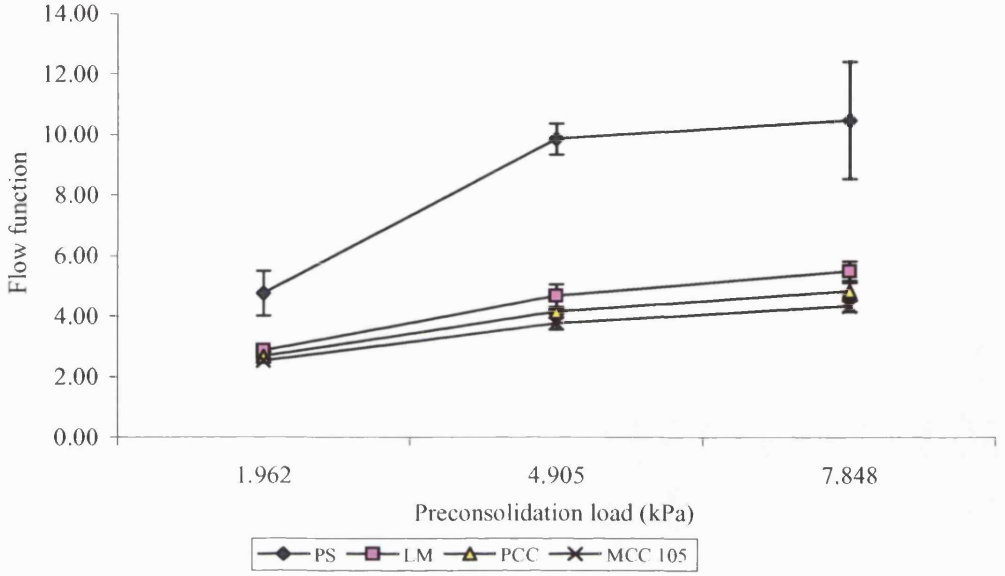

Figure 3.14c *Effect of preconsolidation load on flow function (mean and s.d. for 3 replicates)*

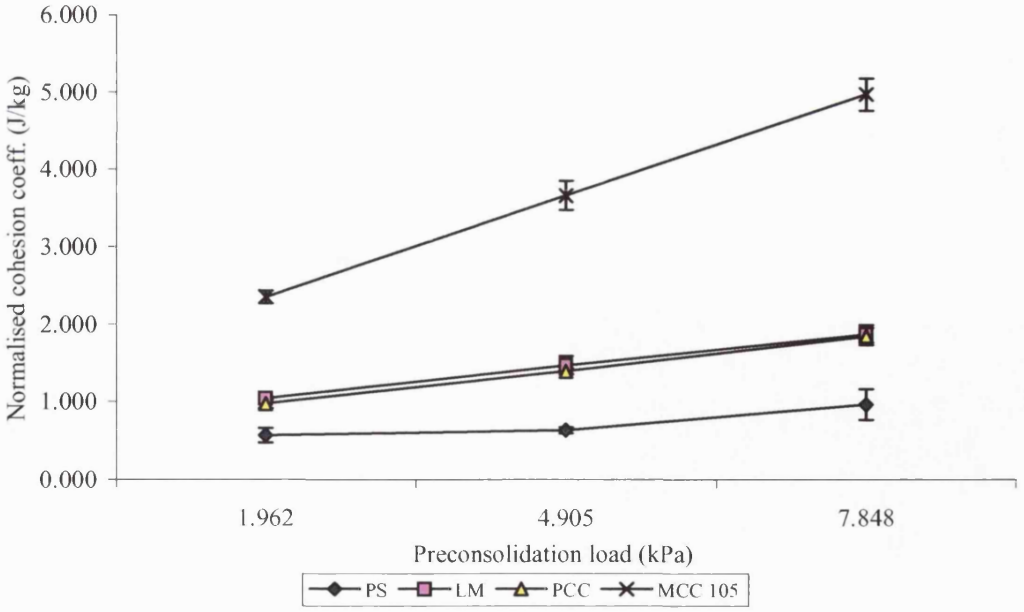

Figure 3.14d *Effect of preconsolidation load on normalised cohesion coefficient (mean and s.d. for 3 replicates)*

Table 3.18 shows that a significant difference exists between the angles of internal friction of the powders when a different preconsolidation load was used. As shown in Figure 3.14a, using the lowest (1.962 kPa) load gave the lowest angle of internal friction. Increase in the angle of internal friction was observed when the loads were increased with no statistical difference on increasing the load to the highest (7.848 kPa) as shown in Table 3.19a. As shown in Table 3.19b, pregelatinised starch and calcium carbonate belong to separate groups, while the angles of friction of α-lactose monohydrate and microcrystalline cellulose type 105 are similar. Generally, the angle of internal friction increases as the load increases for all the powders. In addition, visual observation revealed that the least amount of powder was ejected between the cell base and ring for all the powders (most especialy calcium carbonate) when 1.962 kPa load was used. This is expected, as the increase in weight facilitates particle-particle interaction and reduction in voidage.

The effect of varying the preconsolidation load on the effective angle of friction is shown in Figure 3.14b. A significant difference exists only between the effective angle of friction and the powders as shown in Table 3.18.

Table 3.18 *Tests of significance for effects of preconsoildation load*

SOURCE	df	Angle of Internal Friction		Effective Angle of friction		Flow Function		Normalised cohesion coefficient	
		F	*p*	F	*p*	F	*p*	F	*p*
Precon.load	3	98.93	<0.001	0.90	0.416	74.81	< 0.001	295.72	<0.001
Powder	3	76.62	<0.001	477.64	<0.001	110.64	< 0.001	1092.6	<0.001
Precon.load*P	9	0.59	0.735	1.74	0.154	8.08	< 0.001	52.53	<0.001

P - Powder

Precon.load - Preconsolidation load

The post hoc test indicated that the effective angles of the powders are not identical (see Table 3.19c) and are all individually grouped unlike the angle of internal friction that grouped them into three subsets. The graphical illustration (Fig. 3.14b) confirms this. This grouping as shown by the post hoc test indicates that the powders do indeed have different flow behaviour.

Table 3.19a *Post hoc test for preconsolidation load*

Homogenous Subsets- Angle of internal friction

Scheffé

PRECONSOLIDATION LOAD	N	Subset	
		1	2
Preconsolidation load 1.962 kPa	12	30.5	
Preconsolidation load 4.905 kPa	12		34.3
Preconsolidation load 7.848 kPa	12		35.1
Sig.		1.000	0.088

Table 3.19b *Post hoc test for powder*

Homogenous Subsets- Angle of internal friction

Scheffé

		Subset		
		1	2	3
POWDER	N			
PS	9	30.5		
PCC	9		31.9	
LM	9			35.2
MCC 105	9			35.6
Sig.		1.000	1.000	0.808

Table 3.19c *Post hoc test for powder*

Homogenous Subsets- Effective angle of friction

Scheffé

POWDER	*N*	*Subset*			
		1	*2*	*3*	*4*
PS	9	34.1			
PCC	9		39.4		
LM	9			41.7	
MCC 105	9				43.6
Sig.		1.000	1.000	1.000	1.000

Table 3.19d *Post hoc test for preconsolidation load*

Homogenous Subsets- *Flow function*

Scheffé

PRELOAD	N	Subset		
		1	2	3
1.962 kPa	12	3.22		
4.905 kPa	12		5.57	
7.848 kPa	12			6.29
Sig.		1.000	1.000	1.000

Table 3.19e *Post hoc test for powder*

Homogenous Subsets- Flow function

Scheffé

POWDER	N	Subset	
		1	2
MCC 105	9	3.49	
PCC	9	3.89	
LM	9	4.35	
PS	9		8.37
Sig.		0.070	1.000

Figures 3.14c – d illustrate the effect of preconsolidation on the flow function and normalised cohesion coefficient of the model powders. Table 3.18 shows that a significant difference exists in the flow function and normalised cohesion coefficient of the powders when different loads were used. Further analysis using the Scheffé test (Table 3.19e) indicates similarity in the flow behaviour of microcrystalline cellulose type 105, calcium carbonate and α-lactose monohydrate as they are grouped together with the exception of pregelatinised starch. Table 3.18 indicates that an interaction exists between the preconsolidation load and the powder as the value of p of the interaction term correspondes to < 0.001.

The effect of preconsolidation load on the normalised cohesion coefficient is illustrated in in Figure 3.14d. Statitical evaluation indicates that a significant difference exits between the powders and that an interaction exists between the powders and the preconsolidation load with p corresponding to < 0.001 in each case. Further analysis indicates that the normalised cohesion coefficient values of precipitated calcium carbonate and α – lactose monohydrate share the same subset (Figure 3.19g). This may be attributed to similar powder behaviour. The remaining powders occupy different subsets and hence, have different powder behaviour. This is in agreement with the graphical illustration shown in

Figure 3.1.4d. The curves are grouped into three with that of MCC type 105 at the top end, pregelatinised starch at the lower end and those of precipitated calcium carbonate and lactose monohydrate almost overlapping. The normalised cohesion coefficient of the powders increased on increasing the preconsolidation load. The increase in normalised cohesion coefficient is not surprising as the increase in load encouraged close packing; hence more energy is required to induce flow. The order of cohesion coefficient initially obtained (pregelatinised starch < α-lactose monohydrate < calcium carbonate < microcrystalline cellulose) is different to that obtained for the normalised cohesion coefficient (Fig. 3.14d): pregelatinised starch < calcium carbonate < α-lactose monohydrate < microcrystalline cellulose. After normalisation, calcium carbonate and α-lactose monohydrate curves were almost identical. The normalisation of the cohesion coefficient is very important as it prevents false ranking of powders based on their cohesion coefficient values. Visual observation of the consolidation stages using 1.962, 4.905, 7.848 kPa load indicates that only the 4.905 kPa load gave a curve that reached a *limiting value* otherwise called shear stress at failure indicating satisfactory consolidation. On the other hand, a curve which indicates that the sample had been over consolidated was observed when the 7.848 kPa load was used. Hence, pharmaceutical powders (almost all pharmaceutical powders would behave similarly due to their physical properties) should be tested using a consolidation load of 4.905 kPa.

Table 3.19f *Post hoc test for preconsolidation load*

Homogenous Subsets- Normalised Cohesion coefficient

Scheffé

PRECON.LOAD	N	Subset		
		1	2	3
1.962 kPa	12	1.23		
4.905 kPa	12		1.84	
7.848 kPa	12			2.41
Sig.		1.000	1.000	1.000

Table 3.19g *Post hoc test for powder*

Homogenous Subsets- Normalised cohesion coefficient

Scheffé

POWDER	N	Subset		
		1	2	3
PS	9	0.721		
LM	9		1.40	
PCC	9		1.46	
MCC 105	9			3.73
Sig.		1.000	0.788	1.000

Statistical evaluation could not detect the preconsolidation load that will give a reliable result. Visual observation of the shearing test has to be considered for this purpose. For pharmaceutical powders the most reliable preconsolidation load appears to be 4.905 kPa. As mentioned before, this is due to the fact that the stress-strain curve obtained is similar to that reached when a limiting value has been attained (also called the shear stress at failure indicating satisfactory flow).

3.5.2.5. *Effect of varying consolidation-step time*

The consolidation-step provides powders of similar/comparable conditions i.e. density and other properties influencing the yield locus. The consolidation-step time is the time used to apply a maximum allowable sample load valid for the actual yield locus. This stage is called the consolidation-step and it precedes the shear-step. The consolidation-step times used were 1, 2, 3 and 5 minutes and the effects of varying the consolidation- time are shown graphically in Figure 3.15 a – d. The results are the mean and standard deviation of three replicates.

Figures 3.15a and 3.15b show the effect of consolidation-step time on the angle of internal friction and effective angle of friction, respectively.

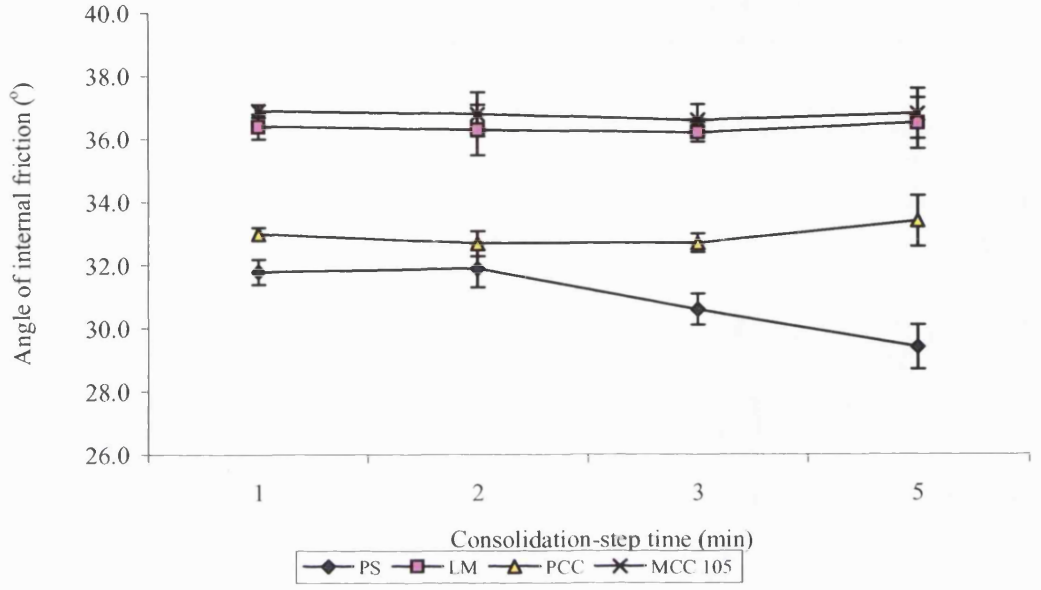

Figure 3.15a *Effect of consolidation-step time on angle of internal friction (mean and s.d. for 3 replicates)*

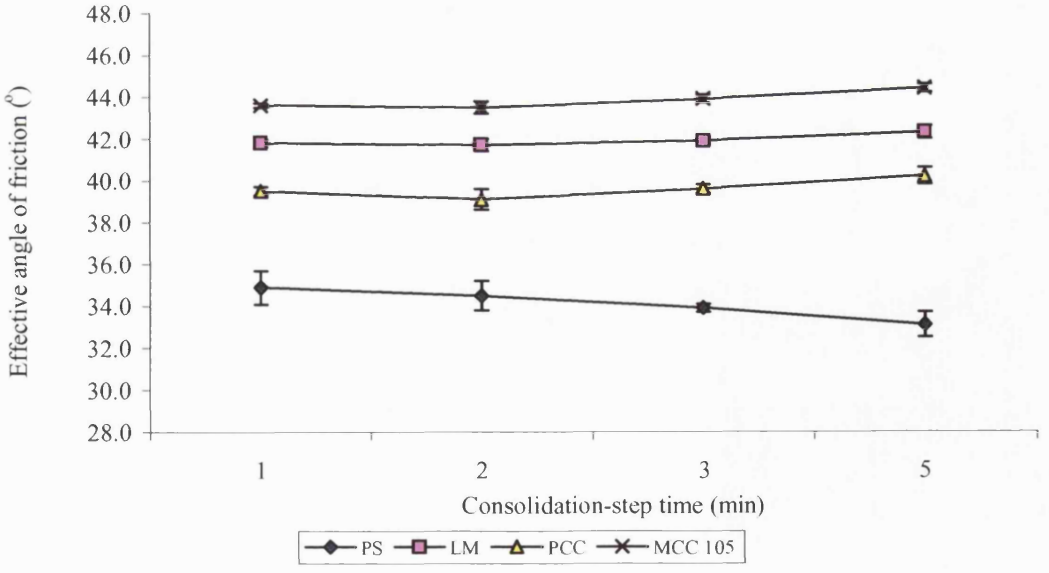

Figure 3.15b *Effect of consolidation-step time on effective angle of friction (mean and s.d. for 3 replicates)*

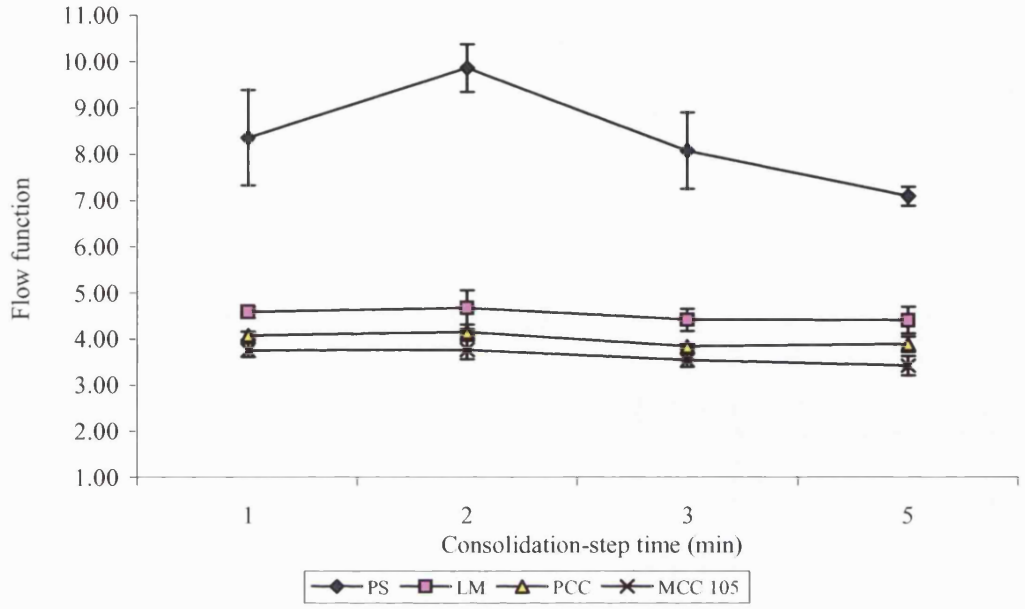

Figure 3.15c *Effect of consolidation-step time on flow function (mean and s.d. for 3 replicates)*

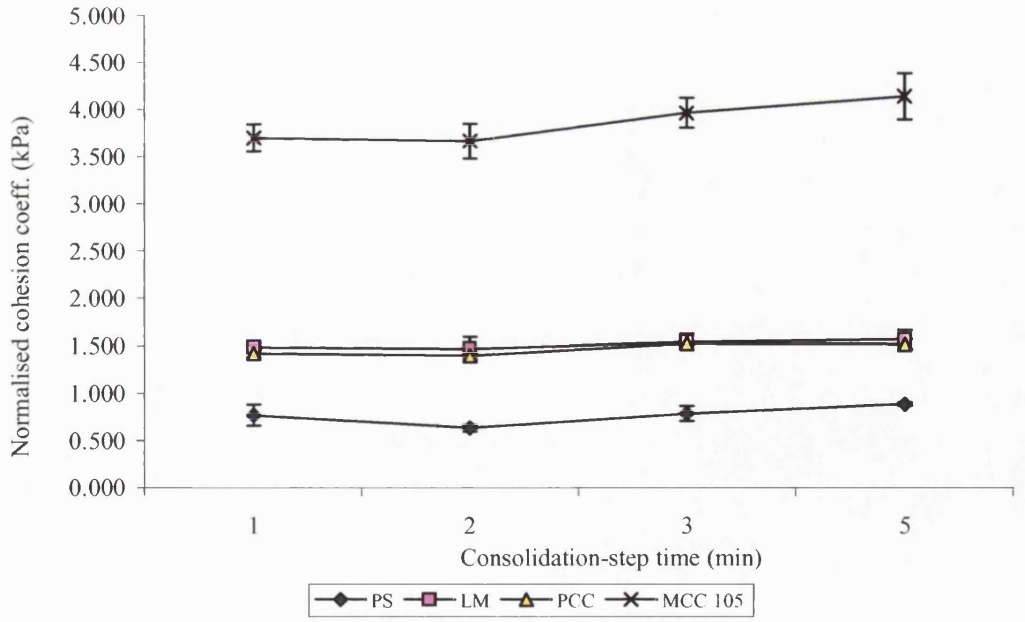

Figure 3.15d *Effect of consolidation –step time on normalised cohesion coefficient (mean and s.d. for 3 replicates)*

A significant difference exists (*p - value of* < *0.001*) between the angles of internal friction and effective angle of friction of the powders when different consolidation time was used as shown in Table 3.20. According to the Scheffé test (Table 3.21a), the angle of internal friction of pregelatinised starch and calcium carbonate are not comparable while that of α-lactose monohydrate and microcrystalline cellulose are. It must also be mentioned that statistically, the consolidation-step time alone did not influence the result, though an interaction between consolidation time and powder exists as shown in Table 3.20.

Table 3.20 *Tests of significance for effects of consolidation-step time*

SOURCE	df	Angle of Internal Friction		Effective Angle of friction		Flow Function		Normalised cohesion coefficient	
		F	*p*	F	*p*	F	*p*	F	*p*
Powder	3	311.91	<0.001	1449.87	<0.001	369.08	<0.001	1887.52	<0.001
Con.time	3	2.30	0.096	1.74	0.177	10.44	<0.001	8.23	<0.001
Powder*Con.time	6	4.67	0.001	6.34	<0.001	5.36	<0.001	1.51	0.185

Con.time - Consolidation-step time (1, 2, 3, 5 min.)

The angle of internal friction of the powders with the exception of pregelatinised starch remained fairly constant except that of pregelatinised starch that decreased progressively after 2 minutes consolidation-step time (Figure 3.1.5a). The plot also replicates the difference as observed when statical evaluation was employed i.e. α-lactose monohydrate and microcrystalline cellulose having comparable flow behaviour, and pregelatinised starch and precipitated calcium carbonate having different flow behaviour. In this case the angles of internal friction of the powders are grouped into three i.e. microcrystalline cellulose type 105 and α-lactose monohydrate at one end while pregelatinised starch and precipitated calcium carbonate are grouped individually.

However in Figure 3.15b, the effective angles of the powders were distinctly grouped i.e. grouped individually, indicating that the powders are different when the effective angles are considered. However, the effective angle of friction of pregelatinsed starch decreased progressively after 1 minute in contrast to that observed for the angle of internal friction. It can be concluded here that the results of pregelatinised starch are clearly dependent on the consolidation time, while those for α-lactose monohydrate, calcium carbonate and microcrystalline cellulose type 105 are not.

Table 3.21a *Post hoc test for powder*

Homogenous Subsets- Angle of internal friction

Scheffé

POWDER	N	Subset		
		1	2	3
PS	12	30.9		
PCC	12		33.0	
LM	12			36.3
MCC 105	12			36.6
Sig.		1.000	1.000	0.568

Table 3.21b *Post hoc test for powder*

Homogenous Subsets- Effective angle of friction

Scheffé

POWDER	N	Subset			
		1	2	3	4
PS	12	34.1			
PCC	12		39.6		
LM	12			41.9	
MCC 105	12				43.8
Sig.		1.000	1.000	1.000	1.000

Table 3.21c *Post hoc test for powder*

Homogenous Subsets- Flow function

Scheffé

POWDER	N	Subset		
		1	2	3
PCC	12	3.58		
MCC 105	12	3.99		
LM	12		4.52	
PS	12			8.35
Sig.		0.112	1.000	1.000

Figures 3.15c and d illustrate the effect of consolidation-step time on the flow function and the normalised cohesion coefficient. The statistical evaluation of the effect of varying the consolidation-step time on the flow function and normalised cohesion coefficient of the powders are shown in Table 3.21d – f. From Table 3.20 it can be seen that a significant difference exists between the flow functions of the powders when different consolidation-step time was used.

Table 3.21d *Post hoc test for consolidation-step time*

Homogenous Subsets- Flow function

Scheffé

CONSOLIDATION TIME	N	Subset		
		1	2	3
5 min	12	4.70		
3 min	12	4.97	4.97	
1 min	12		5.20	5.20
2 min	12			5.57
Sig.		0.445	0.576	0.169

Table 3.21e *Post hoc test for powder*

Homogenous Subsets-Normalised cohesion coefficient

Scheffé

POWDER	N	Subset		
		1	2	3
PS	12	0.768		
LM	12		1.46	
PCC	12		1.52	
MCC 105	12			3.91
Sig.		1.000	0.732	1.000

Table 3.21f *Post hoc test for consolidation-step time*

Homogenous Subsets-Normalised cohesion coefficient

Scheffé

CONSOLIDATION-STEP TIME	*N*	Subset	
		1	2
2 min	12	1.84	
1 min	12	1.84	
3 min	12	1.95	1.95
5 min	12		2.02
Sig.		0.105	0.470

The result of the post hoc test (Table 3.21c) performed on the powders indicates that the flow functions of precipitated calcium carbonate and microcrystalline cellulose type 105 are similar while α-lactose monohydrate and pregelatinised starch are different as they are

in different subsets. This view is supported by the graphical illustration (Fig. 3.15c), as the curve obtained for each powder on varying the consolidation-step time is grouped individually. However, the curves obtained for precipitated calcium carbonate and microcrystalline cellulose type 105 are not so distinctly far from each other. In Table 3.21d, the post hoc test shows that no significant difference exists between 5 and 3 minutes, 3 and 1 minute, 1 and 2 minutes consolidation time. Statistically, it is correct, however, to conclude that the consolidation-step time has an influence on the flow function values obtained as there was an interaction between the two factors.

A significant difference exists between the normalised cohesion coefficients of the powders (see Table 3.20). The normalized cohesion coefficient grouped the powders into three groups as shown in Table 3.21e. The post hoc test indicates that α-lactose monohydrate and precipitated calcium carbonate possesses similar flow behaviour, with pregelatinised starch and microcrystalline cellulose having different powder flow behaviour. This is confirmed graphically in Figure 3.15d, with precipitated calcium carbonate and α-lactose monohydrate's curves overlapping, and pregelatinised starch and microcrystalline cellulose type 105 curves distinctively grouped. The post hoc test on consolidation-step time (Table 3.21f) shows that 2, 1, and 3 minutes are related and no significant difference exists between 3 and 5 minutes consolidation time. The table also indicates that a difference exists between 2 and 1 minute consolidation-step time and 5 minutes consolidation- step time.

Based on visual observation of the shear test, 2 minutes consolidation time is recommended. The longer the consolidation time, the longer is the shear test and more ejection of powders between the cell base and the cell ring occurs.

3.5.2.6. Effect of varying the shear-step time

The shear-step time is the time interval specified for the execution of the shear-step. The shear-step follows the consolidation-step. The effect of varying the shear-step time on the failure properties of the model powders is shown in Figure 3.16a - d. The results are the mean and standard deviation of three replicates.

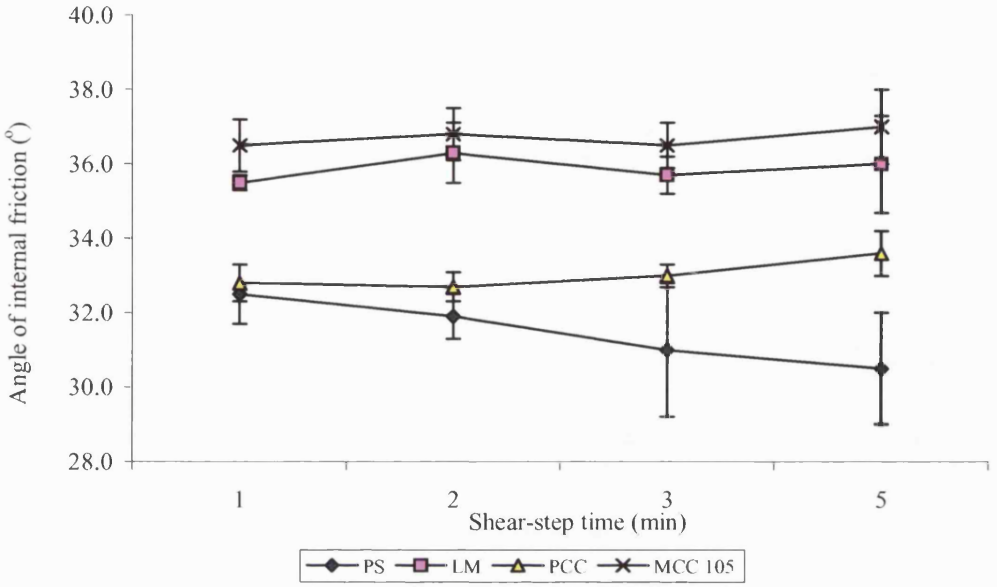

Figure 3.16a *Effect of shear-step time on angle of internal friction (mean and s.d. for 3 replicates)*

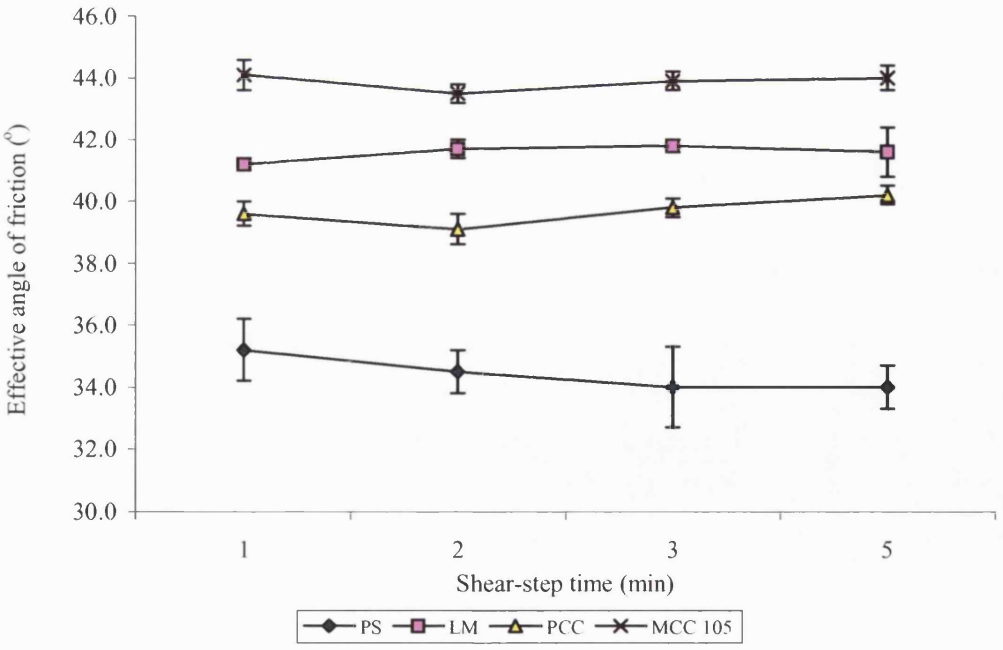

Figure 3.16b *Effect of shear-step time on effective angle of friction (mean and s.d. for 3 replicates)*

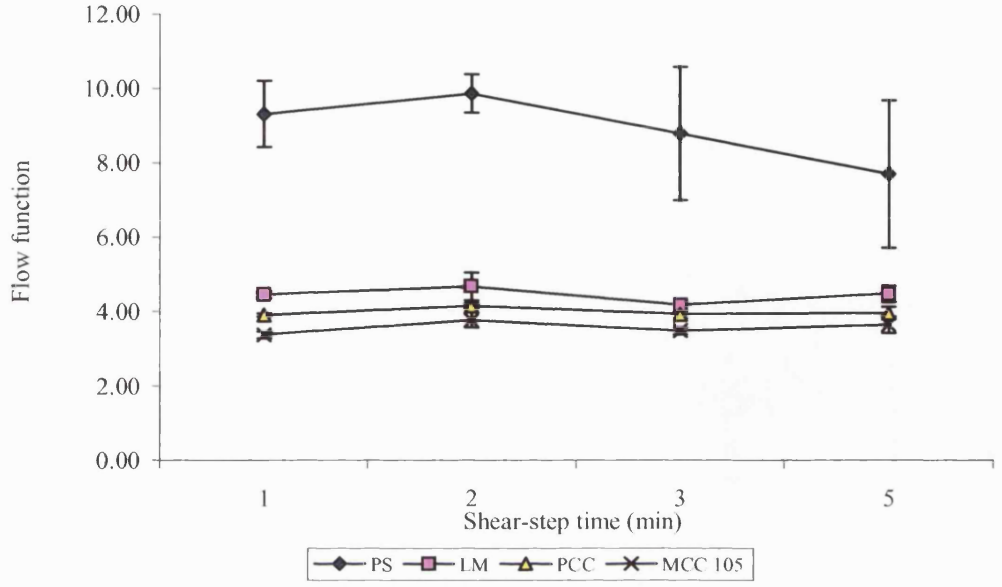

Figure 3.16c *Effect of shear-step time on flow function (mean and s.d. for 3 replicates)*

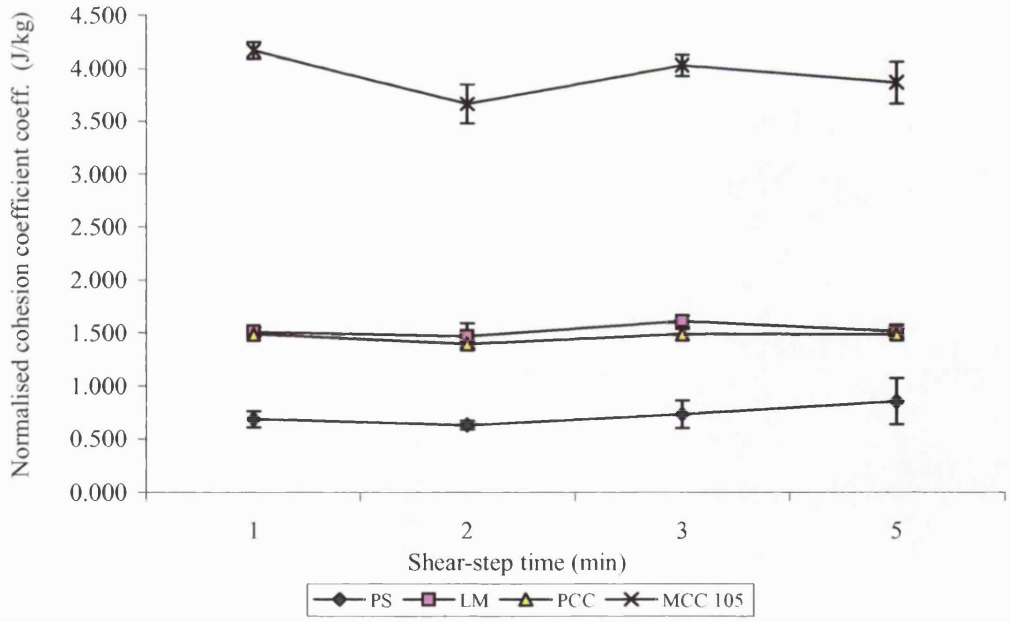

Figure 3.16d *Effect of shear-step time on normalised cohesion coefficient (mean and s.d. for 3 replicates)*

Table 3.22 shows that a significant difference exists between the angles of internal friction and effective angles of friction of the powders, respectively, when the shear-time was varied. The post hoc test shows that all the effective angles of friction of the powders are different, hence, grouped individually. On the other hand, the angles of internal friction of the powders are separated into three groups with α-lactose monohydrate and microcrystalline cellulose showing no significant difference (see Table 3.23a). Statistical evaluation revealed that the shear-step time is not a significant factor if each individual powder is studied ($p > 0.050$).

From Figure 3.16a, it can be seen that varying the shear-step time did not have a significant impact on the angles of internal friction of microcrystalline cellulose type 105, precipitated calcium carbonate and α-lactose monohydrate. The angles of internal friction obtained at each shear step are comparable. On the other hand, the angles of internal friction of pregelatinsed starch decreased progressively on varying the shear-step time. The apparent influence of the shear-step time on the powders could be attributed to the enhanced re-arrangement of the particles as the shear-time increased. The longer shear step time might have facilitated particle-particle adhesion leading to higher values for the angle of internal friction.

Table 3.22 *Tests of significance for effects of shear-step time*

SOURCE	df	Angle of Internal Friction		Effective Angle of friction		Flow Function		Normalised cohesion coefficient	
		F	*p*	F	*p*	F	*p*	F	*p*
Powder	3	111.10	<0.001	0.63	<0.001	181.05	<0.001	2024.01	<0.001
S-S time	3	0.32	0.860	624.75	0.638	1.31	0.282	2.31	0.074
Pow.*S-S time	6	1.32	0.243	1.21	0.306	1.10	0.386	1.40	0.205

Pow. - Powder

Shear-step time (S-S time) – 1, 2, 3 and 5 minutes

The same pattern is apparent for the effective angle of friction (Fig. 3.16b), except that the powders are all grouped individually, suggesting that the powders do have different flow behaviour.

Table 3.23a: *Post hoc test for powder*

Homogenous Subsets-Angle of internal friction

Scheffé

POWDER	N	Subset		
		1	2	3
PS	15	31.5		
PCC	15		32.9	
LM	15			36.0
MCC 105	15			36.6
Sig.		1.000	1.000	0.281

Table 3.23b: *Post hoc test for powder*

Homogenous Subsets- Effective angle of friction

Scheffé

POWDER	N	Subset			
		1	2	3	4
PS	15	34.4			
LM	15		39.6		
PCC	15			41.6	
MCC 105	15				43.8
Sig.		1.000	1.000	1.000	1.000

Table 3.23c *Post hoc test for powder*

Homogenous Subsets-Flow function

Scheffé

POWDER	N	Subset		
		1	2	*3*
MCC 105	15	3.54		
PCC	15	3.96	3.96	
LM	15		4.52	
PS	15			8.84
Sig.		0.465	0.206	1.000

Table 3.23d *Post hoc test for powder*

Homogenous Subsets-Normalised cohesion coefficient

Scheffé

POWDER	N	Subset		
		1	2	3
PS	15	0.733		
PCC	15		1.47	
LM	15		1.50	
MCC 105	15			3.96
Sig.		1.000	0.926	1.000

The effect of varying the shear-step time on the flow function of the powders is shown in Figure 3.16c. In Table 3.22, a significant difference was found for the flow function of the powders. In addition, the flow functions of the powders also showed similar pattern of

powder grouping as observed for the normalised cohesion coefficient (see Table 3.23c and d). It can be seen from these tables that pregelatinised starch and microcrystalline cellulose type 105 have different flow behaviour, while the flow behaviour of calcium carbonate and lactose monohydrate appears to be similar. No significant difference was found when using the shear-step time as influence factor.

Figure 3.16d shows the effect of shear-step time on the normalised cohesion coefficient of the powders. As seen in Table 3.22, a significant difference was found for the normalised cohesion coefficient of the powders. Using the Scheffé test, the statistical significance between the powders was determined. Table 3.23d shows that all the powders are different in terms of their normalised cohesion coefficients. While the normalised cohesion coefficient of calcium carbonate and α-lactose monohydrate are similar (Table 3.23d), the other powders are clearly different, hence the different subsets. The graphical illustration (Figure 3.16d) is in agreement with the statistical evaluation. Here, there is an overlap between the curves obtained for precipitated calcium carbonate and α-lactose monohydrate, while those of pregelatinised starch and microcrystalline cellulose type 105 could be found at the opposite ends of the plot.

Visual observations during the experiment revealed, that the longer the shear-step time was, the greater was the powder ejection between the cell base and ring. Hence, despite the differences seen, a 2 minutes shear-step time is recommended for the shear test as a standard parameter.

3.5.2.7. Effect of varying the expansion time

During the shear test, there is a transition from the static to the shear stage. At this point, the powder expands, and hence, the expansion time is the time allowed for the expansion of powder to occur during the transition stage. Figures 3.17a – d shows the effect of expansion time on the shear properties of the powders. The results are the mean and standard deviation of three replicates.

Figure 3.17a shows the angle of internal friction of the powders as a function of expansion time. Statistical analysis (Table 3.24) indicates that varying the expansion time had no significant effect on the angle of internal friction. However, a significant difference exists between the angles of internal friction of the powders when this parameter was considered. Using the the post hoc test, the statistical significance between the powders was determined. From Table 3.25a it could be seen that similar flow behaviour was experienced by α-lactose monohydrate and microcrystalline cellulose type 105 as they share the same subset. However, pregelatinised starch and precipitated calcium carbonate powders do possess different flow behaviour, as each occupies a different subset. This indication is confirmed by the graphical illustration (see Fig. 3.17a) i.e. microcrystalline cellulose and lactose monohydrate in one group, and precipitated calcium carbonate and pregelatinised starch in another group. Although statistical analysis indicated a significant difference between precipitated calcium carbonate and pregelatinised starch, the graphical illustration seems to group them as a one. An interaction exists between the powder and the expansion time when the angle of internal friction was considered, which is indicated by the F-value of 3.15 corresponding to an error probability of $p = 0.020$. This indicates that the expansion time is a significant factor if each powder is studied individually.

Figure 3.17b shows the effect of varying the expansion time on the effective angle of friction of the powders. A significant difference exists between the effective angle of friction of the powders (Table 3.24). Using the post hoc test, the statistical significance between the powders was determined. Table 3.25b shows that each powder is different from the other as each occupies a separate subset, indicating different flow behaviour when this parameter is considered. The graphical illustration (Fig. 3.17b) also shows this difference clearly, as the powders are grouped individually. From Table 3.24, it can be seen that using a different expansion time did not have any significant effect alone on the angle of internal friction or effective angle of friction of the powders.

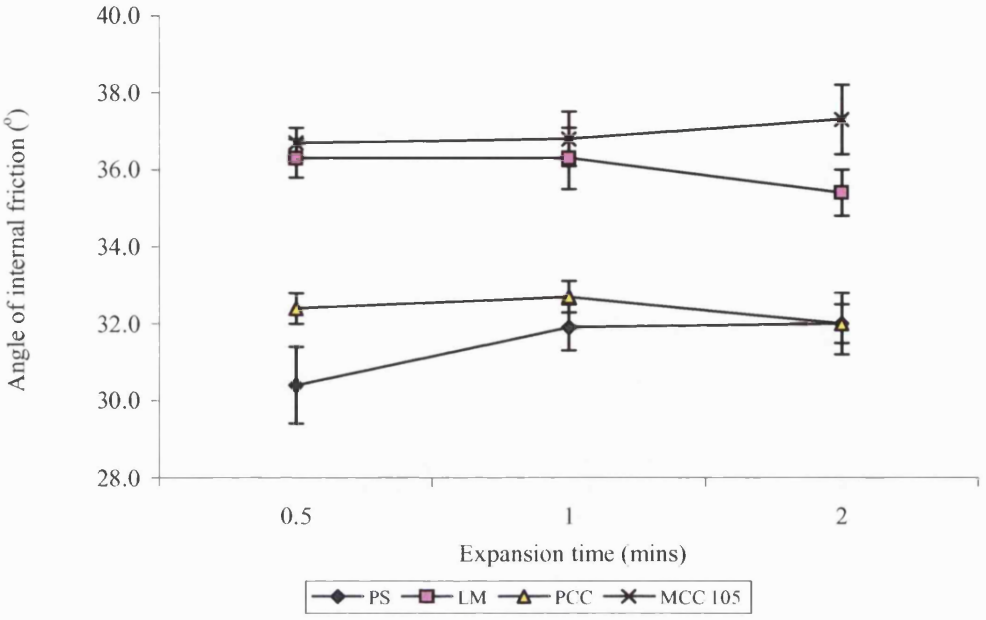

Figure 3.17a *Effect of expansion time on angle of internal friction (mean and s.d. for 3 replicates)*

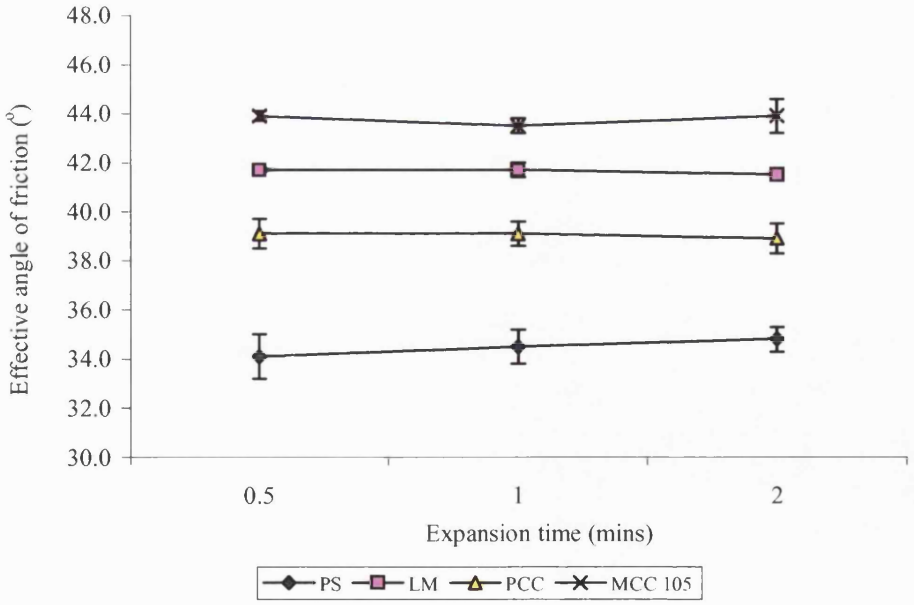

Figure 3.17b *Effect of expansion time on the effective angle of friction (mean and s.d. for 3 replicates)*

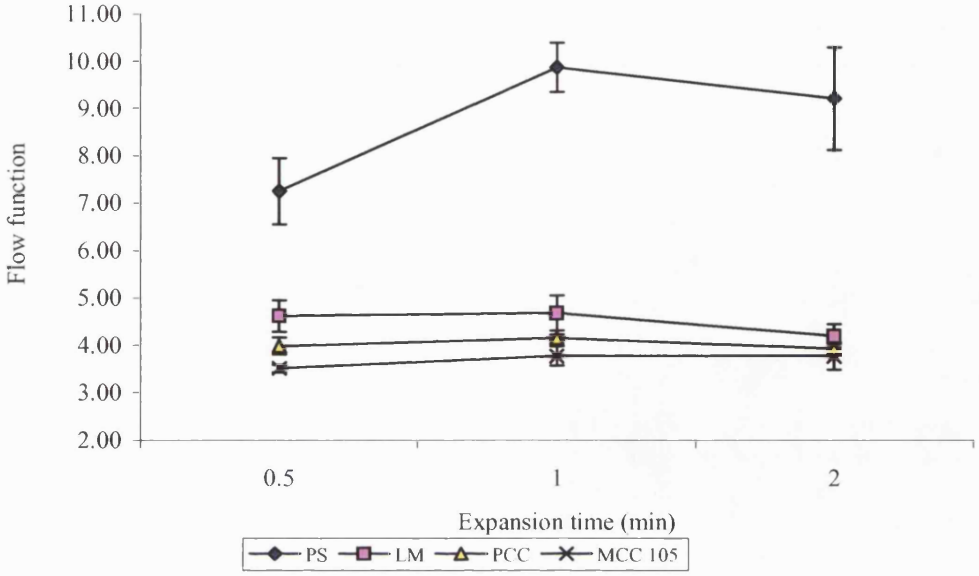

Figure 3.17c *Effect of expansion time on flow function (mean and s.d. for 3 replicates)*

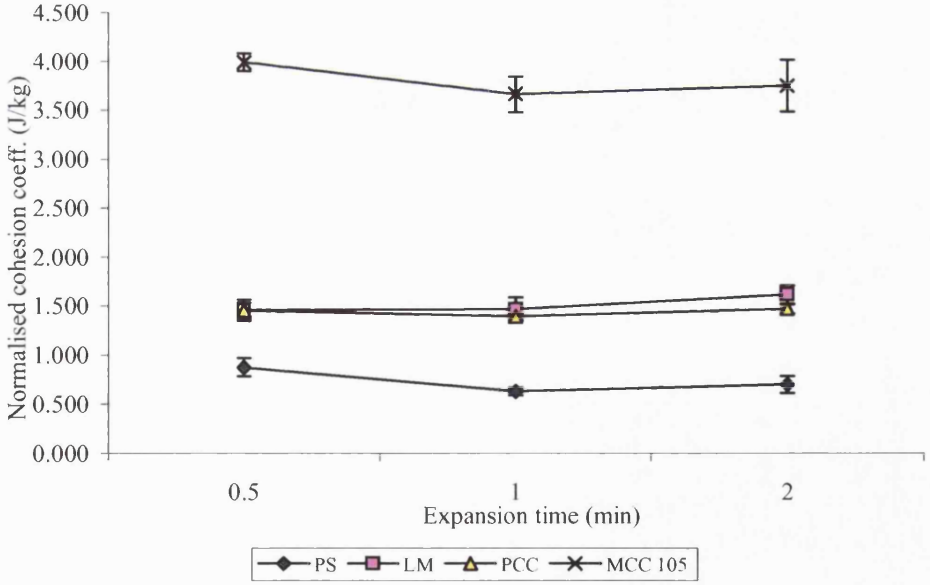

Figure 3.17d *Effect of expansion time on normalised cohesion coefficient (mean and s.d. for 3 replicates)*

Table 3.24 *Tests of significance for effects of expansion time*

SOURCE	df	Angle of Internal Friction		Effective Angle of friction		Flow Function		Normalised cohesion coefficient	
		F	*p*	F	*p*	F	*p*	F	*p*
Powder	3	151.42	<0.001	571.69	<0.001	257.88	<0.001	1193.12	<0.001
Expantime	2	0.86	0.436	0.10	0.905	8.05	0.002	2.61	0.094
Powder*Expantime	6	3.15	0.020	0.864	0.535	7.03	0.020	2.02	0.103

Expantime – 0.5, 1, 2 minutes expansion time

Table 3.25a *Post hoc test for powder*

Homogenous Subsets - Angle of internal friction

Scheffé

POWDER	N	Subset		
		1	2	3
PS	9	31.4		
PCC	9		32.4	
LM	9			36.0
MCC 105	*9*			36.8
Sig.		1.000	1.000	1.000

Table 3.25b *Post hoc test for powder*

Homogenous Subsets- Effective angle of friction

Scheffé

POWDER	N	Subset			
		1	2	3	4
PS	9	34.4			
PCC	9		39.0		
LM	9			41.6	
MCC 105	9				43.7
Sig.		1.000	1.000	1.000	1.000

Table 3.25c *Post hoc test for powder*

Homogenous Subsets-Flow function

Scheffé

POWDER	N	Subset		
		1	2	3
MCC 105	9	3.62		
PCC	9	4.02	4.02	
LM	9		4.50	
PS	9			8.78
Sig.		0.345	0.189	1.000

Table 3.25d *Post hoc test for expansion time*

Homogenous Subsets- Flow function

Scheffé

EXPANSION TIME	N	Subset	
		1	2
expantime 0.5 min	12	4.84	
expantime 2 min	12	5.27	5.27
expantime 1 min	12		5.57
Sig.		0.085	0.272

Figure 3.17c shows the flow function as a function of expansion time. Table 3.24 shows that a significant difference exists between the flow functions of the model powders when the expansion time was varied. From the significant interaction between powder and expansion time, it can be concluded that the influence of the expansion time on the flow function varies with the powder tested. Using the post hoc test, the statistical difference between the mean of the flow functions was determined. Based on the flow function (see Table 3.25c), the powders are divided into three groups with pregelatinised starch in its own subset by virtue of having the largest mean flow function and hence, a different powder behaviour. This is hardly surprising, as, for example, the rugosity, surface area and particle shape could be attributed to the high flow function value observed for pregelatinised starch (see section 3.1). Figure 3.17c shows that for pregelatinised starch, there was an increase in the flow function value when the expansion time was increased from 0.5 to 1 minute and further increment did not have any major impact on the flow function. Table 3.25d shows that no significant difference exists between 0.5 and 2 minutes expansion time as well as 2 and 1 minute expansion time.

The effect of expansion on the normalised cohesion coefficient values of the powders is considered graphically in Figure 3.17d. Table 3.24 shows that a statistical difference exists

between the normalised cohesion coefficients of the powders. In Table 3.25e, the powders are separated into three groups with lactose monohydrate and precipitated calcium carbonate sharing on subset, while pregelatinised starch and microcrystalline cellulose type 105 could be found in separate subsets. This trend is repeated in the graphical illustration (see Fig. 3.17d). In addition, a slight overlap of the calcium carbonate curve and lactose monohydrate curve can be seen. This may indicate similar flow behaviour. The large normalised cohesion coefficient value experienced for microcrystalline cellulose type 105 may be due to the interlocking of the elongated particle shape, as particles with such morphology tend to orientate themselves so that such mechanism prevails.

Choosing the right expansion time is very crucial as increasing the expansion time to more than required will lead to more ejection of powder from the cell and also to an increase in analysis time.

Table 3.25e *Post hoc test for powder*
Homogenous Subsets-Normalised cohesion coefficient
Scheffé

POWDER	N	Subset		
		1	2	3
PS	9	0.736		
PCC	9		1.44	
LM	9		1.52	
MCC 105	*9*			3.87
Sig.		1.000	0.621	1.000

According to Cleaver et al., (2000), during shearing powders expand to accommodate stress and the only direction in which the expansion can take place is vertically upwards. As such this may have contributed to the lifting of the cell ring leading to higher amounts of powder being ejected when the expansion time was increased to 2 minutes.

Hence, measurement time should be kept as short as possible but not too short to prevent powder sample expansion. From the results obtained there is no evidence that a prolonged

expansion time would improve the results in any way, but an expansion time of less than 1 minute appeared to suppress powder expansion. Hence, 1 minute expansion time is recommended.

3.5.2.8. Effect of varying the number of shear-steps

In this experiment, three variations were considered utilising 4.095 kPa as initial load. The variations are as follows:

5 shear-steps: only five shear steps were utilised using 4.095, 3.924, 2.943, 1.962 and 0.981 kPa load.
6 shear-steps: 4.905, 3.924, 2.943, 1.962, 0.981 and 0.491 kPa. This is the standard shear-step setting.
10 shear-steps: 4.905, 4.415, 3.924, 3.434, 2.943, 2.453, 1.962, 1.472, 0.981 and 0.491 kPa.

The results are shown graphically in Figure 3.19a - d. and are the mean and standard deviations of three replicates.

Figures 3.18a and b show the effect of varing the shear-step number on the angle of internal friction and effective angle of friction, respectively. As can be seen from Table 3.26, a significant difference exists between the powders and the shear-steps number (error probability was smaller than 0.05). Using the post hoc test, the statistical difference between the mean angles of internal friction and effective angles of friction was determined (see Table 3.27a - c). No statistical difference exists between pregelatinised starch and calcium carbonate, and there is also no difference between α-lactose monohydrate and microcrystalline cellulose (Table 3.27a). The graphical illustration (Fig. 3.18a) also shows that the powders are grouped into two distinct groups, with microcrystalline cellulose and α-lactose monohydrate at the top end while calcium carbonate and pregelatinised starch can be found at the lower end of the graph. On the contrary, this trend is not repeated by the effective angle of friction of the powders on varying the number of shear-steps. In this case, each powder is distinct from the other (Fig. 3.18a).

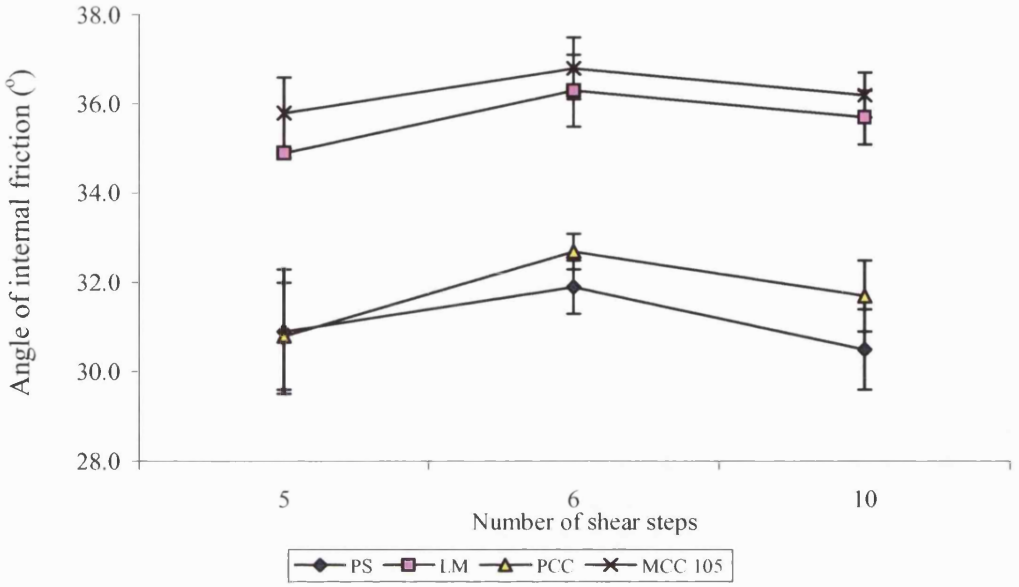

Figure 3.18a *Effect of varying shear-step on angle of internal friction (mean and s.d. for 3 replicates)*

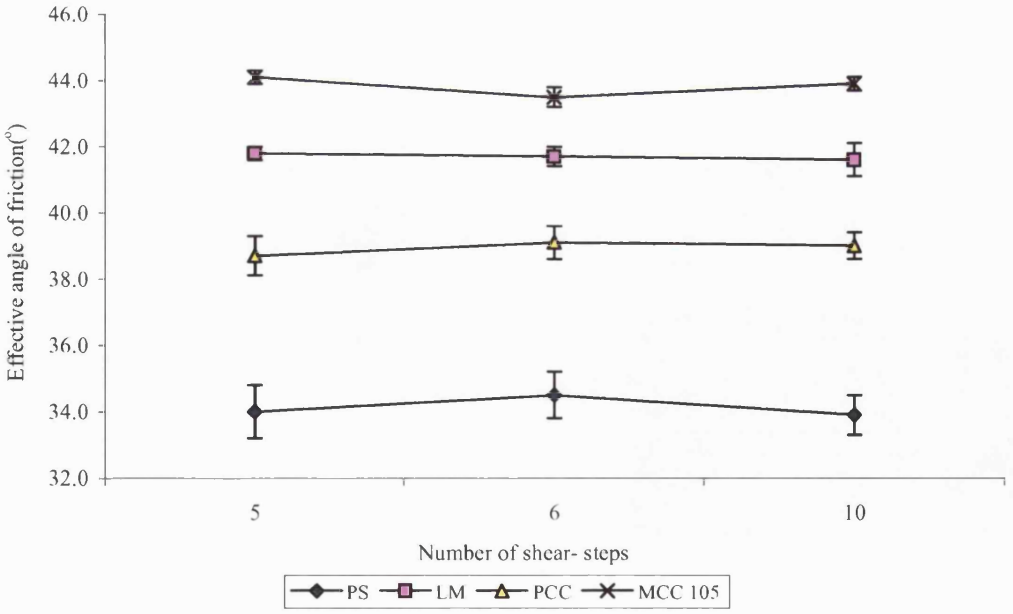

Figure 3.18b *Effect of varying shear-step on effective angle of friction (mean and s.d. for 3 replicates)*

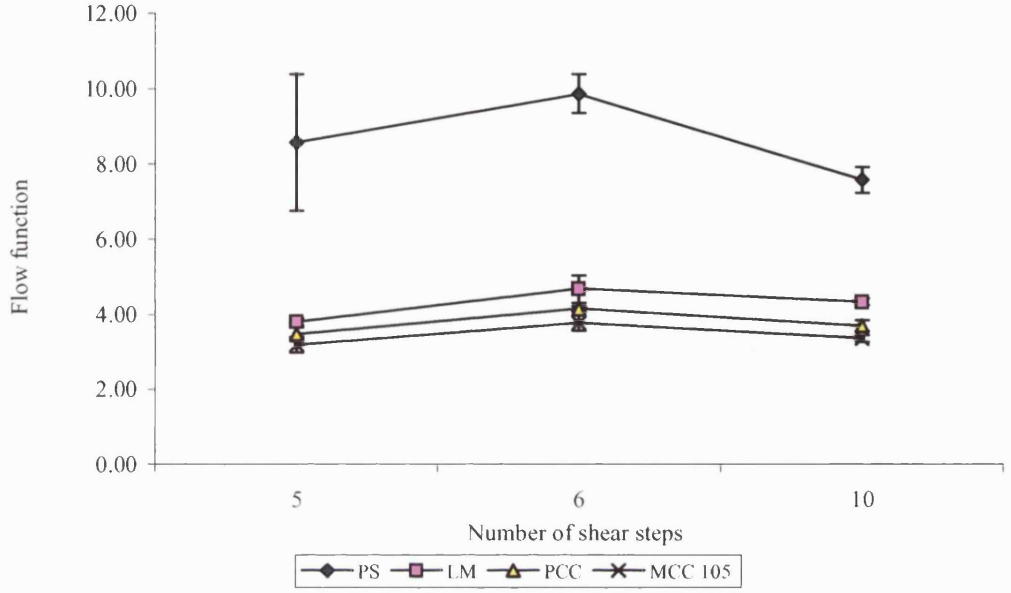

Figure 3.18c: *Effect of varying the shear-step time on flow function (mean and s.d. for 3 replicates)*

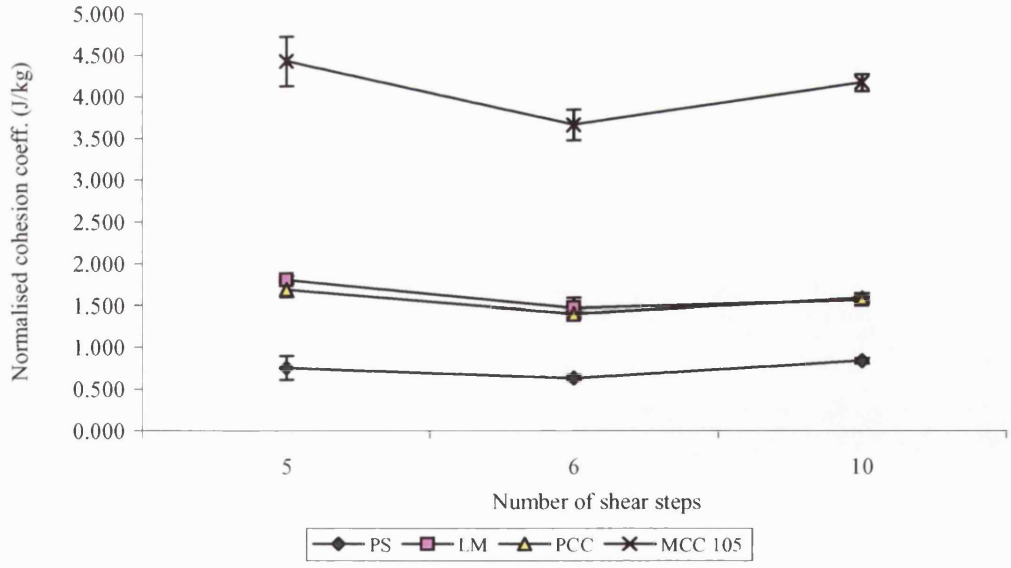

Figure 3.18d: *effect of varying the shear-step on normalised cohesion coefficient (mean and s.d. for 3 replicates)*

The post hoc test indicated that there was no difference between using 5 shear-steps or 10 shear-steps and 10 shear-steps or 6 shear-steps (Table 3.27b).

Figure 3.18c and show the flow function and normalised cohesion coefficients of the powder as a function of shear-step number, respectively. From Table 3.26, it can be seen that there is a significant difference in the flow function of the powders, which is further explored in Table 3.27d. A similar trend as for the effective angle of friction of the powders (Fig. 3.18b) could be observed. The only exception is that pregelatinised starch is distinctly separate (Fig. 3.18c) from the other powders and not grouped with any other powder.

Table 3.26 *Tests of significance for effect of number of shear-steps*

SOURCE	df	Angle of Internal Friction		Effective Angle of friction		Flow Function		Normalised cohesion coefficient	
		F	*p*	F	*p*	F	*p*	F	*p*
Powder	3	98.93	<0.001	699.98	<0.001	165.11	<0.001	1308.25	< 0.001
Shear-step No.	2	7.18	0.004	0.04	0.953	8.21	0.002	21.92	< 0.001
Powder*S-S No.	6	0.87	0.529	1.09	0.392	2.34	0.063	2.29	0.069

Shear-step No. (S-S No.) – 5, 6 and 10 number of shear-steps

Statistical evaluation also reveals that a significant difference exists between the shear-step numbers (Table 3.26). Further analysis shows (see Table 3.27e) that no significant difference exists in the results if 10 or 5 shear-steps are used, whereas a significant difference exists between the results of these set-ups and the 6 shear-step findings.

Table 3.27a *Post hoc test for powder*

Homogenous Subsets- Angle of internal friction
Scheffé

POWDER	N	Subset	
		1	2
PS	9	31.1	
PCC	9	31.7	
LM	9		35.6
MCC 105	9		36.1
Sig.		0.447	0.662

Table 3.27b *Post hoc test for number of shear-steps*

Homogenous Subsets- Angle of internal friction
Scheffé

NUMBER OF SHEAR-STEPS	N	Subset	
		1	2
5 shear-steps	9	33.1	
10 shear-steps	9	33.5	33.5
6 shear-steps	9		34.3
Sig.		0.424	0.075

Table 3.27c *Post hoc test for powder*

Homogenous Subsets- Effective angle of friction
Scheffé

POWDER	N	Subset			
		1	2	3	4
PS	9	34.2			
LM	9		39.0		
PCC	9			41.6	
MCC 105	9				43.8
Sig.		1.000	1.000	1.000	1.000

Table 3.27d *Post hoc test for powder*

Homogenous Subsets- Flow function

Scheffé

POWDER	N	Subset		
		1	*2*	3
MCC 105	9	3.38		
PCC	9	3.77	3.77	
LM	9		4.27	
PS	9			8.67
Sig.		0.559	0.364	1.000

Table 3.27e *Post hoc test for number of shear-steps*

Homogenous Subsets- Flow function

Scheffé

NUMBER OF SHEAR-STEPS	N	Subset	
		1	2
10 shear-steps	12	4.74	
5 shear-steps	12	4.76	
6 shear-steps	12		5.57
Sig.		0.997	1.000

Table 3.27f *Post hoc test for powder*

Homogenous Subsets- Normalised cohesion coefficient

Scheffé

POWDER	N	Subset		
		1	2	3
PS	9	0.740		
PCC	9		1.55	
LM	9		1.61	
MCC 105	9			4.15
Sig.		1.000	1.000	1.000

Table 3.27g *Post hoc test for number of shear-steps*

Homogenous Subsets- Normalised cohesion coefficient

Scheffé

NUMBER OF SHEAR-STEPS	N	Subset	
		1	2
6 shear-steps	12	1.84	
10 shear-steps	12		2.03
5 shear-steps	12		2.17
Sig.		1.000	0.052

Similarly, a significant difference exists between the normalised cohesion coefficient values of the powders and when this parameter was considered (see Table 3.26). In Table 3.27f, the post hoc test shows that apart from pregelatinised and microcrystalline cellulose 105, the other powders have similar normalised cohesion coefficient values. The graphical illustratioalso confirms this. Here, the powders are grouped into three groups, with microcrystalline cellulose and pregelatinised starch distinctively separate from the other powders.

Hence, it can be concluded that, using 6 shear-steps would give reproducible results.

3.5.2.9. Effect of varying the standard deviation value from linear approximation

In the software version available with the Peschl shear cell (Peschl, 2000), it is assumed that a linear model can be used to describe the yield locus. The software hence uses linear regression to approximate the yield locus. In linear regression, the deviation of the original data from the regression line can be quantified by calculating the standard deviation of the data from the regression line. In the ideal case all experimental data will lie precisely on the

regression line, and in such case the standard deviation would be zero. Experimental data however, will never fit completely and hence the standard deviation of the regression line will be larger than zero. Peschl uses hence the standard deviation as a measure of goodness of fit. Peschl suggests that the standard deviation should not exceed a value of 0.029 kPa and he used this value as a quality criterion in his software.

The effect of varying the standard deviation of measured points from the automatically calculated linear approximation was also assessed using three different specified standard deviation values (0.020, 0.029 and 0.049 kPa). This is particularly crucial for quality control purposes, where limits are required before a material is accepted or rejected. It should be noted that, varying the standard deviation of the measured points to the automatically calculated values should not have any effect on the obtained flow properties/ flow parameters used i.e. angle of internal friction, effective angle of friction etc. Table 3.28 shows the error probability of the effect of varying the standard deviation value. As seen from Table 3.28, varying the standard deviation of the measured points from the automatically calculated ones did not have any impact on the obtained flow parameters.

Table 3.28 *Tests of significance for effects of varying the standard deviation value for the linear approximation of the yield locus*

SOURCE	df	Angle of Internal Friction		Effective Angle of friction		Flow Function		Normalised cohesion coefficient	
		F	*p*	F	*p*	F	*p*	F	*p*
Powder	3	137.65	<0.001	699.98	<0.001	175.31	<0.001	1763.39	<0.001
Std - dev	2	2.91	0.073	1.40	0.265	4.36	0.024	2.90	0.074
Powder*Std-dev	6	1.19	0.341	8.56	0.541	2.72	0.037	0.56	0.754

Std- dev – standard deviation

However, significant differences exist between the powders as they possess different flow properties. This is not suprising, as this was found when the effect of varying the acceleration of vibration and sieve size was considered using 0.029 kPa standard deviation as operating parameter (see Table 3.12).

The standard deviation of measured points from the automatically calculated values has an implication for in-process control. The acceptable standard deviation for each powder should not be too high such that all measurements pass and not be too low so that measurements are not rejected often. Based on this, the 0.029 kPa is suggested as a guide, further analysis could be performed using various type of powder with different flow properties to ascertain a reliable limit for each group of powder.

3.5.2.10. Effect of varying the shear measurement

In this experiment, the shear measurement was varied using either the full or standard measurement. In the standard measurement, shearing continued until ten points after the peak. However, in the full measurement, shearing of the powder continued until 100 points after the peak. The results obtained for the full measurement are compared with those of the standard measurement in Figure 3.20a - d. The results are the mean and standard deviations of three replicates.

Statistical analysis (see Table 3.29) did not reveal any difference between the flow properties obtained when the standard shear measurement (10 points after the shear peak) was used and when the full measurement was used i.e. 100 points after the shear peak. From Figure 3.20a – d it can be seen that there is little or no variability in the flow properties of the powders when full measurement was used as opposed to when standard measurement was used. In addition, the measurement time was longer for the full measurement than for the standard measurement.

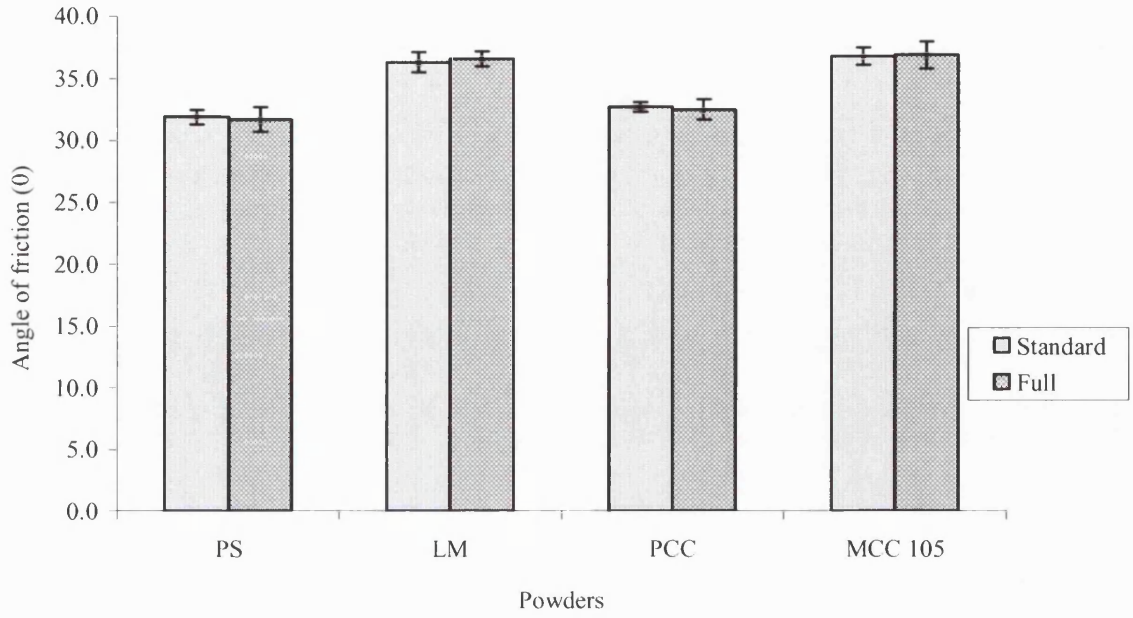

Figure 3.19a *Effect of varying the shear measurement on angle of internal friction (mean and s.d. for 3 replicates)*

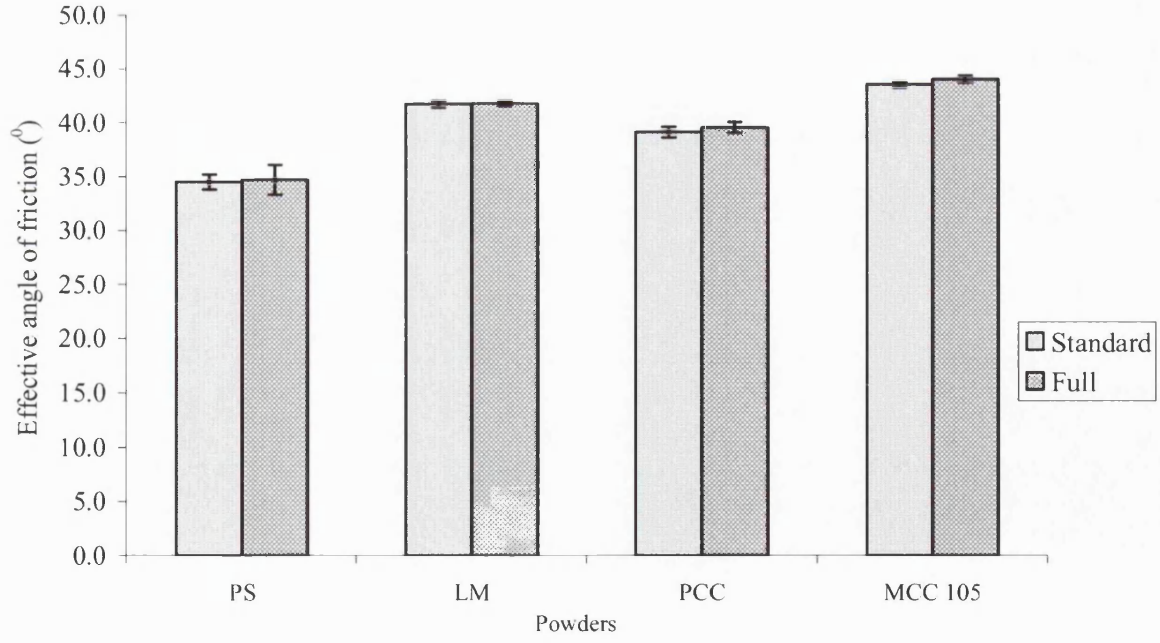

Figure 3.19b *Effect of varying the shear measurement on effective angle of friction (mean and. s.d. for 3 replicates)*

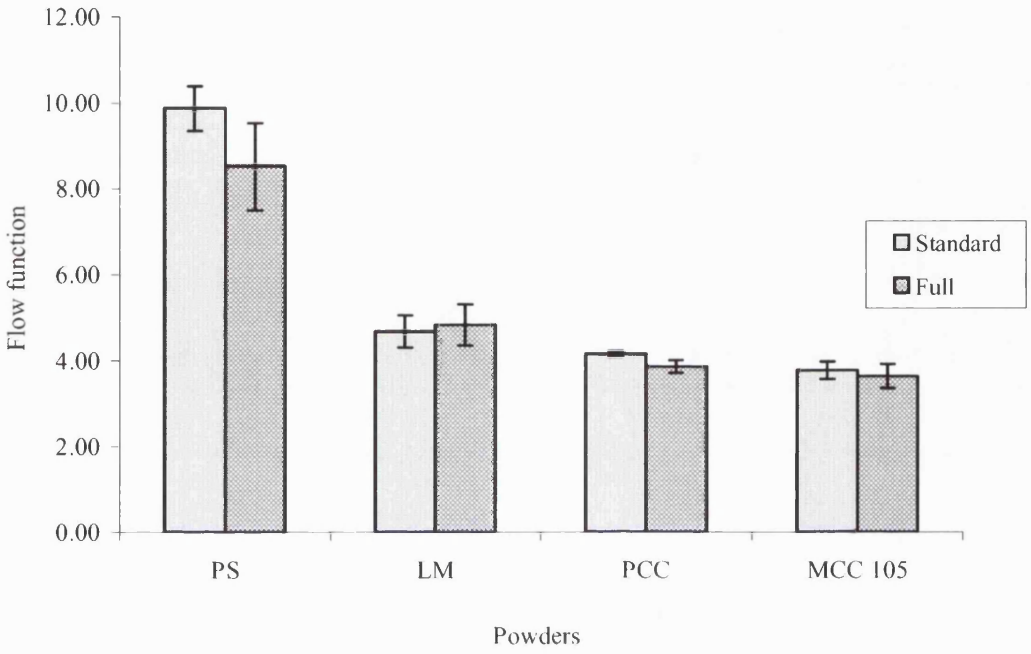

Figure 3.19c *Effect of varying the shear measurement on flow function (mean f and s.d. or 3 replicates)*

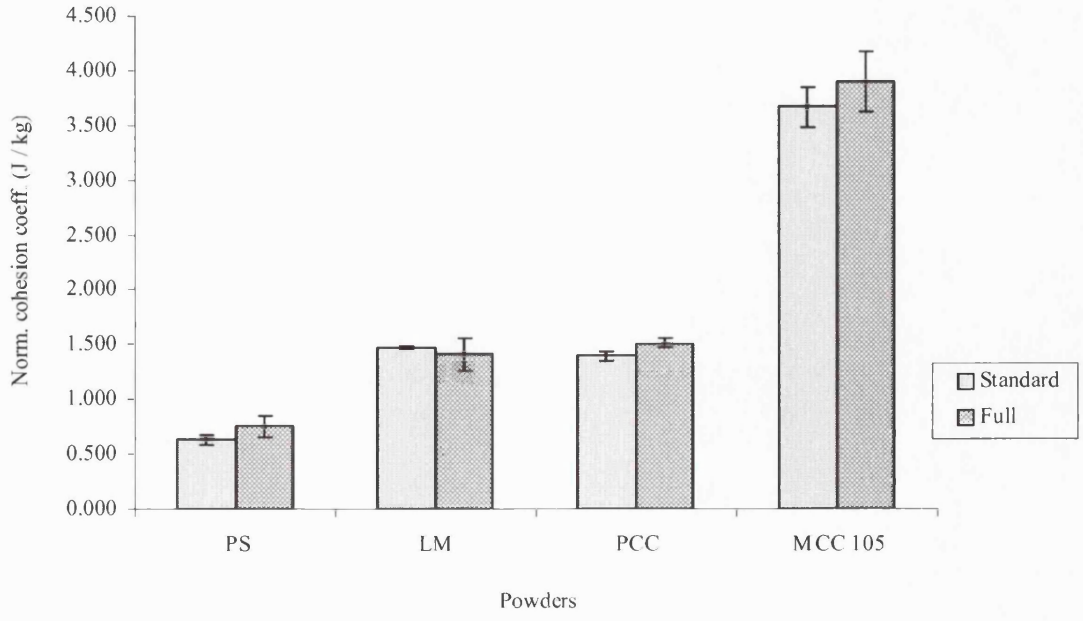

Figure 3.19d *Effect of varying the shear measurement on normalised cohesion coefficient (mean s.d. for 3 replicates)*

Table 3.29 *t - Test for effect of shear time on powder flow properties*

SOURCE	df	Angle of Internal Friction		Effective Angle of friction		Flow Function		Normalised cohesion coefficient	
		F	*p*	F	*p*	F	*p*	F	*p*
PS	4	1.13	0.346	0.87	0.404	2.05	0.225	2.76	0.172
LM	4	0.12	0.746	2.88	0.165	0.10	0.762	0.02	0.879
PCC	4	0.72	0.442	0.16	0.710	1.02	0.368	0.00	0.969
MCC 105	4	0.67	0.457	0.60	0.481	0.47	0.530	0.58	0.487

PS – Pregelatinised starch

LM – lactose monohydrate

PCC – Precipitated calcium carbonate

MCC 105 – Microcrystalline cellulose type 105

Physical observation during the experiment showed that using the full measurement increases not only the duration of shearing but also enhanced powder ejection between the cell base and the cell ring. In addition, the use of full shear measurement produced large variability in results as shown graphically. Taking all these aspects into account, the best shear measurement appears to be the standard shear measurement.

3.5.3. SUGGESTED STANDARD OPERATING PROCEDURE FOR THE PESCHL SHEAR TESTER WITH A STANDARD CELL

The suggested standard operating procedure as deduced from the evaluation of the operating parameters of the calibrated RO - 200 semi automated rotational split-level shear tester (Peschl shear tester) is given below:

3.5.3.1. Preparation of Peschl shear cell/Sample preparation

1. Switch on power supply, computer, monitor, air supply and the micro filtration unit.
2. Place the cell ring with the notches facing upward on top of the cleaned cell base ensuring alignment of the cell ring with the cell base before tightening the three centering pins.
3. Weigh the empty shear cell before placing the protection ring on top of the shear cell followed by the fill ring (1 cm ring for free-flowing powder and 2 cm for cohesive powders)
4. Fill the shear cell with the powder sample using the fill sieve with the fill sieve acceleration of vibration setting at 18.5 m/s^2 and the sieve size of 2.1 mm to remove agglomerates and to ensure uniform filling.
5. Remove small amount of excess powder at a time with the scraper/blade provided to prevent subjecting the powder specimen to a downward force (consolidation).
6. Scrape off powder above the upper edge of the fill ring and place the 'porous' consolidation lid on top of the powder as carefully as possible.
7. Place the shear cell on the consolidation bench, load with 4.905 kPa and preconsolidate for 8 minutes.
8. Remove the shear cell after completion from the consolidation bench and also remove the porous consolidation lid.
9. Remove the fill ring gently and any additional powder above the top of the shear cell scraping it off.
10. Using a fine brush, remove spilled powder from the shear cell.
11. Weigh the shear cell with the powder sample and determine the weight of the powder by subtracting the weight of the empty shear cell from the final weight.

3.5.3.2. Procedure for shear cell assembly

1. Place the three – legged top lid of the shear cell gently on the shear base ensuring that the loading lid (top cover) of the shear cell did not make any contact with the powder in the shear cell.

2. Lower the loading lids gently until the top cover touches the powder and tighten the three clamp screws immediately.

3.5.3.2. Mounting of the shear cell on the shear tester

1. Loosen the three screws on the turntable of the shear tester and place the shear cell assembly on the shear tester.
2. Position the shear cell such that the loading arm on the shear cell connects with the loading linkage on the shear tester.
3. Fix the shear cell to the turntable using the three screws and connect loading bar to the shear cell.
4. Loosen the centering screws gently so as not to disturb the powder packing and to ensure that the top cover could move freely.
5. Connect the air supply.

3.5.3.3. Measurement

1. Insert a floppy disc (all data will be stored automatically on this).
2. From the main menu, select 1 for "measure density", followed by 5 for "set up parameters for measurement" and '1' for yield locus. Use the measurement parameters for analysis given below:

Consolidation step load of 50 g/cm^2	- (4.905 kPa)
Shear step value per step	- 10 g/cm^2 (0.981 kPa)
Minimum/last shear step	- 5 g/cm (0.490 kPa)
Time factor consolidation step	- 2 min
Time factor shear step	- 2 min
Expansion time	- 1 min
Measurement type	- Standard
Data input	- 1 yield locus
Standard deviation	- 0.029 kPa (from linear approximation)

3. Enter a 'set up code'
4. Enter the sample details including the weight of powder sample.
5. Enter '0' to commence analysis.
6. Follow the instructions on the monitor for consolidation and shear tests analysis with regards to the loading and unloading process.

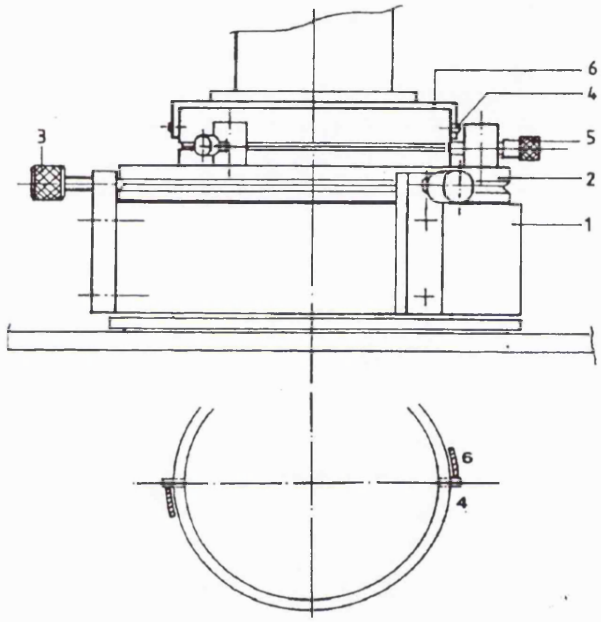

Figure 3.20 *Shear cell assembly on shear tester (Taken from Peschl shear tester Operating manual)1. Turntable, 2. Cell base, 3. Clamp screws for fixing the cell, 4. Pin on cell ring, 5. Centering screw for cell ring, 6. Lips on loading lid*

3.5.3.4. Evaluation of data

1. Return to main menu
2. Select option '4' for evaluation program.
3. Select '1' for yield locus
4. Enter test number of the data required.
5. Select '3' for full report.
6. Select '1' for correction of vertical load.
7. Select '1' for automatic correction according to measured density type.

3.5.3.5. Shut Down

1. After the completion of the analysis switch off the compressed air, micro filtration unit, shut down computer and switch off electric supply from mains.
2. Clean the equipment and surrounding area.

3.5.3.6. Maintenance

1. Ensure that the water collecting glass of the micro filtration unit and that of the compressed air are routinely emptied.
2. Ensure that the instrument is clean and calibrated before use.
3. For the replacement of filters in the compressed air and in the micro filtration units, consult the manufacturer's manual for guidance.

3.5.4. THE INFLUENCE OF RELATIVE HUMIDITY OF AIR ON SHEAR PROPERTIES

The graphical and statistical evaluation of the influence of relative humidity of air on shear properties are given below with each powder considered separately. Table 3.31 shows the effect of moisture (relative humidity of air) on the shear properties of the powders considered. The results are the mean and standard deviations of three replicates.

3.5.4.1. Pregelatinised starch

The effect of varying the relative humidity of the storage air on the flow properties of pregelatinised starch is shown in Table 3.30. Statistical evalustion did not reveal any significant difference ($p > 0.05$) in the angles of internal friction and ht eeefective angle of friction obtained after exposing the powder samples to different relative humidity of air. Thus, although slight differences appear to exist between the angles of internal friction as shown in Table 3.30, the variation is not large enough to result in significant changes in the angle of internal friction or effectve angle of friction.

The effect of relative humidity of air on the flow function of pregelatinised starch is shown in Table 3.30. Increasing the RH to 76 % led to a decrease in the powder flow as shown by the statistically significant ($p < 0.05$) reduction in the flow function (Table 3.31a). Though

the flow function values obtained after exposure to 76 and 35% RH share the same subset (see Table 3.31a) despite the large difference in values, the post hoc test utilised (Scheffé test) is highly conservative. The reason being that in the Scheffé test, a larger difference is required for significance. The increase in moisture content may have enhanced the presence of capillary forces in the powder bulk, and hence reduced the powder flow. Pregelatinised starch being hydrophilic will absorb much greater amounts of moisture into the powder bulk at corresponding humidities with no tendency to go into solution (Craik and Miller, 1958).

Table 3.30 *Flow properties of the model powders after exposure to different relative humidity of storage air (results are the mean and s.d. of 3 replicates)*

POWDER	Relative Humidity (%)	Angle of internal friction (°)	Effective angle of friction (°)	Flow function	Normalised cohesion coefficient (J/kg)
Pregelatinised starch	35	31.2 ± 0.4	34.0 ± 0.2	9.22 ± 0.87	0.53 ± 0.05
	45	32.0 ± 1.1	34.9 ± 0.6	9.69 ± 0.44	0.57 ± 0.10
	53	31.9 ± 0.7	34.5 ± 0.9	9.75 ± 1.15	0.51 ± 0.07
	76	30.3 ± 1.4	34.1 ± 1.0	6.92 ± 0.64	0.72 ± 0.07
α – lactose monohydrate	35	35.4 ± 0.2	41.6 ± 0.2	4.14 ± 0.07	1.14 ± 0.04
	45	35.9 ± 0.5	41.8 ± 0.2	4.28 ± 0.16	1.11 ± 0.04
	53	35.5 ± 0.5	41.7 ± 0.4	4.15 ± 0.06	1.15 ± 0.03
	76	36.0 ± 0.7	41.9 ± 0.3	4.30 ± 0.26	1.11 ± 0.07
Precipitated calcium carbonate	35	32.0 ± 0.6	39.0 ± 0.5	3.85 ± 0.03	1.06 ± 0.01
	45	32.7 ± 0.4	39.6 ± 0.4	3.84 ± 0.05	1.07 ± 0.02
	53	32.9 ± 0.3	39.7 ± 0.2	3.88 ± 0.12	1.06 ± 0.04
	76	32.6 ± 0.4	39.2 ± 0.1	4.02 ± 0.22	1.02 ± 0.06
Microcrystalline cellulose Type 105	35	36.6 ± 0.5	43.5 ± 0.3	3.71 ± 0.11	2.72 ± 0.07
	45	36.7 ± 0.2	43.8 ± 0.1	3.57 ± 0.10	2.84 ± 0.10
	53	36.8 ± 0.4	43.7 ± 0.3	3.67 ± 0.10	2.75 ± 0.11
	76	37.1 ± 0.2	44.1 ± 0.4	3.61 ± 0.14	2.88 ± 0.15

However, the extent of moisture absorption depends on the prevailing humidity and time of exposure. The sorption-desorption curves (Figure 3.10a) of this powder show that there was a progressive increase in water sorbed on increasing the relative humidity. This is an indication of the "hygroscopicity" (moisture absorption into the powder bulk rather than adsorption at the particle surfaces) of this powder.

Using the annular shear cell, Teunou and Fitzpatrick (1999) reported a decrease in the flowability of flour and whey on increasing the relative humidity of the storage air as a result of the moisture absorbing nature of the powders. Shotton and Harb (1966) concluded that the cohesiveness of the different types of starch powders considered was maximium after exposure to 66 % relative humidity of air. Increasing the relative humidity led to a decrease in the cohesiveness of the starch powders. This the authors attributed to the formation of starch granules from starch powder aggregates.

Table 3.31a *Post hoc test on relative humidity (OTHER)*

Homogenous subsets – Flow function
Scheffe

OTHER (RH)	N	Subset	
		1	2
RH 76 %	3	6.92	
RH 35 %	3	9.22	9.22
RH 45 %	3		9.69
RH 53 %	3		9.75
Sig		0.055	0.886

The storing of powder in a higher relative humidity environment had an effect on the normalised cohesion coefficient as indicated statistically i.e. $p < 0.05$ and in Table 3.30. Table 3.31b shows where the difference in the normalised cohesion coefficient values lies. As before, there was an increase in this value on exposing the powder to RH in excess of 53 %. This increase may have been the result of the presence of capillary forces at elevated relative humidity. The amount of moisture absorbed at lower relative humidities was not enough to hinder powder flow as the amount of moisture was not critical. Exceeding the RH above 53 % led to a significant decrease in the flow function and increase in the normalised cohesion coefficient, respectively (Table 3.30). This increase was also found to be statistically significant after exposure to 76 % RH. This finding is supported by the DVS

studies (see Chapter 3, section 3.2.3), where it was shown that pregelatinised starch sorbed moisture progressively on increasing the RH.

Table 3.31b *Post hoc test on relative humidity (OTHER)*

Homogenous subsets – Normalised cohesion coefficient
Scheffe

OTHER	N	Subset	
		1	2
RH 53 %	3	0.504	
RH 35 %	3	0.530	0.530
RH 45 %	3	0.571	0.571
RH 76 %	3		0.716
Sig		0.765	0.760

Using the tilting plate method, Shotton and Harb (1966) concluded that the cohesiveness of some starches (maize, wheat and potato) was maximal at about 66 % RH. A further increase in RH led to a decrease in this flow property. This was attributed to the capillary effect of surface moisture. This is contrary to the findings for the normalised cohesion coefficient, which increased on exposing pregelatinised starch to RH in excess of 53 % (see Table 3.30). The difference may lie in the water absorbing capability of the powders. Wurster et al. (1982) found that the amount of water bound by corn starch was lower than that of starch 1500. This variation may probably indicate that, exceeding the critical level as stipulated by Shotton and Harb (1966) may have enhanced the lubricating property of water or even resulted in the softening of the partice surfaces leading to an increase in powder flow.

3.5.4.2. α – lactose monohydrate

The flow properties of α – lactose monohydrate stored under varying RH are shown in Table 3.30. Statistical evaluation showed that the powder is not truly affected by the variation in the relative humidity of air ($p > 0.05$).

3.5.4.3. Precipitated calcium carbonate

The flow properties of precipitated calcium carbonate are shown in Table 3.30. The values obtained for each of the parameter considered on exposing precipitated calcium carbonate to different relative humidity of air were found not to be significant ($p > 0.05$). This could indicate that little or no moisture was adsorbed onto the surface of the powder particles. This was confimed by the DVS studies, which indicated minute weight gain for this powder on increasing the RH value (see Chapter 3, section 3.2.3). This is hardly surprising as calcium carbonate is hydrophobic in nature and the total amount sorbed (about 0.2 %) agrees with that obtained by Tan and Newton (1990a).

3.5.4.4. Microcrystalline cellulose type 105

The flow properties of MCC 105 exposed to different relative humidity of air are shown in Table 3.30. Similarly, no statistical significant difference was found when the flow parameters were considered on exposing the microcrystalline cellulose to different relative humidity of storage air ($p > 0.05$).

3.5.5. INFLUENCE OF PARTICLE SIZE AND RELATIVE HUMIDITY OF AIR ON SHEAR PROPERTIES OF POWDERS

The sensitivity of the rotational split-level shear tester to changes in particle size and the influence of relative humidity of air on the shear properties using the fractions of pregelatinised starch and α – lactose monohydrate were evaluated jointly.

3.5.5.1. Pregelatinised starch size fractions

Table 3.32 shows the flow properties of pregelatinised starch fractions after exposure to different levels of relative humidity (RH). Statistical evaluation reveals that no significant difference ($p > 0.05$) exists between the values of the flow properties of each fraction obtained after exposure to different relative humidity of storage air. However, from Table 3.32, it can be seen that exposing the larger size fraction to 76 % RH had an effect on the powder flow as indicated by the flow function value. At this RH, the powder experienced a poor powder flow. This is contrary to the result obtained for the angle of internal friction at that relative humidity. This shows that the flow function depends on other particle

properties such as particle size and shape and not on the surface properties such as particle surface texture.

Table 3.32 *Flow properties of the powder fractions after exposure to different relative humidity of storage air (results are the mean and s.d. of 3 replicates)*

POWDER	Relative Humidity (%)	Angle of internal friction (°)	Effective angle of friction (°)	Flow function	Normalised cohesion coefficient (J/kg)
Pregelatinised starch > 56 μm	35	33.5 ± 0.7	34.7 ± 0.6	20.42 ± 2.29	0.25 ± 0.03
	45	33.8 ± 0.9	35.1 ± 0.7	19.98 ± 3.74	0.26 ± 0.06
	53	34.1 ± 0.1	35.2 ± 0.2	20.38 ± 1.34	0.25 ± 0.02
	76	32.9 ± 0.5	34.5 ± 0.5	16.39 ± 0.98	0.31 ± 0.02
Pregelatinised starch < 56 μm	35	33.0 ± 0.8	37.2 ± 0.4	5.89 ± 0.33	1.11 ± 0.11
	45	32.0 ± 0.6	36.8 ± 0.9	5.48 ± 0.67	1.12 ± 0.15
	53	32.2 ± 0.3	37.1 ± 0.6	5.38 ± 0.40	1.12 ± 0.11
	76	31.9 ± 0.4	37.1 ± 0.9	5.06 ± 0.50	1.19 ± 0.16
α – lactose monohydrate > 56 μm	35	35.4 ± 0.6	36.8 ± 0.4	18.42 ± 1.69	0.24 ± 0.03
	45	35.8 ± 0.5	37.2 ± 0.5	17.70 ± 0.74	0.26 ± 0.01
	53	35.7 ± 0.5	37.0 ± 0.5	17.89 ± 0.74	0.25 ± 0.01
	76	35.8 ± 0.3	37.1 ± 0.4	17.52 ± 1.18	0.25 ± 0.02
α – lactose monohydrate < 56 μm	35	35.7 ± 0.3	43.4 ± 0.4	3.43 ± 0.12	1.58 ± 0.08
	45	35.6 ± 0.3	43.5 ± 0.1	3.31 ± 0.10	1.61 ± 0.05
	53	35.5 ± 1.2	43.4 ± 0.8	3.33 ± 0.13	1.61 ± 0.07
	76	35.5 ± 1.0	43.6 ± 0.5	3.27 ± 0.14	1.65 ± 0.09

This indicates that the higher the moisture content or atmospheric humidity the poorer the powder flow. The difference in *FF* value is more pronounced for the bigger size fraction on exposure to 76% RH than for the smaller size fraction. The normalised cohesion coefficient results of the pregelatinised starch size fractions are shown in Table 3.32. A close observation of the normalised cohesion coefficient of each fraction shows that the difference in the values for each powder after exposure to different relative humidity is not pronounced. Storing the powder in the 76% RH produced the highest effect on the larger size fraction. This shows that the amount of moisture absorbed not only enhanced the swelling of the powder particles, but also the formation of liquid bridges and ultimately the powder cohesiveness. However, this difference was found to be statistically insignificant.

Further analysis carried out to ascertain if any difference exists between the flow properties of the powders at similar RH, revealed that no statistical difference exists between the angles of internal friction of the powder fractions when exposed to 35, 53 or even 76 % RH. However, a significant difference exists when exposed to 45% RH. However, the effect of RH on the effective angle of friction of pregelatinised starch size fractions was not significant when exposed to 45% RH, but significant at the remaining relative humidities ($p < 0.05$). The value of δ of 34.0° obtained for pregelatinised starch > 56 μm size at 35% RH is equal to that obtained by Tan and Newton (1990a) at 35 ± 5% RH environment condition, using an annular shear cell similar in design to that of Carr and Walker (1967/68).

The flow functions of each size fraction at similar RH were found to be statistically different. This finding supports that of Tan and Newton (1990a), who found that the *FF* of pregelatinised starch fractions increased as the particle size increased using the annular shear cell. This strongly indicates that the *FF* could be a useful flow criterion to differentiate between powders where the angle of internal friction or even effective angle of friction fails to do so. Similarly, the normalised cohesion coefficient of each size fraction at similar RH differs significantly ($p < 0.05$).

It can be concluded that the bigger size fraction (> 56 μm) is less cohesive than the < 56 μm size fraction as revealed by the *FF* and normalised cohesion coefficient values, and the effect of varying the relative humidity of storage air is more pronounced in the bigger size fraction. This may be due to the bigger pores evident in the the bigger size fraction (see SEM, Chapter 3, Fig. 3.2 – 3.3 and also Table 3.5 for apparent particle density values) and hence, the capability of absorbing more moisture than the smaller size fraction on increasing the RH of storage air. The < 56 μm size fraction behaved differently in the presence of varying amount of relative humidity of air. The angle of internal friction of the larger size fraction of pregelatinised starch was found to be higher than that of the smaller size fraction. A likely reason could be the surface texture of the bigger size fraction. The values obtained for rugosity revealed that pregelatinsed starch (> 56 μm) has a large rugosity value of 4.641, as opposed to 3.578 obtained for the smaller size fraction (see

Chapter 3, section 3.1.6). The rugosity value, which is an indication of particle roughness and angularity (Robertson and Emödi, 1943), indicates that the larger pregelatinised starch size fraction has a particle surface texture which may have encouraged stronger particle-particle contact and hence, a high angle of internal friction. However, no significant difference ($p > 0.05$) exists between the angles of internal fricton of the two size fractions after exposure to different relative humidity of air.

3.5.5.2. α – lactose monohydrate size fractions

The flow properties of α – lactose monohydrate size fractions are shown in Table 3.32. Statistical evaluation indicates that no significant difference exists ($p > 0.05$) between the angles of internal fricition obtained for each size fraction on exposure to different RH. In addition, the difference between the angles of internal friction of the bigger size fraction and the smaller size fraction on exposing to various RH is minimal. This may be attributed to the fact that lactose monohydrate belongs to the group of powders that adsorb moisture onto the particle surfaces and hence, little or no differences in the angles of internal friction were found. No statistical difference could be found when the effective angles of friction were evaluated. There is no major difference in the *FF* values obtained for each powder at different relative humidity. Statistical analysis revealed that no significant difference exists between the *FF* values of each fraction at similar RH. The same trend is repeated for the normalised cohesion coefficient values i.e. varying the relative humidity of the storage air did not have any statistically significant impact on the values obtained for each size fraction at different RH.

Statistical evaluation indicates that no significant difference exists between the the angles of internal friction of the size fractions at similar RH. However, the effective angles of frction differ statistically when each fraction was evaluated at similar RH. A statistically significant diffence also exists between the *FF* values of each fraction at similar RH. The pattern shown by the flow functions differs from that of the angle of internal friction. Here there is a clear distinction between the flow function of the bigger size fraction and the smaller size fraction. The trend obtained for the normalised cohesion coefficient (Table

3.32) is as expected, as high *FF* values correspond to a lower interparticulate attraction and hence lower powder cohesiveness and ultimately better powder flow. Similarly, statistical evaluation revealed that a statistical difference ($p < 0.05$) exists between the normalised cohesion coefficient values of the two fractions obtained at similar RH (i.e. the normalised cohesion coefficient values of the smaller size fraction differ from those of the bigger size fraction). Here, the smaller size fraction is more cohesive than the bigger size fraction.

In conclusion, it can be said that the only tested storage condition that had an effect on one of the powders (pregelatinised starch) was 76% RH. This value is in agreement with the critical humidity values (65 – 80% RH) quoted by Turner and Balasubramanian (1974). The effect observed on the powder bulk depends on the ability of the powder to take up moisture (as shown by the larger size fraction of pregelatinised starch), the particle size, time of exposure and the amount of moisture present in the atmosphere.

3.6 COMPARISON OF THE DIFFERENT METHODS

In the pharmaceutical industry, the success of a tabletting or capsule filling operation is dependent amongst other things on the flow and packing properties of the powder blend. Hence, there arises a need for a method which when used can accurately predict/evaluate the flowbility of the powder. In this research, different methods have been applied such as flow through an orifice, tapping, from which packing characteristics such as Carr's compressibility index, compaction constant and angle of internal flow were deduced and used to assess the flowability of the various powders. In the literature, little or no attempt has been made to compare/relate the results obtained from the aforementioned methods to those obtained from shear test experiments using a rotational split – level shear tester (Peschl shear cell) to assess powder flowability. The values obtained from the various methods employed to assess powder flowability were ranked, ranging from number one (indicating best flow) to number eight (poor powder flow behaviour). The correlation between the rank orders of the flow parameters was assessed statistically by the rank correlation of Spearman, r_s (Snedecor, 1980). The rank orders of the different flow parameters for different powders are shown in Table 3.35.

This section aims to correlate the data obtained from tapping experiments and critical orifice diameter with that of the flow parameters derived using the Peschl's rotational split

– level shear tester. The values used are those obtained after storage of powder at 45% RH (with the exception of the results obtained for the COD, which were used as supplied), as this was the RH of the environment when the experiments were carried out.

Table 3.33 *Summary of powder ranking*

POWDER	C_S	C_F	T_S	T_F	$AIFL_S$	$AIFL_F$	*COD*	*AIF*	*EAF*	*FF*	*NCC*
PS	3	3	3	1	2	2	4	1	1	3	3
α-LM	6	5	4	2	1	1	6	7	6	5	5
PCC	8	8	8	8	7	7	5	3	5	6	4
MCC 105	7	7	6	7	8	8	6	8	8	7	8
PS > 56 μm	2	2	1	3	5	4	1	4	2	1	1
PS < 56 μm	4	4	5	4	6	5	3	1	3	4	6
α-LM > 56 μm	1	1	2	6	3	3	2	6	4	2	2
α-LM < 56 μm	5	6	7	5	4	6	6	5	7	8	7

The lowest number (1) is the most desirable powder flow behaviour.

C_S, C_F - Carr's index for slow and fast tapping respectively; T_S, T_F – Compaction constant for slow and fast tapping respectively; $AIFL_S$, $AIFL_F$ – Angle of internal flow for slow and fast tapping respectively; COD – Critical orifice diameter; AIF- Angle of internal friction; EAF – Effective angle of friction; FF – Flow function; NCC – Normalised cohesion coefficient.

See Table 3.7 for abbreviations of powders.

From Table 3.34 it can be seen that depending on the ranks selected for comparison, the Spearman's correlation coefficient values obtained show significance at 0.01 or at 0.05

level, or no significant correlation beween the two ranks. When parameters commonly used to assess powder flowability, such as Carr's compressibility, critical orifice diameter, flow function and recently, the compaction constant, T_s are compared, they either show values that are highly significant at 0.01 level or at 0.05 level. This implies that comparable results will be obtained if any of the aforementioned methods is used for evaluating powder flowability. However, the critical orifice diameter shows a significant correlation with the effective angle of friction and flow function at 0.05 and 0.01, level respectively; angle of internal friction with flow function and normalised cohesion coefficient at 0.05 and 0.01 level, respectively.

Using the slow tapping technique, the Carr's compressibility index obtained, C_S is highly correlated to the compaction constant, T_S (r_s = 0.857**). In contrast, this flow parameter (i.e. C_S) is not significantly correlated with the angle of internal flow ($AIFL_S$), and T_S is also not significantly correlated with $AIFL_S$. On comparing the C_S with other flow parameters, it was observed that this parameter shows a significant correlation with the flow function (*FF*) and the critical orifice diameter (COD).

Some correlations were found by Tan and Newton (1990a) between coefficient of variation of the fill weight of capsules and the flow parameters Carr's compressibility, Hausner's ratio, angle of repose, Kawakita's equation constant and Jenike's flow function (obtained using an annular shear cell). Podczeck and Newton (2000), found an agreement between the coefficient of fill weight variation of capsules filled with lubricated granulated cellulose powder at maximum compression and shear cell results. However, the workers could not arrive at a definite conclusion on the relationship between the Jenike flow function and the Carr's index using an annular shear cell.

No significant correlation could be found between this parameter (i.e. C_S) and $AIFL_s$, $AIFL_F$, T_F, AIF, EAF or with NCC. For the fast tapping technique, the Carr's compressibility index C_F, did not correlate with the compaction constant, T_F and the angle of internal flow ($AIFL_F$).

Table 3.34 *Values of Spearman's Rank correlation Coefficient for various rank orders*

	C_S	C_F	T_S	T_F	$AIFL_S$	$AIFL_F$	COD	AIF	EAF	FF	NCC
C_S	---	**0.976****	**0.857****	0.452	0.452	0.548	**0.781***	0.228	0.667	**0.810***	0.667
C_F		---	**0.929****	0.524	0.524	0.667	**0.781***	0.180	0.690	**0.881****	**0.714***
T_S			---	0.595	0.500	0.690	**0.708***	0.024	0.643	**0.905****	**0.738***
T_F				---	**0.738***	**0.810***	0.171	0.299	0.571	0.452	0.310
$AIFL_S$					---	**0.929****	0.024	0.000	0.310	0.333	0.381
$AIFL_F$						---	0.268	0.108	0.524	0.595	0.548
COD							---	0.479	0.805	**0.903****	**0.805***
AIF								---	**0.766***	0.323	0.323
EAF									---	**0.833***	**0.762***
FF										---	**0.881****
NCC											---

** Correlation is significant at the 0.01 level

* Correlation is significant at the 0.05 level

For abbreviations, see Table 3.34

However, a significant correlation exists between the compaction constant, T_F and the angle of internal flow - $AIFL_F$ ($r_s = 0.810$, $p < 0.05$ level). $AIFL_F$ significantly correlates with $AIFL_s$. No significant correlation exists between $AIFL_F$ and COD, AIF, FF, NCC and T_s.

For the shear cell experiments, the angle of internal friction (AIF), one of the flow parameters, was found to show significant correlation with the effective angle of friction (EAF) at the 0.05 level. No significant correlation was observed between this flow parameter and flow function and normalised cohesion coefficient (NCC). The effective angle of friction (EAF) was found to correlate highly with the flow function (FF) and the

normalised cohesion coefficient (NCC) at the 0.05 level. In addition the flow function (FF) was found to correlate significantly with the normalised cohesion coefficient and the critical orifice diameter at the 0.01 level.

With regards to the ranking obtained using the slow and fast tapping technique, it can be seen that different rankings were obtained when the two techniques were employed, and as such may influence decision making during research and development. Methods that correlate significantly (by virtue of the flow parameters obtained) or flow parameters that correlate significantly by virtue of the similarity in ranking order, could be selectively used, or flow parameter values could be considered and still one would arrive at the the same conclusion for the powder flow behaviour.

Using the non-parametric statistical analysis (Spearman's correlation coefficient ranking order, r_s), it can be seen that the flow function (FF) significantly correlates with the normalised cohesion coefficient (NCC), critical orifice diameter (COD), compaction constant (T_s) and Carr's compressibility indices (C_s and C_f).

The implications of the above findings could be looked at from different angles. For instance, the compaction constant T_s, one of the flow parameters obtained using the slow tapping technique, correlates with the shear cell findings i.e. the flow function (FF) and the normalised cohesion coefficient (NCC). However, there is no such correlation when using the fast tapping machine. This is an excellent indication of the benefits of using the slow tapping equipment over the fast tapping instrument. A method that can detect or be related to the physical properties of powders is much more useful especially in the pharmaceutical industry. In addition, a formulator/researcher would like to be armed with knowledge of different techniques that would give comparable results. This could be very crucial when decisions have to be made with regards to the instrument to be obtained when there is a financial constraint.

According to Pilpel and Varthalis (1976) a strong relationship exists between the angle of internal flow (AIFL) and the angle of internal friction. In this work no correlation was

found between the angle of internal flow or any flow parameters obtained using the shear cell, hence the findings from this work are not in agreement with that of the authors. This may be attributed to the fact that the authors used binary powder mixtures, which may undergo different particle arrangement as opposed to single powders used in this work. This may be an indication that the angle of internal flow and the angle of internal friction are dependent on or measure different powder properties.

The critical orifice diameter, a measure of arch formation in cylinders was found to correlate significantly with the Compressibility indices, compaction constant (T_s), angle of internal friction (EAF), flow function (FF) and the normalised cohesion coefficient (NCC) and not with the angle of internal friction or the angle of internal flow. This is hardly surprising, as the flow function, described by Jenike (1964) as the relationship between the unconfined yield strength as a function of the consolidating pressure or major consolidation pressure of the powder could be analysed to determine the minimum outlet diameter of hoppers or bins to prevent the formation of arches. The flow function and the normalised cohesion coefficient depend on the bulk properties rather than the surface properties. Lee et al., (2000) found that similarities exist between the flow properties ranking obtained from Carr's Compressibility index and the critical orifice diameter of the powders they studied. However, Marshall and Sixsmith (1976) could not find any relationship between the critical orifice diameter and the shear cell measurements using the Jenike shear cell when the flow properties of different tableting grades of microcrystalline cellulose powders were assessed using different techniques. However, a good correlation exists between the powder cohesiveness, coefficient of internal friction and the flow function of the powders, with spray dried lactose exhibiting the best flow properties.

CHAPTER FOUR

GENERAL CONCLUSIONS AND FUTURE WORK

4.1 GENERAL CONCLUSIONS

- From the data of the particle density measurements (pre-drying data not shown), it was deduced that drying of the powder samples prior to analysis had an effect upon the final result obtained. Better results were obtained with dried samples, which were more similar to literature values. Hence, it is recommended that pharmaceutical excipients should be dried prior to particle density determination so as to remove contaminants from the pores and surface of the powder particles.

- The results for the specific surface area clearly show that the surface area of a powder is also a function of, for example, surface texture as suggested by Robertson and Emődi (1943).

- From the data of the particle density determination, precipitated calcium carbonate had the largest particle density. This powder also possessed the largest compaction constant value in comparison to other powders using the slow tapping technique. Overall, precipitated calcium carbonate has also the largest Carr's compressibility index using the slow and fast tapping technique. The compaction constant *T* gave a clear distinction of all the powders as opposed to other flow parameters obtained using the tapping technique. Using the slow tapping technique, the threshold values for densification as proposed by Mohammadi and Harnby (1997) though erroneously interpreted by the workers, were confirmed. However, the values obtained using the fast tapping technique gave very large *T* values, which made interpretation more difficult.

- The Carr's compressibility values obtained using the slow tapping technique (C_s) correlate significantly with those obtained using the fast tapping technique (C_f), but not with the other flow parameters obtained using the fast tapping technique.

- The ranking of powders obtained using the critical orifice diameter (COD) was quite different to that obtained based on Carr's compressibility index. The COD and the compaction constant both ranked pregelatinised starch > 56 μm the same i.e. as being

the powder with the best flow properties. In contrast, α - lactose monohydrate > 56 μm gave the smallest Carr's index, hence the best flow when the slow tapping technique was used.

- A good significant correlation is shown between the flow function and the normalised cohesion coefficient (NCC), critical orifice diameter (COD), compaction constant (T_s) and Carr's compressibility index (C_s and C_f).

- The Peschl shear tester, a rotational split-level tester, provided useful data which were able to differentiate between the properties of the powders.

- For quality control purposes where quick results are required or where there is capital constraint, the slow tapping technique could be applied most utilising the compaction constant, T as the flow indicator. The measurement of flow parameters using the shear tester could take longer than for instance the use of the critical orifice diameter. However, the method is ideal especially for powders with poor flow behaviour and when in-depth information of how a powder will behave during processing/handling is required.

- The influence of relative humidity of air on the flow properties of all the powders revealed that powders such as pregelatinised starch, which absorb moisture on exposing to relative humidity in excess of 53 %, are more likely to change their flow properties (flow function and normalised cohesion coefficient) than powders such as lactose monohydrate, which adsorb moisture or calcium carbonate, which is hydrophobic. No significant difference exists between the shear properties of each powder fraction on varying the relative humidity of air, but a significant difference exists between the bulk properties i.e. the flow function and the normalised cohesion coefficient values of the fractions, when compared.

- The Peschl shear tester is sensitive enough to detect changes in powder particle size, as shown by the flow function and normalised cohesion coefficient values of pregelatinised starch and α –lactose monohydrate size fractions.

4.2 FUTURE WORK

- The relationship between the compaction constant, *T* and the tabletting performance of powders could be studied.

- Pharmaceutical actives or excipients with powder flow similar to the model excipients could be studied to ascertain whether the findings obtained are applicable universally regardless of the type of material used.

- Future work should include further characterisation of the four model powders and further assessment of the Peschl cell in regards to, for example, the wall friction coefficient. This could also include the measurement of flow parameters of other pharmaceutical powders.

- Shear properties of narrow particle size fractions could also be assessed using the shear tester.

- The effect of time consolidation on shear properties could also be evaluated.

- A comparison of the data obtained using the 50 cm^3 Peschl standard cell with that of the Pharma-cell (5 cm^3 volume, 1- 5g of powder) should be undertaken. A good correlation would encourage the use of the Pharmacell in the pharmaceutical industry.

- The findings obtained using the Peschl shear tester could be related to interparticulate adhesion and friction forces, studied, for example using atomic force microscopy.

The flow properties of powders are affected by not one but several factors. This calls for a method that would be able to predict the way these collective properties would interact to be able to define the flow behaviour of the powder in the handling system. The flow parameters obtained (the flow function and normalised cohesion coefficient) from the Peschl shear cell correlate significantly with the results obtained based on the critical orifice diameter, Carr's compressibility index and the rate of densification, otherwise called the compaction constant T_s. However, of all the methods studied, only the shear cell measurements gave the most reproducible results, with the flow parameters being able to differentiate between the powders. In addition, the results obtained from this method were well detailed in contrast to the other methods. This could prove useful for instance in the pharmaceutical sector where the knowledge of the flow properties of powders/powder mixtures is very crucial for a successful powder handling operation e.g. tableting processes.

CHAPTER FIVE

REFERENCES

REFERENCES

Abdullah, E.C. and Geldart, D. (1999). The use of bulk density measurements as flowability indicators. *Powder Technol.,* 102, 151- 165.

Aiache, J. M. and Beyssac, E., (1995). Powders as dosage forms. In: Swarbrick, J. and Boylan, J. C., (Eds), Encyclopedia of Pharmaceutical Technology, Marcel Dekker, N. Y., Vol.12, pp.389-420.

Allen, T., (1999). Surface area determination by gas adsorption. In Particle Size Measurement. Kluwer Academic Publishers, Dordrecht, The Netherlands, Fifth edition, Vol. 2, pp. 39 – 96.

Armstrong, N. A., (2000). Calcium carbonate. In: Kibbe, A. H., (Ed), Handbook of Pharmaceutical Excipients, American Pharmaceutical Association. Third edition, pp. 56-59.

Bagster, D. F., (1984). Tests on a very large shear cell. In: Iinoya, K., Beddow, J. K. and Jimbo, G., (Eds), Powder Technology, Hemisphere, Washington D.C., pp.141-149.

Bak, P., Tang, C. and Weisenfeld, K., (1988). Self-organised criticality. *Phy. Rev.,* A38, 364 - 374

Bauer, E. and Wu, W., (1995). A hypoplastic constitutive model for cohesive powders. *Powder Technol. 85*, 1-9.

Berlin, E., Kliman, P. G., Anderson, B. A. and Pallansch, M.J. (1971). Calorimetric measurement of the heat of desorption of water vapour from amorphous and crystalline lactose. *Thermochimica Acta*, 2, 143 – 152.

Bolhuis, G. and Chowhan, Z.T., (1996). Materials for direct compaction. In Alderborn, G. and Nyström C., (Eds), Pharmaceutical Powder Compaction Technology, Marcel Dekker, N.Y., Vol. 71, pp. 419-500.

Bolton, S., (1997). Pharmaceutical Statistics. Marcel Dekker Inc., Third edition, pp. 62 -101.

Brittain, H.G., Bogdanowich, S.J., Bugay, D.E., De Vincentis, J., Lewen, G. and Newman, A.W., (1991a). Physical characterization of pharmaceutical solids: a review. *Pharm. Res.,* 8, 963-973.

Brittain, H.G., Sachs, C.J., Bugay, and Fiorelli, K., (1991b). Physical characterization of pharmaceutical solids: Practical Examples. *Pharm. Technol.,* 15, 38-52.

British Pharmacopoeia, (2003). The Stationery Office, London, Appendix XVII B A337.

Brunauer, S., Emmett, P.H. and Teller, E., (1938). Adsorption of gases in multimolecular layers. *J. Am. Chem. Soc.,* 60, 309 – 319.

Bryman, A. and Cramer, D., (2001). Quantitative Data Analysis with SPSS Release 10 for Windows. Routledge, East Sussex, England, pp. 96 – 157.

BS 2955, 1993. Glossary of Terms Relating to Particle Technology. British Standards Institution, London, p 4.

Buerki, R. A. and Higby, G. J., (1993). History of dosage forms and basic preparations. In: Swarbrick, J. and Boylan, J. C., (Eds), Encylopedia of Pharmaceutical Technology, Marcel Dekker, N.Y., Vol. 7, pp.299-338.

Caligaris, R. E., Topolevsky, R., Maggi, P. and Brog, F., (1985). Compaction behaviour of ceramic powders. *Powder Technol.,* 42, 263-267.

Callahan, J.C., Cleavy, G.W., Elefant, M., Kaplan, K., Kensler, R. and Nash, A., (1982). Equilibrium moisture content of pharmaceutical excipients. *Drug Dev. Ind. Pharm.*, 8, 355 – 369.

Carr, J. F. and Walker, D. M., (1967/1968). An annular shear cell for granular materials. *Powder Technol.* 1, 369-373.

Carr, R. L., (1965). Evaluating flow properties of solids. *Chem. Eng.* 72, 163-168.

Carr, R. L., (1970). Particle behaviour, storage and flow. *Br. Chem. Eng.*, 15, 1541-1549.

Cassidy, O. E. and Thomas, W. I., (2001). An experimental evaluation of powder rheology. *B.P.C. Science Proceedings, Glasgow,* p 256.

Cleaver, J.A.S., (2004). Personal communication.

Cleaver, J.A.S., Nedderman, R.M. and Thorpe, R.B., (2000). Accounting for granular material dilation during the operation of an annular shear cell. *Adv. Powder Technol.*, 11, 385-399.

Coelho, M. C. and Harnby, N., (1978). The effect of humidity on the form of water retention in a powder. *Powder Technol.*, 20, 197 – 200.

Cole, G. C., (1987). Powder characteristics for capsule filling. In: Ridgway, K., (Ed), Hard Capsules: Development and Technology, The Pharmaceutical Press, London, pp.80-86.

Cooper, A. K. and Eaton, L. E., (1962). Compaction behaviour of several ceramic powders. *J. Am. Ceram. Soc.* 45, 97-101.

Craik, D. J. and Miller, B. F., (1958). The flow properties of powders under humid conditions. *J. Pharm. Pharmacol.,* 10, 136T-144T.

Deleiul, M., Chulia, D., and Pourcelot, Y., (1994). Particle and powder dynamics. In: Chulia, D., Deleiul, M., and Pourcelot, Y., (Eds.), Powder Technology and Pharmaceutical Processes, Elsevier, Amsterdam, pp. 115 -163.

Doelker, E., (1993). Comparative compaction properties of various microcrystalline cellulose types and generic products. *Drug Dev. Ind. Pharm.* 19, 2399-2471.

Eiserhart-Rothe, M. U. and Peschl, I. A. S. Z., (1977). Powder testing techniques for solving industrial problems. *Chem. Engrg., 84,* 97-102.

Etzler, F.M. and Sanderson, M.S., (1995). Particle size analysis: A comparative study of various methods. *Part. Part. Syst. Charact.,* 12, 217 – 224.

Esezobo, S. and Pilpel, N., (1974). The effects of moisture content and gelatine binding agent on the mechanical and failure properties of oxytetracycline formulation. *J. Pharm. Pharmacol., suppl.,* 26, 47P -56P.

European Pharmacopoeia (2002)., Fourth Edition, European Department for the Quality of Medicine within the Council of Europe, Strasbourg, France, pp. 207 – 208.

Flemming, J. and Mielck, J.B., (1995). Requirements for the production of microtablets: Suitability of direct-compression excipients estimated from characteristics and flow rates. *Drg Dev. Ind. Pharm.,* 21(19), 2239 – 2251.

Furnas, C.C., (1931). Mathematical relationships for beds of broken solids of maximum density. *Ind. Eng. Chem.,* 23, 1052 – 1058.

Goelema, C. C., Maltby, L. P. and Enstad, C. G., (1993). Use of uniaxial tester for the determination of instantaneous and time consolidated flow properties of powders. *RELPOWFLO II,* EFChE Publication services, Oslo, Vol. 96, pp. 139-152.

Gohil, U.C., (2002). Investigations into the filling properties of powder mixtures into hard shell capsules. PhD Thesis, University of London, p. 111.

Gold, G., Duvall, R.N., Palermo, B.T. and Slater, J.G., (1966a). Powder flow studies I: Instrumentation and applications. *J. Pharm. Sci.,* 55, 1133 – 1136.

Gold, G., Duvall, R.N., Palermo, B.T. and Slater, J.G., (1966b). Powder flow studies II: Effect of glidants on flow rate and angle of repose. *J. Pharm. Sci.,* 55, 1291– 1295.

Grey, R. O. and Beddow, J. K., (1968/69). On the Hausner ratio and its relationship to some properties of metal powders. *Powder Technol.,* 2, 323-326.

Haaker, G. and Rademacher, F. J. C., (1984). A modified triaxial tester for measuring the flow properties of bulk solids. In: Iinoya, K., Beddow, J. K. and Jimbo, G., (Eds), Powder Technology, Hemisphere, Washington D. C., pp. 127-132.

Hanson, W.A., (1998).Dissolution and powder technology. In: Chulia, D., Deleuil, M. and Pourcelot, Y., (Eds), Powder Technology and Pharmaceutical Processes, Marcel Dekker, N.Y., Vol. 9, pp. 545-552.

Harnby, N., Hawkins, A. E. and Vandame, D. (1987). The use of bulk density determination as a means of typifying the flow characteristics of loosely compacted powders under conditions of variable relative humidity. *Chem. Eng. Sci.,* 42, 879-888.

Harwood, C.F., Pilpel, N., (1968). Measurement of flow properties of powders. *Chem. Process Eng.,* 49, 92 – 96.

Harwood, C.F. and Pilpel, N., (1969). The flow of granular solids through circular orifices. *J. Pharm. Pharmacol.,* 21, 721 – 730.

Hauer, V. B., Remmele, T. and Sucker, H., (1993). Gezieltes Entwickeln und Optimieren von Kapselformulierungen mit einer instrumentierten Dosierröhrchen-Kapselfüllmaschine. Part II: Grundlagen der Optimierungsstrategie. *Pharm. Ind.,* 55, 780-786.

Hausner, H.H., (1967). Friction in a mass of metal powder. *Int. J. Powder Metall.* 3, 7-13.

Hawkins, A.E., (1993). The Shape of Powder – Particle Outlines. Research Studies Press Ltd., Taunton, UK.

Held, G.A., Solina, D.H., Keane, D.T., Haig, W.J., Horn, P.M. and Grinstein, G., (1990). Experimental study of critical mass flunctuations in an evolving sand pile. *Phy. Rev. Lett.,* 65, 1120 – 1123.

Heywood, H. (1963). The evaluation of powders. *J. Pharm. Pharmacol.,* 196, 56T –73T.

Howard, S. A., (2002). Flow Properties of Solids. In: Swarbrick, J. and Boylan, J. C (Editors). Encyclopedia of Pharmaceutical Technology, Marcel Dekker Inc., New York, Second edition, Vol. 12, pp. 1264 – 1286.

Hundal, H.S., Rohani, S., Wood, H.C. and Pons, M.N., 1997. Particle shape characterisation using image analysis and neural networks. *Powder Technol.*, 91, 217-227.

Hvorslev, M.J., (1937). Über die Festigkeitseigenschaften gestörter bindiger Böden Ingeniorvidenskabelige, Skrifter, A Nr. 45, 1 – 162.

Jenike, A.W., (1961). Gravity flow of bulk solids. *Utah Eng. Exp. Stn. Bull.* Vol. 108.

Jenike, A. W., (1964). Storage and flow of solids. *Utah Eng. Exp. Stn. Bull.* Vol.123.

Johanson, J. R., (1992). The Johanson indicizer system versus the Jenike shear tester. Bulk Solids Handling, *12, 23 – 240.*

Jolliffe, I.G. and Newton, J.M., 1982. Capsule filling by dosator nozzle system. *J. Pharm.Pharmacol.,* 34, 293-298.

Jones, T.M., and Pilpel, N. (1966). The flow properties of granular magnesia. *J. Pharm. Pharmacol.,* 18, 81 – 93.

Jordan, R. P. and Rhodes, C. T., (1979). Recording powder flow meters and their use in pharmaceutical technology. *Drug Dev. Ind. Pharm.,* 5, 151-167.

Kamath, S., Puri, V. M., Manbeck, H. B. and Hogg, R., (1993). Flow properties of powders using four testers: measurement, comparison and assessment. *Powder Technol.* 76, 277-289.

Kamath, S. and Puri, V. M., (1997). Measurement of powder flow constitutive model parameters using a cubical triaxial tester. *Powder Technol.* 90, 59-70.

Kawakita, K. and Lüdde, K.H., (1970/71). Some considerations on powder compression equations. *Powder Technol.,* 4, 57-60.

Kaye, B. H., Gratton, J. and Clark, G. G., (1992). Characterizing the flow properties of powders by studying avalanching behaviour. *Proc. Tech. Prog. Chicago,* pp. 231-234.

Kaye, B.H., Liimatainen, J. and Faddis, N., (1995). The effect of flow agents on the rheology of a plastic powder. *Part. Part. Syst. Charact.,* 12, 194 -197.

Kaye, B. H., (1997). Powder Mixing, Chapman and Hall, London, UK, pp. 106 – 124.

Kibbe, A. H., (2000). Lactose. In: Kibbe, A. H., (Ed), Handbook of Pharmaceutical Excipients, American Pharmacuetical Association. Third edition, pp. 227-285.

Klausner, J. F., Chen, D. and Renwei, M., (2000). Experimental investigation of cohesive powder rheology. *Powder Technol.* 112, 94-101.

Kočova, S. and Pilpel, N., (1971/72). The failure properties of lactose and calcium carbonate powders. *Powder Technol.,* 5, 329 - 343.

Kočova, S. and Pilpel, N., (1973). The tensile properties of mixtures of cohesive powders. *Powder Technol.* 7, 51-67.

Ladipo, D. D. and Puri, V. M., (1997). Computer controlled shear cell for measurement of flow properties of particulate materials. *Powder Technol.* 92, 135-146.

Lavoie, F., Cartilier, L. and Thibert, R., (2002). New methods characterising avalanche behaviour to determine powder flow. *Pharm. Res.,* 19(6), 887 – 893.

Lee, Y.S.L., Poynter, R., Podczeck, F. and Newton, J.M. (2000). Development of a dual approach to assess powder flow from avalanching behaviour. *AAPS Pharm.Sci. Technol.,* 1 (3), article 21 (http://www.pharmscitech.com).

Lordi, N. G. and Rowley, G., (2000). Starch, pregelatinized. In: Kibbe, A.H., (Ed), Handbook of Pharmaceutical Excipients, American Pharmaceutical Association. Third edition, pp. 528-530.

Lowes, T. M. and Perry, M.G., (1965). The measurement of cohesion in powders. *Rheol. Acta,* 4, 166-177.

Lüdde, K.H. and Kawakita, K., (1966). Die Pulverkompression. *Pharmazie,* 21, 393-403.

Luerkens, D.W., Beddow, J.K. and Vetter, A.F., (1987). Structure and morphology – The science of form applied to particle characterisation. *Powder Technol.,* 50, 93 – 101.

Luukkonen, P., Schæfer, T., Podczeck, F., Newton, M., Hellén, L and Yliruusi, J., (2001). Characterisation of microcrystalline cellulose and silicified microcrystalline cellulose wet masses using a powder rheometer. *Eur. J. Pharm. Sci.,* 13, 143 –149.

Madichie, C., (2003). Personal communication. GlaxoSmithKline, Harlow Town, Essex, UK.

Magreiter, H. and Schlocker, W., (2002). Effect of the addition of coarse particle fractions on the flow properties of micronised lactose. *Proc. 4th World Meeting ADRITELF/APGI/APV, Florence, Italy, 8 – 11 April,* pp. 149 – 150.

Maltby, L. P., Enstad, G. G. and de Silva, S. R., (1993). Characterization of flow properties and quality control of cohesive particulate solids by means of a uniaxial tester. *Powder and Bulk Solids Conference/ Exhibition,* Chicago, pp. 15-27.

Marinelli, J. (2003). Factors that Impact a Bulk Solid's Flowability, http://www.powderandbulk.com, pp. 1-2.

Marshall, K., (1986). Compression and consolidation of powdered solids. In: Lachman, L., Lieberman, H. and Kanig, J.,(Eds), The Theory and Practice of Industrial Pharmacy, Lea Febiger, Philadelphia, Third edition, pp. 66-99.

Martin, A., (1993). Physical Pharmacy, Lea and Febiger, Philadelphia, U.S.A., Fourth edition p 423 – 452.

Miller, J.C. and Miller, J.N., (1993). Statistics for Analytical Chemistry. Third edition, Ellis Horwood Ltd., Chichester, England, pp. 53 - 77.

Mohammadi, M. S. and Harnby, N., (1997). Bulk density modelling as a means of typifying the microstructure and flow characteristics of cohesive powders. *Powder Technol.* 92, 1-8.

Moreton, R.C., (2000). Calcium carbonate. In: Kibbe, A. H., (Ed), Handbook of Pharmaceutical Excipients, American Pharmaceutical Association. Third edition, pp. 56 – 62.

Neumann, B. S., (1967). The flow properties of powders. In: Bean, H. S., Beckett, A. H. and Carless, J. E., (Eds.), Advances in Pharmaceutical Sciences, Academic Press, London, pp. 181-220.

Newman, A.W., Mueller, R. L., Vitez, I. M., Kiesnowski, C.C., Buggay, D.E., Findlay, W.P. and Rodriguez, C. (1996). Starch. In: Brittain, H.G (Ed.), Analytical Profiles of Drug Substances and Excipients, Academic Press, San Diego, pp. 523 – 577.

Newton, J.M. and Bader, F., (1981). The prediction of the bulk densities of powder mixtures, and its relationship to the filling of hard gelatin capsules. *J. Pharm. Pharmacol.*, 33, 621 – 626.

Nyqvist, H., (1983). Saturated salt solutions for maintaining specified relative humidities. *Int. J. Pharm. Technol. Prod. Mfr.*, 4, 47 – 48.

Orband, J. L. R. and Geldart, D., (1997). Direct measurement of powder cohesion using a torsional device. *Powder Technol.*, 92, 25-33.

Orr, C. and Dallavalle, J. M., (1959). Fine Particle Measurement, The Macmillan Company, New York, pp. 164 – 204.

Patel, R. and Podczeck, F., (1996). Investigation of the effect of type and source of microcrystalline cellulose on capsule filling. *Int. J. Pharm.*, 128, 123-127.

Peschl, I. A. S. Z., (1984). New developments in the field of shear test equipment and their application in industry. In: Iinoya, K., Beddow, J. K. and Jimbo, G.,(Eds), Powder Technology, Hemisphere Publishing Corporation, Washington D.C, pp. 150-164.

Peachl, I.A.S.Z., (2000). Operating Manual for Peschl Shear Tester R0-200 Semi-Automatic IPT, Liechtenstein, pp. 37 – 39.

Pharmaceutical Codex (1979). Pharmaceutical Press, London. Eleventh edition, p.124.

Pilpel, N., (1965). Flow properties of non cohesive powders. *Chem. Proc. Eng.*, 4, 167-179.

Pilpel, N., (1971). Cohesive Pharmaceutical Powders. In: Bean, H.S., Becket, A.H. and Carless, J.E., (Eds), Advances in Pharmaceutical Sciences, Academic Press, London, Vol. 3, pp. 173-219.

Pilpel, N. (1964). The flow properties of magnesia. *J. Pharm. Pharmacol.*, 16, 705 -716.

Pilpel, N. and Esezobo, S., (1974). The effects of moisture content and gelatine binding agent on the mechanical and failure properties of oxytetracycline formulation. *J. Pharm Pharmacol.*, 26, Suppl. 47P – 56P.

Podczeck, F., 1997. A shape factor to assess the shape of particles using image analysis. Powder Technol., *93, 47-53.*

Podczeck, F., (1998). Particle-Particle Adhesion In Pharmaceutical Powder Handling, Imperial College Press, London, pp. 95-140.

Podczeck, F., (1999a). Rheological studies of the physical properties of powders used in capsule filling: I. *Pharm. Technol. Eur.,* 11(9), 16-24.

Podczeck, F., (1999b). Rheological studies of the physical properties of powders used in capsule filling: II. *Pharm. Technol. Eur.,* 11(10), 34 - 42.

Podczeck, F. and Lee-Amies, G., (1996). The bulk volume changes of powders by granulation and compression with respect to capsule filling. *Int. J. Pharm.* 142, 97 – 102.

Podczeck, F. and Miah, Y., (1996). The influence of particle size and shape on the angle of Internal friction and the flow factor of unlubricated and lubricated powders. Int. J. Pharm., 144, 187-194.

Podczeck, F. and Sharma, M., (1996). The influence of particle size and shape of components of binary powder mixtures on the maximum volume reduction due to packing. *Int. J. Pharm.,* 137, 41-47.

Podczeck, F. and Newton, J. M., (1999). Powder filling into hard gelatine capsules on a tamp filling machine. *Int. J. Pharm.* 185, 237-254.

Podczeck, F. and Newton, J. M., (2000). Powder and capsule filling properties of lubricated granulated cellulose powder. *Int. J. Pharm. Biopharm.,* 50, 373-377.

Podczeck, F. and Wood, A. V., (2003). The relationship between granule growth mechanism, amount of liquid binder added and properties of the wet powder mass determined using a split bed shear tester. *Int. J. Pharm.,* 257, 57 - 67.

Prescott, J.K. and Barnum, R.A., (2001a). On powder flowability: I. *Pharmaceutical Technol.,* 13, 36 – 43.

Prescott, J.K. and Barnum, R.A., (2001b). On powder flowability: II. *Pharmaceutical Technol.,* 13, 44 – 53.

Rhodes, M., (1998). Introduction to Particle Technology, John Wiley and Sons, Chichester, pp. 193 – 221.

Richards, J. C., (1966). Bulk solids in motion. In: Richards, J. C., (Ed), the Storage and Recovery of Particulate Solids, Institution of Chemical Engineers, London, pp. 57-94.

Ridgway, K. and Rupp, R., (1969). The effect of particle shape on powder properties. *J. Pharm. Pharmacol.,* 21, *Suppl.,* 30S – 39S.

Robertson, R. H. S. and Emödi, B. S., (1943). Rugosity of granular solids. *Nature,* 152, 539 –540.

Rowley, G., (2003). Pregelatinised Starch, In: Rowe, R. C., Sheskey, P. J. and Weller, P.J., (Ed.) Handbook of Pharmaceutical Excipients. Pharmaceutical Press, London, Fourth edition, pp. 609 – 611.

Rudzinski, W. and Everett, D.H., (1992). Adsorption of Gases on Heterogeneous Surfaces. Harcourt Brace Jovanovich, London, pp. 351 – 419.

Rhodes, M., (1999). Introduction to Particle Technology. John Wiley, Chichester, England, pp. 55 – 80.

Rumpf, H., (1962). The strength of granules and agglomerates. In: Int. Symposium on Agglomeration. Knepper, W.A. (ed.), Interscience, New York, pp. 379 – 418.

Rupp, R. (1977). Flow and other properties of granulates. *Boll. Chim. Farm.* 116, 251 – 266.

Scarlett, B. and Todd A.C., (1968). A split ring annular shear cell for the determination of the shear strength of a powder. *Journal of Scientific Instruments,* 1, 655 – 656.

Schneiderhöhn, P., (1954). Eine vergleichende Studie über Methoden zur quantitativen Bestimmung von Abrundug und Form an Sandkörnern. Heiderlb. Beitr. Miner. Petrogr. 4, 172 – 191.

Schwedes, J., (1984). Measurement of flow properties of bulk solids. In: Iinoya, K., Beddow, J. K. and Jimbo, G., (Eds), Powder Technology, Hemisphere Publishing Corporation, Washington D.C., pp. 89-98.

Schwedes, J., (1996). Measurement of flow properties of bulk solids. *Powder Technol.,* 88, 285-290.

Schwedes, J. and Schulze, D., (1990). Measurement of flow properties of bulk solids. *Powder Technol.,* 61, 59-68.

Shah, R. D., Kabadi, M., Pope, D. G. and Augsburger, L. L., (1995). Physiomechanical characterisation of the extrusion-spheronisation process. II. Rheological determinants for successful extrusion and speronisation. *Pharm. Res.,* 12, 498 -507.

Shangraw, R.F., (1989). Compressed Tablets by Direct Compression. In: Lieberman, H.A., Lachman, L., Schwartz, J.B., (Eds), Pharmaceutical Dosage Forms: Tablets, Second edition, Marcel Dekker, Inc., New York, Vol. 1, pp. 195 -245.

Shotton, E. and Harb, N., (1966). The effect of humidity and temperature on cohesion of powders, *J. Pharm. Pharmacol.,* 18, 175 – 178.

Skoog, D.A., Holler, F.J. and Nieman, T.A., (1998). Principles of Instrumental Analysis. Saunders College Publishing, London, pp. 535 – 561.

Snedecor, G.W. (1950). Statistical Methods, Fourth edition, The Iowa State College Press, Iowa, pp. 138 -168.

SPSS Training Manual (2000). Building Anova Models SPS 10.0. SPSS, Woking, Surrey.

Staniforth, J.N., (2002). Powder Flow. In: Aulton, M.E. (Ed), Pharmaceutical Science and Dosage Form Design. Churchill Livingstone, Edinburgh, Second edition, pp. 600-615.

Staple, W.J., (1975). The influence of size distribution on the bulk density of uniformly packed glass particles. *Soil Sci. Soc. Am. Proc.,* 404 – 408.

Szabó-Révész, P., Pintye-Hódi, K., Kásayr, P. and Selmeczi, B., (1995). Study of flowability and compressibility of microcrystalline cellulose with different morphological characteristics. *Proc. 1st World Meeting APGI/APV,* Budapest, pp. 209-210.

Tan, S. B. and Newton, J. M, (1990a). Powder flowability as an indication of capsule filling performance. *Int. J. Pharm.,* 61, 145 – 155.

Tan, S. B. and Newton, J.. M, (1990b). Capsule filling performance of powders with dosator nozzles of different wall texture. *Int. J. Pharm.,* 66, 207 – 211.

Teunou, E. and Fitpatrick, J.J. and Synnott (1999a). Characterisation of food powder flowability. *J. of Food Engineering.* 39, 31 – 37.

Teunou, E. and Fitpatrick, J.J., (1999b). Effect of relative humidity and temperature on food powder flowability. *J. of Food Engineering.* 42, 109 – 116.

Teunou, E. and Vasseur, J. (1996). Time flow function; Means to estimate water effect on dissoluble bulk materials flow. *Powder Handling and Processing*, 8, 111 – 116.

Turner, G.A. and Balasubramanian, M., (1974). Investigations of the contributions to tensile strength of weak particulate masses. Powder Technol., 10, 121 – 127.

The, R., Couch, S. W. and Bell, T. A., (1995). Characterisation of flow properties of low bulk density materials.*Powder and Bulk Solid Conference and Exhibition, Chicago,* pp. 77-87.

Thomson, F. M., (1997). Storage and flow of particulate solids. In: Fayed, M. E. and Otten,L., (Eds), Handbook of Powder Science and Technology, Chapman and Hall, N.Y., pp. 389-480.

Train, D., (1958). Some aspects of the property of angle of repose of powders. *J. Pharm. Pharmacol.,* 10, 127T-135T.

Tripodi, M. A., Puri, V. M. and Manbeck, H. B., (1992). Constitutive models for cohesive powders: preliminary tests. *Proc. Tech. Prog. Chicago* ,pp. 247-255.

Tripodi, M. A., Puri, V. M., Manbeck, H. B. and Messing, G. L., (1994). Triaxial testing of dry, cohesive powder and its application to a modified Cam-clay constitutive model. *Powder Technol.,* 80, 35-43.

Tripodi, M. A., Puri, V. M., Manbeck, H. B. and Messing, G. L., (1995). Elastoplastic finite element model development and validation for low pressure uniaxial compaction of dry cohesive powder. *Powder Technol.*, 85, 241-251.

Turner, G.A. and Balasubramanian, M., (1974). Ivestigations of the contributions to tensile strength of weak particulate masses. *Powder Technol.,* 10, 121 – 127.

Varthalis, S. and Pilpel, N., (1976). Anomalies in some properties of powder mixtures. *J. Pharm. Pharmacol.,* 28, 415-419.

Wade, A., (1980). Pharmaceutical Handbook, Pharmaceutical Press, London, Nineteenth edition, pp. 592.

Walker, D. M., (1966). An approximate theory for pressures and arching in hoppers. *Chem. Eng. Sci.,* 21, 975-997.

Wanibe, Y. and Itoh, T., (1998). New Quantitative Approach to Powder Technology, Wiley and Sons, Chichester, pp. 7-18.

Washington, C., 1992. Particle Size Analysis in Pharmaceutics and Other Industries, Ellis Horwood Ltd. Chichester, England, pp. 9-39.

Weller, P. J., (2003). Microcrystalline cellulose, In: Rowe, R. C., Sheskey, P. J. and Weller,P.J., (Ed.) Handbook of Pharmaceutical Excipients. Pharmaceutical Press, London, Fourth edition, pp. 609 – 611.

Westman, A.E.R. and Hugill, H.R., (1930). The packing of particles. *J. Am. Ceram. Soc.,* 13, 767 -779.

Wheatley, T.A., (2000). Cellulose, Microcrystalline. In: Kibbe, A.H., (Ed), Handbook of Pharmaceutical Excipients. American Pharmaceutical Association. Third edition, pp. 102-106.

Wurster, D. E., Peck, G. and Kildsig, D. O., (1982). A comparison of the moisture adsorption-desorption properties of corn starch U.S.P and directly compressible starch. *Drug Dev. Ind. Pharm.*, 8, 342 - 354.

York, P., (1975). The use of glidants to improve the flowability of fine lactose powder. *Powder Technol.*, 11, 197 - 198.

Young, G., (2000). Powder flow meter that measures solid particulate flow. U.S Patent

598653.

Zeng, X.M., Martin, G.P. and Marriott, C., (2001). Particulate Interactions in Dry Powder Formulations for Inhalation. Taylor and Francis, New York, pp. 31 – 132.

Zheng, J., Johnson, P.F. and Reed, J.S., (1990). Improved equation of the continuous particle size distribution for dense packing, *J. Am. Ceram. Soc.,* 73, 1392 – 1398.

Zimon, A.D., (1980). Adhesion of Dust and Powder. 2nd edition, Consultants Bureau, New York, pp. 168